Elucidation of hyperglycaemia mediated mitochondrial dysfunction and associated complications in heart and evaluation of ferulic acid against the same

By
Salin Raj P
10BB15A39025

A thesis submitted to the
Academy of Scientific & Innovative Research
for the award of the degree of

DOCTOR OF PHILOSOPHY
in
SCIENCE

Under the supervision of
Prof. (Dr) K G Raghu

CSIR – National Institute for Interdisciplinary Science and Technology (NIIST), Thiruvananthapuram, Kerala – 695 019, India

Academy of Scientific and Innovative Research
AcSIR Headquarters, CSIR-HRDC campus, Sector 19,
Kamla Nehru Nagar, Ghaziabad, U.P. – 201 002, India

September 2020

DECLARATION

I hereby declare that the work incorporated in this thesis entitled, "*Elucidation of hyperglycaemia mediated mitochondrial dysfunction and associated complications in heart and evaluation of ferulic acid against the same*", submitted to the Academy of Scientific and Innovative Research (AcSIR) in fulfilment of the requirements for the award of the Degree of *Doctor of Philosophy* in *Biological Sciences*, embodies original research work carried-out by me under the supervision of Prof (Dr) KG Raghu, Senior Principal Scientist, Agro-Processing and Technology Division, CSIR-National Institute for Interdisciplinary Science and Technology (CSIR-NIIST), Thiruvananthapuram, Kerala India. I, further declare that this work has not been submitted to any other University or Institution in part or full for the award of any degree or diploma.

Salin Raj P

09/09/2020

Thiruvananthapuram

राष्ट्रीय अंतर्विषयी विज्ञान तथा प्रौद्योगिकी संस्थान

NATIONAL INSTITUTE FOR INTERDISCIPLINARY SCIENCE AND TECHNOLOGY

वैज्ञानिक तथा औद्योगिक अनुसंधान परिषद् | Council of Scientific and Industrial Research

इंडस्ट्रियल एस्टेट पी. ओ, पाप्पनंकोड, तिरुवनंतपुरम, भारत - 695 019 | Industrial Estate P.O., Pappanamcode, Thiruvananthapuram, India – 695 019

CERTIFICATE

This is to certify that the work incorporated in this Ph.D. thesis entitled, "*Elucidation of hyperglycaemia mediated mitochondrial dysfunction and associated complications in heart and evaluation of ferulic acid against the same*", submitted by *Salin Raj P* to the Academy of Scientific and Innovative Research (AcSIR) in fulfillment of the requirements for the award of the Degree of *Doctor of Philosophy* in *Biological Sciences*, embodies original research work carried-out by the student. We, further certify that this work has not been submitted to any other University or Institution in part or full for the award of any degree or diploma. Research materials obtained from other sources and used in this research work have been duly acknowledged in the thesis. Images, illustrations, figures, tables etc., used in the thesis from other sources, have also been duly cited and acknowledged.

Salin Raj P
09/09/2020

Dr. K G Raghu
09/09/2020

Tel: 91 471 2515486 / 9495902522 Fax: 91 471 2491712 E-mail: raghukgopal@niist.res.in Website: http//www.niist.res.in

STATEMENTS OF ACADEMIC INTEGRITY

I, Salin Raj P, a Ph.D. student of the Academy of Scientific and Innovative Research (AcSIR) with Registration No. 10BB15A39025 hereby undertake that, the thesis entitled "Elucidation of hyperglycaemia mediated mitochondrial dysfunction and associated complications in heart and evaluation of ferulic acid against the same" has been prepared by me and that the document reports original work carried out by me and is free of any plagiarism in compliance with the UGC Regulations on *"Promotion of Academic Integrity and Prevention of Plagiarism in Higher Educational Institutions (2018)"* and the CSIR Guidelines for "*Ethics in Research and in Governance (2020)"*.

09/09/2020
Thiruvananthapuram

It is hereby certified that the work done by the student, under my supervision, is plagiarism-free in accordance with the UGC Regulations on *"Promotion of Academic Integrity and Prevention of Plagiarism in Higher Educational Institutions (2018)"* and the CSIR Guidelines for "*Ethics in Research and in Governance (2020)".*

Dr. K G Raghu
09/09/2020
Thiruvananthapuram

PLAGIARISM DECLARATION

I, Salin Raj P, bearing AcSIR Registration No. 10BB15A39025 declare that:

(a) My thesis entitled, "Elucidation of hyperglycaemia mediated mitochondrial dysfunction and associated complications in heart and evaluation of ferulic acid against the same" is plagiarism free in accordance with the UGC Regulations on *"Promotion of Academic Integrity and Prevention of Plagiarism in Higher Educational Institutions (2018)"* and the CSIR Guidelines for "*Ethics in Research and in Governance (2020)".*

(b) I would be solely held responsible if any plagiarised content in my thesis is detected, which is violative of the UGC regulations 2018.

09/09/2020
Thiruvananthapuram

ACKNOWLEDGEMENTS

Undertaking this PhD has been a truly life-changing experience for me, and it would not have been possible to do without the support and guidance that I received from many people. Over the past few years, I had the privilege of meeting many influential persons, whose knowledge and passion in doing science have inspired me all through my work. I am indebted to many people, and I would like to extend my sincere gratitude and appreciation to all those who made this PhD thesis possible.

First and foremost, I would like to extend my sincere gratitude to my supervisor Prof. (Dr) KG Raghu for introducing me to this exciting field of science and for his dedicated help, advice, inspiration, encouragement and continuous support, throughout my PhD. His enthusiasm, integral view on research and mission for providing high-quality work, has made a deep impression on me. During our course of interaction during the last seven and half years, I have learnt extensively from him, including how to raise new possibilities, how to regard an old question from a new perspective, how to approach a problem by systematic thinking, data-driven decision making and exploiting serendipity. I owe his lots of gratitude for having me shown this way of research. I am delighted to be associated with a person like Dr Raghu KG in my life. I could not have imagined having a better advisor and mentor for my PhD study.

It is my privilege to thank Dr Suresh Das, former Director and Dr A. Ajayaghosh, Director, CSIR-NIIST for allowing me to be a part of this organization and providing the necessary infrastructure for the completion of my thesis. I also wish to express my gratitude to Dr A Sundaresan, and Mr MM Sreekumar, former Heads of Division, and Dr. K G Raghu, HOD, Agro-Processing and Technology Division for allowing me to be a part of this division and for the constant support and efforts provided.

Besides my advisor, I would like to thank the Doctoral Advisory Committee: Dr Rajeev K Sukumaran, Dr Kaustabh Kumar Maiti, and Dr P Jayamurthy, for their insightful comments and encouragement, but also for the

hard question which incented me to widen my research from various perspectives. I am grateful to the AcSIR coordinators Dr Mangalam S Nair, Dr Luxmi Verma, and Dr C H Suresh for guiding me throughout the working tenure concerning proper fulfilments of the AcSIR requirements for the completion of this thesis. My sincere gratitude also goes to Dr M Arumugam, who has been an excellent support for the fulfilment of the AcSIR requirements in the faculty of biological sciences.

I am grateful to Dr S. Priya, Senior Scientist, Agro-Processing and Technology Division who support me in my western blot analysis, DNA oxidation analysis, and other analysis which helped my work to attain the current status.

Also, I wish to thank the scientists, Dr P. Nisha, Dr BS. Dileep Kumar, Dr MV. Reshma, Mr Venugopalan VV, Dr Anjineyulu Kothakota, Dr Venkatesh R, and Mr Venkatesh T; and Technical staffs Dr Beena Joy, Sri Soban Kumar DR and Mrs Divya Mohan of Agro-Processing and Technology Division for their fruitful comments during the divisional meetings and I am thankful to one and all for their kind gesture.

I am also indebted to the Director, Jubilee Mission Medical College &Research Institute (JMMC&RI), Thrissur, Kerala, India for hosting and allowing me to conduct my animal experiments in the Small Animal Research Facility centre of the institute. In this regard, I would also like to thank Dr Rajankutty, Head, Small Animal Research Facility, JMMC&RI, Thrissur, Kerala. Had it not been his consent to work in the lab and use the animal bleeding, sacrificing, specimen collecting facility, my work would have never been able to attain the current status. I also extend my sincere gratitude to Dr. P R Varghese, Research Coordinator; Dr Ranjith S, Adjunct Faculty, Anatomy; Dr Mathew John, Dr Sureshkumar, Dr Alex George, Ms Gracy, Ms Kalyani of JMMC&RI, Thrissur for their constant support in the completion of my animal experiments.

My sincere thanks also go to Dr A. Prathapan, who guided me to join this team as M Sc project trainee and later as project assistant, and who gave

access to this laboratory and research facilities. Without his precious support it would not be possible to conduct this research.

I also extend my sincere thanks to, Dr Soumya RS, Dr Riya Mariam Philip, Dr Antu K. Antony, Dr Anusree SS, Dr Nisha VM, Dr Priyanka A, Dr Vineetha VP, Dr Reshma PL, Dr Priya Rani, and Dr Vandana Sankar, who provided helpful directions for me about the laboratory and research facilities and gave precious support as their team member. I will always cherish the warmth shown by them.

I would also like to thank my labmates, who have been an excellent support for the past few years. Worth mentioning are Ms Preetha Rani MR, Ms Anupama Nair, Dr Shyny GL, Dr Sindhu G, Dr Genu George, Ms Swapna Sasi, Ms Sreelekshmi Mohan, Ms Sruthi CR, Ms Roopsree OJ, Ms Poornima MS, Dr Sithara Thomas, Ms Jubi Jacob, Ms Evlin M Anto, Ms Anaga Nair, Mr Billu Abraham, Ms Lekshmi K, Ms Lekshmi S, Ms Anusha, Ms Tanya, Ms Sannya, Ms Shini VS, Ms Reshmitha TR, Mr Pratheesh S. Nair, Mr Sreejith, and all other colleagues of Agro-Processing and Technology Division for the stimulating discussions, and for all the fun we have had in the past few years. Also, I thank my seniors and friends in other divisions of NIIST for their help and support.

I want to express my gratitude to all the members of the library, administrative, academic programme committee and technical staff of NIIST for their help and support. I am also indebted to Council of Scientific and Industrial Research (CSIR) and Department of Health Research (DHR), New Delhi, India for financial assistance in the form of research fellowship and Young Scientist Fellowship.

My special regards to my teachers because of whose teaching at different stages of education has made it possible for me to see this day. Because of their kindness, I feel, was able to reach a stage where I could write this thesis.

I owe my deep sense of gratitude and regard to my mother, wife, brother, and sisters for their prayers, affection, encouragements, inspiration,

patience and support which smoothly paved my path towards the successful completion of the research work.

I owe my deepest gratitude towards my mother, brother and sisters for their unlimited support and understanding of my goals and aspirations. Their unfailing love and support have always been my strength. Their patience and sacrifice will remain my inspiration throughout my life, and without their help, I would not have been able to complete much of what I have done and become who I am. It will be ungrateful on my part if I am not acknowledging my wife Ms Lijisha JS. I am thankful to her for giving me happiness during the last few months of my studies.

A special thanks to my brother-in-law for their love and affection. My hearty regard goes to my father-in-law, mother-in-law, sister-in-law and her family, for their love and moral support. As always it is impossible to mention everybody who had an impact on this work; however, there are those whose spiritual support is even more important. I am also very much grateful to all my family members for their constant inspiration and encouragement.

Finally, I humbly bow before the almighty God Jesus for showering his blessings upon me and giving me the strength, and wisdom to reach this important milestone in my academic life.

Salin Raj P

TABLE OF CONTENTS

Sl. No.	Contents	Page
1.	Title page	i
2.	Declaration	ii
3.	Thesis certificate	iii
4.	Statement of academic integrity	iv
5.	Plagiarism declaration	v
6.	Acknowledgement	vi - ix
7.	Table of contents	x
8.	Chapter contents	xi - xv
9.	List of figures	xvi - xviii
10.	List of tables	xix- xx
11.	Chapter text	1-150
12.	Abstract of thesis	151
13.	List of publication	152-153
14.	List of conferences presentations	154-155
15.	Published paper	156-169
16.	Annexure I – List of proteins	170
17.	Annexure II – AcSIR course work	171

CHAPTER CONTENTS

No.		Headings	Page
		Chapter 1	
		Introduction and literature reviews	**1-45**
1.1		**Diabetes mellitus**	**1-2**
	1.1.1.	Type 1 diabetes mellitus	3
	1.1.2.	Type 2 diabetes mellitus	4-6
	1.1.3.	Gestational diabetes mellitus	7
1.2.		**Cardiovascular disorders**	**8-79**
1.3.		**Diabetic cardiomyopathy**	**10-12**
	1.3.1.	Stages of diabetic cardiomyopathy	13
	1.3.2.	Characteristics of diabetic cardiomyopathy	14
	1.3.3.	Cardiac metabolism in diabetic cardiomyopathy	15-17
	1.3.4.	Mitochondrial function in diabetic cardiomyopathy	18-19
	1.3.5.	Oxidative stress and diabetic cardiomyopathy	20-21
	1.3.6.	Calcium homeostasis and diabetic cardiomyopathy	22
	1.3.7.	MAM and diabetic cardiomyopathy	23-26
	1.3.8.	Apoptosis and diabetic cardiomyopathy	27-28
1.4.		**Currently available medications**	**29-31**
1.5.		**Natural products and diabetic cardiomyopathy**	**32-34**
1.6.		**Ferulic acid**	**35-36**
1.7.		**Hypothesis and Objectives**	**37**
		References	**38-45**
		Chapter 2	
		Hyperglycaemia induces oxidative stress in H9c2 rat cardiomyocyte and the possible beneficial effect of ferulic acid	**46-72**
2.1.		**Introduction**	**46-47**
2.2.		**Materials and Methods**	**48-54**

	2.2.1.	Chemicals and reagents	48
	2.2.2.	Cell culture and induction of hyperglycaemia	48
	2.2.3.	Estimation of Atrial natriuretic peptide (ANP) and brain natriuretic peptide (BNP)	49
	2.2.4.	Morphometric analysis	50
	2.2.5.	Extraction and estimation of protein concentration	50
	2.2.6.	Cytotoxicity assay	51
	2.2.6.1.	MTT assay	51
	2.2.6.2.	Lactate dehydrogenase (LDH) leakage assay	51
	2.2.7.	Analysis of intracellular ROS by bio-imaging and cytometry	52
	2.2.8.	Lipid peroxidation (TBARS) assay	52
	2.2.9.	Protein carbonyl content assay	53
	2.2.10.	Intracellular Ca^{2+}overload assay	54
	2.2.11.	Western blot	54
		Statistical analysis	55
2.3.		**Results**	**55-64**
	2.3.1.	Hyperglycaemia induced cell death in H9c2 cells	55
	2.3.2.	HG induced intracellular Ca^{2+} ([Ca^{2+}]i) overload in H9c2 cardiomyoblast	56
	2.3.3.	HG induced ROS production in H9c2 cardiomyoblasts	57
	2.3.4.	HG upregulated the cellular pro-oxidants and downregulated the antioxidant proteins and enzymes	58-59
	2.3.5.	HG induces damage to lipids and proteins	60
	2.3.6.	HG caused H9c2 cell injury	61
	2.3.7.	HG induced alteration in fibrosis	62
	2.3.8.	HG induced alteration in myocyte morphology	63-64
2.4.		**Discussion**	**64-67**
		References	**68-72**

	Chapter 3	
	Investigation on mitochondrial dysfunction during hyperglycaemia in *in vitro* model and amelioration with ferulic acid	**73-108**
3.1.	**Introduction**	**73-75**
3.2.	**Materials and Methods**	**76-82**
3.2.1.	Chemicals and reagents	76
3.2.2.	Cell culture and induction of hyperglycaemia	76
3.2.3.	Mitochondrial permeability transition pore (mPTP)	77
3.2.4.	Mitochondrial transmembrane potential (ΔΨm)	78
3.2.5.	Estimation of mitochondrial superoxide production	78
3.2.6.	Mitochondrial superoxide dismutase (MnSOD) activity	79
3.2.7.	Analysis of SERCA/PLN pathway	79
3.2.8.	Analysis of mitochondria associated ER membrane (MAM) function	79
3.2.9.	Evaluation of mitochondrial biogenesis and dynamics	80
3.2.10.	Isolation of mitochondria	80
3.2.11.	Determination of OxPhos function	80
3.2.12.	ATP content assay	81
3.2.13.	Evaluation of expression of apoptotic proteins	81
3.2.14.	Annexin V-FITC/propidium iodide (PI) double staining assay for apoptosis	81
3.2.15.	Western blot	82
	Statistical analysis	82
3.3.	**Results**	**83-96**
3.3.1.	HG induced the opening of mPTP by altering the protein expressions in H9c2 cells	83-84
3.3.2.	HG induced dissipation of mitochondrial membrane potential (ΔΨm) in H9c2 cells	85
3.3.3.	HG increases the mitochondrial superoxide production in H9c2 cells	86
3.3.4.	HG reduces the activity of MnSOD in H9c2 cells	87

3.3.5.	Effect of HG on the MAM and calcium transport	88
3.3.6.	Effect of HG on the SERCA/PLN/PKA Cα pathway	89-90
3.3.7.	Effect of HG on the mitochondrial biogenesis and dynamics	91
3.3.8.	Effect of HG on the mitochondrial OxPhos function and ATP production	92-93
3.3.9.	HG induces apoptosis through mitochondrial Cyt c/Casp3, Smac/Arts/ HtrA2/XIAP, and Aif/EndoG pathways in H9c2 cells	94-96
3.4.	**Discussion**	**97-104**
	References	**104-108**
	Chapter 4	
	Investigation on alteration in the heart metabolism during T2DM	**109-146**
4.1.	**Introduction**	**109-111**
4.2.	**Materials and methods**	**112-121**
4.2.1.	Chemicals and reagents	112
4.2.2.	Animal model and treatment protocol	112-113
4.2.3.	Morphology analysis and estimation of body mass index (BMI) and heart mass index (HMI)	114
4.2.4.	Estimation of fasting blood glucose (FBG)	115
4.2.5.	Estimation of serum glycated haemoglobin (HbA1c)	115
4.2.6.	Estimation of serum insulin and HOMA-IR	115
4.2.7.	Serum atrial and b-type natriuretic peptide (ANP & BNP)	116
4.2.8.	Activity of serum glutamate oxaloacetate transaminase (SGOT)	116
4.2.9.	Analysis of lipid profile	117
4.2.10.	Serum lactate dehydrogenase (S-LDH) & creatine kinase-MB (CK-MB)	118
4.2.11.	Serum myeloperoxidase (MPO) enzyme activity	119
4.2.12.	Analysis of biochemical markers of heart	119
4.2.13.	Estimation of serum cardiac troponin I-interacting kinase (TNNI3K)	119

	4.2.14.	Mitsugumin 53 mediated insulin resistance and fatty acid oxidation	120
	4.2.15.	Western blot	120
	4.2.16.	Histological studies	121
		Statistical analysis	121
4.3.		**Results**	**122-132**
	4.3.1.	Diabetes increased the morphometric parameters	122
	4.3.2.	Diabetes induces insulin resistance	123
	4.3.3.	Diabetes induces lipotoxicity	124-125
	4.3.4.	Diabetes induces cardiac hypertrophy	126
	4.3.5.	Diabetes induces cardiac dysfunction	127
	4.3.6.	Diabetes induces systolic dysfunction and myocardial infarction	128-129
	4.3.7.	MG 53 up regulation induced diabetic cardiomyopathy	130-131
	4.3.8.	Diabetes induced cardiomyocyte fibrosis	132
4.4.		**Discussion**	**133-141**
		References	**142-146**
		Chapter 5	
		Summary and conclusion	**147-150**
5.1.		Summary	147-148
5.2.		Conclusion	149
5.3		Future prospects	149-150

LIST OF FIGURES

Sl. No.	Title	Page
1.1.	Global statistics on diabetes	1
1.2	Risk factors of T2DM	4
1.3	Secondary complications of T2DM	6
1.4	Different types of cardiovascular disorders	9
1.5	Definition of cardiomyopathy	12
1.6.	Different stages of diabetic cardiomyopathy	14
1.7.	Pathophysiology mechanisms of diabetic cardiomyopathy	17
1.8.	Mitochondrial dynamics in diabetic cardiomyopathy	19
1.9.	Oxidative stress in the development of diabetic cardiomyopathy	21
1.10.	Calcium and diabetic cardiomyopathy	23
1.11.	MAM and diabetic cardiomyopathy	24
1.12.	Apoptotic mechanisms in diabetic cardiomyopathy	28
1.13.	Ferulic acid	36
2.1.	Hyperglycaemia increases the intracellular Ca^{2+} ($[Ca^{2+}]i$) in H9c2 rat cardiomyoblast	57
2.2	Hyperglycaemia increases the ROS formation in H9c2 rat cardiomyoblast	58
2.3.	Hyperglycaemia upregulates stress proteins and downregulates stress relieving proteins	59
2.4.	Hyperglycaemia upregulates the cardiac injury (hypertrophy) markers Anp and Bnp in H9c2 cells	62

2.5.	Hyperglycaemia increases the total protein content in H9c2 rat cardiomyoblast	63
2.6.	Hyperglycaemia increases the cell volume in in H9c2 rat cardiomyoblast	64
3.1.	Mitochondrial permeability transition pore (mPTP)	74
3.2.	Hyperglycaemia induces the opening of mitochondrial permeability transition pore (mPTP) in H9c2 cells	83
3.3.	Hyperglycaemia induces dissipation of mitochondrial membrane potential (ΔΨm) in H9c2 cells	85
3.4.	Hyperglycaemia increases the mitochondrial superoxide production in H9c2 rat cardiomyoblast	86
3.5.	Hyperglycaemia reduces the MnSOD activity in H9c2 rat cardiomyoblast	87
3.6.	Hyperglycaemia causes alterations in the expression of various vital proteins of mitochondria-associated endoplasmic reticulum membranes (MAMs) in H9c2 rat cardiomyoblasts	88
3.7.	Hyperglycaemia causes alterations in the expression of SERCA/PLN/PKACα pathway of calcium transport in H9c2 rat cardiomyoblasts	90
3.8.	Hyperglycaemia downregulates the marker proteins of mitochondrial biogenesis and fusion and upregulates fission in H9c2 rat cardiomyoblasts	91
3.9.	Hyperglycaemia down regulates the various complexes of OxPhos and reduces ATP synthesis in H9c2 rat cardiomyoblasts	92
3.10.	Hyperglycaemia upregulates the mitochondrial caspase-dependent and independent apoptotic pathways in H9c2 rat cardiomyoblasts	94
3.11.	Hyperglycaemia induced apoptotic cell death in H9c2 rat cardiomyoblasts	96

4.1.	Signalling pathways involved in MG53-induced DCM	111
4.2.	Experimental flow chart of in vivo study	113
4.3.	Diabetes causes the increase in morphologic parameters in Wistar rats	122
4.4.	Diabetes causes the increase in cardiac biomarkers, indicating diabetic cardiomyopathy in Wistar rats	129
4.5.	Diabetes causes the increase in cardiomyopathy markers in Wistar rats	131
4.6.	Diabetes induces cardiomyocyte fibrosis in Wistar rats	132
5.1	Schematic representation of the effect of ferulic acid against DCM	148

LIST OF TABLES

Sl. No.	Title	Page
1.1.	Criteria for the diagnosis of diabetes - American Diabetes Association	2
1.2.	Historical findings on diabetic cardiomyopathy	10
1.3.	Protein composition and functions of MAMs	25
1.4	Compounds targeting fatty acid metabolism as a treatment for diabetic cardiomyopathy	30
1.5.	Effect of natural products on various diabetic cardiomyopathy models	33-35
2.1.	Hyperglycaemia causes significant cytotoxicity in H9c2 rat cardiomyoblasts	56
2.2.	Densitometry analysis blots of oxidative stress marker proteins in H9c2 cells	59
2.3.	Hyperglycaemia causes the significant increase in lipid peroxidation and protein oxidation in H9c2 cells	60
2.4.	Hyperglycaemia causes the significant release of cardiac injury (hypertrophy) markers - atrial natriuretic peptide (ANP), and b-type natriuretic peptide (BNP) in H9c2 rat cardiomyoblasts	61
3.1.	Densitometry analysis blots of mPTP proteins in H9c2 cells	84
3.2.	Densitometry analysis of proteins of MAM of H9c2 cells	89
3.3.	Densitometry analysis of proteins of SERCA pathway of H9c2 cells	90
3.4.	Densitometry analysis of proteins of mitochondrial dynamics of H9c2 cells	91
3.5.	Densitometry analysis of proteins of complexes of OxPhos of H9c2 cells	93

3.6.	Densitometry analysis of apoptotic and anti-apoptotic proteins of H9c2 cells	95
4.1.	Diabetes induces alteration in glucose homeostasis in male Wistar rats	124
4.2.	Diabetes induces lipotoxicity in male Wistar rats	125
4.3.	Diabetes causes significant release of cardiac hypertrophy markers in the blood	126
4.4.	Diabetes increases the activities of cardiac enzymes	127
4.5.	Densitometry analysis of protein markers of cardiac dysfunction	130
4.6.	Densitometry analysis of MG53, insulin signalling and lipid metabolism pathway	131

Chapter 1

Introduction and literature reviews

1.1. Diabetes mellitus

Diabetes mellitus (DM) is one of the chronic metabolic diseases distinguished by raised levels of glucose in the blood (hyperglycaemia). A persistent hyperglycaemia for long time will lead to severe damage to other organs such as kidneys, eyes, blood vessels, heart, and nerves to become lethal. The people living in low and middle-income countries are more prone to DM. The International Diabetes Federation (2020) reported that, about 463 million DM patients worldwide in 2019, and it directly ascribed to death of 1.6 million every year. The prevalence of diabetes has steadily increasing in past few decades, and predicted to prolong in the next decade (**Fig. 1.1**).

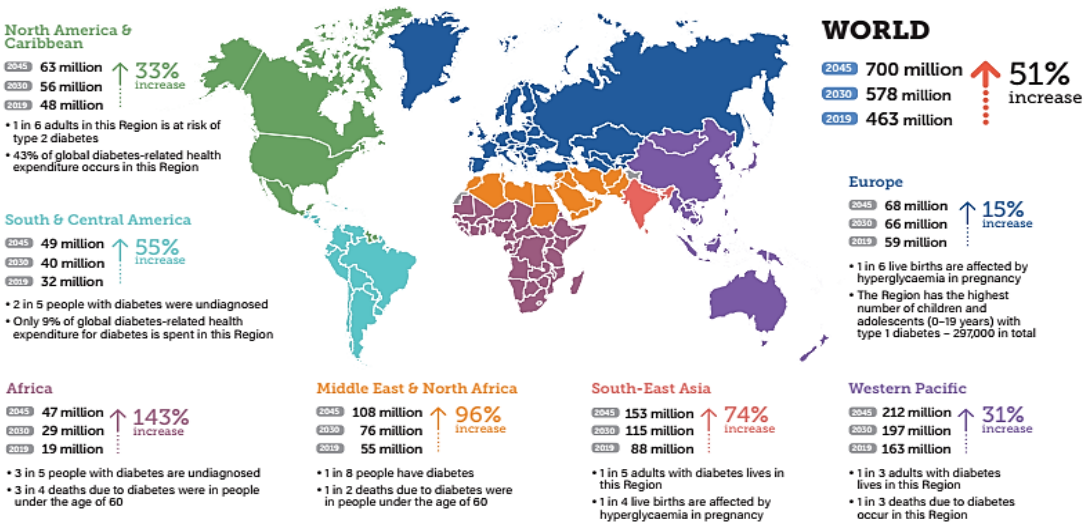

Figure.1.1. Global statistics on diabetes Number of adults aged 20 - 79 years with diabetes worldwide; Global Fact sheet (IDF, 2020).

The diagnosis criteria of DM in earlier days was based on fasting plasma glucose (FPG) or oral glucose tolerance test (OGTT), but in 2010, the American Diabetes Association included the assessment of glycated haemoglobin (HbA1c) into the diagnosis criteria (ADA, 2013). **Table. 1.1** summarises the specific criteria used to diagnose the DM.

Marker	Diagnosis criteria	Method
HbA1c	≥ 6.5 %	NGSP certified method and standardised to the DCCT assay*
FPG	≥ 126 mg/dL (7.0 mM)	No caloric intake for at least 8 h)*
2 h PG	≥ 200 mg/dL (11.1 mM)	OGT test (75 g glucose in water) *
RPG	≥ 200 mg/dL (11.1 mM)	Patients with symptoms of hyperglycaemia

Table.1.1. Criteria for the diagnosis of diabetes - American Diabetes Association. FPG indicates fasting plasma glucose; RPG random plasma glucose; NGSP, National Glycohaemoglobin Standardization Program; DCCT, Diabetes Control and Complications Trial; and OGT, Oral Glucose Tolerance. * In the absence of unequivocal hyperglycaemia (ADA, 2013).

The polyuria, polydipsia, polyphagia, weight loss, and blurred vision are the early symptoms of DM. The chronic hyperglycaemia may be susceptible to certain infections and in children, it imparts impairment of growth. The acute condition of DM occurs if uncontrolled, which becomes lethal with ketoacidosis or the non-ketotic hyperosmolar syndrome (HHNS). The retinopathy (vision loss), nephropathy (renal failure), neuropathy (foot ulcers, amputations, and Charcot foot), gastrointestinal, genitourinary and sexual dysfunction, and cardiovascular symptoms are the major long term complications of DM.

Based on the pathogenic processes involved in the development of diabetes, it is classified mainly into three types. The chronic diabetic condition seen in juveniles with little insulin production due to the defective pancreas is termed as type 1 diabetes (T1DM), which is also known as insulin-dependent diabetes. The most common type of diabetes, type 2 diabetes (T2DM), develops when the body becomes resistant to the insulin or the non-functional insulin, and usually occurs in adults. The third one is the gestational diabetes (GDM) occurred in pregnant women.

1.1.1. Type 1diabetes mellitus (T1DM)

T1DM is an autoimmune disorder with the destruction of the insulin producing pancreatic β cells. T1DM develops mainly between the ages of five to seven years. Initially, it was thought T1DM as a disorder of children and adolescents, but the recent findings revealed the symptomatic onset of T1DM in aged people also. The diagnostic hallmarks in children and adolescents include polydipsia, polyphagia, and polyuria, along with hyperglycaemia. Sometimes T1DM tends to develop more slowly in adults than it does in children. The latent autoimmune diabetes of adulthood is the T1DM, and seen in adults over 35 years of age, which is sometimes misdiagnosed as T2DM. Also, the T2DM diagnosed with islet autoantibodies (5 to 15%) in some occasions are having T1DM (Tuomi, 2005).

The symptoms of T1DM such as polydipsia, polyphagia, polyuria and weight loss when comes above the average, and not treated immediately, it may become lethal. T1DM may lead to significant risk with initial hyperglycaemia and ketoacidosis, which can lead to the development of macrovascular and microvascular complications. The common macrovascular complication of T1DM is cardiovascular diseases which have a higher risk for myocardial infarction, stroke, angina, and coronary artery vascularisation, when compared to the non-diabetic people (Melendez-Ramirez et al. 2010).

An immediate exogenous insulin replacement is a requirement for T1DM, and lifetime treatment is needed. The major microvascular complications of T1DM such as retinopathy, nephropathy and neuropathy have been ameliorated with insulin treatment. Also, the immune-based therapies using cyclosporine were attempted to reverse T1DM nearly three decades before. Even now, the autoimmune destruction of β-cells remains untreatable. One of the breakthrough protocols in the T1DM treatment was the transplantation of islet without the use of glucocorticoids for immune suppression. However, only 10% of patients remained independent of exogenous insulin (Ryan et al. 2005). Nowadays, the primary research

interests on T1DM are immunomodulation and improvement of vascularisation by biomaterials instead of islet transplantation.

1.1.2. Type 2 diabetes mellitus (T2DM)

T2DM is the most common form of DM, which accounts for 90 to 95% of all diabetic patients (Tripathi & Srivastava, 2006). T2DM was the first described component of metabolic syndrome. The defective metabolisms of carbohydrate, proteins and lipids, insulin resistance or impairment in insulin secretion are the significant characteristics of T2DM. The pre-existence of insulin resistance in the skeletal muscle, liver and adipose tissue and the directing impairment in the insulin secretion by pancreatic beta cells is thought to be the leading cause of T2DM (**Fig. 1.2**).

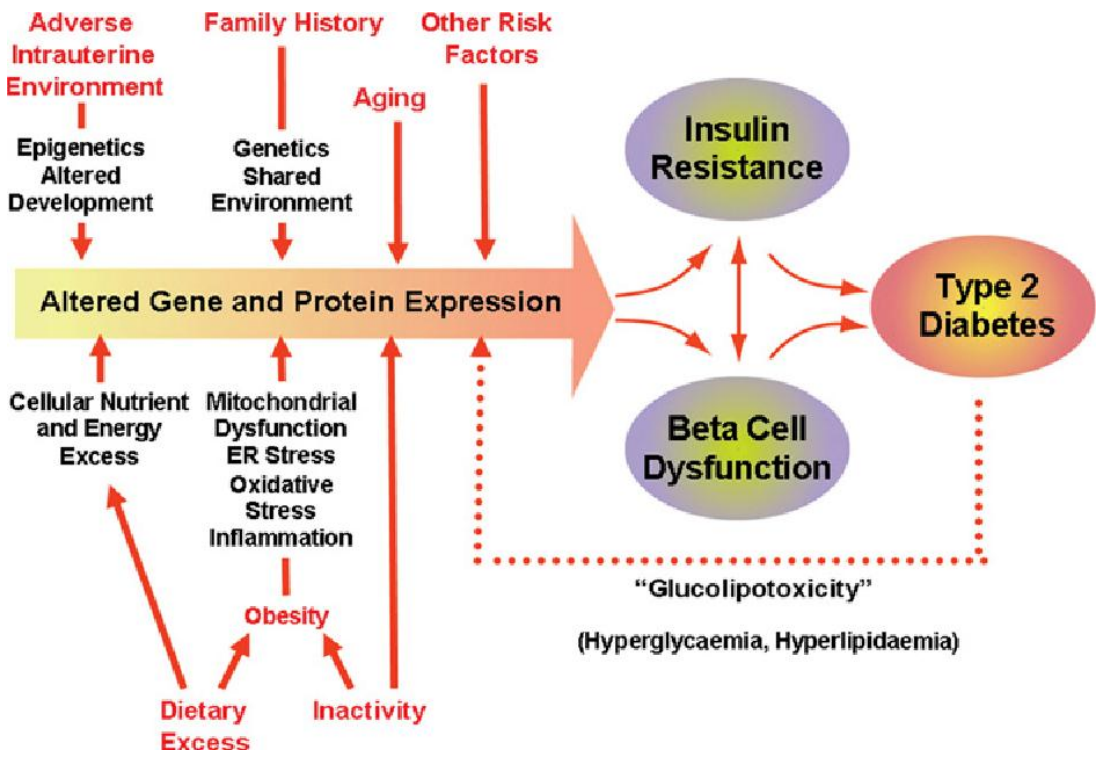

Figure.1.2. Risk factors of T2DM (Jin & Patti, 2009, Clinical Science 116:99–111)

Since a large number of people are affected by T2DM and remain asymptomatic and are in prediabetic stage, screening is an essential need, and ~30 % of individuals are reported to be undiagnosed. The asymptomatic T2DM patients present severe hyperglycaemia or lethal ketoacidosis on

diagnosis. These days, T2DM is self-manageable by controlling abnormal glucose levels, lipid profiles and blood pressure along with the continuous medical care.

The development of secondary microvascular complications like retinopathy, nephropathy and neuropathy, and macrovascular complications such as heart attack and stroke can be prevented or minimised. T2DM patients have two to three-fold increases in the risk of heart attacks and strokes due to the increased atherosclerosis, peripheral arterial and cerebrovascular disease (**Fig. 1.3**). Diabetes and its associated complications lower the quality of people's lives and generate enormous economic and social burdens. The elucidation of molecular pathways and the development of effective interventions are the immediate requirements for the exact cure of T2DM.

The higher level of C-reactive protein, interleukin-6 (IL-6), tumour necrosis factor (TNF), branched-chain and aromatic amino acids, and lower levels of sex hormone-binding globulins in the blood (Wang et al. 2013) are some of the novel biomarkers in the pathophysiology of T2DM. They are associated with an increased risk of T2DM. A high concentration of adiponectin is associated with reduced risk due to its anti-inflammatory effects (Li et al. 2009). The prediction of future risk of T2DM is a novel aim on diabetic research and the gut flora metabolites aid in that.

The gut microbiota plays a vital role in the control of metabolism of diets, levels of metabolic endotoxins in the blood, chronic inflammation, and alteration in some gene expression (Esteve et al. 2011). Even though there is no total reversal of T2DM with drugs, it can be potentially manageable, and it is estimated up to 90 %. The maintenance of BMI less than 25 kg/m^2, 30 min exercise per day, keeping away from smoking and alcohol consumption, and a healthy diet is advised for fruitful management of T2DM.

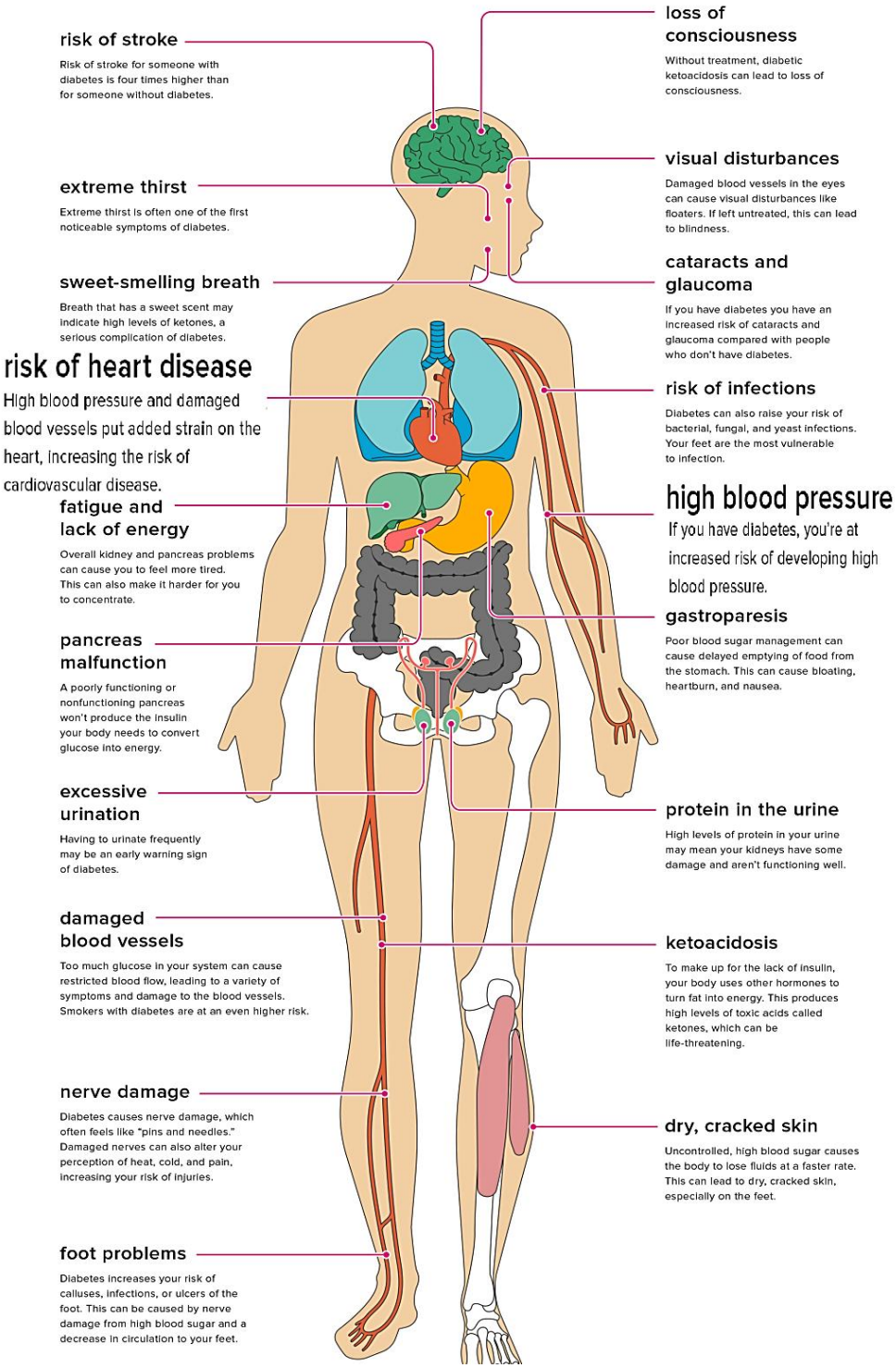

Figure.1.3. Secondary complications of T2DM (https://www.healthline.com/health/diabetes/effects-on-body#1)

One another condition is known as prediabetes, in which normal glucose homeostasis is compromised. Impaired fasting plasma glucose (100-

125 mg/dL), glucose tolerance (140-199 mg/dL), and/ or high HbA1c level (5.7-6.4 %) are the prime characteristics of prediabetes. In comparison with peoples with normal glucose values, the prediabetics have three to seven-fold increased risk of developing T2DM. Also, the chronic complications of T2DM such as microalbuminuria, retinopathy, and neuropathy are identified during the prediabetic state. The risk for CVD is two to three times higher in prediabetic patients compared with normal individuals (Levitzky et al. 2008). The early diagnosis of prediabetes is, therefore, advisable to minimise the complications of impending T2DM.

1.1.3. Gestational diabetes mellitus (GDM)

GDM is another type of diabetes developing as pregnancy complications. The GDM is expounded as the development of chronic hyperglycaemia during gestation, in women without a previously diagnosed DM. The pancreatic beta cell dysfunction manifest the GDM with chronic insulin resistance. GDM affects approximately 16.2% of pregnancies worldwide, representing approximately 18 million births annually. GDM is set to increase with the escalating obesity epidemic.

The higher maternal age, a family history of insulin resistance or DM, overweight or obesity, deficiency in micronutrient, and Westernized diet are the major risk factors of GDM. In the mother, GDM may increase the risk for T2DM and CVDs, and in the child, it induces future CVDs, obesity, T2DM, or GDM, if it is not cleared following the delivery. There is no treatment or prevention strategy for GDM, except the lifestyle interventions like diet and exercise. However, in some cases, insulin therapy is advisable (Plows et al. 2018).

The massive increase in DM in the present century is predicted not only due to an increase in incidence, but also the result of better healthcare improvement and life expectancy. Also, the awareness of prediabetes is minimal. Even though there is an immense advance in health care, the DM remains as one of the leading metabolic syndromes of premature mortality,

and this is predicted due to the associated CVDs. According to the IDF, it is estimated 4.2 million deaths worldwide are imputable to DM in 2019 (IDF, 2020).

1.2. Cardiovascular disorders (CVDs)

CVDs affect the heart and blood vessels. The leading CVDs are hypertension, coronary heart disease, cerebrovascular and peripheral vascular disease, rheumatic and congenital heart diseases, and the cardiomyocyte disorders like cardiomyopathies (**Fig. 1.4**). CVDs are the dominant cause of death globally; 17.9 million people die each year due to CVDs, that is an estimated 31% of all deaths worldwide (WHO, 2020). There observed an increase in blood pressure, glucose and lipids levels with obesity and overweight individuals at risk of CVDs. The risk factors for CVD include metabolic/physiological risk factors like high blood pressure (hypertension) and higher concentrations of blood sugar or glucose (diabetes) and cholesterol or lipid (dyslipidaemia), along with the behavioural risk factors such as unhealthy diet, tobacco and alcohol use and inadequate physical activity.

A large percentage of CVDs can be prevented through the reduction of behavioural risk factors since unhealthy behaviours lead to metabolic/ physiological changes. These factors are predicted to start in childhood, prolonged over many years and demonstrated as heart attacks and strokes in people of middle age via atherosclerosis in coronary and cerebral blood vessels. Diabetes is a significant risk factor of CVD, and cardiovascular risk increases with raised glucose values (Boden-Albala et al. 2008).

It is estimated that 60% of all mortality in people with DM accounts in the CVDs. In DM patients, two to three times higher risk of developing the CVDs, which is estimated higher in women. Also, the incidence of stroke rate showed two-fold increase in DM of some age groups (Tun et al. 2017). The diagnosis also reported failing in most DM patients after a CVD. The DM augments the CVDs through the glycated proteins induced arterial stiffness,

fibrillation, and oxidative stress-induced myopathy of heart (van Heerebeek et al. 2008).

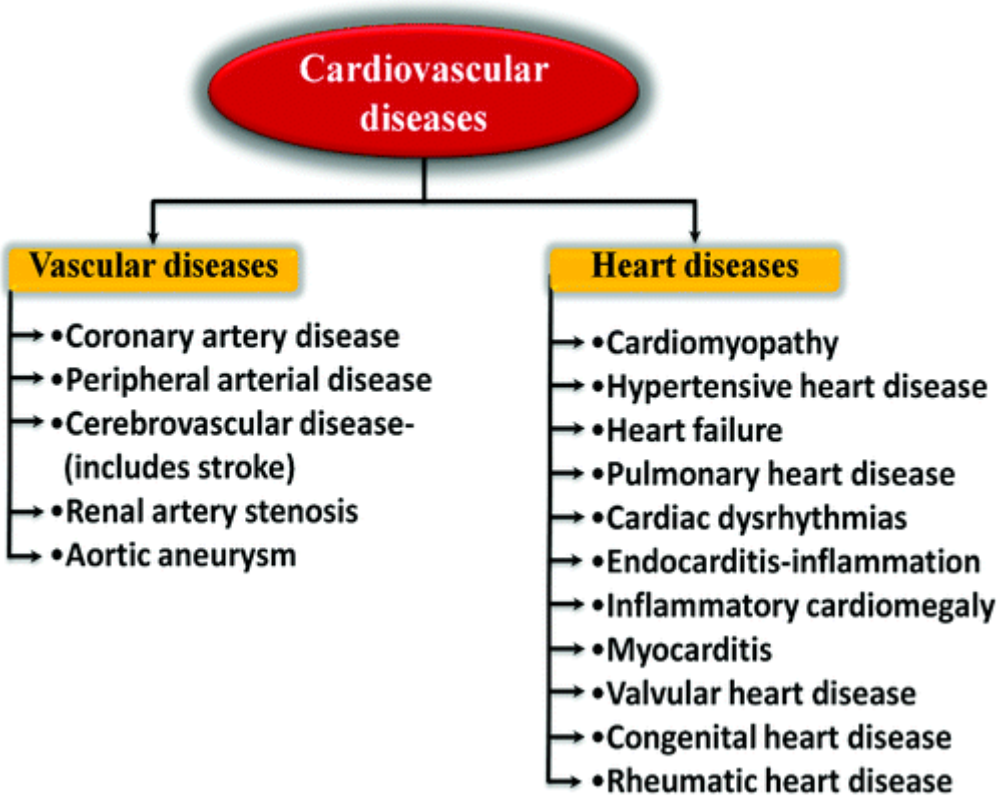

Figure.1.4. **Different types of cardiovascular disorders** (Parsanathan & Jain, 2020; Metab Syndr Relat Disord 18(1):10-30)

Cardiomyopathy refers to diseases of the heart muscle, manifested with enlarged, thick or rigid cardiac muscles. The weakening of heart, inability to pump blood, irregular heartbeats (arrhythmias), problems with heart valves, and heart failure are predicted series with the worsening of cardiomyopathy. There observed different types of cardiomyopathy based on the myopathic lesions, among this, the leading types of cardiomyopathies are dilated, hypertrophic, restrictive, transthyretin amyloid cardiomyopathies, and arrhythmogenic right ventricular dysplasia. Diabetic cardiomyopathy is recently identified in DM patients. Cardiomyopathy affects all age people, but middle-aged group men are more prone to this disorder.

1.3. Diabetic cardiomyopathy (DCM)

As mentioned previously, DM persuades the affected individuals to severe cardiovascular complications in two to three folds, implicated as the leading cause of diabetic associated morbidity and mortality. The DM urges to develop heart disease at a younger age than those without diabetes. In order to develop proper therapeutic interventions for DCM, there needs an authentic clinical understanding of the role of DM in the pathophysiology of structural and functional cardiac abnormalities. The increases in atherosclerosis, vascular dysfunction, prothrombosis, hypertension, dyslipidaemia, and insulin resistance are the prime reasons underlying cardiovascular dysfunction in DM. Over the years of research, it has become apparent that the increased risk of diabetic heart failure prevails independent of other cofactors such as hypertension or coronary artery disease (**Table. 1.2**).

Year	Author	Description
1876	Schmitz	Severe insufficiency of cardiac action. A common and notable complication of diabetes mellitus
1881	Leyden	Heart failure was a 'frequent and noteworthy complication of diabetes mellitus
1888	Mayer	Association between diabetic-associated heart disease and metabolic abnormalities
1954	Lundbaek	Myocardial dysfunction as a common complication in elderly diabetic patients
1969	Lundbaek	Suggested the need for developing specific diagnostic criteria for myocardial dysfunction associated with diabetes mellitus
1972	Rubler	New type of cardiomyopathy associated with diabetic glomerulosclerosis
2004	Fang	The existence of diabetic heart disease or cardiomyopathy—referring to myocardial disease in diabetic subjects that cannot be ascribed to hypertension, coronary artery disease or any other known cardiac disease—has remained controversial
2007	Boudina	Diabetic cardiomyopathy has been defined as ventricular dysfunction that occurs independently of coronary artery disease and hypertension
2008	Aneja	Diabetic cardiomyopathy is the presence of myocardial dysfunction in the absence of coronary artery disease and hypertension. Diabetic cardiomyopathy can be clinically defined by the presence of abnormal myocardial performance or structure in the absence of epicardial coronary artery disease, hypertension and significant valvular disease. Diabetic cardiomyopathy is defined by echocardiography with myocardial structural or functional abnormalities in the absence of hypertension and coronary disease

2009	Asghar	Diabetic cardiomyopathy is a distinct primary disease process, independent of coronary artery disease, which leads to heart failure in patients with diabetes
2010	Boudina	Diabetic cardiomyopathy describes diabetes-associated changes in the structure and function of the myocardium that is not directly attributable to other confounding factors such as coronary artery disease or hypertension
2010	Voulgari	Diabetic cardiomyopathy is defined as the cardiovascular damage present in diabetes patients, which is characterised by myocardial dilatation and hypertrophy, as well as a decrease in the systolic and diastolic function of the left ventricle, and its presence is independent of the coexistence of ischaemic heart disease or hypertension
2011	Tarquini	A distinct entity characterised by the presence of abnormal myocardial performance or structure in the absence of epicardial coronary artery disease, hypertension and significant valvular disease
2013	Miki	The current typical definition of diabetic cardiomyopathy comprises structural and functional abnormalities of the myocardium in patients with diabetes without coronary artery disease or hypertension
2013	Ryden	Diabetic cardiomyopathy is a clinical condition diagnosed when ventricular dysfunction occurs in the absence of coronary atherosclerosis and hypertension
2014	Trachanas	Diabetic cardiomyopathy, defined as the presence of myocardial involvement in patients with diabetes, characterised by dilatation and hypertrophy of the left ventricle, with the concomitant appearance of diastolic and/or systolic dysfunction, and its presence is independent of the coexistence of ischaemic or hypertensive or valvular heart disease
2016	Matshela	Diabetic cardiomyopathy refers to diabetes-associated structural and functional myocardial dysfunction not related to other confounding traditional factors such as coronary artery disease, hypertension, congenital heart diseases or valvular heart diseases
2017	Lorenzo-Almoros	The minimal criteria to be diagnosed with diabetic cardiomyopathy include left ventricular diastolic dysfunction and/or reduced left ventricular ejection fraction, pathological left ventricle hypertrophy and interstitial fibrosis

Table. 1.2. Historical findings in diabetic cardiomyopathy (Albakri, Med. Clin. Arch. 2018, 2(3):1-13; Lee, et al. Heart. 2019, 105:337-345)

A pivotal study by Rubler et al. (1972) in post-mortem pathological analysis of four diabetic patients who exhibited heart failure symptoms without any signs of coronary artery or valve disorders developed the concept of “diabetic cardiomyopathy” (**Fig. 1.5**)

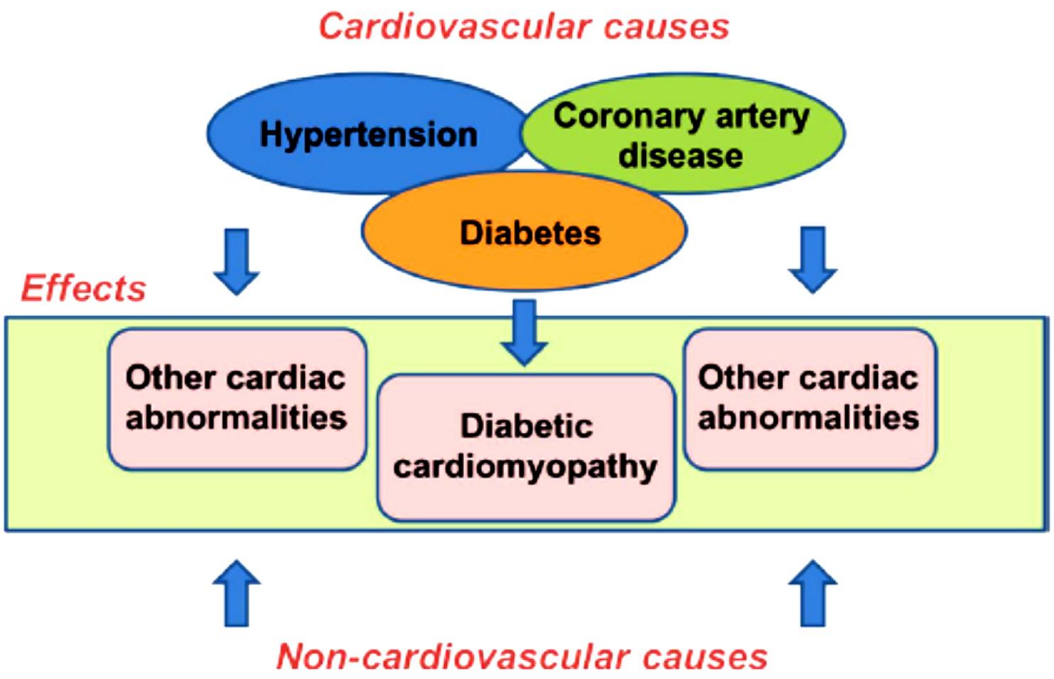

Figure.1.5. Definition of cardiomyopathy (Lee, et al. Heart, 2019; 105:337-345)

There was a 5-fold prevalence of heart failure in diabetic women and 2.4 fold in men after adjusting the other cardiovascular risk factors, such as age, coronary heart disease, and hypertension in a Framingham heart study. Later the cardiovascular research groups from the American college of cardiology foundation, the American heart association, and the European society of cardiology in collaboration with the European Association for the study of diabetes defined DCM as “a clinical condition of ventricular dysfunction that occurs in the absence of coronary atherosclerosis and hypertension in patients with diabetes mellitus” (Yancy et al. 2013).

About five decades since the landmark study of Rubler et al. (1972), the DCM has still required much research for the exact mechanism underlying it because most of them were controversial. The current study is also focusing on the identification of fundamental mechanisms of DCM, to obtain right drug development platforms and biomarkers for the management of this disorder.

1.3.1. Stages of diabetic cardiomyopathy

The progress of DCM has been grouped into different stages based on the ejection fraction and phenotypic changes in left ventricles (**Fig. 1.6**). In the early stages of its evolution, DCM is usually asymptomatic. The initial pathophysiological symptoms include the left ventricular (LV) hypertrophy, impaired diastolic filling, increased atrial filling, and prolonged isovolumetric relaxation. The metabolic dysregulation such as altered glucose and lipid metabolisms, and defective intracellular calcium and other ions homeostasis (Jia et al. 2016) were also observed in the early stages. There documented many pathological factors underlying the development of DCM. The hyperglycaemic stress, increased free fatty acids, systemic and cardiac tissue insulin resistance, inflammation, and malfunction of renin-angiotensin-aldosterone (RAAS) and sympathetic nervous systems (SNS) are some of the prime factors. The inefficient sequestration of sarcoplasmic reticulum Ca^{2+} also contributes the diastolic cardiac dysfunction through reduced calcium (Ca^{2+}) pump activity (Jia et al. 2016).

The second stage is followed with noticeable LV hypertrophy due to the loss of myocytes via apoptosis, fibrosis and cardiac remodelling, which advances through diastolic cardiac dysfunction and the resultant clinical indications of heart failure without alteration in the ejection fraction (Jia et al. 2016). The third stage is depicted with an enlarged LV chamber and the proceeding reduction in ejection fraction, period, and prolonged pre-ejection rate developed as a consequence of diastolic and systolic dysfunction, and reduced cardiac compliance, leads to increased resistance to filling with increased filling pressures (Jia et al. 2016). The abnormalities in the expression of contractile and regulatory protein such as cardiac myosin heavy chain isoforms V1 to V3, myosin light chain-2, troponin contributes to the impaired cardiomyocyte contraction and systolic cardiac dysfunction. The terminal stage is heart failure with marked remodelling, ischemia or infraction.

The principal factor in the development of DCM is the hyperglycaemia mediated cardiac metabolic dysregulation, hypertrophy, myocyte remodelling, fibrosis, steatosis, apoptosis, and necrosis. These were occurring as a chain of deformities and gave a precise platform for different stage-wise progression of DCM. The structural modifications influenced cardiac dysfunction in DCM had ended up in an initial diastolic dysfunction followed by altered systolic function and heart failure (Muralidaran & Viswanathan, 2015).

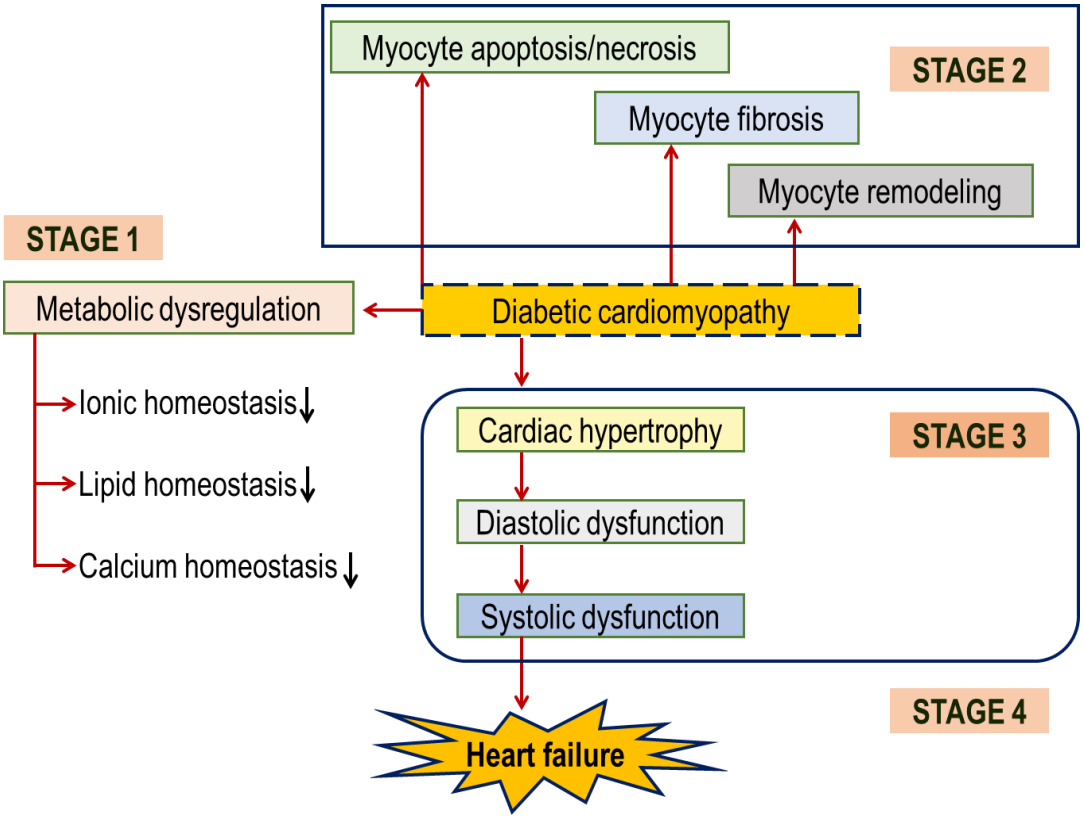

Figure.1.6. Different stages of diabetic cardiomyopathy (Muralidaran & Viswanathan, 2015; 6:1-15)

1.3.2. Characteristics of diabetic cardiomyopathy

The initiation and prolongation of diabetic cardiomyopathy or “diabetic heart muscle disease” to the heart failure shows various physiological and pathological adaptations in the heart with an initial asymptomatic diastolic dysfunction (slowing in relaxation kinetics) and the progressive systolic function, which increases morbidity and mortality (Schannwell et al. 2002). The DCM is characterised by myocardial fibrosis, dysfunctional remodelling,

diastolic and systolic dysfunction, and the leading heart failure. In the development and progression of DCM, the heart showed various cardiac tissue abnormalities such as increased oxidative stress, reduced nitric oxide bioavailability, cardiac metabolic abnormalities, impaired insulin signalling, advanced glycation end products, microvascular dysfunction, cardiomyocyte and extracellular matrix stiffness due to collagen fibrosis as the consequence of hyperglycaemia.

The mitochondrial dysfunction, defects in mitochondrial and cardiomyocyte Ca^{2+} handling, endoplasmic reticulum stress, inflammation are the significant intracellular abnormalities of DCM. In the heart, the activation of RAAS and SNS, and cardiac autonomic neuropathy were also observed (Jia et al. 2018). The hypertrophic marker genes such as atrial natriuretic peptide (ANP), B-type natriuretic peptide (BNP), and β-myosin heavy chain were found upregulated in the DCM heart (Huynh et al. 2010). Also, the activation of transforming growth factor β1 (TGFβ1) pathway in the cardiomyocyte with the impaired insulin signalling pathways, increased the myocardial fibronectin and collagen content, and cardiac interstitial fibrosis is characteristic of DCM (Bando & Murohara, 2014).

1.3.3. Cardiac metabolism in diabetic cardiomyopathy

During diabetes or insulin resistance, the heart modifies its energy metabolism with augmented fatty acid and decreased glucose consumption. This alteration of cardiac metabolism has been suggested playing a vital role in the development of cardiomyopathy (Jia et al. 2018). In normal physiological conditions, the heart can utilise fatty acids, carbohydrate, amino acids, and ketones and 70% of ATP generation is through fatty acids oxidation and the remaining 30% from glucose and lactate. The chronic hyperglycaemia evoked by insulin deficiency or resistance in DM damages the myocardium by altering glucose metabolism.

The reduction in expression of glucose transporters, increased the expression of pyruvate dehydrogenase kinase-4 (PDK4), increased flux of

glucose into hexosamine, pentose and polyol pathways were also reported. These changes in the metabolic pathways increased the implication of advanced glycation end products (AGEs) formation and reduced the fatty acid energy production (Bugger & Abel, 2014). The increased formation of AGEs stimulates the collagen cross-linking and myocardial fibrosis. Also, it increases the oxidative stress through activation of AGE receptor (RAGE), and inflammation by nuclear factor-κB (NF-κB) signalling (Bugger & Abel, 2014). Thus in DM, glucose uptake, glycolysis, and pyruvate oxidation were impaired during the insulin resistance.

However, the heart can rapidly switch its substrate selection to accommodate different physiological and pathophysiological conditions, and this substrate switching is essential to ensure continuous ATP generation to maintain heart function (Young et al. 2002). The lack of insulin function augments lipolysis, and the heart rapidly adapts to using fatty acids exclusively for ATP generation.

High fatty acids uptake and metabolism augments the accumulation of fatty acid intermediates and triglycerides or ceramide resulted in lipotoxicity leading to cardiomyocyte steatosis and hypertrophy. The intra-myocardial lipid deposits, formed due to this increased uptake of fatty acids from circulating very low-density lipoproteins and targeted cardiac-specific overexpression of human lipoprotein lipase, with normal cardiac function reveals the metabolic disturbances precede the onset of left ventricular dysfunction in DCM (**Fig. 1.7**; Yagyu et at. 2003).

In mouse models of cardiac steatosis and reduced heart function, there was increased fatty acid utilisation with restricted expressions of membranes fatty acid transporter – long-chain acyl-coenzyme A synthetase 1, fatty acid transport protein 1 and the transcription factor for fatty acid uptake and oxidation activation - peroxisome proliferator-activated receptor α (Finck et al. 2002). In the cardiomyocyte, approximately 75% of cytosolic fatty acids are transported to the mitochondria and utilised in the OxPhos and ATP

generation, and the rest is stored in the form of TAG (Stanley et al. 2005). In the mitochondria, fatty acids were metabolised through β- oxidation pathway to acetyl CoA and NADH, which is then utilised for ATP production via tricarboxylic acid cycle and OxPhos.

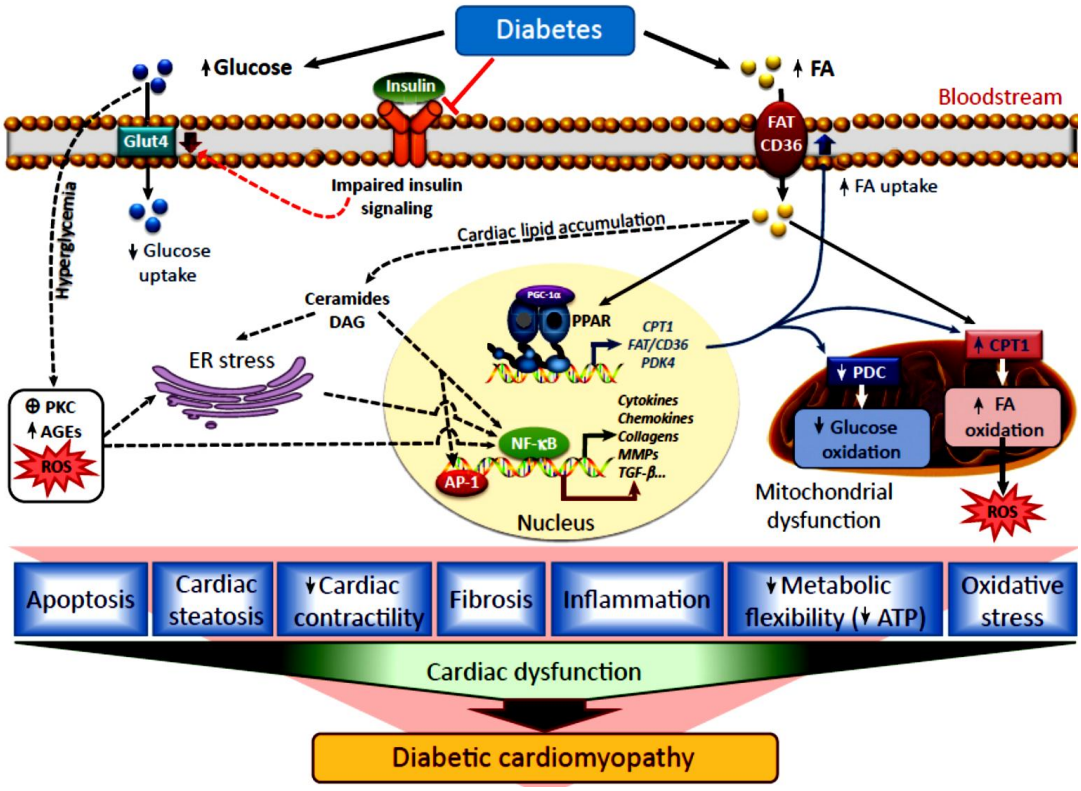

Figure.1.7. Pathophysiology mechanisms of diabetic cardiomyopathy (Palomer, et al, Trend. Pharmacol. Sci. 2018; 39(5):452-467)

The fatty acid oxidation decreases glucose oxidation through the activation of pyruvate dehydrogenase kinase (PDK) and inhibition of the pyruvate dehydrogenase (PDH) enzyme complex (Randle cycle; Randle et al. 1963), and this allows the heart to switch sources for energy production based on nutritional status. The dependence of fatty acid over glucose for the generation of ATP needs more oxygen, which also alters the features of cardiac energetics like shuttling of cellular ATP, noncontractile energy expenditure, mitochondrial uncoupling, along with overproduction reactive oxygen and nitrogen species (ROS/RNS), and ER stress (Bugger & Abel, 2014). The mitochondrial uncoupling and increased ROS triggers the calcium

mishandling, cardiomyocyte apoptosis, and chronic low-grade inflammation in DM. These metabolic abnormalities in diabetic hearts contribute to the development of impaired contractility observed in DCM. The change from glucose to fatty acids for energy production during diabetes in the heart has thus become an essential determinant in the genesis of DCM.

1.3.4. Mitochondrial function in diabetic cardiomyopathy

Cardiac dysfunction in diabetic patients is caused by multiple pathologic mechanisms. Most of these mechanisms are associated with mitochondrial dysfunction (abnormalities), which has been proposed to be an etiological factor in the pathophysiology of diabetic heart disease and these derangements in cardiac energy metabolism plays a vital role in the genesis of DCM.

The irregular mitochondrial dynamics, defective mitochondrial electron transport chain (oxidative phosphorylation) activity, decreased peripheral mitochondrial DNA (mtDNA) copy number, and mutation in mtDNA are the prime mitochondrial abnormalities resulted due to the shifted substrate utilisation, and altered ion homeostasis. These mitochondrial deformities lead to increased formation of MitoROS. The mitochondria make up 30% of the volume of a single cardiomyocyte, and the heart contraction depends mostly on ATP produced by the mitochondrial oxidative phosphorylation system, so the malfunction in cardiomyocyte mitochondrial energetics appear to contribute substantially in DCM (Liu et al. 2014). It plays a variety of roles in the cardiomyocyte beyond its function as ATP producing ‘powerhouse’ of the cell in cellular survival. It has a critical role as an arbitrator of cell death. In diabetic people there observed an inverse relationship between the HbA1c level and mitochondrial respiratory capacity. Also, in all diabetic patients even with a low HbA1c value of 6.0, the mitochondrial function was found altered (Anderson et al. 2009).

The mitochondrial switch from glucose to free fatty acids oxidation for ATP production is accompanied by increased mitochondrial ROS generation and impaired oxidative phosphorylation (**Fig. 1.8**). Also, the hyperglycaemia

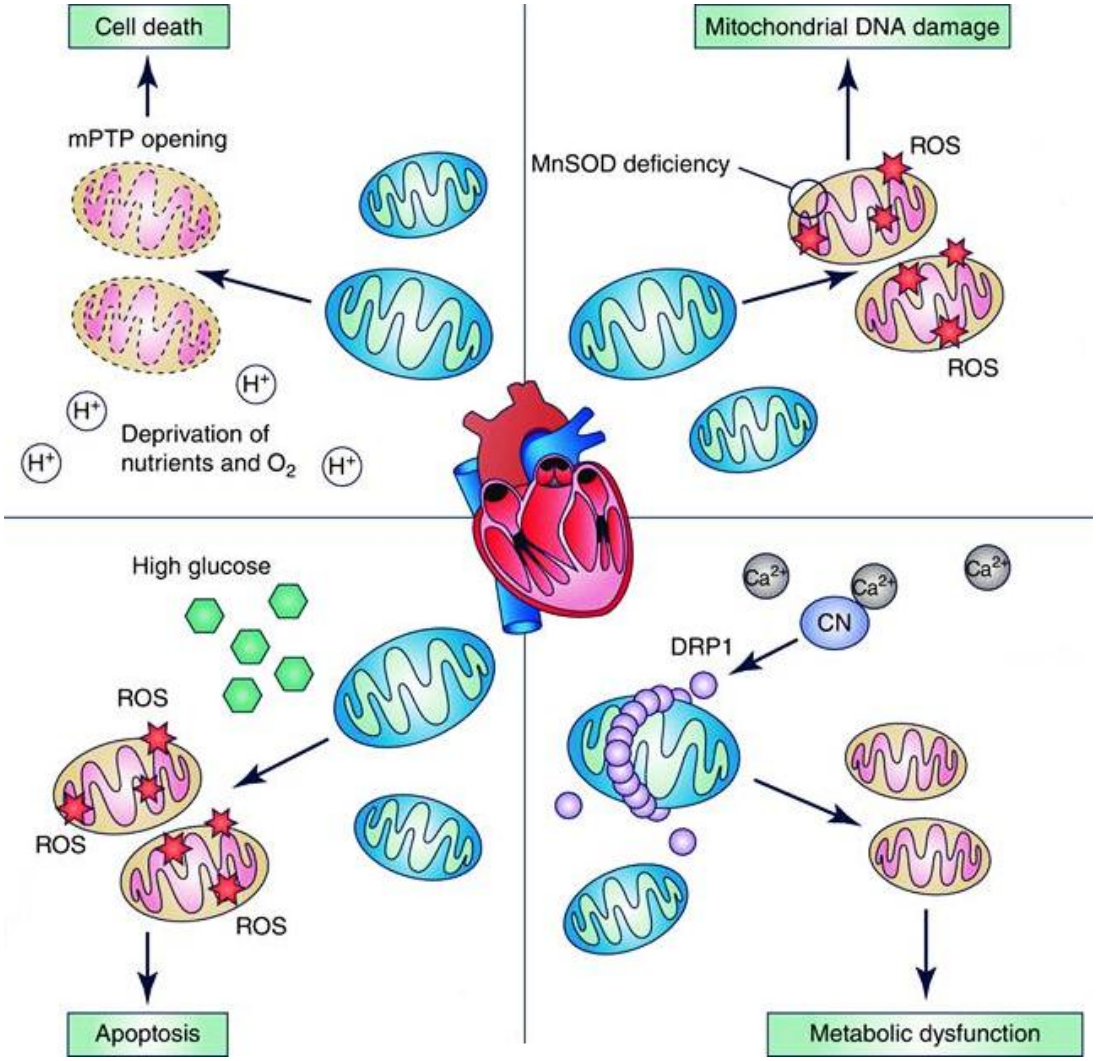

Figure.1.8. Mitochondrial dynamics in diabetic cardiomyopathy (Vasquez-Trincado et al, J Physiol. 2016; 594(3):509–525)

and insulin resistance induce the mitochondrial dysfunction via increasing the NAD and FAD flux to the mitochondrial electron transport chain (ETC), resulted in inner mitochondrial membrane hyperpolarisation, inhibition of electron transport in complex III, and overproduction ROS (Teshima et al. 2014). Increased cardiomyocyte NAD phosphate oxidase, an essential source

of cardiomyocyte ROS, activity has been reported in diet-induced obesity and systemic and cardiac insulin resistance (Jia et al. 2018).

The altered mitochondrial Ca^{2+} handling further promotes mitochondrial respiratory dysfunction leading to cell death (Anderson et al. 2009). The mitochondrial dysfunction induced by the hyperglycaemic stress also persuades the Ca^{2+} overload and mitochondrial permeability transition pore opening, which will terminate in cardiomyocyte autophagy and necrosis (Anderson et al. 2011). Dysfunctional mitochondria release pro-death factors such as cytochrome C, apoptosis-inducing factor, and Smac/DIABLO (Shen et al. 2006) and directly involved in the apoptotic cell death.

1.3.5. Oxidative stress and diabetic cardiomyopathy

Multiple potential mechanisms are underlying the genesis of DCM, but most of the pathophysiologic factors are either generated from the oxidative stress or result of it. Oxidative stress is the pathological condition when there is an imbalance between reactive oxygen species or reactive nitrogen species formation and the antioxidant defences for their neutralisation. ROS and RNS formed due to hyperglycaemia play a critical role in diabetic injury in multiple organs via the oxidative damage in DNA, protein, lipids and carbohydrates. Hyperglycaemia in both T1DM and T2DM is associated with increased ROS and RNS production in mitochondria. The loss of myocardial cells via apoptosis plays the condemnatory role in the genesis of DCM. Studies showed that oxidative stress activated the signal pathways of apoptosis in the gene expression and signal transduction stages (**Fig. 1.9**).

In the diabetic heart, multiple pathways are involved in the generation of ROS. The most studied mechanisms are the mitochondrial electron transport chain leakage, increased activities of enzymes such as nicotinamide adenine dinucleotide phosphate oxidase (NOX), xanthine oxidase and 12/15 lipoxygenase, nitric oxide synthase uncoupling, protein kinase C activation, and the interaction between the receptor for advanced glycation end-products (RAGE) and AGE (Kayama et al. 2015).

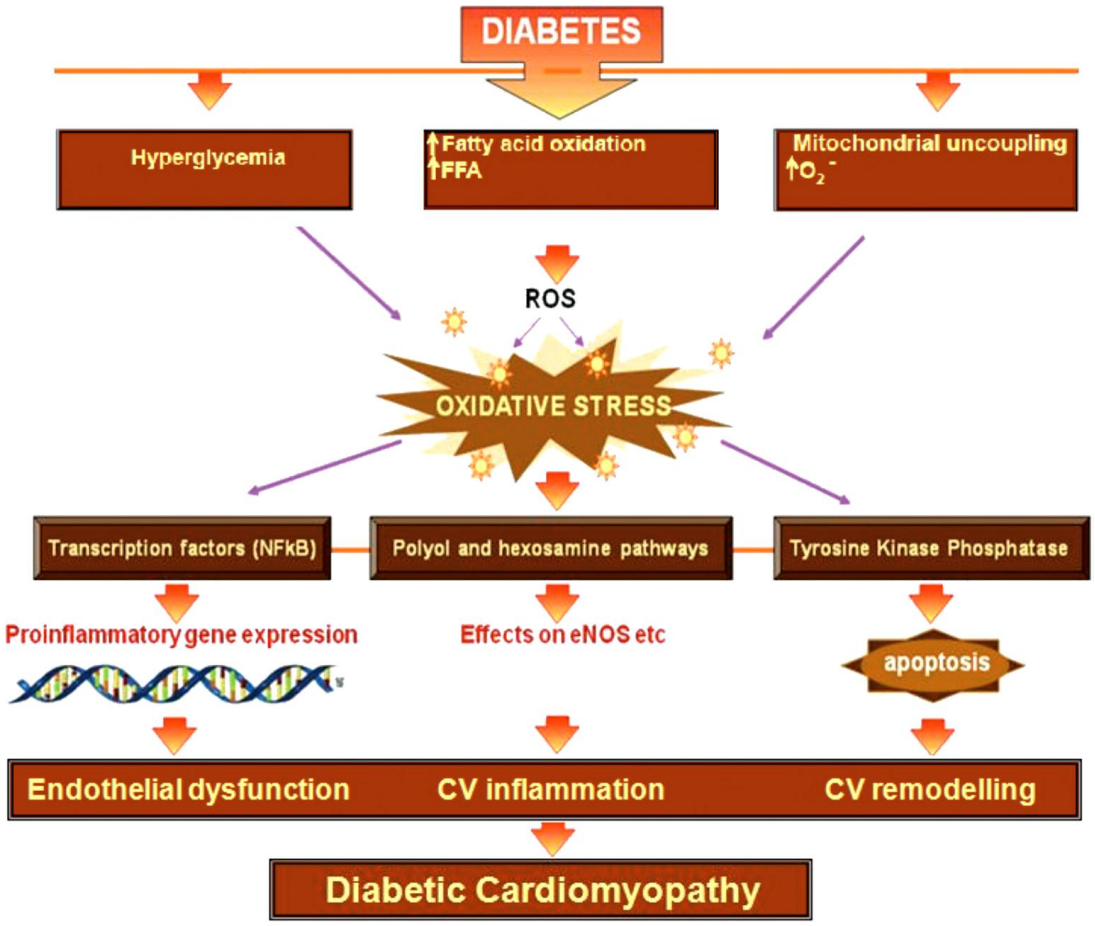

Figure.1.9. Oxidative stress in the development of diabetic cardiomyopathy (Khullar et al, Can. J. Physiol. Pharmacol. 2010; 88:233-240)

Mitochondria are the primary site of ROS production, and in the heart the cardiac myocytes, endothelial cells and neutrophils are the cellular sources of ROS generation. The mitochondria produce approximately 90% of basal cellular ROS in cardiomyocytes. The superoxide radicals are generated from ETC as an unprecedented by-product from complexes I and III. The ROS, when interfered with nitric oxide, advanced to the cellular damage by oxidation, modulation of intracellular signalling pathways, and induction of apoptosis (Liu et al. 2014). Activated NOX produce superoxide, which combines with NO form highly reactive and damaging peroxynitrite species, also stimulate oxidative stress. The oxidative stress activates matrix metalloproteinase and modulates signal transduction pathways involved in

cardiomyocyte hypertrophy and apoptosis, which together alter the morphology of the extracellular matrix (Takano et al. 2003).

1.3.6. Calcium homeostasis and diabetic cardiomyopathy

Calcium (Ca^{2+}) homeostasis is essential for the normal myocardium contraction and relaxation cycle. In diabetic patients, the abnormal Ca^{2+} handling and succeeding ventricular excitation-contraction coupling are the crucial contributors to cardiac dysfunction. The activation of the cardiac ryanodine calcium-sensitive receptor by the Ca^{2+} ions, entered through the L-type Ca^{2+} channels, induces the Ca^{2+} release from the sarcoplasmic reticulum (SR), which initiates the myocyte contraction. This sudden rise of intracellular free Ca^{2+} ion concentration results in the myocardial contraction by promoting the activation of myofilament and shortening of the myocytes. Any disruption of Ca^{2+} homeostasis can cause an increase in cytosolic Ca^{2+} due to leakage from the SR or increased cell membrane influx. This disruption activates, $[Ca^{2+}]i$ dependent protein calpain, which degrades intracellular proteins, cellular membranes, and nuclear DNA (Whitehead et al. 2006) thereby cause cell death.

The decreased activity of the sarco/endoplasmic reticulum Ca^{2+}-ATPase 2 (SERCA2a) and sodium (Na^{+})-Ca^{2+} exchanger (NCX) impaired ryanodine receptor (RyR2) function, and reduced phospholamban phosphorylation has been reported to be responsible for the dysfunctional Ca^{2+} handling in DCM (Belke et al. 2004; **Fig. 1.10**). These molecular abnormalities accord to the systolic and diastolic dysfunction associated with DM. In the diabetic heart, during the conditions of high $[Ca^{2+}]i$, the mitochondrial Ca^{2+} uptake is also found defected which weakens the Ca^{2+} buffering system. Also in DM patients, the sensitivity to Ca^{2+} ions in the mitochondrial permeability transition pore of myocardium increases, which induces the metabolic and oxidative stress, and the resulted cardiomyocytes autophagy and necrosis (Anderson et al. 2011). In the pathophysiological conditions like DCM, the mitochondrial Ca^{2+} uptake modulates the metabolism

of fatty acids, tricarboxylic acid cycle, OxPhos, and different apoptotic pathways through the Ca^{2+}- dependent proteins and enzymes participating in the pathways (Wang & Wei, 2017).

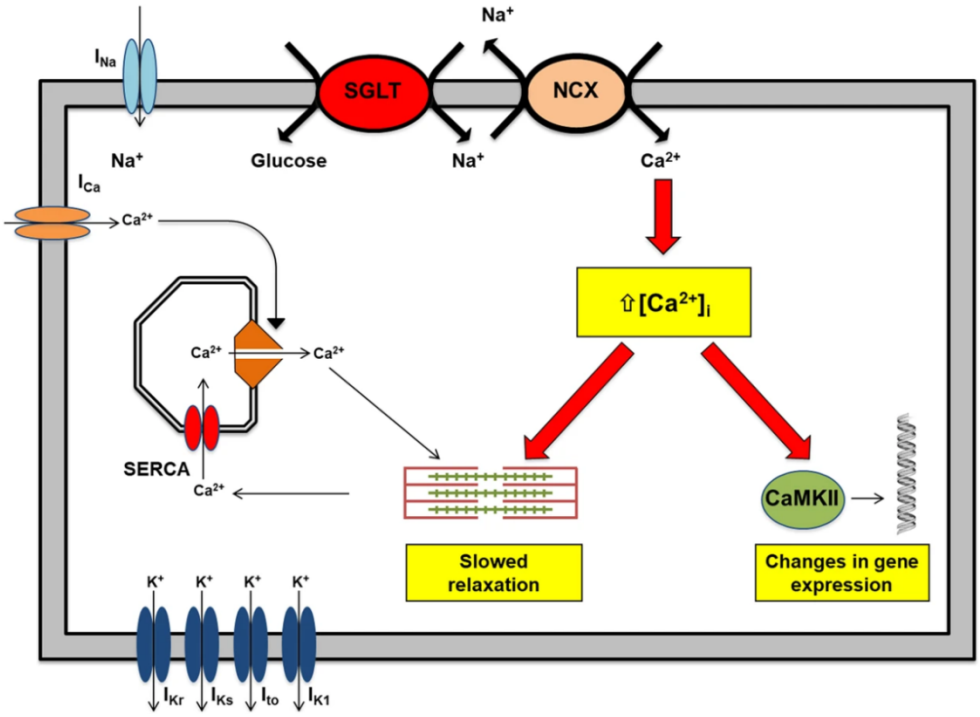

Figure.1.10. Calcium and diabetic cardiomyopathy (Ng et al, Sci. Rep. 2018; 8:14872)

The mitochondria couple cellular metabolic state by regulating Ca^{2+} levels through entire cellular Ca^{2+} signalling network. This is achieved through efficient communication between the ER and mitochondria via specialised structures between them known as mitochondria-associated ER membranes (MAMs) (Wang & Wei, 2017).

1.3.7. MAM and diabetic cardiomyopathy

The intracellular organelles, which are in close proximity, may form membrane contact sites, membranes are closely apposed and tethered through protein-protein or protein-lipid tether complexes; and exist in almost every type of subcellular organelle (**Fig. 1.11**). The shape and functions of the subcellular organelles were altered by exchanging their contents directly or indirectly through these contact sites, and appear to be essential for

maintaining fundamental cellular functions ranging from lipid metabolism to cell death (Lackner & Voelt, 2017).

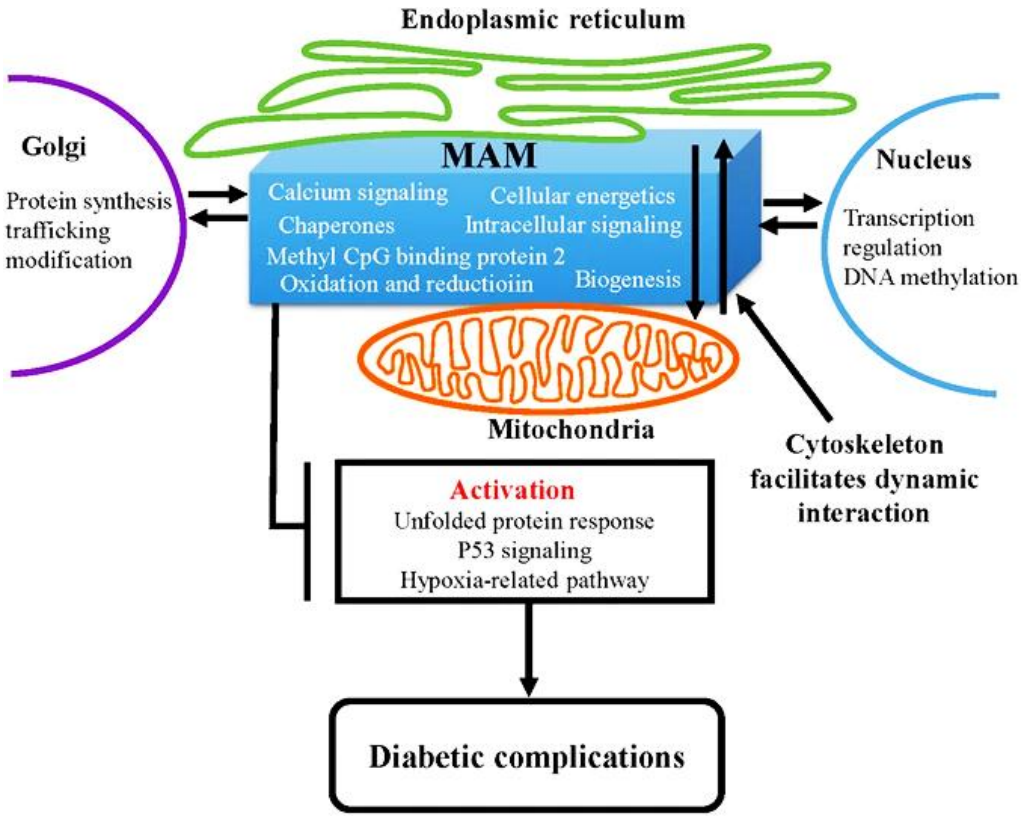

Figure.1.11. MAM and diabetic cardiomyopathy (Ma et al, Sci. Rep. 2017; 7:2062)

Since mitochondria and endoplasmic reticulum (ER) are the two organelles involved in the primary cellular functions; studies over the past few decades focus more on the interactions of both organelles. This lead to the demonstration of ER and mitochondrial physically connected junctions termed it as mitochondria-associated membranes (MAMs) with gap distances of 6 to 15 nm (Csordas et al. 2006). The MAMs fraction was first identified by Vance (1990), and membrane fragments from both the ER and outer mitochondrial membrane were identified in the isolated MAM fractions. The proteomics studies on the MAM fraction from human fibroblast and mouse brain (Poston et al. 2013) showed that more than 1000 “MAM proteins” reside in the fraction.

MAMs provides an excellent scaffold for crosstalk between the ER and mitochondria, also functions as a platform for many fundamental cellular functions, like metabolic shifts, lipid metabolism, Ca^{2+} ion homeostasis,

Functions	Proteins
Ca^{2+} transfer	Ip3r, Akt, Pp2a, Pml, Mfn2, Fundc1, RyR, Sig1R, p53, Pdzd8, Gsk3β, CypD
Lipid synthesis and transfer	Serac1, Facl1/4, acyl-CoA desaturase, Fatp4, Pemt2, Sig1R
Mitochondrial fission	Drp1, Fundc1, Rab7, Fis1
Autophagy	Fundc1
Intracellular trafficking	Miro
Unfolded protein response (UPR)	Grp75, Mfn2, Vapb, Bip, Calnexin, Calreticulin, ERp57/44, Sig1R
Inflammasome formation	Nlrp3, Asc, Txnip

Table. 1.3. Protein composition and functions of MAMs (Wu & Zou, Arch. Biochem. Biophys. 2019).

mitochondrial biogenesis, autophagy, apoptosis, and tumour growth (Missiroli et al. 2017) (**Table.1.3**). MAMs allow rapid exchange of biological molecules to maintain cellular health; therefore, MAMs act as a critical feature of cell destiny. So the alterations in the composition of MAMs and the abnormal induction of this lead to various disorders.

A key pathological factor in T2DM is that it induces MAM formation in the heart. Wu et al. (2017) reported that, during DM in the MAMs of cardiomyocytes, the outer mitochondrial membrane protein FUNDC1 and the SR protein IP3R2 were interacted to form a new protein bridge. MAM is thought to promote the mitochondrial Ca^{2+} signalling by local Ca^{2+} delivery from the ER to the mitochondrial matrix, induces a pathological Ca^{2+} overload in mitochondria which causes impairment in mitochondrial function, a vital contributor to heart failure.

MAMs play a predominant role in mitochondrial dynamics, especially the fission; it marks the division sites via the mitochondrial fission factor, and mitochondrial fission 1 protein (Fis1). Also, the FUNDC1 and MAMs actively participate in the development of heart failure evident with FUNDC1-MAMs formation was significantly suppressed in the patients with heart failure. The restoration of the proper function of MAMs should be an emerging target for treating heart failure (Wu et al. 2017). The FUNDC1 protein localised MAMs regulates Ca^{2+} concentrations in the cell and mitochondria through its control on the functions and levels of IP3R2. A decreased level of mitochondrial and intracellular Ca^{2+} was observed due to reduction of FUNDC1 in MAMs, which will guide the inhibition of the CREB/Fis1 pathway, mitochondrial elongation, impairment in mitochondrial function, and ensuing cardiac dysfunction (Wu et al. 2019).

Another protein of MAM, Grp75 forms a tripartite complex with IP3R and VDAC, involved in the regulation of energy metabolism, oxidative stress, and mitochondrial Ca^{2+} overload (Tubbs et al. 2014). The mitochondrial Ca^{2+} overload leads to opening the mPTP via its component proteins in MAMs and activates apoptosis and necrosis pathways. The MAMs' binding mechanisms also regulate the activity of the calcium loading mediated by SERCA, thus the local transfer of Ca^{2+} from the SR to mitochondria. The SERCA activity is decreased by the MAM enzyme glutathione peroxidase-8 and thus regulates the Ca^{2+} ion storage and mobility (Yoboue et al. 2017).

MAMs also take part in the early phase of autophagosome formation during autophagy. MAM alters the phenotype of vascular smooth muscle cells (VSMCs) in hypertension and atherosclerosis. A multifunctional sorting protein PACS-2 in MAM, in human VSMCs, is responsible for low-density lipoprotein (LDL) damage, mitophagy, integration of ER-mitochondria communication, ER homeostasis, and apoptosis (Moulis et al. 2017). Sig-1R regulates the production of reactive oxidants through the MAM (Natsvlishvili et al. 2015).

MAMs also have a specific role in the glucose homeostasis, as it is a hub of hormonal and nutrient signalling in insulin-sensitive tissues and glucose levels appears the principal regulator of MAM integrity during the nutritional transition (Theurey et al. 2016). The pentose phosphate-protein phosphatase 2A (PP2A) pathway activation during the hyperglycaemia alters the MAM integrity and function (Theurey et al. 2016). Since the significant proteins of insulin signalling like Akt, glycogen synthase kinase 3β (GSK3β), mammalian target of rapamycin complex 2 (mTORC2), phosphatase and tensin homolog (PTEN), and PP2A were located at MAM interface, its' alteration is associated with hepatic (Theurey et al. 2016) and skeletal muscle insulin resistance, and β-cell dysfunction in the pancreas of T2DM patients (Tubbs et al. 2018).

1.3.8. Apoptosis and diabetic cardiomyopathy

Apoptosis or programmed cell death is an active, precisely regulated, and energy-requiring process which is orchestrated by genetic programs. It plays a crucial role in normal tissue development and the regulation of proliferating cell populations in adult tissues. The prime reason underlying the pathogenesis and progression of various chronic diseases like atherosclerosis, endothelial dysfunction, ischemia-reperfusion, myocardial infarction, and cardiomyopathies is the myocardial cell death (Cai & Kang, 2003). The myocardial cell apoptosis and necrosis occurred in DM and played a significant role in the development of DCM. High blood sugar induced apoptosis through activating phosphoinositide- 3-kinase/protein kinase B (PI3K/Akt) signalling pathway, which was related to GSK-3β gene expression changes (Song et al. 2009).

There observed a significant increase in cardiomyocyte death at the early stage of T1DM mice induced by streptozotocin and cardiac specimens from T2DM patients. Also, cardiomyocyte apoptosis has been observed in humans following acute myocardial infarction. When compared with the remote regions of the myocardial infarction, the peri‑infarct border region

showed a high prevalence of cardiomyocyte apoptosis in the myocardium of chronic heart failure secondary to ischemic cardiomyopathy. In animal models of chronic heart failure produced by intracoronary microembolisation also showed similar effects (Stanley et al. 2005).

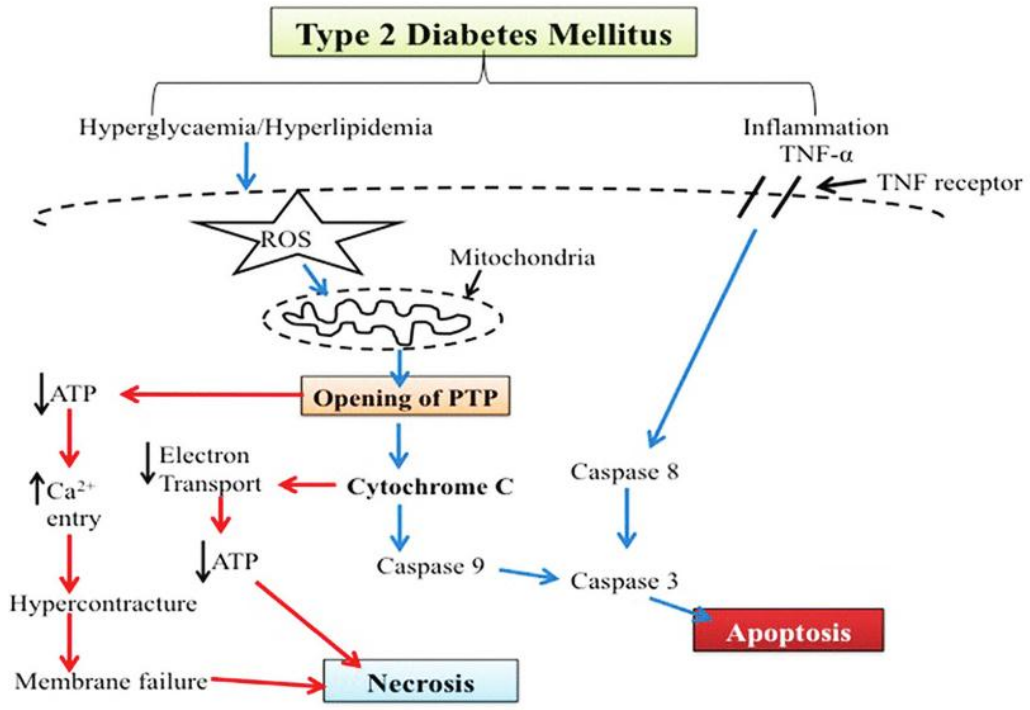

Figure.1.12. Apoptotic mechanisms in diabetic cardiomyopathy (Munasinghe & Katare, Int J Clin Exp Physiol 2016; 3:155-65)

Different pathologic and molecular factors trigger apoptosis in the myocardium. The pathological factors of cardiomyocyte apoptosis include the formation of ROS, exposure to hypoxia, excess levels of angiotensin-II, norepinephrine, and cytokines such as TNFα. There are a lot of molecular triggers involved in the apoptosis of cardiomyocytes (**Fig. 1.12**). The Bcl2 of the multigene family of Bcl-2-like proteins inhibits apoptosis whereas Bax promotes apoptosis, and acts as apoptosis regulators. The tumour suppressor p53 protein, involved in cell cycle arrest, also induces apoptosis in response to DNA damage.

Many studies showed caspases as one of the primary regulators of apoptosis. The apoptotic factor found induced in the infarct myocytes bordering is the caspase 3, but it is induced to a lesser extent in failing hearts due to DCM. In rats following myocardial ischemia and reperfusion, the apoptotic cardiomyocytes showed a co-localisation of caspase3 (Scarabelli et al. 2001). One of the critical pathways involved in the activation of caspases resulting in apoptosis and heart failure in ischemic rats is the release of cytochrome c and apoptosis-inducing factor from mitochondria. Also, the internucleosomal cleavage of DNA by Ca^{2+} and Mg^{2+} dependent endonucleases was found to be increased during apoptosis. The deoxyribonuclease I is found significantly increased in the myocardium of patients with heart failure (Mughal & Kirshenbaum, 2011).

1.4. Currently available medications

Despite all the available therapies, DCM carries an abysmal prognosis. There are no specific morphological changes, biochemical markers, or clinical manifestations for the diagnosis of DCM, and a definitive diagnosis is still challenging since the symptoms usually overlap with other complications of diabetes and also asymptomatic in the early stages. The use of non-invasive imaging technologies, such as echocardiography, magnetic resonance imaging (MRI), transmitral and tissue doppler imaging, provide detailed information about cardiac morphology and functions (Levelt et al. 2018).

The abnormalities in the initial passive transmitral inflow velocity (E) and medial mitral annulus velocity (e’) ratio, which are measured by Doppler imaging, correlate with the development of heart failure and increased mortality which is independent of other threat factors like hypertension and CAD (From et al. 2010). MRI can analyse the pathological alterations in the diastolic function, left ventricular mass, myocardial fibrosis, and steatosis. The myocardial metabolic abnormalities can be assessed with the positron emission tomography (PET). The DCM could be diagnosed at very early

stages using these new imaging techniques, but needed expertise to interpret the results (Palomer et al. 2018).

In the diagnosis or treatment of DCM patients, despite the growing interest in its pathophysiology, there are no specific guidelines for the diagnosis or formulating a treatment regimen in clinical practice. Still, the antihyperglycaemic drugs are crucial in the management of DCM by effectively reducing microvascular complications beyond their ability to control glycaemia, and several drugs used currently can improve cardiac health also. The blood glucose-lowering drugs like glucagon-like peptide 1 receptor agonists (GLP-1RAs) and sodium-glucose co-transporter 2 (SGLT2) inhibitors have been found to have a direct effect on myocardium and could be beneficial for the cardiovascular disorders (von Lewinski et al. 2017).

The GLP-1RAs such as lixisenatide, exenatide, liraglutide, and semaglutide showed potential cardioprotective effects. They attenuate cardiovascular risk factors like hypetglycaemia, obesity, high blood pressure, and dysfunctional lipid profile (**Table. 1.4**). In several animal models of ischemic heart disease, the GLP-1RAs treatment decreased the infarct size and improved cardiac function. In endothelial cells of diabetic rats, treatment with the GLP-1RAs drug exenatide reduced the glucose-induced ROS generation and apoptosis, and in the human endothelial cells, it stimulated proliferation and NO synthase activity (Ding & Zhang, 2012).

Class	Examples	Mechanism of Action
Fatty acid (FA) uptake inhibitors	Etomoxir	Irreversible inhibition of CPT1
	Perhexiline	Reversible inhibition of CPT1
Malonyl-CoA decarboxylase (MCD) inhibitors	CBM-301106	Allosteric inhibition of CPT1 by increasing malonyl-CoA
Mitochondrial β-oxidation partial inhibitors	Trimetazidine	Inhibition of 3-ketoacyl-CoA thiolase (3-KAT)
	Ranolazine	Inhibition of late sodium current, partial inhibition of FA oxidation

Pyruvate dehydrogenase kinase (PDK) inhibitors	Dichloroacetate	Inhibition of a negative regulator of glucose oxidation
Glucose–insulin–potassium (GIK)	GIK therapy	Increase glucose uptake, decrease circulating plasma free FA (FFA) levels
Nicotinic acid	Acipimox	Decrease circulating plasma FFA levels through reduction in lipoprotein lipase (LPL)
Glucagon-like peptide (GLP)–1agonists	Liraglutide	Increase insulin secretion, decrease glucagon release, delay gastric emptying
β-adrenoreceptor antagonists (β-blocker)	Carvedilol	Decrease circulating plasma FFAs, inhibit mitochondrial FA uptake

Table. 1.4. Compounds targeting fatty acid metabolism as a treatment for diabetic cardiomyopathy (Bayeva et al, J Am Heart Assoc. 2013; 2:e000433)

Also, the dipeptidyl peptidase-4 (DPP-4) inhibitors such as sitagliptin, alogliptin, saxagliptin, linagliptin increase myocardial glucose uptake, pave the way to the beneficial use of these compounds in the progression of DCM. In mouse models of insulin resistance and obesity, DPP-4 inhibitors attenuated the fibrosis and oxidative stress thus averted the diastolic cardiac dysfunction (Bostick et al. 2014). The DPP-4 inhibitors also improved ventricular remodelling, reduced the severity of HF, and increased the survival rate in various models of HF. Nevertheless, the therapeutic potential of different DPP-4 inhibitors in the DCM patients is not yet fully understood.

The SGLT2i such as empagliflozin and canagliflozin remarkably improved CV outcomes, including all causes of mortality in patients treated with these antidiabetic drugs. The glucose-lowering effect, weight loss, and blood pressure reduction, hemodynamic effects, direct vascular effects, osmotic diuresis, and natriuresis properties of SGLT2i may contribute to the CV effects.

The uses of modulators of oxidative stress are also recommended in case of HF in diabetic patients. Coenzyme Q_{10} (CoQ_{10}), a potent antioxidant has been explored the efficacy in reducing oxidative stress and pathological remodelling of the heart. The treatment with CoQ_{10} in DM patients resulted in

improved systolic and diastolic blood pressure, thus acting as a vasodilator (Chew et al. 2008). In T1 and T2DM mouse models, CoQ_{10} supplementation decreased the cardiac inflammation, fibrosis, and hypertrophy (Huynh et al. 2010). Thus the dietary compounds with antioxidant properties are proposed to be beneficial against the DCM.

1.5. Natural products and diabetic cardiomyopathy

The exact mechanisms behind the development and progression of DCM in humans are still partly understood. In order to understand DCM in details, both T1DM and T2DM *in vitro* and *in vivo* models have been used. Both the T1 and T2DM models show increased fatty acid utilisation, decreased glucose utilisation, and mitochondrial dysfunction, but slight differences also exist between the two phenotypes. Both T1 and T2DM models helped the understanding on DCM progression, even though there are differences in between the models. The natural products are utilised for the exploration of various mechanisms of development of DCM with different models for many years, and many of them are showing promising outcomes.

The new chemical entities from medicinal plants as well as the plant extracts were analysed in vitro and in vivo models with different doses and periods. Many of the natural products were found to be effective against DCM in different pathological alterations such as the increase in blood glucose, inflammation, hypertrophy, fibrosis, cardiac dysfunction, remodelling; and also in the molecular level alterations of AMPK, HO-1, GSK, and Glut2/4. Some of the natural products studied with different DCM models, and their effects are listed in **Table.1.5**.

Compound	DM model & dose	Effect
Sulforaphane	STZ-induced diabetic C57BL/6J mice with 0.5 mg/kg/d for 3 months	Decreased cardiac oxidative damage, inflammation, hypertrophy, fibrosis, and dysfunction.
	HFD/STZ-induced diabetic C57BL/6J mice with 0.5 mg/kg/d for 4 months	Upregulated cardiac LKB1/AMPK; decreased lipotoxicity, fibrosis, inflammation, and dysfunction.
	HFD/STZ-induced diabetic C57BL/6J WT and Nrf2 KO mice; 129 s WT and Mt KO mice with 0.5 mg/kg/d for 4 months	Increased cardiac MT, HO-1, NQO1, reduced oxidative damage, inflammation, fibrosis, hypertrophy, and dysfunction.
Curcumin	STZ-induced diabetic Wistar rats with 200 mg/kg/d for 6 weeks	Reduced myocardial capillary sclerosis.
	STZ-induced diabetic Wistar rats with 100 or 200 mg/kg/d for 16 weeks	Reduced AGE accumulation, cardiac fibrosis, myocardial dysfunction, upregulated Akt and GSK-3*β* phosphorylation.
	High glucose-treated neonatal rat cardiomyocyte with 10 μmol/L for 30 min	Reduced HG-induced oxidative stress and apoptosis.
	STZ-induced diabetic Sprague-Dawley rats with 100 mg/kg/d for 8 weeks	Reduced blood glucose, cardiac oxidative stress, cardiomyocyte hypertrophy, increased antioxidant activity, left ventricular dysfunction, lipid peroxidation, and myocardial fibrosis.
	STZ-induced diabetic rats with 20 mg/kg/d for 45 days	Reduced expression of ANP, MEF2A, MEF2C, and P300; and increased left ventricular function.
Icariin	STZ-induced diabetic Sprague-Dawley rats with 30 or 120 ml/kg/d for 8 weeks	Reduced myocardial collagen deposition, ventricular hypertrophy, body weight loss, and increased cardiac function.
Flos puerariae	STZ-induced diabetic C57BL/6J mice with100 or 200 mg/kg/d for 10 weeks	Reduced cardiac remodelling and apoptotic cardiac cell death.

Betanin	High fructose feed-induced diabetic Sprague-Dawley rats with 25 or 100 mg/kg/d for 60 days	Reduced cardiac fibrosis, TGF-β1 and CTGF.
Chrysin	STZ-induced diabetic Wistar rats with 60 mg/kg for 28 days	Increased cardiac CAT, MnSOD, GSH; and reduced AGEs/RAGE, apoptosis and cardiac dysfunction.
Aralia taibaiensis	High glucose-treated H9c2 cells with 25, 50, or 75 μg/ml	Decreased apoptosis, ROS, and oxidative damage.
Magnolia plant extract	High-fat diet-induced obese C57BL/6 mice with BL153 at 5 or 10 mg/kg/d, for 24 weeks	Reduced cardiac lipid accumulation, inflammation, oxidative stress, and apoptosis
	High-fat diet-induced obese C57BL/6 mice with 4-O-methylhonokiol with 0.5 or 1.0 mg/kg/d for 24 weeks	Reduced cardiac oxidative stress, lipid accumulation, hypertrophy, and dysfunction
Abroma augusta L. leaf	STZ/nicotinamide-induced type 2 diabetic rats with 100 or 200 mg/kg/d for 4 weeks	Reduced hyperglycaemia, hyperlipidaemia, membrane disintegration, cardiac oxidative stress and oxidative stress-induced cell death
Aegle marmelos leaf extract	Alloxan-induced diabetic rats with 200 mg/kg/d for14 days	Reduced cardiac necrosis and inflammation
Dendrobium officinale extract	STZ-induced Kunming diabetic mice with 300 mg/kg/d for 8 weeks	Reduced cardiac MDA, lipid accumulation, and the expression of inflammatory and fibrotic factors
Fermented *rooibos* extract	H2O2-treated cardiomyocytes isolated from the hearts of STZ-induced rats with 1 or 10 μg/ml for 6 hours	Reduced ROS generation and apoptosis
Ficus racemosa stem bark extract	STZ-induced diabetic Wistar rats with 200 or 400 mg/kg/d for 8 weeks	Reduced cardiac MDA

Ginkgo biloba	STZ-induced diabetic rats with 100 mg/kg/d, for 3 months	Increased creatine kinase activity; reduction of myofibril loss, and myocyte diameter
Kalpaamruthaa	HFD/STZ-induced diabetic Sprague- Dawley rats with 200 mg/kg/d for 28 days	Reduced blood glucose, cardiac lipid peroxides, cardiac lipid accumulation, cardiac remodelling, chromatin condensation and marginalisation, insulin resistance, matrix metalloproteinase-2 and 9, and carbonyl content, proinflammatory cytokines; increased hepatic antioxidants and pancreatic antioxidants
North American ginseng	STZ-induced diabetic C57BL/6J type 1 diabetic mice or db/db type 2 diabetic mice with 200 mg/kg/d for 2 or 4 months	Decreased cardiac extracellular matrix proteins and vasoactive factors, hypertrophy, and dysfunction
Pongamia pinnata	STZ/nicotinamide-induced type 2 diabetic rats with100 mg/kg/d for 4 months	Increased cardiac SOD and GSH; reduced MDA, remodelling, dysfunction, biomarkers for cardiac injury, and blood glucose
Syzygium cumini	High glucose-treated H9c2 cells with 9 µg/ml for 48 h	Reduced hypertrophy and accumulation of extracellular matrix

Table.1.5. Effect of natural products on various diabetic cardiomyopathy models (Yan et al., J. Diab. Res. 2017).

1.6. Ferulic acid

Since dietary factors play a crucial role in the development and prevention of human diseases, including diabetes and cardiovascular diseases, we have selected ferulic acid (FA) for evaluation of its potential against DCM. FA, an edible mono phenolic phytochemical, is a dominant constituent of medicinal herbs like *Cimicifuga racemosa*, *Angelica sinensis*, and *Ligusticum chuanxiong* (Ou & Kwok, 2004). It is also habitually seen in

commelinid plants like oats, pineapple, rice and wheat; and also in artichoke, beans, coffee, fruits, grains, peanut, and in vegetables.

The phenolic acid FA is present abundantly in most of the plants, and its amount varies from species to species, estimated at 5 to 50g/kg in the cereals. FA was found either in free form or covalently linked to biopolymers like lignin in the seeds and leaves. In the cell walls, FA is commonly seen in the form of cross-linked esters with polysaccharides like arabinoxylans (grasses), pectin (spinach and sugar beet), and xyloglucans (bamboo). The phenolic nucleus and the extended side chain of the FA aided the conjugation with carbohydrates and proteins. The potent antioxidant potential is accomplished with its ability to the rapid formation of resonance stabilized phenoxy radical.

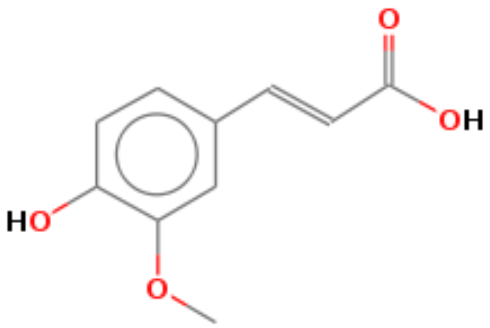

Figure.1.13. Ferulic acid or trans-Ferulic acid: A trans-cinnamic acid with the phenyl ring having methoxy and hydroxy substituents in the 3rd and 4th positions respectively ($C_{10}H_{10}O_4$; Molecular weight - 194.18 g/mol).

FA has been widely utilised for UV induced skin damage, Alzheimer's disease, blood pressure, cardiovascular disorders, cancer, diabetes, ischemic diseases, kidney disorders, and pulmonary disorders (Alam, 2019). It also has strong anti-inflammatory and antiapoptotic properties and reduces gluconeogenesis (Narasimhan et al. 2015). In order to reduce the oxidative damage induced disorders, a nutritional approach could be appraised with curcumin and ferulic acid as food supplementation. Trans-ferulic acid can be absorbed by the small intestine and excreted through the urine. All these qualities make it an attractive phytochemical for bioevaluation against DCM,

and it has not been evaluated so far against myocardial protection during diabetes.

1.7. Hypothesis and Objectives

The prevalence of DM and the increased lethality due to the DCM need active research for the identification of the exact mechanism underlying this metabolic syndrome associated with cardiac complications and also to develop novel biomarkers for it. There exists a gap in research on diabetes and associated complications such as DCM, which remains incurable due to the unknown mechanisms of its origin, and absence of proper treatments. The importance of mitochondria in the general function of the heart is well established. However, the detailed studies on various aspects of mitochondria during the DCM are missing in the literature. From the functional point, mitochondria are expected to be involved in the genesis of DCM. Based on this hypothesis, detailed investigations are planned on mitochondria and associated cellular structure such as MAMs in this thesis. Besides, to find suitable bioactive from natural resources against DCM, ferulic acid was selected based on preliminary results.

In order to evaluate the pathophysiological mechanisms of the DCM emphasising the importance of mitochondria, the present study aims to

- evaluate the alterations in innate antioxidant status in H9c2 cells during hyperglycaemia and possible attenuation by FA
- analyse the functional alterations in mitochondria during hyperglycaemia and possible amelioration by FA in H9c2 cells
- analyse the alterations in bioenergetics during hyperglycaemia and possible modulation by FA in H9c2 cells
- analyse the role of MAMs in the mitochondrial function, Ca^{2+} homeostasis and cardiomyocyte death during hyperglycaemia and the effect of FA
- evaluate the alterations in heart biochemistry and function for the biomarker identification in DCM and possible beneficial role of FA

References

1. Alam MA, 2019. Anti-hypertensive effect of cereal antioxidant ferulic acid and its mechanism of action, Front. Nutr. 6:121.
2. Albakri A, 2018. Diabetic cardiomyopathy: a review of literature on clinical status and meta-analysis of tissue doppler diagnostic method and the clinical value of intensive glycemic control. Med. Clin. Arch. 2(4):1-12.
3. American Diabetes Association, 2013. Standards of medical care in diabetes -2013. Diabetes Care. 36:S11-S66.
4. Anderson EJ, Kypson AP, Rodriguez E, et al. 2009. Substrate-specific derangements in mitochondrial metabolism and redox balance in the atrium of the type 2 diabetic human heart. J. Am. Coll. Cardiol. 54:1891-1898.
5. Anderson EJ, Rodriguez E, Anderson CA, et al. 2011. Increased propensity for cell death in diabetic human heart is mediated by mitochondrial-dependent pathways. Am. J. Physiol. Heart. Circ. Physiol. 300:H118–H124.
6. Bando YK, Murohara T, 2014. Diabetes-related heart failure. Circ. J. 78:576-583.
7. Bayeva M, Sawicki KT, Ardehali H, 2013. Taking diabetes to heart--deregulation of myocardial lipid metabolism in diabetic cardiomyopathy. J. Am. Heart Assoc. 2(6):e000433
8. Belke DD, Swanson EA, Dillmann WH, 2004. Decreased sarcoplasmic reticulum activity and contractility in diabetic *db/db* mouse heart. Diabetes Metab. Res. Rev. 53:3201-3208.
9. Boden-Albala B, Cammack S, Chong J, et al. 2008. Diabetes, fasting glucose levels, and risk of ischemic stroke and vascular events: Findings from the Northern Manhattan Study (NOMAS). Diabetes Care. 31:1132-1137.
10. Bostick B, Habibi J, Ma L, 2014. Dipeptidyl peptidase inhibition prevents diastolic dysfunction and reduces myocardial fibrosis in a mouse model of Western diet induced obesity. Metabolism. 63(8):1000-1011.

11. Bugger H, Abel ED, 2014. Molecular mechanisms of diabetic cardiomyopathy. Diabetologia. 57(4):660-671.
12. Cai L, Kang YJ, 2003. Cell death and diabetic cardiomyopathy. Cardiovasc. Toxicol. 3(3):219-228.
13. Chew GT, Watts GF, Davis TM, 2008. Hemodynamic effects of fenofibrate and coenzyme Q10 in type 2 diabetic subjects with left ventricular diastolic dysfunction. Diabetes Care. 31(8):1502-1509.
14. Csordas G, Renken C, Varnai P, et al., 2006, Structural and functional features and significance of the physical linkage between ER and mitochondria, J. Cell Biol. 174(7):915-921.
15. Ding L, Zhang J, 2012. Glucagon-like peptide-1 activates endothelial nitric oxide synthase in human umbilical vein endothelial cells. Acta Pharmacol. Sin. 33:75-81.
16. Esteve E, Ricart W, Fernandez-Real JM, 2011. Gut microbiota interactions with obesity, insulin resistance and type 2 diabetes: did gut microbiote co‐evolve with insulin resistance? Curr. Opin. Clin. Nutr. Metab. Care 14:483-490.
17. Finck BN, Lehman JJ, Leone TC, et al. 2002. The cardiac phenotype induced by PPARalpha overexpression mimics that caused by diabetes mellitus. J. Clin. Invest. 109(1):121-130.
18. From AM, Scott CG, Chen HH, 2010. The development of heart failure in patients with diabetes mellitus and pre-clinical diastolic dysfunction a population-based study. J. Am. Coll. Cardiol. 55(4):300-5.
19. https://www.healthline.com/health/diabetes/effects-on-body#1
20. Huynh K, Mcmullen JR, Julius TL, et al. 2010. Cardiac-specific IGF-1 receptor transgenic expression protects against cardiac fibrosis and diastolic dysfunction in a mouse model of diabetic cardiomyopathy. Diabetes. 59:1512-1520.
21. International Diabetes Federation, 2020. IDF Diabetes Atlas. 9th ed, Brussels, Belgium.

22. Jia G, DeMarco VG, Sowers JR, 2016. Insulin resistance and hyperinsulinaemia in diabetic cardiomyopathy. Nat. Rev. Endocrinol. 12(3):144-153.
23. Jia G, Hill MA, Sowers JR, 2018. Diabetic cardiomyopathy: an update of mechanisms contributing to this clinical entity. Circ. Res. 122:624-638.
24. Jin W, Patti ME, 2009. Genetic determinants and molecular pathways in the pathogenesis of type 2 diabetes. Clin. Sci. 116:99-111.
25. Kayama Y, Raaz U, Jagger A, et al. 2015. Diabetic cardiovascular disease induced by oxidative stress. Int. J. Mol. Sci. 16(10):25234-25263.
26. Khullar M, Al-Shudiefat AA, Ludke A, Binepal G, Singal PK, 2010. Oxidative stress: a key contributor to diabetic cardiomyopathy. Can. J. Physiol. Pharmacol. 88(3):233-240.
27. Lackner LL, Voeltz GK, 2017. The mechanisms and functions of inter organelle interactions. Mol. Biol. Cell. 28(6):703-704.
28. Lee MMY, McMurray JJV, Lorenzo-Almorós A, et al. 2019. Diabetic cardiomyopathy. Heart. 105(4):337-345.
29. Levelt E, Gulsin G, Neubauer S, McCann GP, 2018. Mechanisms in Endocrinology- Diabetic cardiomyopathy: pathophysiology and potential metabolic interventions state of the art review. Eur. J. Endocrinol. 178(4):R127-R139.
30. Levitzky YS, Pencina MJ, D'Agostino RB, et al., 2008. Impact of impaired fasting glucose on cardiovascular disease: the Framingham Heart Study. J. Am. Coll. Cardiol.51:264-270.
31. Li S, Shin HJ, Ding EL, van Dam RM, 2009. Adiponectin levels and risk of type 2 diabetes: a systematic review and meta-analysis. JAMA. 302:179-188.
32. Liu Q, Wang S, Cai L, 2014. Diabetic cardiomyopathy and its mechanisms: Role of oxidative stress and damage. J. Diabetes Invest. 5(6):623-634.
33. Ma JH, Shen S, Wang JJ, et al. 2017. Comparative proteomic analysis of the mitochondria-associated ER membrane (MAM) in a long-term type 2 diabetic rodent model. Sci Rep. 7(1):2062

34. Melendez-Ramirez LY, Richards RJ, Cefalu WT, 2010. Complications of type 1 diabetes. Endocrinol. Metab. Clin. North Am. 39:625-40.
35. Missiroli S, Danese A, Iannitti T, et al., 2017. Endoplasmic reticulum-mitochondria Ca^{2+} crosstalk in the control of the tumor cell fate. Biochim. Biophys. Acta. Mol. Cell Res. 1864(6):858-864.
36. Moulis M, Grousset E, Faccini J, et al. 2019. The multifunctional sorting protein PACS-2 controls mitophagosome formation in human vascular smooth muscle cells through mitochondria-ER contact sites. Cells. 8(6):638.
37. Mughal W, Kirshenbaum LA, 2011. Cell death signalling mechanisms in heart failure. Exp. Clin. Cardiol. 16(4):102-108.
38. Munasinghe PE , Katare R, 2016. Maladaptive autophagy in diabetic heart disease. Int. J. Clin. Exp. Physiol. 3:155-65
39. Muralidaran Y, Viswanathan P, 2015. Diabetic cardiomyopathy: A new perspective of mechanistic approach, J. Diabetes Metab. 6:605.
40. Narasimhan A, Chinnaiyan M, Karundevi B, 2015. Ferulic acid exerts its antidiabetic effect by modulating insulin-signalling molecules in the liver of high-fat diet and fructose-induced type-2 diabetic adult male rat. Appl. Physiol. Nutr. Metab. 40:769-781.
41. Natsvlishvili N, Goguadze N, Zhuravliova E, Mikeladze D, 2015. Sigma-1 receptor directly interacts with Rac1-GTPase in the brain mitochondria. BMC Biochem. 16:11.
42. Ng KM, Lau YM, Dhandhania V, et al. 2018. Empagliflozin ammeliorates high glucose induced-cardiac dysfuntion in human iPSC-derived cardiomyocytes. Sci Rep. 8(1):14872
43. Ou S, Kwok KC, 2004. Ferulic acid: pharmaceutical functions, preparation and applications in foods, J. Sci. Food. Agric. 84:1261-1269.
44. Palomer X, Pizarro-Delgado J, Vazquez-Carrera M, 2018. Emerging actors in diabetic cardiomyopathy: Heartbreaker biomarkers or therapeutic targets? Trends Pharmacol. Sci. 39(5):452-467.

45. Parsanathan R, Jain SK, 2020. Novel invasive and noninvasive cardiac-specific biomarkers in Oobesity and cardiovascular diseases. Metab. Syndr. Relat. Disord. 18(1):10-30.
46. Plows JF, Stanley JL, Baker PN, Reynolds CM, Vickers MH, 2018. The pathophysiology of gestational diabetes mellitus. Int. J. Mole. Sci. 19(11):3342.
47. Poston CN, Krishnan SC, Bazemore-Walker CR, 2013. In-depth proteomic analysis of mammalian mitochondria-associated membranes (MAM). J. Proteomics 79:219-230.
48. Randle PJ, Garland PB, Hales CN, Newsholme EA, 1963. The glucose fatty-acid cycle. Its role in insulin sensitivity and the metabolic disturbances of diabetes mellitus. Lancet. 1(7285):785-789.
49. Rubler S, Dlugash J, Yuceoglu YZ, Kumral T, 1972. New type of cardiomyopathy associated with diabetic glomerulosclerosis. Am. J. Cardiol. 30:595-602.
50. Ryan EA, Paty BW, Senior PA, et al. 2005. Five-year follow-up after clinical islet transplantation. Diabetes. 54:2060-2069.
51. Scarabelli T, Stephanou A, Rayment N, et al. 2001. Apoptosis of endothelial cells precedes myocyte cell apoptosis in ischemia/reperfusion injury. Circulation. 104(3):253-256.
52. Schannwell CM, Schneppenheim M, Perings S, et al. 2002. Left ventricular diastolic dysfunction as an early manifestation of diabetic cardiomyopathy. Cardiology. 98:33-39.
53. Shen X, Zheng S, Metreveli NS, Epstein PN, 2006. Protection of cardiac mitochondria by overexpression of MnSOD reduces diabetic cardiomyopathy. Diabetes. 55:798-805.
54. Song JQ, Teng X, Cai Y, Tang CS, Qi YF, 2009. Activation of Akt/GSK-3beta signaling pathway is involved in intermedin(1-53) protection against myocardial apoptosis induced by ischemia/reperfusion. Apoptosis. 14(9):1061-1069.

55. Stanley WC, Fabio A. Recchia, Lopaschukl GD, 2005. Myocardial substrate metabolism in the normal and failing heart. Physiol. Rev. 85:1093-1129.
56. Takano H, Zou Y, Hasegawa H, et al. 2003. Oxidative stress-induced signal transduction pathways in cardiac myocytes: involvement of ROS in heart diseases. Antioxid. Redox. Signal. 5:789-794.
57. Teshima Y, Takahashi N, Nishio S, Saito S, Kondo H, 2014. Production of reactive oxygen species in the diabetic heart. Roles of mitochondria and NADPH oxidase. Circ. J. 78:300-306.
58. Theurey P, Tubbs E, Vial G, et al. 2016. Mitochondria-associated endoplasmic reticulum membranes allow adaptation of mitochondrial metabolism to glucose availability in the liver. J Mol Cell Biol. 8(2):129-143.
59. Tripathi BK, Srivastava AK, 2006. Diabetes mellitus: complications and therapeutics. Med. Sci. Monit. 12(7):RA130-147.
60. Tubbs E, Chanon S, Robert M, et al. 2018. Disruption of mitochondria-associated endoplasmic reticulum membrane (MAM) integrity contributes to muscle insulin resistance in mice and humans. Diabetes. 67(4):636-650.
61. Tubbs E, Theurey P, Vial G, et al. 2014. Mitochondria-associated endoplasmic reticulum membrane (MAM) integrity is required for insulin signaling and is implicated in hepatic insulin resistance. Diabetes. 63:3279-3294.
62. Tun NN, Arunagirinathan G, Munshi SK, Pappachan JM, 2017. Diabetes mellitus and stroke: A clinical update. World J. Diabetes. 8(6):235-248.
63. Tuomi T, 2005. Type 1 and type 2 diabetes: what do they have in common? Diabetes. 54(S2):S40-45.
64. van Heerebeek L, Hamdani N, Handoko ML, et al. 2008. Diastolic stiffness of the failing diabetic heart: importance of fibrosis, advanced glycation end products, and myocyte resting tension. Circulation. 117(1):43-51.

65. Vance JE, 1990. Phospholipid synthesis in a membrane fraction associated with mitochondria. J. Biol. Chem. 265:7248-7256.
66. Vasquez-Trincado C, Garcia-Carvajal I, Pennanen C, et al. 2016. Mitochondrial dynamics, mitophagy and cardiovascular disease. J. Physiol. 594(3):509-525.
67. von Lewinski D, Kolesnik E, Wallner M, Resl M, Sourij H, 2017. New anti-hyperglycemic drugs and heart failure: Synopsis of basic and clinical data. Biomed. Res. Int. 2017:1253425.
68. Wang CH, Wei YH, 2017. Role of mitochondrial dysfunction and dysregulation of Ca^{2+} homeostasis in the pathophysiology of insulin resistance and type 2 diabetes. J. Biomed. Sci. 24(1):70.
69. Wang X, Bao W, Liu J, et al., 2013. Inflammatory markers and risk of type 2 diabetes: a systematic review and meta‐analysis. Diabetes Care. 36:166-175.
70. Whitehead NP, Yeung EW, Allen DG, 2006. Muscle damage in mdx (dystrophic) mice: Role of calcium and reactive oxygen species. Clin. Exp. Pharmacol. Physiol. 33:657-662.
71. World Health Organization: Cardiovascular disease. https://www.who.int/health-topics/cardiovascular-diseases#tab=tab1/2020
72. Wu S, Lu Q, Ding Y, et al. 2019. Hyperglycaemia-driven inhibition of AMP-activated protein kinase α2 induces diabetic cardiomyopathy by promoting mitochondria-associated endoplasmic reticulum membranes in vivo. Circulation. 139(16):1913-1936.
73. Wu S, Lu Q, Wang Q, et al, 2017. Binding of FUN14 domain containing 1 with inositol 1,4,5-Trisphosphate receptor in mitochondria-associated endoplasmic reticulum membranes maintains mitochondrial dynamics and function in hearts in vivo. Circulation. 136:2248-2266.
74. Wu S, Zou MH, 2019. Mitochondria-associated endoplasmic reticulum membranes in the heart. Arch. Biochem. Biophys. 662:201-212.
75. Yagyu H, Chen G, Yokoyama M, et al. 2003. Lipoprotein lipase (LpL) on the surface of cardiomyocytes increases lipid uptake and produces a cardiomyopathy. J. Clin. Invest. 111(3):419-426.

76. Yan B, Ren J, Zhang Q, et al. 2017. Antioxidative effects of natural products on diabetic cardiomyopathy. J. Diabetes Res. 2017:2070178.
77. Yancy CW, Jessup M, Bozkurt B, et al. 2013. 2013 ACCF/AHA guideline for the management of heart failure: a report of the American College of Cardiology Foundation/American Heart Association Task Force on Practice Guidelines. J. Am. Coll. Cardiol. 62(16):e147-e239.
78. Yoboue ED, Rimessi A, Anelli T, Pinton P, Sitia R, 2017. Regulation of calcium fluxes by GPX8, a type-II transmembrane peroxidase enriched at the mitochondria-associated endoplasmic reticulum membrane, Antioxid. Redox Signal. 27: 583-595.
79. Young ME, McNulty P, Taegtmeyer H, 2002. Adaptation and maladaptation of the heart in diabetes: Part II: potential mechanisms. Circulation. 105:1861-1870.

Chapter 2

Hyperglycaemia induces oxidative stress in H9c2 rat cardiomyocyte and the possible beneficial effect of ferulic acid

2.1. Introduction

One of the most common metabolic disorders, experienced in the human population is the diabetes mellitus (DM). The existence of hyperglycaemia for an extend period may impart damages through different modes of action on different vital organs such as the heart, and kidney. (Miki et al. 2013). Cardiovascular disorders like coronary heart disease, hypertension, and DCM are the principal complications of DM induced morbidity and mortality. Among this, the DCM is the major complication and accounts for nearly 80% of the mortality due to DM (Hayat et al. 2004). The DCM has reported being the result of an enduring process in the myocardium before the diagnosis of DM, in which the myocardium has been affected at a very early stage via the changes in the metabolism (Marcinkiewicz et al. 2017).

Oxidative stress and multiple associated complications are primarily responsible for the development of DCM (Kayama et al. 2015). Oxidative stress causes direct and indirect harmful effects in the heart. The oxidative stress occurred due to excess of ROS formation. It can cause damage to proteins, lipids, and DNAs in cardiomyocytes, once it is not being balanced or removed by the endogenous antioxidant enzymes and molecules or by the action of exogenous antioxidant molecules (Kayama et al. 2015). The increased formation of AGEs and expression of AGE receptors, activation of protein kinase C and pathological pathways such as polyol and hexosamine pathways are reported to be the result of hyperglycaemia induced oxidative stress and increased mitochondrial superoxide production in DM patients (Giacco & Brownlee, 2010). In the diabetic heart, these deleterious effects in due course lead to cardiac remodelling and dysfunction.

The existence of a crosstalk between redox status and calcium (Ca^{2+}) homeostasis in the cells has been well established. Literature reveals that DM alters Ca^{2+} homeostasis (Kumar et al. 2012). The facilitated Ca^{2+}

homeostasis suggested as a potential choice for the treatment of DCM (Huang et al. 2018). There are some reports available on mechanisms underlying HG-induced intracellular calcium ([Ca^{2+}]i) overload in H9c2 cells. Kumar et al. (2012) reported that HG treated H9c2 cells showed increased [Ca^{2+}]i with a concomitant increase in intra-mitochondrial calcium ([Ca^{2+}]m) which resulted in enhanced reactive oxygen species (ROS) generation, mitochondrial dysfunction and apoptosis.

In recent years, extensive investigations have been conducted on the antioxidant effect of natural products on the attenuation of DCM, and many of them showed promising outcomes (Singh et al. 2013). Reports showed that natural products such as sulforaphane, curcumin, icariin, betanin, chrysin, were found useful in the prevention of diabetes-induced cardiac oxidative damage, inflammation, hypertrophy, fibrosis, myocardial capillary sclerosis, apoptosis, extracellular protein accumulation, preserve left ventricular function and dysfunction, through a different mechanism such as activation of Nrf2 signalling, PPAR-*γ* activation, upregulation of CAT, MnSOD, and GSH; inhibition of AGE/RAGE signalling (Bai et al. 2013; Han et al. 2015; Rani et al. 2016).

The present study uses ferulic acid (FA), an edible mono phenolic phytochemical first isolated from the medicinal plant *Ferula asafoetida*. FA is an principal component of many medicinal herbs and also commonly found fruits, leaves, seeds, cereals, pulses, coffee, and artichoke (Ou & Kwok, 2004). FA is known for its potent antioxidant property, and it has been widely utilised for UV induced skin damage, ageing, Alzheimer's disease, blood pressure, cardiovascular disorders, cancer, diabetes, ischemic diseases, kidney disorders, and pulmonary disorders (Alam, 2019; Sahu et al. 2019). It also has strong anti-inflammatory and antiapoptotic properties and reduces gluconeogenesis (Narasimhan et al. 2015). However, the precise role of FA and the details of the underlying mechanism of HG-induced DCM remain unclear. All these qualities make it an attractive phytochemical for bioevaluation against DCM. In the present study, H9c2 cardiomyoblast cells

have been used as a model system for in vitro experiments. H9c2 cells exhibit most of the biochemical, electrophysiological and pharmacological characteristic features of adult cardiac myocytes. So this has been widely preferred for heart-related *in vitro* experiments (Wu & Zou, 2018; Bock &Tait, 2020).

2.2. Materials and methods

2.2.1. Chemicals and reagents

Ferulic acid, metformin hydrochloride, D-glucose, mannitol, 2',7'-dichlorofluorescin diacetate (DCFDA), 1-(4,5-Dimethylthiazol -2-yl)-3,5-diphenyl formazan (MTT), dimethyl sulfoxide (DMSO), Krebs-Ringer bicarbonate buffer (KRB), radioimmunoprecipitation assay (RIPA) buffer and protease inhibitor cocktail were purchased from Sigma-Aldrich, USA. Dulbecco's Modified Eagle's Medium (DMEM), foetal bovine serum (FBS), Hank's Balanced Salt Solution (HBSS), penicillin-streptomycin solution and trypsin-EDTA solution were from GIBCO®, Life Technologies, USA. Fura-2 AM was purchased from Invitrogen™, Fisher Scientific, USA. Primary and secondary western blot antibodies were purchased from Cell Signalling Technology, USA. All other solvents and reagents used were of analytical grade unless/otherwise mentioned.

2.2.2. Cell culture and induction of hyperglycaemia

H9c2 cardiomyoblast cells (American Type Culture Collection, CRL-1446; Rockville, MD, USA) were maintained in DMEM supplemented with 10% FBS, 1% penicillin-streptomycin solution and incubated at 5% CO_2 and 37°C in a humidified incubator (Eppendorf, USA). The hyperglycaemia was induced according to the previous protocol (Cai et al. 2002). Briefly, when the cell populations reached 50-60 % confluence, the cultures were exposed to d-glucose in a final concentration of 33 mM in cultures for treatment with high glucose (HG) for 48 h, and the one maintained in 5.5 mM d-glucose (NG) as control. An osmotic control group with 27.5 mM mannitol and 5.5 mM d-

glucose was also run in the preliminary screening to rule out the osmotic effect.

Experimental groups:

C - Control (5.5 mM d-glucose)

HG - High glucose (33 mM d-glucose)

HGF1 - High glucose + FA (10 µM)

HGF2 - High glucose + FA (25 µM)

HGM - High glucose + metformin (Met -10 µM)

CF - Control + FA (25 µM)

OC - Control + mannitol (27.5 mM)

The FA and Met were co-treated with the HG for 48 h in the experimental groups.

2.2.3. Estimation of atrial natriuretic peptide (ANP) and brain natriuretic peptide (BNP)

The level of ANP in the medium was estimated by a competitive ELISA method using the Rat ANP ELISA kit (Elabscience®, Texas, USA). The ANP in the sample (cell culture medium) competes with a fixed amount of ANP on the solid phase supporter for sites on the biotinylated detection antibody specific to ANP. Then it was incubated with avidin conjugated to horseradish peroxidase (HRP) and a TMB substrate solution. The enzyme-substrate reaction was terminated by the addition of stop solution, and the colour change was measured spectrophotometrically at a wavelength of 450 nm. The concentrations of ANP were determined from the standard curve, and the results were expressed as pg/ml.

The BNP level was determined using RayBio® Human/Mouse/Rat Brain Natriuretic Peptide EIA Kit (RayBiotech, Inc. USA). The samples were added to the plate pre-coated with the anti-BNP antibody. The biotinylated BNP peptide competes with endogenous (from the sample) BNP for binding to the anti-BNP antibody. After a wash step, any bound biotinylated BNP then interacts with horseradish peroxidase (HRP)-streptavidin, which catalyses a

colour development reaction. The intensity of the colourimetric signal is directly proportional to the amount of captured biotinylated BNP peptide and inversely to the amount of endogenous BNP in the samples. The concentrations of BNP were determined from the standard curve; and expressed as pg/ml.

2.2.4. Morphometric analysis

For morphometric analysis, a total of 5 x 10^4 cells per well were seeded in a 24 well plate. On reaching 50 - 60% confluence, the cells were subjected to various treatments accordingly (*section 2.2.2*). After respective treatment, cells from all experimental groups were initially checked for morphological alterations, and after that, the cells were made to detach via trypsinisation. Then cells were observed under Nikon Eclipse TS-100 inverted phase-contrast microscope (Nikon, Tokyo, Japan) under 40X magnification and images were captured using Nikon DS-Fi1 digital camera (Prathapan et al. 2013). The cell size was measured using NIS- Elements D (Nikon, Japan) imaging software, and cell volume was calculated using the equation for the volume of a sphere ($4/3\pi r^3$). The diameter of individual cells was measured, and 100 cells per experimental group were measured randomly.

2.2.5. Extraction and estimation of protein concentration

The proteins from the cells were extracted in the RIPA buffer. Briefly, after the respective treatments, the cell culture dishes were taken and placed on ice and washed the cells with ice-cold PBS. The PBS was aspirated and added an ice-cold cell lysis buffer containing RIPA buffer with 10% protease inhibitor cocktail. The adherent cells were scraped using a cold plastic cell scraper, and then gently transferred the cell suspension into a pre-cooled microcentrifuge tube. This was kept at constant agitation for 30 min at 4°C and subjected to freeze/ thaw for five times and centrifuged in a cold centrifuge at 4°C for 20 min at 12,000 rpm. Then the supernatant was aspirated gently into another set of fresh tubes placed on ice, and the pellets were discarded.

Then protein concentration was estimated using the Protein Assay Kit (Thermo Scientific™, Rockford, Illinois, USA). Briefly, 200 µL of the working reagent (made in a concentration of 50:1 as per the protocol) was added to 25 µL of standards and samples. The plate was mixed thoroughly on a plate shaker for 30 sec and incubated at 37°C for 30 min in the dark. It was cooled to room temperature and measured the absorbance at 562 nm on a plate reader (Tecan Infinite M200PRO, Tecan, Austria). A standard curve was prepared, and the protein concentration of each sample was determined.

2.2.6. Evaluation of cytotoxicity

2.2.6.1. MTT assay

The cell viability was determined by MTT assay (Mosmann, 1983). Briefly, 1 x 10^4 cells were seeded in each well of 96-well plate and incubated in the humidified CO_2 (5 %) incubator at 37 °C, and allowed to attach to the substrate. When cells grew to 50-60% confluence, they were subjected to various treatments. Then the cells were incubated with MTT solution (5 mg/mL MTT in DMEM) at 37 °C for 4 h. The viable cells with an active metabolism reduce MTT into a purple-coloured formazan product with an absorbance maximum near 570 nm. When the cells die, they lose the ability to convert MTT into formazan. We dissolved the formazan crystals formed in DMSO. We read the plate after 45 min of incubation at room temperature using a microplate reader (Tecan Infinite M200PRO, Austria) at 570 nm.

2.2.6.2.Lactate dehydrogenase (LDH) leakage assay

The LDH leakage was determined by monitoring the rate of conversion of NADH to NAD^+ using an assay kit (Clontech Laboratories, Inc. USA). Briefly, the H9c2s cells were treated as indicated in section 2.2.2 in a 96 well plate. At the end of the treatment period, the plate was centrifuged at 250 x g for 10 min, and 100 µl of supernatant was transferred into the corresponding wells of another optically clear 96-well flat-bottom plate. Then, 100 µl of the freshly prepared reaction mixture (from the kit) was added to each well and

incubated in the dark for 30 min at room temperature. The absorbance was then measured at 490 nm using a multi-well plate reader (Tecan Infinite M200PRO, Austria), and the percentage toxicity was calculated.

2.2.7. Analysis of intracellular ROS by bio-imaging and cytometry

For bioimaging analysis, 1 x 10^4 cells were plated in each well of 96 well transparent bottom black bioimaging plate (BD), placed in the humidified 5% CO_2 incubator at 37°C and allowed to attach to the substrate. At 40-50 % confluence, the cells were subjected to various treatments. After respective treatment, 2', 7'- dichlorofluorescin diacetate (DCFH-DA) was added (3 µg/ml in PBS) to cultures and kept at 37 °C for 20 min. Since DCFH-DA enters cells and the acetate group on DCFH-DA is cleaved by cellular esterases, trapping the non-fluorescent DCFH inside the cells and the subsequent oxidation by ROS yields an increase in the fluorescent product 2', 7'- dichlorofluorescin (DCF). DCF fluorescence imaging was done (Ex. 488 nm; Em. 525 nm) to detect the difference in the intensity of fluorescence emitted using a spinning disk fluorescent microscope (BD Pathway™ Bioimager system, USA) at 20X magnification.

For the determination of ROS, the cells were cultured in 6-well plates at 3x 10^5 cells per well. After the induction of hyperglycaemia and treatment, the cells were collected in flow tubes by trypsin-EDTA detraction, and it was washed. Then DCFH-DA dye was added in a ratio of 1: 1000 in PBS buffer in each tube and incubated for 20 min and measurements were carried out using BD FACS Aria II flow cytometer (BD Biosciences, San Jose, CA, USA). Acquisition and analysis of flow cytometric data were carried out using BD FACS Diva software.

2.2.8. Lipid peroxidation (TBARS) assay

The lipid peroxidation (LPO) assay was done using the MDA assay kit (Sigma-Aldrich, St. Louis, MO, USA). For the assay, the cells were cultured in 6 well plates at 3x 10^5 cells per well). After the treatment, the cells were

collected and homogenised on ice in 300 µL of the MDA lysis buffer, centrifuged at 13,000 x g for 10 min to and the supernatant was collected. Briefly, to form the MDA-TBA adduct, 600 µL of the TBA solution was added into each tube and incubated at 95°C for 60 min, cooled to room temperature in an ice bath for 10 min. Pipetted out 200 µL from each reaction mixture into a transparent bottom 96 well plate, and measured the absorbance at 532 nm using a multimode plate reader (Tecan Infinite). The protein concentration was determined using the Pierce™ BCA Protein Assay kit (Thermo Scientific™, Rockford, Illinois, USA). A set of standard MDA was also run simultaneously, and the results were expressed as nM of MDA per mg protein.

2.2.9. Protein carbonyl content assay

Protein carbonylation (PCO) is a type of protein oxidation that can be promoted by reactive oxygen species. The protein carbonyl content was measured using the Cayman protein carbonyl colourimetric assay kit (USA). Briefly, 3x 10^5 cells were cultured in 6-well plate and treated as in *section 2.2.2.* After the respective treatments, the cells were collected by centrifugation at 2000 x g for 10 min at 4 °C. The cell pellets were homogenised on an ice cold phosphate buffer (50 mM, pH 6.7) and centrifuged at 10,000 x g for 15 min at 4°C. The supernatant was collected and stored on ice for assay. Initially, the absorbance of the supernatant was measured at 280 and 260 nm for nucleic acid contamination and found there was no nucleic acid contamination (280/260 nm was less than 1).

Then 200 µL supernatants were pipetted out 2 mL microcentrifuge tubes, and 800 µL of DNPH (kit reagent) was added to sample tubes and 800 µL of 2.5 M HCl (kit reagent) to the control tube. The tubes were incubated in the dark at room temperature for 1 h. Then 1 ml of 20 % TCA (kit reagent) was added to all the tubes and kept on ice for 5 min. The tubes were centrifuged at 10,000 x g for 10 min at 4°C, and the pellets were again resuspended in 1 ml of 20 % TCA was added to all the tubes and kept on ice

for 5 min. The tubes were again centrifuged at 10,000 x g for 10 min at 4°C and the pellets collected. It was washed with ethanol/ethyl acetate mixture (1:1, kit reagent) by suspending the pellet in the mixture and centrifugation at 10,000 x g for 10 min at 4°C, and repeated for eight times. After washing, the pellets were re-suspended in 500 µL of guanidine hydrochloride (kit reagent) and centrifuged at 10,000 x g for 10 min at 4°C. The absorbance of the supernatant was measured at 385 nm using the multimode plate reader (Tecan Infinite). The protein carbonyl content was calculated and expressed as nmol/mg protein.

2.2.10. Intracellular Ca^{2+}overload assay

For intracellular calcium overload analysis, 1 x 10^4 cells were cultured in each well of 96 well transparent bottom black plate, placed in the humidified 5% CO_2 incubator at 37°C and allowed to attach to the substrate and subjected to various treatments. The intracellular calcium overload was detected after staining the cells with the high-affinity, intracellular calcium indicator fura-2 AM for 20 min at 37 °C and visualised (BD Pathway™ 855 High-Content BioImager, BD Biosciences, USA) at an excitation/emission of 375/510 nm wavelengths. The images were analysed using ImageJ software.

2.2.11. Western blot

After the respective treatment, the total protein was extracted in RIPA buffer (Priyanka et al. 2017), and quantified using the Pierce™ BCA Protein Assay Kit (Thermo Scientific™, Rockford, Illinois, USA). Equal amounts of proteins (25 µg) were separated by 10% SDS-PAGE and transferred to PVDF membranes using the Trans-Blot® Turbo™ Transfer system (Bio-Rad, USA). The membranes were blocked with 5% skimmed milk in TBST (50 mM Tris, pH 7.5; 150 mM NaCl; 0.01% Tween-20) for 1h at room temperature. The membrane was washed 3 times with TBST for 10 min each. The membrane was incubated at 4°C overnight in primary antibodies of Anp, Bnp, Hdac1, Rac1, Ho-1, Hsp 60, 70, and 90, Gapdh, and β-actin proteins. After washing with TBST, the membrane was incubated with HRP-conjugated corresponding

secondary antibodies for 1h at room temperature. Again washed three times with TBST, then the membranes were developed using Western BLoT Hyper HRP Substrate (Takara Bio Inc. USA), and the protein bands were analysed by stain-free imaging capabilities of the Bio-Rad ChemiDoc MP imaging systems, using image lab software (Bio-Rad, USA).

Statistical analysis

The results were presented as the mean ± standard deviation (SD) for the control and experimental groups. All statistical analyses were carried out using the Statistical Package for Social Science (IBM SPSS Statistics for Windows, Version 22.0. Armonk, NY). Data were subjected to one-way ANOVA, and the differences among the means for the groups were assessed using Duncan's multiple range tests to determine which mean values were significantly different at $p < 0.05$.

2.3. Results

2.3.1. Hyperglycaemia (HG) induced cell death in H9c2 cells

The HG caused a significant increase in the cell death (27.80 % compared to control; $p \leq 0.05$, **Table.2.1**) and co-treatment with FA (10 and 25 µM) reduced the cell death (15.89 and 10.24 % respectively compared to HG, $p \leq 0.05$). The treatment with positive control Met also showed a significant reduction in cell death compared to HG (7.38 %). The osmotic control group treated with mannitol and FA alone treated group showed no significant cell death (**Table.2.1**).

Further, the myocyte damage was confirmed by LDH leakage assay (expressed as % cytotoxicity) which showed a significant release of the enzyme with HG (12.16 %; $p \leq 0.05$) whereas co-treatment with FA significantly reduced the LDH leakage (9.98 and 6.93 % respectively, $p \leq 0.05$; **Table.2.1**) comparable with Met (5.91 %; $p \leq 0.05$). These results

showed that, FA can protect the cardiac myocyte from the HG induced cell injury.

Groups	Percentage cytotoxicity	
	MTT assay	LDH leakage assay
C	0.00	0.00
HG	27.80 ± 1.54*	12.16 ± 1.63*
HGF1	15.89 ± 0.47#	9.98 ± 0.41#
HGF2	10.24 ± 0.45#	6.93 ± 0.51#
HGM	7.38 ± 0.26 #	5.91 ± 0.90#
CF	1. 73 ± 0.13	1.43 ± 0.33
OC	1.92 ± 0.16	1.89 ± 0.27

Table.2.1. Hyperglycaemia causes significant cytotoxicity in H9c2 rat cardiomyoblasts. Analysis of cell death in H9c2 cells grown under the conditions of NG (5.5 mM d-glucose), HG (33 mM d-glucose), FA (10 or 25 µM), or Met (10 µM) conditions for 48 h (mean ± SD, n=6, * $p < 0.05$ vs. control and # $p < 0.05$ vs. hyperglycaemia). **C**, indicates control (NG); **HG**, high glucose, **HGF1**, high glucose + 10 µM FA; **HGF2**, high glucose + 25 µM FA, **HGM**; high glucose + Met (10 µM); **CF**, NG + 25 µM FA; **OC**, osmotic control (27.5 µM mannitol + 5.5 µM d-glucose); FA, ferulic acid; and Met, metformin.

Here also, the osmotic control group treated with mannitol showed no significant cell death, and which was very much similar to the FA alone treated group. Since there was no cell injury induced by mannitol, the osmotic stress was ruled out, and this group was eliminated for further analysis. The FA also showed no significant cell death or cell injury, and this group was not included in the protein expression (western blot) analysis (**Table.2.1**).

2.3.2. HG induced intracellular Ca^{2+} ($[Ca^{2+}]i$) overload in H9c2 cardiomyoblasts

Intracellular calcium was found increased significantly with the HG group evident by the increased blue (fura 2) fluorescence. The treatment with FA and Met decreased the $[Ca^{2+}]i$ overload shown by diminished blue fluorescence (**Fig. 2.1A**). This was again confirmed by fluorescent intensity

analysis with a plate reader and found that 31% increase of $[Ca^{2+}]i$ concentration in HG compared with control (n=6, $p \leq 0.05$). The FA treatment decreased $[Ca^{2+}]i$ overload (16% and 20% with 10 and 25 µM respectively; **Fig. 2.1B**), which was comparable to Met (23 %). These results reveal the efficacy of FA in maintaining the $[Ca^{2+}]i$ homeostasis during HG.

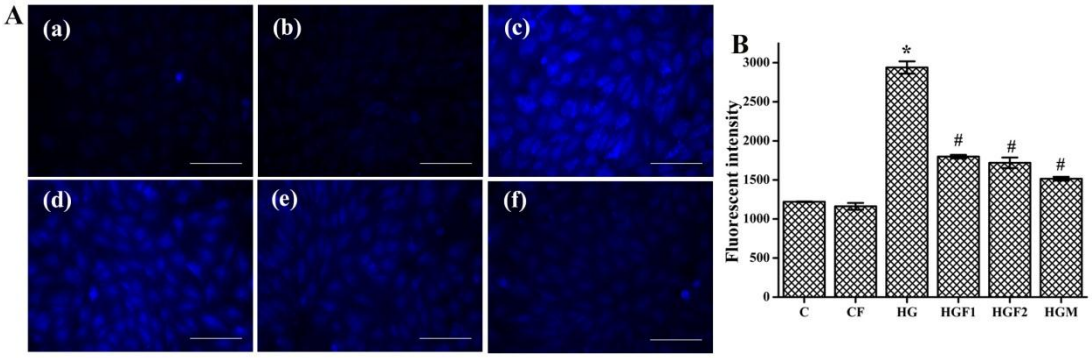

Figure. 2.1. Hyperglycaemia increases the intracellular Ca^{2+} ($[Ca^{2+}]i$) in H9c2 rat cardiomyoblast. A, Analysis of intracellular Ca^{2+} overload (fura2-AM fluorescence) in H9c2 cells grown under the treatment of (a) NG (5.5 mM d-glucose), (b) FA (25 µM), (c) HG (33 mM d-glucose), (d & e) FA (10 or 25 µM), or (f) Met (10 µM) conditions for 48 h. Images are representative of six independent (n=6) experiments. Scale bar - 50 µm. **B,** Fluorescent intensity analysis of intracellular Ca^{2+} (mean ± SD, n=6, * $p < 0.05$ vs. control and # $p < 0.05$ vs. hyperglycaemia). C, indicates control (NG); CF, NG + 25 µM FA; HG, hyperglycaemia; HGF1, high glucose + 10 µM FA; HGF2, high glucose + 25 µM FA; HGM; high glucose + Met (10 µM); FA, ferulic acid; and Met, metformin.

2.3.3. HG-induced ROS production in H9c2 cardiomyoblasts.

We analysed the cytosolic ROS production, and HG showed increased production evidenced by the increase in green fluorescence, while FA prevented ROS, which was comparable to Met (**Fig. 2.2A**). This was again confirmed by the fluorescent intensity analysis and showed a significant (60 % compared with control) production of ROS in HG whereas the treatment with FA (10 and 25 µM) showed 10 % and 22 % reduction of the ROS production respectively ($p < 0.05$). The Met application also caused ROS reduction (30 %) compared to the HG group (**Fig. 2.2B**). Further confirmatory analysis by flow cytometry also showed the same trend (**Fig. 2.2C**).

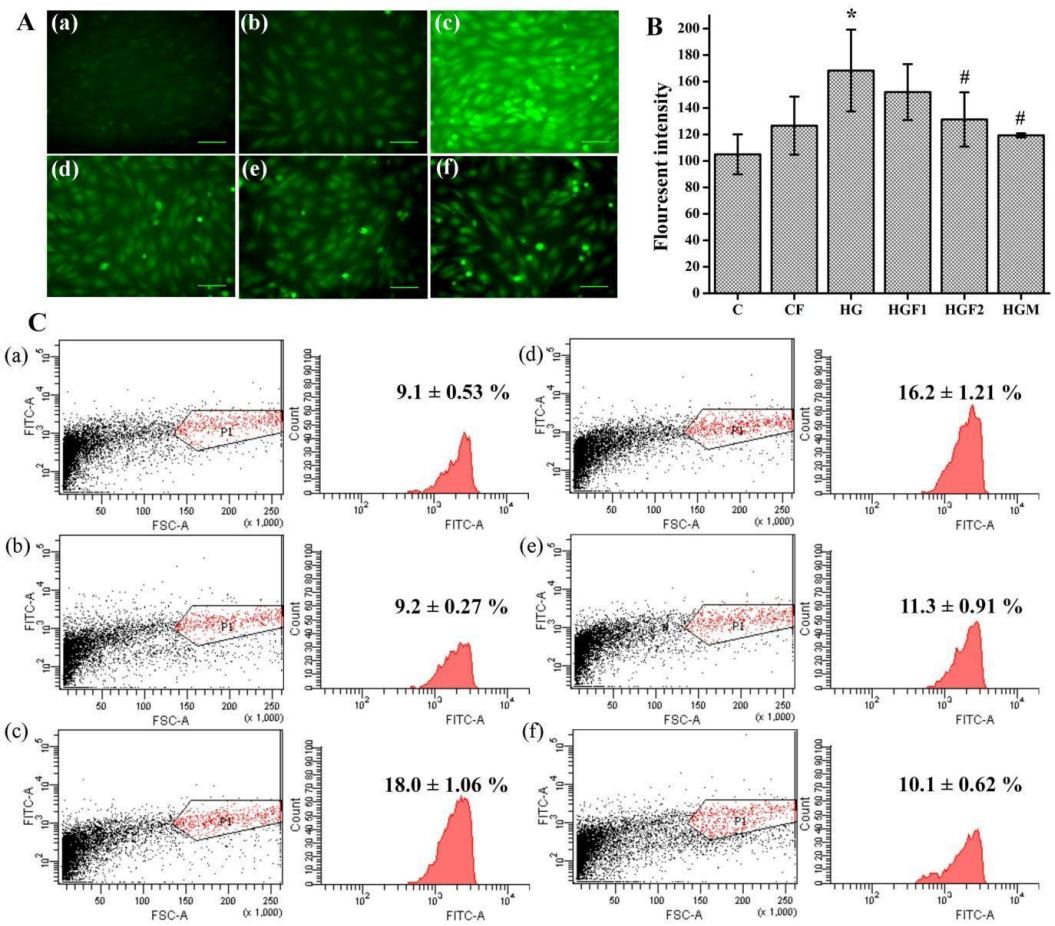

Figure. 2.2. Hyperglycaemia increases the ROS formation in H9c2 rat cardiomyoblast. A, Analysis of ROS formation (dichlorofluorescin florescence) in H9c2 cells grown under the treatment of (a) NG (5.5 mM d-glucose), (b) FA (25 µM), (c) HG (33 Mm d-glucose), (d & e) FA (10 or 25 µM), or (f) Met (10 µM) conditions for 48 h. Images are representative of six independent (n=6) experiments. Scale bar - 50 µm **B,** Fluorescent intensity analysis of ROS (mean ± SD, n=6, * $p < 0.05$ vs. control and # $p < 0.05$ vs. hyperglycaemia). C, indicates control (NG); CF, NG + 25 µM FA; HG, hyperglycaemia; HGF1, high glucose + 10 µM FA; HGF2, high glucose + 25 µM FA; HGM; high glucose + Met (10 µM); FA, ferulic acid; and Met, metformin. **C**, Flow cytometry analysis of ROS formation, images are representative of six independent (n=6) experiments (mean ± SD, n=6, * $p < 0.05$ vs. control and # $p < 0.05$ vs. hyperglycaemia).

2.3.4. HG upregulated the cellular pro-oxidants and downregulated the antioxidant proteins and enzymes.

Hereafter group of stress proteins from cytoplasm such as the heat shock proteins (HSPs) were examined and found Hsp 60 was upregulated

(2.27 fold), and stress relieving Hsp 70 and 90 were downregulated (0.69 and 0.62 fold respectively) in HG, and co-treatment with FA and Met showed significant protection ($p < 0.05$) (**Fig. 2.3** & **Table. 2.2**). The stress-responsive proteins Rac1 and Hdac1 were upregulated in HG (4.5 and 13.0 respectively). However Ho-1 was found downregulated (0.9 fold). Co-treatment with FA (10 and 25 µM) was effective in bringing back the enzyme level to normal (**Fig. 2.3** & **Table. 2.2**).

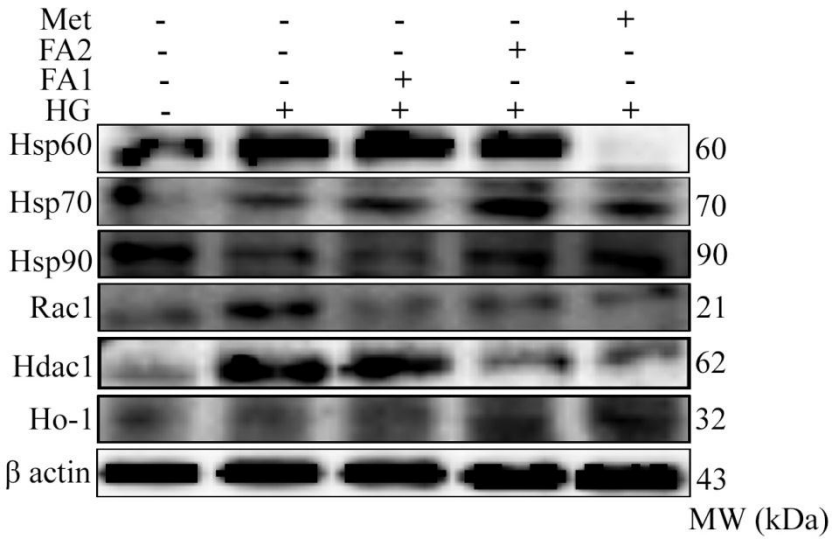

Figure.2.3. Hyperglycaemia upregulates stress proteins and downregulates stress-relieving proteins. Western blot analysis of the proteins of interest in cellular stress in the cell lysate prepared H9c2 cells grown under the treatment of NG (5.5 mM d-glucose), HG (33 mM d-glucose), FA (10 or 25 µM), or Met (10 µM) conditions for 48 h. Images are representative of three independent (n=6) experiments. NG indicates control; HG, hyperglycaemia; FA, ferulic acid; and Met, metformin.

Groups / Proteins	**Protein folds of control**			
	HG	**HGF1**	**HGF2**	**HGM**
Hsp60	2.27 ± 0.47*	3.23 ± 0.42#	2.76 ± 0.40#	0.21 ± 0.01
Hsp70	0.69 ± 0.09*	2.15 ± 0.36#	3.30 ± 0.93#	3.15 ± 0.94#
Hsp90	0.62 ± 0.06*	0.84 ± 0.08#	1.12 ± 0.14#	1.74 ± 0.34#
Rac1	4.54 ± 0.85*	2.25 ± 0.59#	3.53 ± 0.09	2.76 ± 0.19#
Hdac1	13.08 ± 1.58*	10.41 ± 0.94#	0.98 ± 0.18#	0.65 ± 0.09#
Ho-1	0.93 ± 0.12	1.84 ± 0.27#	2.246 ± 0.46#	4.16 ± 0.69#

Table.2.2. Densitometry analysis blots of oxidative stress marker proteins in H9c2 cells. Fold difference values of intensity of proteins analysed by western blot. Values were fold difference of control, as control normalised to 1 (mean ± SD, n=6, * $p < 0.05$ vs. control and # $p < 0.05$ vs. hyperglycaemia). **HG**, indicates high glucose (33 mM d-glucose); **HGF1**, high glucose cells treated with FA - 10 µM; **HGF2**, high glucose cells treated with FA- 25 µM; **HGM**, high glucose cells treated with Met -10 µM; FA, ferulic acid; and Met, metformin.

2.3.5. HG induces damage to lipids and proteins.

In addition, HG-induced lipid peroxidation and protein carbonylation were also investigated. HG caused a significant increase in lipid peroxidation and protein carbonylation (1.70 and 3.33 fold respectively; compared to control; **Table. 2.3**). The treatment with FA (10 and 25 µM) reduced lipid peroxidation (1.45 and 1.52 fold) and protein carbonylation (1.45 and 1.84 fold) significantly (compared to HG; $p \leq 0.05$) in a dose-dependent manner which was comparable to Met (1.96 fold; **Table. 2.3**)

	Lipid peroxide (nM/µl)		Protein carbonyl (nM/mg)	
Groups	**Mean ± SD**	**Fold change**	**Mean ± SD**	**Fold change**
C	0.20 ± 0.02		0.27 ± 0.03	
HG	0.34 ± 0.02	1.70*	0.90 ± 0.14	3.33*
HGF1	0.24 ± 0.07	1.45#	0.62 ± 0.09	1.45#
HGF2	0.22 ± 0.05	1.52#	0.49 ± 0.11	1.84#
HGM	0.17 ± 0.02	1.99#	0.46 ± 0.09	1.96#
CF	0.22 ± 0.02		0.25 ± 0.02	

Table.2.3. Hyperglycaemia causes a significant increase in lipid peroxidation and protein oxidation in H9c2 cells. Analysis of lipid peroxidation and protein carbonyl content in H9c2 cells grown under the conditions of NG (5.5 mM d-glucose), HG (33 mM d-glucose), FA (10 or 25 µM), or Met (10 µM) conditions for 48 h (mean ± SD, n=6, * $p < 0.05$ vs. control and # $p < 0.05$ vs. hyperglycaemia). **C**, indicates control (NG); **HG**, high glucose, **HGF1**, high glucose + 10 µM FA; **HGF2**, high glucose + 25 µM FA, **HGM**; high glucose + Met (10 µM); **CF**, NG + 25 µM FA; FA, ferulic acid; and Met, metformin.

2.3.6. HG caused H9c2 cell injury.

HG-induced cell injury was evaluated by measuring cardiac health markers such as BNP and ANP release into the medium. H9c2 cardiomyoblasts treated with HG showed significant release of BNP and ANP (9.73 and 2.47 fold respectively, $p \leq 0.05$; **Table.2.4**) and co-treatment with FA significantly reduced the release of both NPs (BNP – 3.94 and 6.10 fold; ANP – 1.33 and 1.81 fold; $p \leq 0.05$; Table.2.4) in a dose-dependent manner (for 10 and 25 µM respectively which is comparable with positive control Met (BNP – 5.25 and ANP – 1.91 fold; **Table.2.4**).

The western blot analysis showed 42.28 and 65.01 fold increase in ANP and BNP, respectively in HG and the treatment with FA reduced the release of these proteins significantly (**Fig. 2.4A &B**). The FA treatment reduced the ANP release in a dose-dependent manner (4.44 and 10.65 fold reduction for 10 and 25 µM respectively). FA also reduced the BNP release in dose-dependent manner (3.63 and 5.96 fold). The positive control metformin also reduced the release of these markers significantly (3.57 fold for ANP and 19.43 fold for BNP, **Fig. 2.4**). The results revealed the protective effect of ferulic acid against the hyperglycaemia induced cell injury.

Groups	ANP (pg/ml)		BNP (pg/ml)	
	Mean ± SD	Fold change	Mean ± SD	Fold change
C	149.80 ± 24.88		48.83 ± 4.89	
HG	369.48 ± 4.85	2.47*	475.01 ± 30.90	9.73*
HGF1	277.18 ± 9.92	1.33#	120.32 ± 18.81	3.95#
HGF2	218.67 ± 0.05	1.81#	77.93 ± 0.72	6.10#
HGM	193.03 ± 23.25	1.91#	90.46 ± 8.52	5.25#
CF	176.59 ± 16.59	0.18	57.93 ± 3.55	0.18

Table.2.4. Hyperglycaemia causes a significant release of cardiac injury (hypertrophy) markers - atrial natriuretic peptide (ANP), and b-type natriuretic peptide (BNP) in H9c2 rat cardiomyoblasts. Analysis of markers of cardiac hypertrophy in H9c2 cells grown under the conditions of NG (5.5 mM d-glucose), HG (33 mM d-glucose), FA (10 or 25 µM), or Met

(10 µM) conditions for 48 h (mean ± SD, n=6, * p < 0.05 vs. control and # p < 0.05 vs. hyperglycaemia). **C** indicates control (NG); **HG**, high glucose, **HGF1**, high glucose + 10 µM FA; **HGF2**, high glucose + 25 µM FA; **HGM**; high glucose + Met (10 µM); **CF**, NG + 25 µM FA; FA, ferulic acid; and Met, metformin.

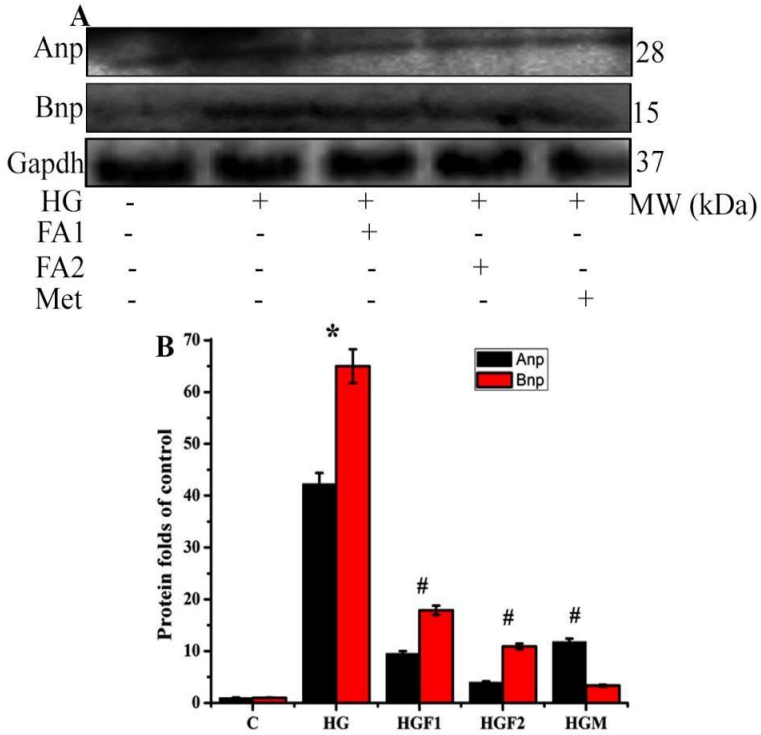

Figure.2.4. Hyperglycaemia upregulates the cardiac injury (hypertrophy) markers Anp and Bnp in H9c2 cells. A, Western blot analysis of proteins of interest of cardiac injury (hypertrophy) in the cell culture medium of H9c2 cells grown under the treatment of NG (5.5 mM d-glucose), HG (33 mM d-glucose), FA (10 or 25 µM), or Met (10 µM) conditions for 48 h. Images are representative of six independent (n=6) experiments. **B,** Densitometric analysis of the blots (mean ± SD, n=6, * p < 0.05 vs. control and # p < 0.05 vs. hyperglycaemia). **C** Indicates control (NG); **HG**, high glucose; **HGF1**, high glucose + 10 µM FA; **HGF2**, high glucose + 25 µM FA; **HGM**; high glucose + Met (10 µM); FA, ferulic acid; and Met, metformin.

2.3.7. HG-induced increase in cellular protein level.

In order to analyse the hyperglycaemia induced fibrosis, we measured the protein concentration in the cells. The HG induced a 27 % increase in the protein content in H9c2 cells (**Fig. 2.5**). The treatment with FA reduced the proteins content significantly in a dose-dependent manner (4 and 12% with 10

and 25µM respectively). The Met treatment also reduced the protein level by 23 % (**Fig. 2.5**).

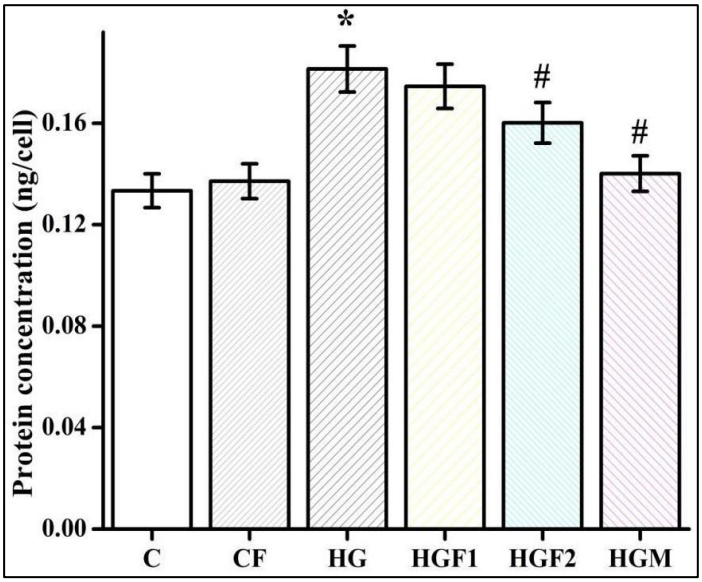

Figure.2.5. Hyperglycaemia increases the total protein content in H9c2 rat cardiomyoblast. Cellular protein content determined from the H9c2 cells grown under the treatment of NG (5.5 mM d-glucose), HG (33 mM d-glucose), FA (10 and 25 µM), or Met (10 µM) conditions for 48 h (mean ± SD, n=6, * $p < 0.05$ vs. control and # $p < 0.05$ vs. hyperglycaemia). **C** indicates control (NG); **CF**, NG + 25 µM FA**; HG**, high glucose; **HGF1**, high glucose + 10 µM FA; **HGF2**, high glucose + 25 µM FA; **HGM**; high glucose + Met (10 µM); FA, ferulic acid; and Met, metformin.

2.3.8. HG-induced alteration in myocyte morphology.

The morphometric examination showed that hyperglycaemia induced a significant increase in the cell size of H9c2 cells and the cells showed flaccid appearance (**Fig. 2.6A**). The treatment with the positive control metformin and the two concentrations of FA reduced the cell size significantly in a dose-dependent manner (**Fig. 2.6A**). The cell size measurement showed a 47 % increase in the cell volume in hyperglycaemia (**Fig. 2.6B**). The treatment with FA reduced cell size by 36 and 45 %, and this was comparable to the Met treatment, which reduced the size of the cells by 46%. FA was found effective against the hyperglycaemia induced cardiac cell hypertrophy and fibrosis.

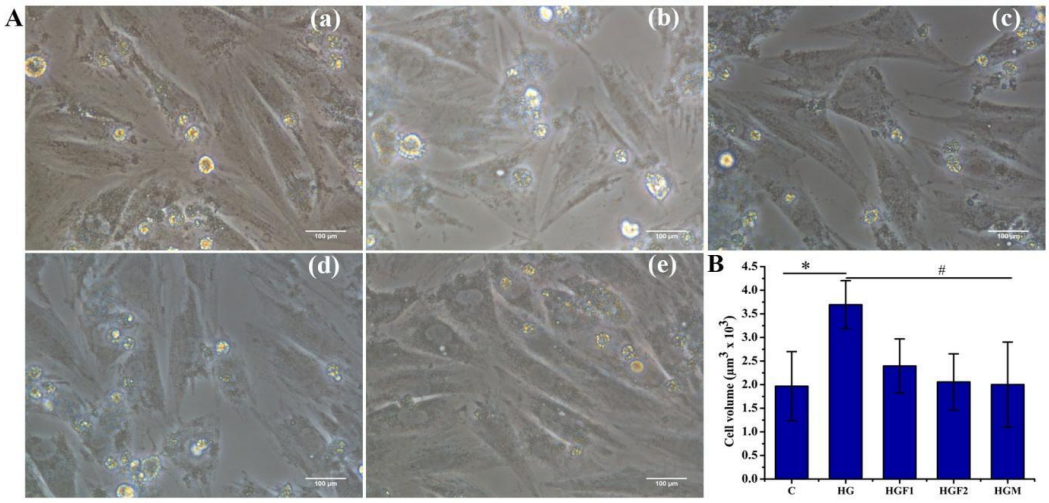

Figure.2.6. Hyperglycaemia increases the cell volume in H9c2 rat cardiomyoblast. A, Photomicrograph of H9c2 cells grown under the treatment of **(a)** NG (5.5 mM d-glucose), **(b)** HG (33 mM d-glucose), **(c & d)** FA (10 or 25 µM), or **(e)** Met (10 µM) conditions for 48 h. Images are representative of six independent (n=6) experiments. Scale bar - 100 µm. **B,** Cell volume determined from the radius measured using NIS Element imaging software (mean ± SD, n=6, * $p < 0.05$ vs. control and # $p < 0.05$ vs. hyperglycaemia). **C** Indicates control (NG); **HG**, Hyperglycaemia; **HGF1**, high glucose + 10 µM FA; **HGF2**, high glucose + 25 µM FA; **HGM**; high glucose + Met (10 µM); FA, ferulic acid; and Met, metformin.

2.4. Discussion

The pathogenesis of diabetic cardiomyopathy (DC) is multifactorial in origin, and evidence indicates that the defect in Ca^{2+} homeostasis is a primary pathological reason for cardiac dysfunction (Singh et al. 2018). Herein we describe the sequences of various biochemical processes induced by HG in H9c2 cells which ultimately terminates in oxidative stress via calcium overload and mitochondrial dysfunction. Normal Ca^{2+} homeostasis is very much essential for cardiac function. One of the most detrimental factors in the genesis of various heart diseases is the unbalanced change in Ca^{2+} homeostasis (Dhalla et al. 2001). Ca^{2+} overload in post-ischemic cardiomyocytes is the leading cause of cell death either through apoptosis or necrosis (Soumya et al. 2014). The Ca^{2+} ion flux from the extracellular compartments and internal reservoirs are in tight control for the sufficient regulation of intracellular Ca^{2+} ion concentration (Soumya et al. 2014).

Alteration of this triggers a plethora of effects. There are reports available stating that HG is responsible for the alteration of Ca^{2+} homeostasis in diabetes patients (Kumar et al. 2012).

Role of intracellular calcium in the generation of the oxidative stress is well established in various studies (Soumya et al. 2014; Prathapan et al. 2016). One explanation has been that Ca^{2+} induces a three-dimensional conformation change of the respiratory chain complexes, which leads to surplus mitochondrial ROS generation (Adam-Vizial & Starkov, 2010). There is further evidence that the metabolic state of the mitochondria determines the effects of Ca^{2+} on mitochondrial ROS levels (Jaiswal et al. 2015). We also checked lipid peroxidation and genesis of carbonyl content to confirm alteration in redox status. A significant rise in lipid peroxidation and carbonyl content was found during HG condition.

Research shows that inhibition of Hdac1 protects the heart against myocardial injury and stimulates endogenous angiomyogenesis (Zhang et al. 2012). Nevertheless, Hdac1 was found upregulated during hyperglycaemia in H9c2 cells revealing its negative role in diabetes. The exceptional cardioprotective ability of Ho-1 is well proved by its power to modulate inflammation, various signalling pathways, and mitochondrial function (Otterbein et al. 2003). Its role in mitigating myocardial tissue injury and the progression of proliferative vascular disease has been already reported. Reduced expression of Ho-1 found here during hyperglycaemia may be one mechanism behind inflammation in the heart during DCM.

The small GTP-binding protein Rac1is a critical molecule involved in cardiac myocyte hypertrophy; also, Rac1 is pivotal in hyperglycaemia induced apoptosis in cardiomyocytes (Otterbein et al. 2003). It is functioning through NADPH oxidase activation and mitochondrial ROS generation. The increase of Rac1 protein expression with hyperglycaemia shows the possibility of the development of hypertrophy in H9c2 rat cardiomyoblasts. Other investigators have also reported cardiac hypertrophy during diabetes but through different mechanisms such as decreased GLUT4 translocation, lowered sarcoplasmic reticulum Ca^{2+} pump activity and increasing cardiomyocyte intracellular Ca^{2+},

high insulin induced binding to the IGF-1 receptor (Jia et al. 2018). Here we would like to add the contribution of Rac1 in the genesis of cardiac hypertrophy during diabetes in addition to other mechanisms.

In the normal cardiac myocytes, the heat shock proteins (HSPs) are expressed in the physiological range, but during the oxidative stress and ischemic conditions, their expressions are enhanced into pathological manner. The protein folding and degradation are the primary functions of HSP chaperons. Some of the HSPs have shown to have protective effects against severe stresses. The HSP increases lysosomal activity and protects cardiomyocytes from the damaged mitochondria. Hsp70 is integral for disease prevention and protecting cardiomyocytes from stress (Bernardo et al. 2016). Extracellular Hsp60 has been found to cause cardiac myocyte apoptosis and may be a factor in the progression of heart failure (Chan et al. 2009). We observed upregulation of Hsp60, and downregulation of Hsp70 and 90 proteins in the cell line during hyperglycaemia which shows the cells are in oxidative stress and undergoing physiological (Hsp70) and pathological (Hsp90) adaptation for survival. However, the trend of Hsp60 warns of the forthcoming apoptosis, which is already known during hyperglycaemia. These results reveal the differential role of HSPs during stress and also give clues of forthcoming apoptosis during diabetes.

Oxidative stress causes multiple injuries in the cardiac cell, which is reflected in the surplus secretion of various marker proteins like ANP and BNP (Waldman et al. 2018). HG-induced cardiac dysfunction has been confirmed with the quantification of cardiac markers like BNP and ANP. These proteins have been found increased with incubation of cells with the HG medium. It is established that these natriuretic peptides from the heart are released in response to changes in the physiology of the heart (Sergeeva & Christoffels, 2013; Wong et al. 2017). The level of BNP goes up when heart failure develops or gets worse, and it goes down when the condition is stable. ANP, another marker peptide from the heart is released during stressed conditions like cardiac ischemia and heart failure (Wong et al. 2017). In early heart failure, these peptides have a significant role in keeping the

compensated state of asymptomatic left ventricular dysfunction (Yoshimura et al. 2001). We also found a surplus release of lactate dehydrogenase (LDH) during HG shock, which confirms the cardiac injury during HG concentrations.

Co-treatment with FA was found effective against HG-induced alterations in H9c2 cells. Further, it safeguarded the integrity of mitochondria which is also expected to contribute to the decrease of $[Ca^{2+}]i$ overload. Mitigation of lipid peroxidation and carbonyl content is also observed with FA co-treatment. Finally, FA was able to keep all cardiac pathological indicators like LDH, ANP and BNP in the normal range. LDH is a stable cytoplasmic enzyme released only when the cytoplasmic membrane is damaged, and quantification of it in the cell culture supernatant depicts the depth of cell injury. Our result is in line with a previous study by Song et al. (2016), who reported that FA is effective against HG-induced oxidative stress. The antioxidant properties of FA have been employed for prevention and treatment of various oxidative stress-induced disorders such as Alzheimer's disease (Jin et al. 2005), diabetes (Narasimhan et al. 2015), cancers (Janicke et al. 2011), hypertension, dyslipidemia and atherosclerosis (Suzuki et al. 2007). Besides, its derivatives have been found effective against several inflammatory diseases due to its anti-inflammatory properties (Bumrungpert et al. 2018).

There are reports on FA for its potential against diabetes and associated complications. It improves insulin sensitivity (Roy et al. 2013), hepatic glycogenesis and inhibits gluconeogenesis (Rukkumani et al. 2004). It is also found to reduce diabetic induced complications like nephropathy (Alam et al. 2013), inflammation and stress-mediated splenotoxicity (Ghosh et al. 2018). These pleiotropic effects of FA were attractive for us to work on FA to see its efficacy against HG-induced pathological manifestation in H9C2 cells. The ability of FA to break free radical chain reactions forms the base of most of its pharmacological properties (Nenadis et al. 2003). The positive impacts of FA observed in the present study on calcium homeostasis glorify its status in the drug discovery field.

FDA has approved FA as a food additive and sports food. The remarkable array of pharmacological properties of FA and lack of side effects make it an exciting compound for use as a functional food as well as a substitute for synthetic drugs. However, detailed preclinical and clinical studies are required before recommending FA for human use both as a nutrient supplement as well as a therapeutic agent against human diseases.

References

1. Adam-Vizia V, Starkov AA, 2010. Calcium and mitochondrial reactive oxygen species generation: how to read the facts. J. Alzheimers Dis. 20:S413-S426.
2. Alam MA, 2019. Anti-hypertensive effect of cereal antioxidant ferulic acid and its mechanism of action. Front. Nutr. 6:121.
3. Alam MA, Sernia C, Brown L, 2013. Ferulic acid improves cardiovascular and kidney structure and function in hypertensive rats. J. Cardiovasc. Pharmacol. 61:240-248.
4. Aneja A, Tang WH, Bansila S, Garcia MJ, Farkouh ME, 2008. Diabetic cardiomyopathy: insights into pathogenesis, diagnostic challenges, and therapeutic options. Am. J. Med. 121(9):748-757.
5. Bai Y, Cui W, Xin Y, et al., 2013. Prevention by sulforaphane of diabetic cardiomyopathy is associated with up-regulation of Nrf2 expression and transcription activation. J. Mol. Cell. Cardiol. 57:82-95.
6. Bernardo BC, Weeks KL, Patterson NL, McMullen JR, 2016. HSP70: therapeutic potential in acute and chronic cardiac disease settings. Future Med. Chem. 8:2177-2183.
7. Bock FJ, Tait SWG, 2020. Mitochondria as multifaceted regulators of cell death. Nat. Rev. Mol. Cell. Biol. 2185-100.
8. Bumrungpert A, Lilitchan S, Tuntipopipat S, Tirawanchai N, Komindr S, 2018. Ferulic acid supplementation improves lipid profiles, oxidative stress, and inflammatory status in hyperlipidemic subjects: A randomized, double-blind, placebo-controlled clinical trial. Nutrients. 10:713.

9. Cai L, Li W, Wang G, et al., 2002. Hyperglycaemia-induced apoptosis in mouse myocardium: mitochondrial cytochrome C-mediated caspase-3 activation pathway. Diabetes. 51:1938-1948.
10. Chan KS, Stice JP, Chen L, et al., 2009. Extracellular heat shock protein 60, cardiac myocytes, and apoptosis, Circ. Res. 105:1186-1195.
11. Dhalla NS, Temsah RM, Netticadan T, Sandhu MS, 2001. Calcium overload in ischemia/ reperfusion injury:In Heart physiology and pathophysiology. Academic Press, San Diego. pp: 949-965.
12. Ghosh S, Chowdhury S, Sarkar P, Sil PC, 2018. Ameliorative role of ferulic acid against diabetes associated oxidative stress induced spleen damage. Food Chem. Toxicol. 118:272-286.
13. Giacco F, Brownlee M, 2010. Oxidative stress and diabetic complications. Circ. Res. 107(9):1058-1070.
14. Han J, Tan C, Wang Y, Yang S, Tan D, 2015. Betanin reduces the accumulation and cross-links of collagen in high fructose-fed rat heart through inhibiting non-enzymatic glycation. Chem. Biol. Interact. 227:37-44.
15. Hayat SA., Patel B, Khattar RS, Malik RA, 2004. Diabetic cardiomyopathy: mechanisms, diagnosis and treatment. Clin. Sci. 107(6):539-557.
16. Huang X, Liu S, Wu D, et al., 2018. Facilitated Ca^{2+} homeostasis and attenuated myocardial autophagy contribute to alleviation of diabetic cardiomyopathy after bariatric surgery. Am. J. Physiol. Heart. Circ. Physiol. 315(5):H1258-H1268.
17. Jaiswal N, Maurya CK, Arha D, et al., 2015. Fructose induces mitochondrial dysfunction and triggers apoptosis in skeletal muscle cells by provoking oxidative stress. Apoptosis. 20:930-947.
18. Janicke B, Hegardt C, Krogh M, et al., 2011. The antiproliferative effect of dietary fiber phenolic compounds ferulic acid and p-coumaric acid on the cell cycle of Caco-2 cells. Nutr. Cancer. 63:611-622.
19. Jia G, Hill MA, Sowers JR, 2018. Diabetic cardiomyopathy: an update of mechanisms contributing to this clinical entity. Circ. Res. 122:624-638.

20. Jin Y, Yan EZ, Fan Y, et al., 2005. Sodium ferulate prevents amyloid-beta-induced neurotoxicity through suppression of p38 MAPK and upregulation of ERK-1/2 and Akt/protein kinase B in rat hippocampus. Acta Pharmacol. Sin. 26:943-951.
21. Kayama Y, Raaz U, Jagger A, et al., 2015. Diabetic cardiovascular disease induced by oxidative stress. Int. J. Mol. Sci. 16:25234-25263.
22. Kumar S, Kain V, Sitasawad SL, 2012. High glucose-induced Ca^{2+} overload and oxidative stress contribute to apoptosis of cardiac cells through mitochondrial dependent and independent pathways. Biochim. Biophys. Acta. 1820:907-920.
23. Marcinkiewicz A, Ostrowski S, Drzewoski J, 2017. Can the onset of heart failure be delayed by treating diabetic cardiomyopathy?. Diabetol. Metabol. Syndrom. 9:21,
24. Miki T, Yuda S, Kouzu H, Miura T, 2013. Diabetic cardiomyopathy: pathophysiology and clinical features. Heart Fail. Rev. 18(2):149-166.
25. Mosmann T, 1983. Rapid colorimetric assay for cellular growth and survival: application to proliferation and cytotoxicity assays. J. Immunol. Methods. 65:55-63.
26. Narasimhan A, Chinnaiyan M, Karundevi B, 2015. Ferulic acid exerts its antidiabetic effect by modulating insulin-signalling molecules in the liver of high-fat diet and fructose-induced type-2 diabetic adult male rat. Appl. Physiol. Nutr. Metab. 40:769-781.
27. Nenadis N, Zhang HY, Tsimidou MZ, 2003. Structure-antioxidant activity relationship of ferulic acid derivatives: effect of carbon side chain characteristic groups. J. Agri. Food Chem. 51:1874-1879.
28. Otterbein LE, Soares MP, Yamashita K, Bach FH, 2003. Heme oxygenase-1: unleashing the protective properties of heme, Trends. Immunol. 24:449-455.
29. Otterbein Y, Otsu K, Nishida K, et al., 2003. The small GTP-binding protein Rac1 induces cardiac myocyte hypertrophy through the activation of apoptosis signal-regulating kinase 1 and nuclear factor-κB. J. Biol. Chem. 278:20770-20777.

30. Ou S, Kwok KC, 2004. Ferulic acid: pharmaceutical functions, preparation and applications in foods, J. Sci. Food. Agric. 84:1261-1269.
31. Prathapan A, Salin Raj P, Raghu KG, 2016. Attenuation of oxidative damage by Boerhaavia diffusa L. against different neurotoxic agents in rat brain homogenate. J. Diet Suppl. 13:300-312.
32. Prathapan A, Vineetha VP, Abhilash PA, Raghu KG, 2013. *Boerhaavia diffusa* L. attenuates angiotensin II-induced hypertrophy in H9c2 cardiac myoblast cells via modulating oxidative stress and down-regulating NF-κβ and transforming growth factor β1. Br. J. Nutr. 110:1201-1210.
33. Priyanka A, Shyni GL, Anupama Nair, Salin Raj P, Anusree SS, Raghu KG, 2017. Development of insulin resistance through sprouting of inflammatory markers during hypoxia in 3T3-L1 adipocytes and amelioration with curcumin. Eur. J. Pharmacol. 812:73-81.
34. Rani N, Bharti S, Bhatia J, et al., 2016. Chrysin, a PPAR-*γ* agonist improves myocardial injury in diabetic rats through inhibiting AGE-RAGE mediated oxidative stress and inflammation. Chemi. Biol. Interacti. 250:59-67.
35. Roy S, Metya SK, Sannigrahi S, Rahaman N, Ahmed F, 2013. Treatment with ferulic acid to rats with streptozotocin-induced diabetes: effects on oxidative stress, pro-inflammatory cytokines, and apoptosis in the pancreatic β cell. Endocrine. 44:369-379.
36. Rukkumani R, Aruna K, Suresh VP, Padmanabhan MV, 2004. Hepatoprotective role of ferulic acid: a dose-dependent study. J. Med. Food. 7:456-461.
37. Sahu R, Dua TK, Das S, de Feo V, Dewanjee S, 2019. Wheat phenolics suppress doxorubicin-induced cardiotoxicity via inhibition of oxidative stress, MAP kinase activation, NF-kB pathway, PI3K/Akt/mTOR impairment, and cardiac apoptosis, Food Chem. Toxicol. 125:503-519.
38. Sergeeva IA, Christoffels VM, 2013. Regulation of expression of atrial and brain natriuretic peptide, biomarkers for heart development and disease. Biochim. Biophys. Acta. 1832:2403-2413.

39. Singh R, Kaur N, Kishore L, Gupta GK, 2013. Management of diabetic complications: A chemical constituents based approach. J. Ethnopharmacol. 150(1):51-70.
40. Singh RM, Waqar T, Howarth FC, et al., 2018. Hyperglycaemia-induced cardiac contractile dysfunction in the diabetic heart. Heart Fail. Rev. 23:37-54.
41. Song Y, Wen L, Sun J, et al., 2016. Cytoprotective mechanism of ferulic acid against high glucose induced oxidative stress in cardiomyocytes and hepatocytes. Food Nutr. Res. 60:30323.
42. Soumya RS, Vineetha VP, Salin Raj P, Raghu KG, 2014. Beneficial properties of selenium incorporated guar gum nanoparticles against ischemia/reperfusion in cardiomyoblasts (H9c2). Metallomics. 6:2134-47.
43. Suzuki A, Yamamoto M, Jokura H, et al., 2007. Ferulic acid restores endothelium-dependent vasodilation in aortas of spontaneously hypertensive rats. J. Am. Soc. Hypertens. 20:508-513.
44. Waldman M, Cohen K, Yadin D, et al., 2018. Regulation of diabetic cardiomyopathy by caloric restriction is mediated by intracellular signaling pathways involving 'SIRT1 and PGC-1α'. Cardiovasc. Diabetol. 17:111.
45. Wong PC, Guo J, Zhang A, 2017. The renal and cardiovascular effects of natriuretic peptides. Adv. Physiol. Educ. 41:179 -185.
46. Wu S, Zou MH, 2019. Mitochondria-associated endoplasmic reticulum membranes in the heart. Arch. Biochem. Biophys. 662:201-212.
47. Yoshimura M, Yasue H, Ogawa H, 2001. Pathophysiological significance and clinical application of ANP and BNP in patients with heart failure. Can. J. Physiol. Pharmacol. 79:730-735.
48. Zhang L, Qin X, Zhao Y, et al., 2012. Inhibition of histone deacetylases preserves myocardial performance and prevents cardiac remodeling through stimulation of endogenous angiomyogenesis. J. Pharmacol. Exp. Ther. 341:285-293.

Chapter 3

Investigation on mitochondrial dysfunction during hyperglycaemia in *in vitro* model and amelioration with ferulic acid

3.1. Introduction

Diabetes mellitus (DM) alters cardiac performance in many ways as the secondary complications to the cardiovascular system; one among such complications is diabetic cardiomyopathy (DCM). The cardiomyocyte death and the increase in the dysfunctional cardiac muscle are the major causes for the DCM. The cellular destruction process begins in the subcellular defects. Since myocytes require more energy for the muscle contraction, the mitochondrial mass and function play a vital role in the normal functioning of the heart. Researchers found that hyperglycaemia induced oxidative stress via mitochondria dysfunction is the primary culprit of myocyte apoptosis and destruction. It links mitochondrial function with its membrane integrity and plasticity.

Mitochondrial function is to convert the metabolic intermediates derived from nutrients into heat and ATP, but the mitochondrial dysfunction causes apoptotic and necrotic cell death (Folmes et al. 2012). This directly opposed function of mitochondria is very much crucial in the heart and brain, where over 90 % of the energy demands were supplied by mitochondria (Wallace, 2005). The opening or activation of the mitochondrial permeability transition pore (mPTP) is shown to be the germ point of the mitochondrial functions (Kwong & Molkentin, 2015) at some points. The opening of mPTP causes an immediate rise in the inner mitochondrial membrane permeability to ions and small solute molecules since it is a high conductance channel. These changes also affect the regulation of the mitochondrial membrane potential, calcium homeostasis, reactive oxygen species (ROS) production, ATP production, and cell death (Elrod et al. 2010; Hou et al. 2014; Galluzzi et al. 2009). The mPTP is a significant factor for the health and disease since it is functioning as the primary arbitrator of both cell development and death.

The mPTP is reported to participate in some of the crucial cell death mechanisms. The mPTP channel is involved in the metabolic regulation of cellular processes such as cell energy homeostasis, mitochondrial calcium

transport, and superoxide efflux (Izzo et al. 2016). The outer mitochondrial membrane voltage-dependent anion channel (VDAC), the inner membrane protein - adenine nucleotide translocator (ANT), and the mitochondrial matrix protein cyclophilin D (CyPD) are the three principal proteins of mPTP formation along with the BH3 phosphate carrier, and p53 protein as the mitochondrial interacting molecules (Rao et al. 2014; Elrod & Molkentin, 2013). The mPTP opening also lowers the transmembrane electrochemical gradient (ΔΨm) and increase of mtROS production (Madamanchi & Runge, 2007; **Fig.3.1**)

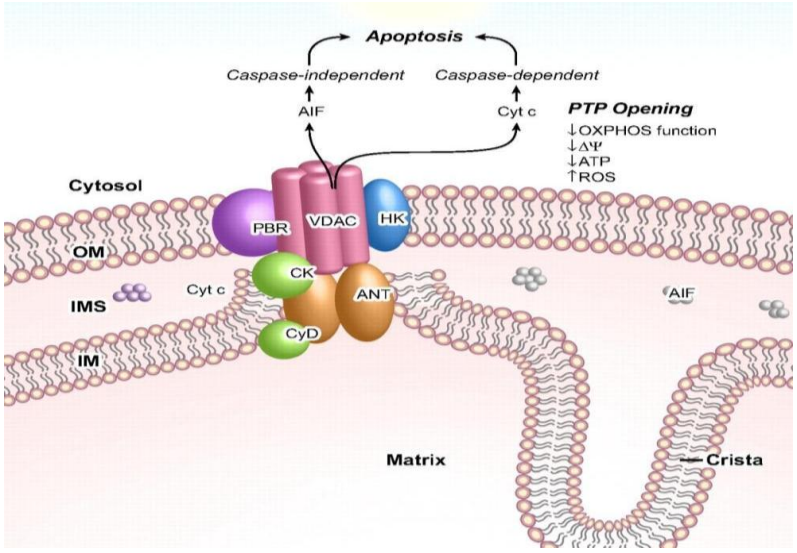

Figure.3.1. Mitochondrial permeability transition pore (mPTP). Schematic representation of proteins in the mPTP complex and their pathologic effects (Madamanchi & Runge, Circ. Res. 2007)

Myocardial cell death via autophagic cell death, apoptosis, and necrosis are observed in the hearts of diabetic patients and animal models (Galluzzi et al. 2018). Some researchers have elucidated the mechanisms and pathway for apoptosis in the myocardium (Riswan & Bhuvaneshwari, 2019). In the normal physiology of the heart, the mPTP was found to be kept closed. One of the mechanisms suggests that under pathological conditions such as hyperglycaemia the mPTP opening allows the entry of solutes and

H_2O, causing the mitochondrial swelling and release of apoptotic factors which ultimately results in apoptosis.

The physiological contact point of endoplasmic reticulum (ER) and mitochondria, the mitochondria associated ER membranes (MAM), is emerging as a novel potential target for various energy metabolism linked pathological conditions. The molecular tethers, a critical protein of mPTP - Vdac1, Ip3r2, Fundc1, glucose-regulated protein 75 (Grp75) chaperone, the mitochondrial shape and dynamics regulators - Drp1 and Mfn2, and the matrix multifunctional sorting protein Pacs2 are the principal elements of MAM (Wu et al. 2019). Since MAMs consist of many crucial proteins, structural disturbances to MAMs may impart pathogenesis in various diseases. MAM is recently known for its exemplary role in energy metabolism and associated diseases (Wu & Zou, 2019; Swapna et al. 2020). The present-day knowledge of inter-organelle communication like MAM has revised the formerly gained “mitochondria-centred” impression that the modulation of crucial activities such as metabolism and cell death, could happen only in a mitochondrion-autonomous (unidirectional) way (Bock & Tait, 2020). Even though mitochondria play a crucial part in cellular health, it is now visible that cellular operations necessary for the cell’s destiny are regulated by the dynamic junction ‘MAM’. Thus, MAMs now is an essential cellular platform for maintaining cellular homeostasis via the exchange of molecular signals and lipid and protein complex formation (Tubbs et al. 2018).

Still, the exact mechanism of apoptotic initiation from MAM, mPTP and $\Delta\Psi m$ dissipation is unclear. Researchers are unable to design a target-oriented strategy for drug development for diabetes and associated complications such as DCM, which is still one of the unmet medical needs. Both the intrinsic and extrinsic pathways of apoptosis were reported in DCM (Chen et al. 2020). However, in-depth knowledge of pathological inducers of apoptosis during hyperglycaemia is not defined in the literature. However, the role of hyperglycaemia induced mitochondrial dysfunction and associated complications leading to DCM is reported (Galloway & Yoon, 2020).

Similarly the defect in Ca^{2+} handling (Swapna et al. 2020) and the role of SERCA/PLN pathway, which play a prominent role during hyperglycaemia, is also not known. So in the present chapter, we explored the role of MAM and SERCA pathway in the genesis of DCM using an in *vitro* model focussing apoptosis in order to elucidate the importance of MAM in the genesis of DCM through multiple pathways. We have focussed our study on apoptosis because of the already known fact that cell death is expected to be the final pathway of cardiomyocyte during DCM. So far, the potential of MAM in the induction of apoptosis via mitochondrial dynamics and OxPhos is not explored by anybody else. So we attempted to check the link of MAM with mitochondrial dynamics and OxPhos in the genesis of apoptosis in H9c2 cells.

3.2. Materials and methods

3.2.1. Chemicals and reagents

Ferulic acid, metformin hydrochloride, D-glucose, mannitol, dimethyl sulfoxide (DMSO), cobalt chloride, mitochondria staining kit, Krebs-Ringer bicarbonate buffer (KRB), radioimmunoprecipitation assay (RIPA) buffer, protease inhibitor cocktail were purchased from Sigma-Aldrich, USA. MitoSox and Calcein AM were purchased from Invitrogen™, Fisher Scientific, USA. Dulbecco's Modified Eagle's Medium (DMEM), fetal bovine serum (FBS), Hank's Balanced Salt Solution (HBSS), penicillin-streptomycin solution and trypsin-EDTA solution were from GIBCO®, Life Technologies, USA. Primary and secondary western blot antibodies were purchased from Cell Signalling Technology, USA. All other solvents and reagents used were of analytical grade unless or otherwise mentioned.

3.2.2. Cell culture and induction of hyperglycaemia

H9c2 cardiomyoblast cells (American Type Culture Collection (ATCC), CRL-1446; Rockville, MD USA) were grown in DMEM supplemented with 10 % FBS, 1 % penicillin-streptomycin solution and incubated at 5 % CO_2 and 37

°C in a humidified incubator (Eppendorf, USA). The hyperglycaemia was induced according to the previous protocol (Cai et al. 2002). Briefly, when the cell populations reached 50-60 % confluence, the cultures for treatment with high glucose (HG) were changed to the DMEM containing a final concentration of 33 mM d-glucose for 48 h, and exposed to 5.5 mM D-glucose (NG) as control. The hyperosmolar effect was excluded through the analysis done in Chapter 2, and not included in the experiments of this chapter.

Experimental groups:

C - Control (5.5 mM glucose)

CF - Control + ferulic acid (FA -25 µM)

HG - High glucose (33 mM glucose)

HGF1 - High glucose + FA (10 µM)

HGF2 - High glucose + FA (25 µM)

HGM - High glucose + metformin (Met -10 µM).

The FA and Met were co-treated with the HG for 48 h in the experimental groups. For the western blot analysis, the CF group was not included since there is no significant effect in this group and is found similar to the control.

3.2.3. Mitochondrial permeability transition pore (mPTP)

The mPTP opening was observed with calcein-AM dye in the presence of CoCl2 as previously described protocol (Bonora et al. 2016). Briefly, after the respective experimental procedure, the culture medium was removed and washed with KRB, and added 1 ml of calcein loading solution (containing 1 µM calcein- AM and 2 mM $CoCl_2$ in KRB); and incubated for 15 min at 37 °C in a 5 % CO_2 atmosphere. Then washed twice with KRB and images of cells were taken (BD Pathway™ 855 High-Content BioImager System, AttoVision software, BD Biosciences, USA); and fluorescent intensity was measured by a microplate reader (Infinite® M200 PRO, Tecan Group Ltd, Switzerland) at excitation/emission of 488/525 nm.

The expression specific proteins of mPTP complex such as Vdac1, Ant1 and the regulatory protein CypD in various treatment groups were

analysed by western blot from the proteins extracted from the cell lysate, after equalising the protein concentration.

3.2.4. Mitochondrial transmembrane potential (ΔΨm)

The change in ΔΨm was detected using the JC-1 mitochondria staining kit (Sigma-Aldrich, St. Louis, MO, USA). Briefly, after the experimental period, 5 µM of JC-1 was added and incubated for 30 minutes at 37 °C. In the live cells, JC-1 exists either as a green-fluorescent monomer at depolarised membrane potentials or as an orange-fluorescent J-aggregate at hyperpolarised membrane potentials. The cell images were taken (BD Pathway™ 855 High-Content BioImager, BD Biosciences, USA) at excitation 490 nm and the emission was collected at 530 nm (monomer) and 590 nm (aggregate) and analysed with ImageJ software. Valinomycin was used as the negative control.

The fluorescent intensity was measured by a microplate reader (Infinite® M200 PRO, Tecan Group Ltd, Switzerland). For JC-1 monomers, the fluorometer was set at ex/em wavelengths of 490/530 nm (green), and for JC-1 aggregates, fluorescence was read at 525/590 nm (red) ex/em wavelengths, and the results were expressed as the ratio of aggregate/ monomer (red/green).

3.2.5. Estimation of mitochondrial superoxide production

The mitochondrial superoxide production was evaluated with MitoSOX™ Red reagent (Molecular Probes, Inc, Invitrogen, Ltd., UK). Briefly, the cells were incubated with MitoSOX (5 µM in HBSS) reagent for 10 min at 37 °C, then washed three times with HBSS and images were taken (BD Pathway™ 855 High-Content BioImager, AttoVision software, BD Biosciences, USA). The fluorescent intensity was analysed at an excitation/emission of 510/580 nm (Infinite® M200 PRO, Tecan Group Ltd, Switzerland)

3.2.6. Mitochondrial superoxide dismutase (MnSOD) activity

The MnSOD activity was measured using the superoxide dismutase assay kit (Cayman chemical, Ann Arbor, MI, USA). Briefly, after treatment, the cells were harvested using a cold plastic cell scraper and collected by centrifugation at 2000 x g for 10 min at 4 °C. Then the pellet was homogenised in a cold sucrose buffer (pH 7.2) and centrifuged at 1500 g for 5 min at 4 °C, and the supernatant was collected. This was then again centrifuged at 10000 x g for 15 min at 4 °C, and the pellets were collected. Then pellet was homogenised in a cold sucrose buffer (pH 7.2) and used for assay as MnSOD source. The assay was conducted in 96 well plates, and for the reactions 200 µl of the diluted radical detector (supplied with kit) and 10 µl of the sample was mixed. Then the reaction was initiated by adding 20 µl of xanthine oxidase enzyme (supplied with kit), mixed well and incubated for 30 min at room temperature on a shaker. The absorbance was read at 460 nm. A set of standards were also run and calculated the activity of MnSOD from the standard curve.

3.2.7. Analysis of SERCA/PLN pathway

The Ca^{2+} homeostasis was evaluated by the SERCA/PLN pathway. The proteins of this pathway, such as Serca 2/1, Pln, pPln, Pkacα, pPkacα were analysed by western blot. The expression level was analysed from the densitometric data calculated using ImageJ software.

3.2.8. Analysis of mitochondria associated ER membrane (MAM) function

The mitochondrial interaction with ER, the MAM was assessed in protein level. The MAM proteins such as Pacs2, Ip3r2, Fundc1, Vdac1, and Mcur1 were examined for their expression studies using western blot. The band intensity was measured using ImageJ software, and densitometric data was calculated to compare the protein expression to control.

3.2.9. Evaluation of mitochondrial biogenesis and dynamics

Mitochondrial biogenesis and dynamics were analysed in protein level from the total protein fraction isolated from H9c2 cells after the respective treatment. The expression of biogenesis factor Pgc1α, mitochondrial fission proteins Fis1 and Drp1; and the fusion proteins such as Mfn2 and Opa1 were analysed by western blot and densitometric analysis were done using the intensity calculated with ImageJ software.

3.2.10. Isolation of mitochondria

The mitochondria were isolated using mammalian mitochondria isolation kit for tissue and cultured cells (BioVision, USA). Briefly, after the treatment, the cells were harvested by centrifugation at 600 x g for 10 min and carefully removed the supernatant. The pellet was homogenised in a mitochondria isolation buffer and centrifuged at 600 x g for 10 min at 4 °C, and the supernatant was collected. The supernatant was again centrifuged at 7000 x g for 10 min at 4 °C and collected the pellet. Then the mitochondrial pellet was washed with a mitochondria isolation buffer and removed the supernatant and stored in the pellet in a storage buffer. Then the protein concentration was seen (Thermo Scientific™, USA) and equalised with the storage buffer and used for western blotting.

3.2.11. Determination of oxidative phosphorylation (OxPhos) function

The activities of complexes (Cx) of OxPhos was analysed with western blot. The OxPhos complex proteins are multi-subunit protein complexes, and the active components of these Cx such as NADH: ubiquinone oxidoreductase 1 beta subcomplex subunit 8 (NDUFB8, CxI), succinate dehydrogenase complex, subunit A (SDHA, CxII), succinate dehydrogenase complex, subunit B (SDHB, CxII), ubiquinol-cytochrome C reductase core protein 2 (UQCRC2, CxIII), mitochondrially encoded cytochrome c oxidase 1 (MTCO 1, CxIV), and ATP synthase F1 subunit alpha (ATP5A, CxV) were selected for expression studies.

3.2.12. ATP content assay

The quantitative bioluminescent determination of ATP content was done using ATP bioluminescent somatic cell assay kit (Sigma-Aldrich, USA). Briefly, after the respective treatment, 2 x 10^5 cells/ mL were collected. 0.1 ml of ATP assay mix working solution was added to an adequate number of vials for test and standards and labelled as reaction vials. It was swirled and kept at room temperature for ~3 min. Then 0.1 ml of 1 X somatic cell ATP releasing reagent, 0.05 ml of ultrapure water and 0.05 ml of the cell sample or ATP standards were swirled briskly. Then 0.1 ml from each tube was transferred to the reaction vial, and immediately measured the amount of light emitted with a luminometer. The ATP content of the cell samples was calculated from the standard curve.

3.2.13. Evaluation of expression of apoptotic proteins

The various apoptotic triggers and the mitochondrial released pro-apoptotic factors such as Jnk, Bax, Aif, EndoG, Smac, HtrA1, Arts, Cytc; and the cytosolic apoptotic effectors such as Apaf1, Casp9, Casp3, Xiap and Ub were analysed by western blot. The β-actin (housekeeping protein) was used as a loading control to normalise the protein expression.

3.2.14. Annexin V-FITC/propidium iodide (PI) double staining assay for apoptosis

The extend of apoptotic and necrotic cell death was assessed by flow cytometric analysis using Annexin V-FITC/propidium iodide (PI) double-staining using the Annexin V-FITC apoptosis detection kit (BioVision Research Products, Linda Vista Avenue, Mountain View, CA, USA.). Briefly, after respective treatments, H9c2 cells were gently trypsinised and collected 1-5 x 10^5 cells by centrifugation; and washed cells once with serum-containing media. The cells were resuspended in 500 µl of 1 X binding buffer, and then added 5 µl of Annexin V-FITC and 5 µl of propidium iodide. It was incubated at room temperature for 5 min in the dark and analysed Annexin V-FITC

binding by flow cytometry (BD FACS Aria II flow cytometer, BD Biosciences, San Jose, CA, USA) at ex/em wavelengths 488/530 nm using FITC signal detector and PI staining by the phycoerythrin emission signal detector. The acquisition and analysis of flow cytometric data were carried out using BD FACS Diva software.

3.2.15. Western blot

For the western blot analysis, equal amounts of proteins (25 µg) were run in a 10 % SDS-PAGE, and transferred to PVDF membranes using Trans-Blot® Turbo™ Transfer system (Bio-Rad, USA). The membranes were then blocked with 5 % defatted (skimmed) milk in TBST (50 mM Tris, pH 7.5, 150 mM NaCl, 0.01% Tween-20) for 1 h at room temperature. The membrane was washed three times with TBST for 10 min each. The membrane was incubated at 4 °C overnight with primary antibodies of various proteins of interest. It was washed with TBST, and the membrane was incubated with HRP-conjugated corresponding secondary antibodies for 1 h at room temperature. The membranes were developed using Western BLoT Hyper HRP Substrate (Takara Bio Inc. USA) after washing three times with TBST, and the protein bands were analysed by stain-free imaging capabilities of the Bio-Rad ChemiDoc MP imaging systems, using image lab software (Bio-Rad, USA). The band intensity was quantified in ImageJ software and normalised to control to analyse the expression pattern.

Statistical analysis

The statistical analyses were done using the SPSS statistics (for Windows, Version 22.0. Armonk, NY). The significant difference at $p < 0.05$ among the means for the groups were assessed using Duncan's multiple range tests after the one-way ANOVA analysis. The results were presented as the mean ± standard deviation (SD) for the control and experimental groups.

3.3. Results

3.3.1. HG-induced the opening of mPTP by altering the protein expressions in H9c2 cells

We evaluated the mPTP opening by calcein-AM/$CoCl_2$ bio-imaging as a marker of mitochondrial dysfunction. The HG showed a decrease in calcein green fluorescence, indicating the aberrant opening of mPTP lead de-compartmentalisation and quenching of mitochondrial matrix calcein fluorescence by cobalt. The co-treatment with FA showed an increase in the compartmentalised calcein green fluorescence (punctiform mitochondria) showing the protection of mPTP (**Fig. 3.2A**). It was further confirmed by

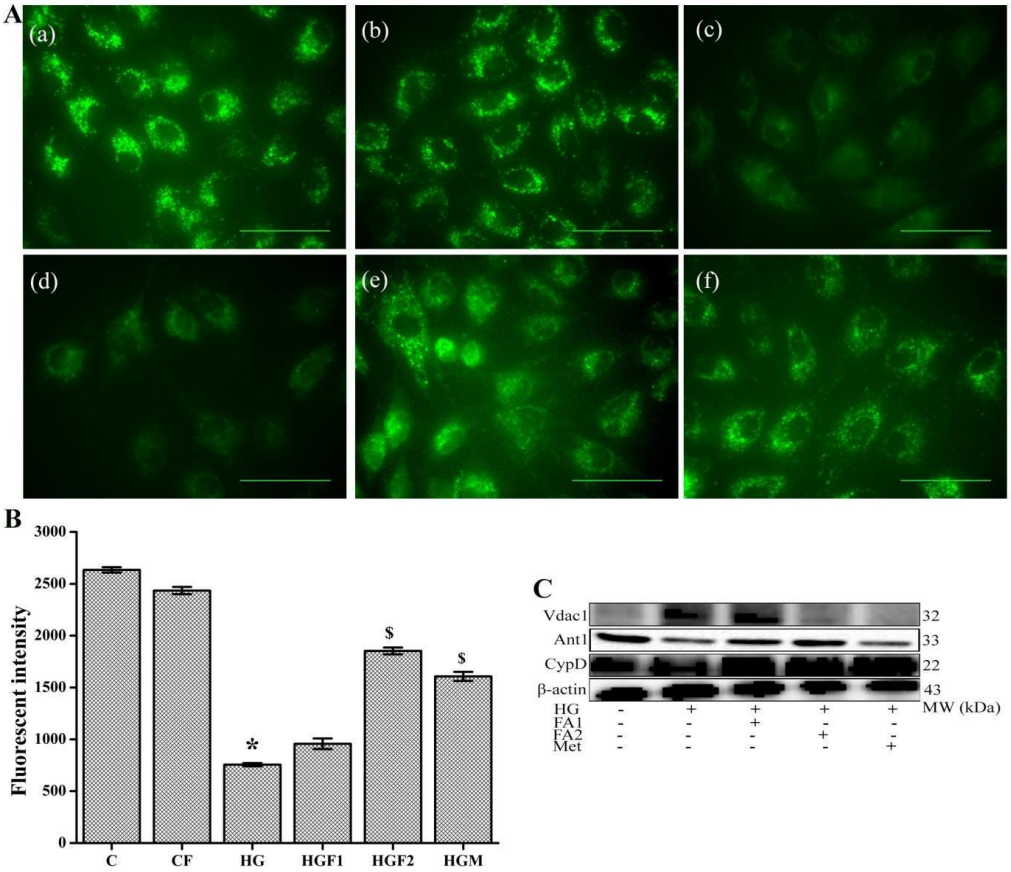

Figure. 3.2. Hyperglycaemia induces the opening of mitochondrial permeability transition pore (mPTP) in H9c2 cells. A, Bioimaging of mPTP opening (calcein fluorescence) in H9c2 cells grown under the treatment of (a) NG (5.5 mM d-glucose), (b) FA (25 µM), (c) HG (33 mM d-glucose), (d & e) FA (10 or 25 µM), or (f) Met (10 µM) conditions

for 48 h. Images are representative of six independent (n=6) experiments. Scale bar - 100 µm. **B,** Fluorescent intensity analysis of calcein fluorescence (mean ± SD, n=6, * $p < 0.05$ vs. control and # $p < 0.05$ vs. hyperglycaemia). C, indicates control (NG); CF, NG + 25 µM FA; HG, hyperglycaemia; HGF1, high glucose + 10 µM FA; HGF2, high glucose + 25 µM FA; HGM; high glucose + Met (10 µM). **C**, Western blot analysis of proteins of interest of mPTP, images are representative of six independent (n=6) experiments. FA indicates ferulic acid; and Met, metformin.

fluorescent intensity analysis (**Fig. 3.2B**). HG showed 71.31 % decrease in the fluorescence and the treatment with FA increased the fluorescence significantly in a dose-dependent manner (21.05 and 48 % for 10 and 25 µM respectively; n=6, $p < 0.05$). The Met also caused increased fluorescent intensity by 37.40 % (**Fig. 3.2B**). The results showed the beneficial effect of FA in maintaining the mitochondrial function during HG in H9c2 cardiomyoblasts.

The effect of HG on mPTP in general, and in particular, the expression of various critical proteins of mPTP such as Vdac1, Ant1, and CypD were analysed. HG caused the loss of integrity of mPTP leading to the aberrant opening of mPTP evidenced by the significant ($p < 0.05$) upregulation in the expression of Vdac1 (8.9 fold) and downregulation of Ant1 (0.5 fold) compared to normal cells. The Cyp D, an activator of Ant1 was also downregulated (0.6 fold) in the HG group. The treatment with FA and Met significantly ($p < 0.05$) safeguarded the integrity by activating CypD and Ant1 and downregulating Vdac1 (**Fig. 3.2C** & **Table. 3.1**).

Groups / Proteins	**Protein folds of control**			
	HG	**HGF1**	**HGF2**	**HGM**
Vdac1	8.95 ± 0.57*	9.39 ± 0.40	3.52 ± 0.27#	2.28 ± 0.36#
Ant1	0.56 ± 0.17*	0.87 ± 0.29#	1.12 ± 0.41#	0.39 ± 0.18
CypD	0.69 ± 0.14*	2.64 ± 0.60#	2.36 ± 0.77#	2.26 ± 0.81#

Table. 3.1. Densitometry analysis of blots of mPTP proteins in H9c2 cells. Fold difference values of intensity of proteins analysed by western blot. Values were fold difference of control, as control normalised to 1 (mean ± SD, n=6, * $p < 0.05$ vs. control and # $p < 0.05$

vs. hyperglycaemia). **HG**, indicates high glucose (33 mM d-glucose); **HGF1**, high glucose cells treated with FA - 10 µM; **HGF2**, high glucose cells treated with FA- 25 µM; **HGM**, high glucose cells treated with Met -10 µM; FA, ferulic acid; and Met, metformin.

3.3.2. HG-induced dissipation of mitochondrial membrane potential (ΔΨm) in H9c2 cells

The ΔΨm was assessed by bio-imaging with mitochondrial staining dye JC-1. In the functional mitochondria, the JC-1 dye was found in aggregate (red) form, and in the dysfunctional mitochondria, the JC-1 was found in monomeric (green) form due to the dissipation of ΔΨm. HG caused increased green fluorescence indicating the dissipation of ΔΨm. The co-treatment with FA (10 and 25 µM) and Met reduced the green fluorescence and increased red fluorescence preventing ΔΨm dissipation (**Fig.3.3A**).

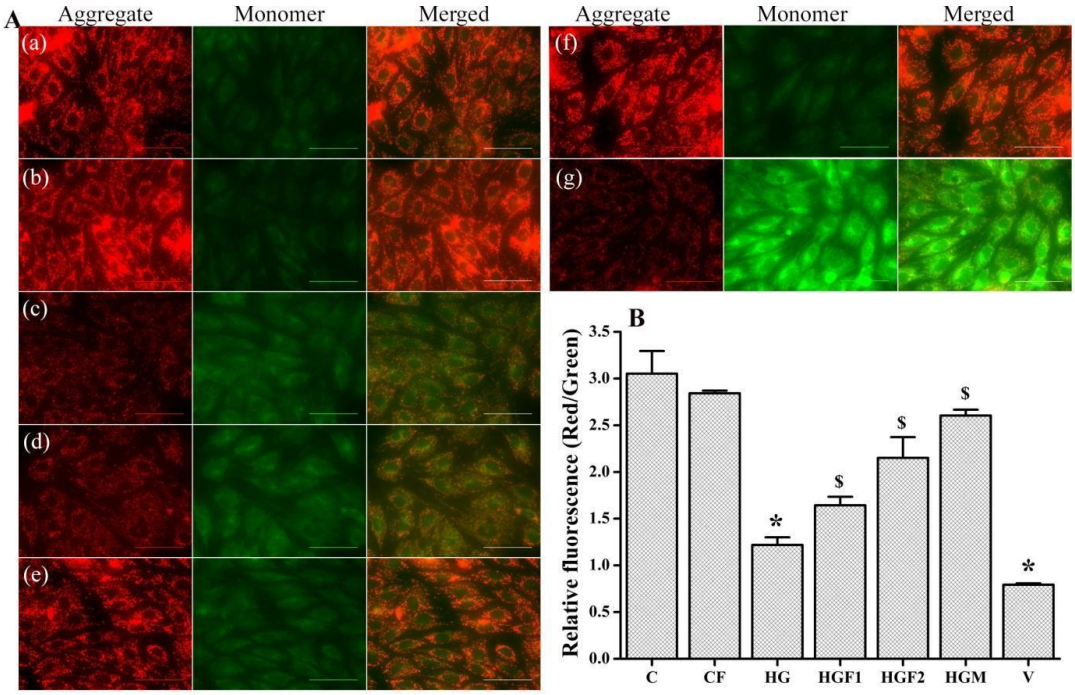

Figure. 3.3. Hyperglycaemia induces dissipation of mitochondrial membrane potential (ΔΨm) in H9c2 cells. A, Bioimaging based analysis of ΔΨm (JC1 fluorescence) in H9c2 cells grown under the treatment of (a) NG (5.5 mM d-glucose), (b) FA (25 µM), (c) HG (33 mM d-glucose), (d & e) FA (10 or 25 µM), (f) Met (10 µM), or (g) valinomycin (negative control) conditions for 48 h. Images are representative of six independent (n=6) experiments. Scale bar - 50 µm. **B,** Fluorescent intensity analysis of JC1 fluorescence – red/green (mean ± SD, n=6, * $p < 0.05$ vs. control and # $p < 0.05$ vs. hyperglycaemia). C, indicates control (NG); CF,

NG + 25 µM FA; HG, hyperglycaemia; HGF1, high glucose + 10 µM FA; HGF2, high glucose + 25 µM FA; HGM; high glucose + Met (10 µM); FA, ferulic acid; and Met, metformin.

This was again confirmed by the fluorescence intensity analysis. HG showed 60.07 % reduction in the aggregate fluorescence indicating the dissipation of ΔΨm. The treatment with FA increased the fluorescence significantly (25.86 and 43.35 % with 10 and 25 µM respectively). Met also protected the membrane potential significantly (53.20 %). The negative control valinomycin causes significant dissipation in ΔΨm (74.04 %; **Fig.3.3B**).

3.3.3. HG increases the mitochondrial superoxide production in H9c2 cells.

In order to evaluate the effect of decreased MnSOD activity in mitochondria, we then analysed the mitochondrial superoxide using MitoSOX™Red reagent. This live-cell permeant and selectively mitochondria-

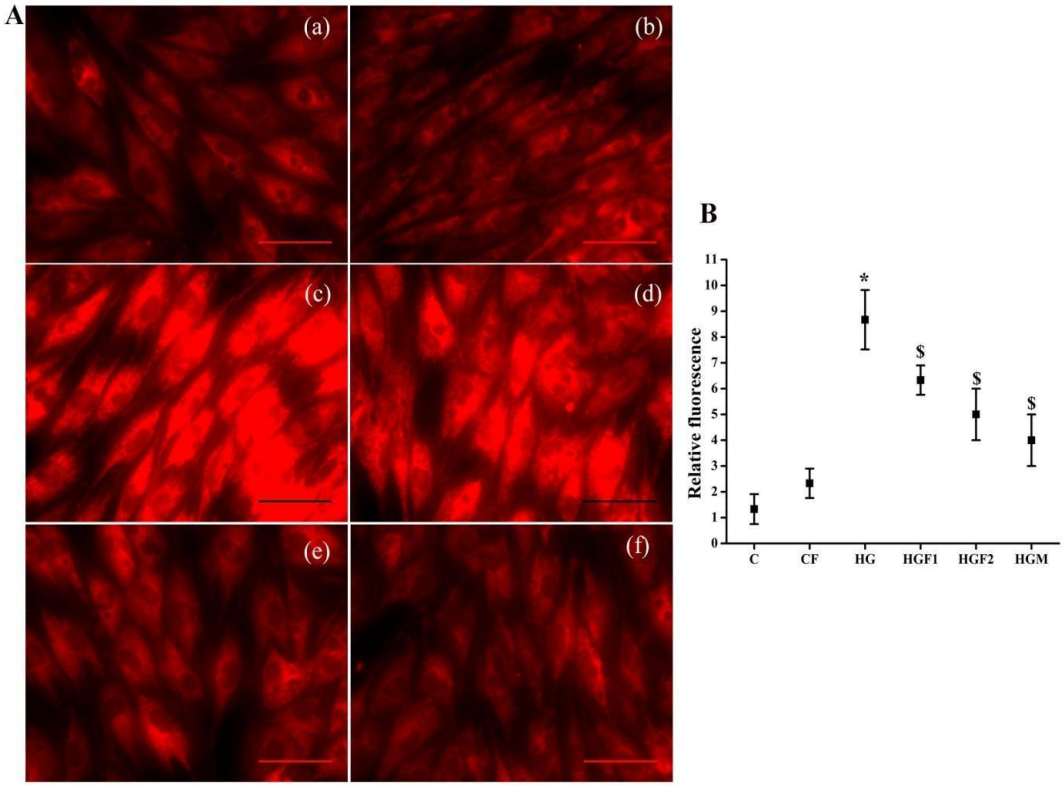

Figure. 3.4. Hyperglycaemia increases the mitochondrial superoxide production in H9c2 rat cardiomyoblast. **A,** Bioimaging based analysis of mitochondrial superoxide

production (MitoSOX™ Red reagent) in H9c2 cells grown under the treatment of (a) NG (5.5 mM d-glucose), (b) FA (25 µM), (c) HG (33 mM d-glucose), (d & e) FA (10 or 25 µM), or (f) Met (10 µM) conditions for 48 h. Images are representative of six independent (n=6) experiments. Scale bar - 100 µm. **B,** Fluorescent intensity analysis of mitochondrial superoxide production (mean ± SD, n=6, * $p < 0.05$ vs. control and # $p < 0.05$ vs. hyperglycaemia). C, indicates control (NG); CF, NG + 25 µM FA; HG, hyperglycaemia; HGF1, high glucose + 10 µM FA; HGF2, high glucose + 25 µM FA; HGM; high glucose + Met (10 µM); FA, ferulic acid; and Met, metformin.

targeted reagent is oxidised by superoxide and exhibits red fluorescence; which is proportional to the superoxide concentration. HG showed increased red fluorescence indicated increased superoxide production. The FA and Met showed a decrease in the fluorescence, revealing the ameliorative effects (**Fig. 3.4A**). This was confirmed by the fluorescent intensity analysis. The HG induced 6.5 - fold increase in the mitochondrial superoxide generation (compared to the control, $p \leq 0.05$), which was reduced significantly by FA (4.75 and 3.5 fold with 10 and 25 µM respectively compared to the control, $p \leq 0.05$; **Fig. 3.4B**). Met also showed a similar trend.

3.3.4. HG reduces the activity of MnSOD in H9c2 cells.

The activity of superoxide radical dismutating enzyme MnSOD was found to have decreased significantly (52.30 %) in hyperglycaemia ($p < 0.05$,

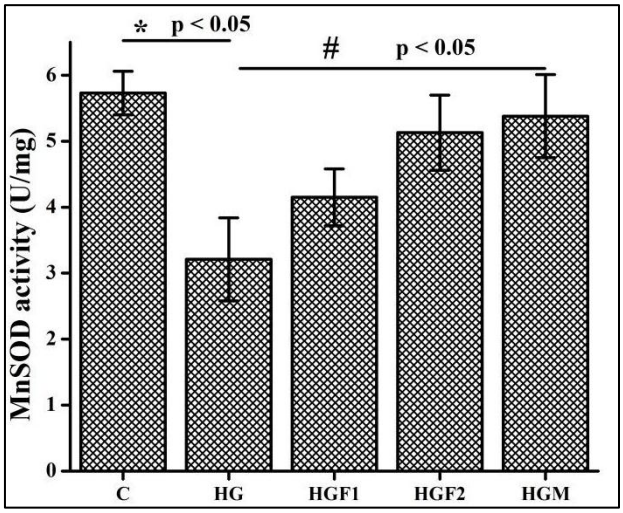

Figure.3.5. Hyperglycaemia reduces the MnSOD activity in H9c2 rat cardiomyoblast. Activity of mitochondrial superoxide dismutase (MnSOD) enzyme in the H9c2 cells grown under the treatment of NG (5.5 mM d-glucose), HG (33 mM d-glucose), FA (10 or 25 µM), or

Met (10 µM) conditions for 48 h (mean ± SD, n=6, * $p < 0.05$ vs. control and # $p < 0.05$ vs. hyperglycaemia). **C** indicates control (NG); **CF**, NG + 25 µM FA**; HG**, high glucose; **HGF1**, high glucose + 10 µM FA; **HGF2**, high glucose + 25 µM FA; **HGM**; high glucose + Met (10 µM); FA, ferulic acid; and Met, metformin.

n=6). The co-treatment with different concentrations of FA (10 and 25 µM) increased the activity of MnSOD significantly by 51.72 and 60.46 % respectively. The metformin also brought back enzyme activity to almost control level (56.44 %, **Fig. 3.5**).

3.3.5. Effect of HG on the MAM and calcium transport

Western blotting showed that HG caused significant upregulation of Pacs2 (3.2 fold), Ip_3r2 (15.2 fold), Vdac1 (8.9 fold), and Fundc1 (3.2 fold) ($p < 0.05$) revealing the physiological importance of MAM in glucose homeostasis **(Fig. 3.6 & Table 3.2)** in H9c2.

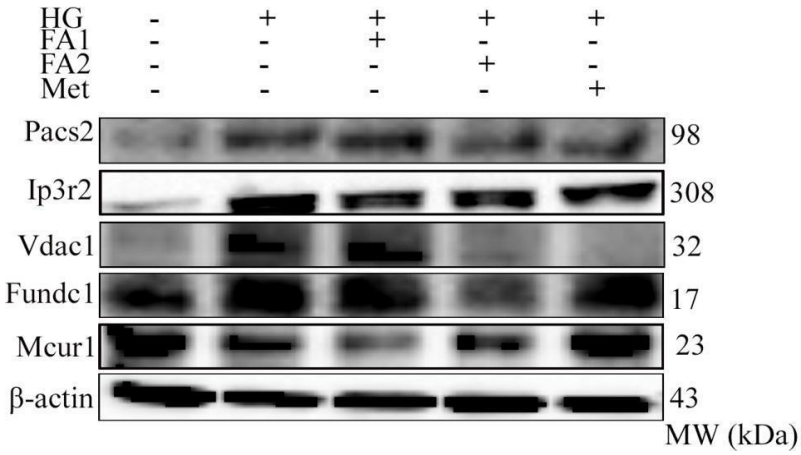

Figure. 3.6. Hyperglycaemia causes alterations in the expression of various vital proteins of mitochondria-associated endoplasmic reticulum membranes (MAMs) in H9c2 rat cardiomyoblasts. Western blot analysis of the proteins of interest in cell lysate prepared from H9c2 cells grown under the treatment of NG (5.5 mM d-glucose), HG (33 mM d-glucose), FA (10 and 25 µM), or Met (10 µM) conditions for 48 h. Images are representative of three independent (n=3) experiments. NG indicates control; HG, hyperglycaemia; FA, ferulic acid; and Met, metformin.

In addition, HG downregulated the master regulator of calcium transport in MAM between ER and mitochondria, Mcur1 significantly (0.8 fold) **(Fig.3.6** & **Table 3.2)**. Co-treatment with FA was useful to bring back most of

the protein (Vdac1, Fundc1, Pacs2, and Mcur1) level to the normal except Ip_3r2 where recovery was slightly less. Met brought back only Vdac11 and Mcur1 to the normal but had little effect on Ip_3r2, Fundc1, and Pacs2.

Groups / Proteins	Protein folds of control			
	HG	HGF1	HGF2	HGM
Pacs2	3.20 ± 0.96*	1.36 ± 0.64#	2.09 ± 0.64	1.99 ± 0.34#
Ip_3r2	15.21 ± 1.03*	11.66 ± 0.82#	13.63 ± 1.48	14.92 ± 1.75
Vdac1	8.95 ± 0.57*	9.39 ± 0.40	3.52 ± 0.27#	2.28 ± 0.36#
Fundc1	3.29 ± 1.29*	3.13 ± 1.21	2.47 ± 0.36#	2.32 ± 0.35#
Mcur1	0.83 ± 0.45*	0.66 ± 0.27	0.96 ± 0.26	1.39 ± 0.69#

Table. 3.2 Densitometry analysis of proteins of MAM of H9c2 cells Folds difference values of intensity of proteins analysed by western blot. Values were folded differences of control, as control normalised to 1. HG indicates high glucose (33 mM d-glucose); HGF1, high glucose cells treated with FA - 10 µM; HGF2, high glucose cells treated with FA- 25 µM; HGM, high glucose cells treated with Met -10 µM. (mean ± SD, n=3, * $p < 0.05$ vs. control and # $p < 0.05$ vs. hyperglycaemia)

3.3.6. Effect of HG on the SERCA/PLN/PKA Cα pathway

To elucidate the mechanism by which HG induces defects in Ca^{2+} homeostasis, we examined the SERCA pathway. The western blot analysis showed that HG downregulated the Serca2 and 1 (0.64 and 0.73 fold), Pln (2.30 fold), Pka cα (1.56 fold) and decreased the expression of pPln (0.44 fold) and pPka cα (0.31 fold), revealing the HG-induced impairment in Ca^{2+} homeostasis. The treatment with FA significantly reversed the effect of HG; it upregulated the SERCA2/1 and increased the phosphorylation of PLN and PKA C-α (n=6) and this was comparable with the positive control Met (**Fig. 3.7**).

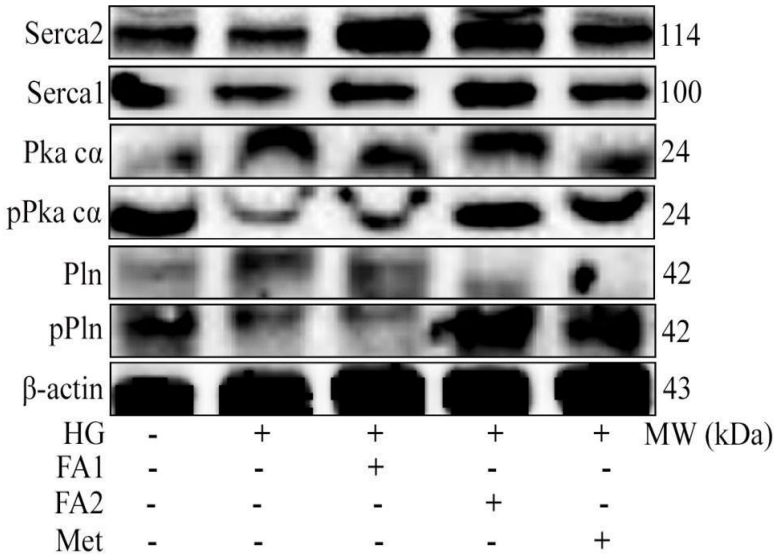

Figure. 3.7. Hyperglycaemia causes alterations in the expression of SERCA/PLN/ PKACα pathway of calcium transport in H9c2 rat cardiomyoblasts. Western blot analysis of the proteins of interest in cell lysate prepared from H9c2 cells grown under the treatment of NG (5.5 mM d-glucose), HG (33 mM d-glucose), FA (10 and 25 µM), or Met (10 µM) conditions for 48 h. Images are representative of three independent (n=6) experiments. NG indicates control; HG, hyperglycaemia; FA, ferulic acid; and Met, metformin.

Groups / Proteins	Protein folds of control			
	HG	HGF1	HGF2	HGM
Serca2	0.64 ± 0.04*	0.99 ± 0.09#	0.92 ± 0.08#	0.79 ± 0.02
Serca1	0.73 ± 0.03*	0.87 ± 0.09	1.03 ± 0.23#	0.77 ± 0.02
Pka cα	1.56 ± 0.06*	1.08 ± 0.15#	1.49 ± 0.28	0.81 ± 0.06#
pPka cα	0.31 ± 0.01*	0.44 ± 0.02	0.64 ± 0.08#	0.59 ± 0.06
Pln	2.30 ± 0.07*	1.97 ± 0.22	0.80 ± 0.06#	0.59 ± 0.03#
pPln	0.44 ± 0.02*	0.26 ± 0.01	1.25 ± 0.07#	0.89 ± 0.06#

Table. 3.3. Densitometry analysis of proteins of SERCA pathway of H9c2 cells Folds difference values of intensity of proteins analysed by western blot. Values were folded differences of control, as control normalised to 1. HG indicates high glucose (33 mM d-glucose); HGF1, high glucose cells treated with FA - 10 µM; HGF2, high glucose cells treated with FA- 25 µM; HGM, high glucose cells treated with Met -10 µM. (mean ± SD, n=6, * $p < 0.05$ vs. control and # $p < 0.05$ vs. hyperglycaemia)

3.3.7. Effect of HG on the mitochondrial biogenesis and dynamics.

Next, we analysed the expression of critical proteins of mitochondrial biogenesis. The biogenesis factor Pgc1α was downregulated (0.7 fold) by HG ($p < 0.05$; **Fig. 3.8** & **Table 3.4**). The treatment with Met and FA prevented the alteration of Pgc1α in a dose-dependent manner. The fusion proteins Mfn2 (0.7 fold) and Opa1 (0.5 fold) were downregulated by HG, and reduced fusion,

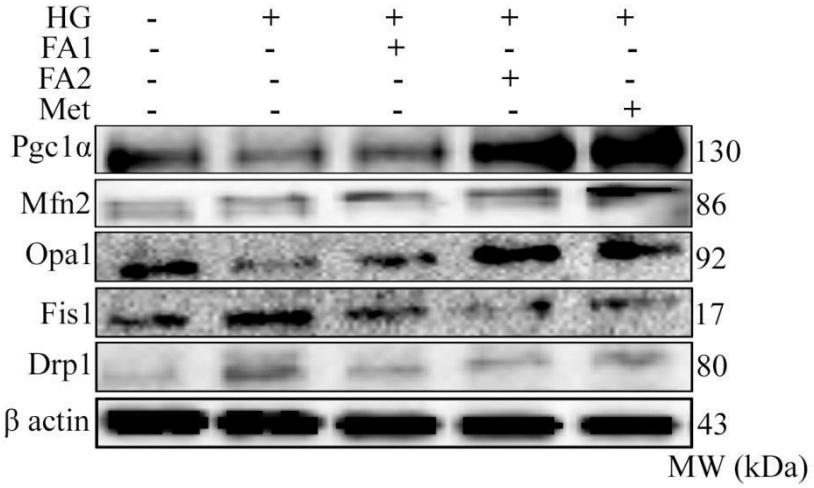

Figure. 3.8. Hyperglycaemia downregulates the marker proteins of mitochondrial biogenesis and fusion and upregulates fission in H9c2 rat cardiomyoblasts. Western blot analysis of the proteins of interest in cell lysate prepared from H9c2 cells grown under the treatment of NG (5.5 mM d-glucose), HG (33 mM d-glucose), FA (10 and 25 µM), or Met (10 µM) conditions for 48 h. Images are representative of three independent (n=3) experiments. NG indicates control; HG, hyperglycaemia; FA, ferulic acid; and Met, metformin.

Groups / Proteins	Protein folds of control			
	HG	HGF1	HGF2	HGM
Pgc1α	0.71 ± 0.27*	0.91 ± 0.65#	1.78 ± 0.73#	2.79 ± 0.79#
Mfn2	0.71 ± 0.15*	1.39 ± 0.35#	1.56 ±0.19#	2.69 ± 0.35#
Opa 1	0.58 ± 0.20*	1.01 ± 0.35#	2.26 ± 0.22#	1.86 ± 0.19#
Fis 1	5.52 ± 0.95*	4.91 ± 0.73	3.02 ± 0.11#	1.23 ± 0.17#
Drp1	8.54 ± 0. 83*	6.82 ± 1.05	4.69 ± 0.96#	4.92 ± 0.09#

Table. 3.4. Densitometry analysis of proteins of mitochondrial dynamics of H9c2 cells Folds difference values of intensity of proteins analysed by western blot. Values were folded differences of control, as control normalised to 1. HG indicates high glucose (33 mM d-

glucose); HGF1, high glucose cells treated with FA - 10 µM; HGF2, high glucose cells treated with FA- 25 µM; HGM, high glucose cells treated with Met -10 µM. (mean ± SD, n=3, * $p < 0.05$ vs. control and # $p < 0.05$ vs. hyperglycaemia).

whereas the co-treatment with FA prevented the downregulation and brought it back to almost normal. The HG caused increased mitochondrial fission by upregulating the fission proteins Fis1 (5.5 fold), and Drp1 (8.5 fold) and the FA treatment blocked the fission process by bringing back the protein level to normal (**Fig. 3.8** & **Table 3.4**). Met also showed the same trend as FA.

3.3.8. Effect of HG on the mitochondrial OXPHOS function and ATP production.

The various OxPhos complex proteins (Cx I NDUFB8, Cx II SDHA and SDHB, Cx III UQCRC2, Cx IV MTCO 1 and Cx V ATP5A) were subjected to

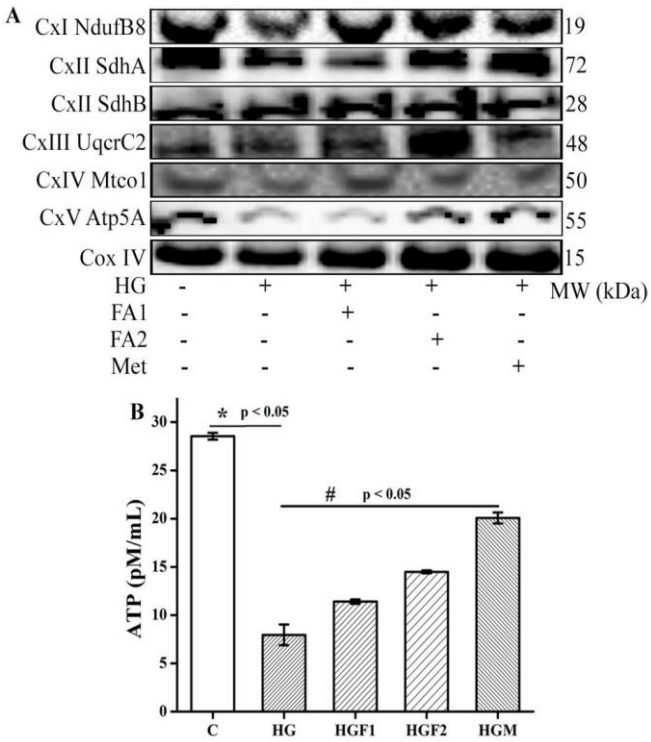

Figure. 3.9. Hyperglycaemia downregulates the various complexes of OxPhos and reduces ATP synthesis in H9c2 rat cardiomyoblasts. A, Western blot analysis of the proteins of interest in mitochondria isolated from H9c2 cells grown under the treatment of NG (5.5 mM d-glucose), HG (33 mM d-glucose), FA (10 and 25 µM), or Met (10 µM) conditions for 48 h. Images are representative of three independent (n=3) experiments. **B,** ATP

concentration determined by bioluminescent assay (mean ± SD, n=6, * $p < 0.05$ vs. control and # $p < 0.05$ vs. hyperglycaemia). NG indicates control (C); HG, hyperglycaemia; FA, ferulic acid; and Met, metformin.

western blotting. The result showed Cx I NDUFB8 (0.6 fold), Cx III UQCRC2 (0.6 fold), Cx IV MTCO 1 (0.5 fold) and Cx V ATP5AIV (0.2 fold) were decreased significantly in HG groups compared to control ($p < 0.05$, n=6). Interestingly Cx II SDHB was not affected. The co-treatment with FA and Met brought back the level to normal ($p < 0.05$, n=6) except Met showed slight inhibition on Cx I. The Cx II subunit SDH A, the connecting link between Krebs cycle and OXPHOS was also studied and found the same has been downregulated (0.6 fold) significantly in HG condition while FA and Met treatment brought the level back to normal (**Fig. 3.9A & Table 3.5**). Similarly, ATP production was found decreased by 72 % in the high glucose condition. Here also applications of FA and Met were found effective to maintain the normal amount of ATP synthesis in a dose-dependent manner (**Fig. 3.9B**).

Groups / Proteins	**Protein folds of control**			
	HG	**HGF1**	**HGF2**	**HGM**
Cx I NDUFB8	0.67 ± 0.05*	1.23 ± 0.49#	1.03 ± 0.07#	0.85 ± 0.02
Cx II SDHA	0.68 ± 0.08*	0.62 ± 0.16	0.94 ± 0.19#	0.99 ± 0.20#
Cx II SDHB	1.08 ± 0.15	1.09 ± 0.07	1.24 ± 0.09	0.94 ± 0.11
Cx III UQCRC2	0.68 ± 0.05*	1.35 ± 0.64#	2.15 ± 0.29#	0.98 ± 0.04
Cx IV MTCO1	0.56 ± 0.09*	2.03 ± 0.48#	0.96 ± 0.12#	0.87 ± 0.05#
Cx V ATP5A	0.20 ± 0.03*	0.34 ± 0.08	0.48 ± 0.05#	0.67 ± 0.08#

Table. 3.5. Densitometry analysis of proteins of complexes of OxPhos of H9c2 cells Folds difference values of intensity of proteins analysed by western blot. Values were folded differences of control, as control normalised to 1. HG indicates high glucose (33 mM d-glucose); HGF1, high glucose cells treated with FA - 10 µM; HGF2, high glucose cells treated with FA- 25 µM; HGM, high glucose cells treated with Met -10 µM. (mean ± SD, n=3, * $p < 0.05$ vs. control and # $p < 0.05$ vs. hyperglycaemia)

3.3.9. HG induces apoptosis through mitochondrial Cyt c/Casp3, Smac/Arts/ HtrA2/XIAP, and Aif/EndoG pathways in H9c2 cells

The analysis of apoptotic stimulants found that Jnk and Bax were upregulated (2.5 and 36.2 fold respectively) in HG. The mitochondrial secretory apoptotic factors Aif and EndoG were also upregulated (1.9 and 1.1 fold respectively) in HG, whereas the treatment with FA downregulated these proteins in a dose-dependent manner (n=6, $p < 0.05$; **Fig. 3.10** & **Table.3.6**). Met downregulated AIF but it has no effect on the release of EndoG.

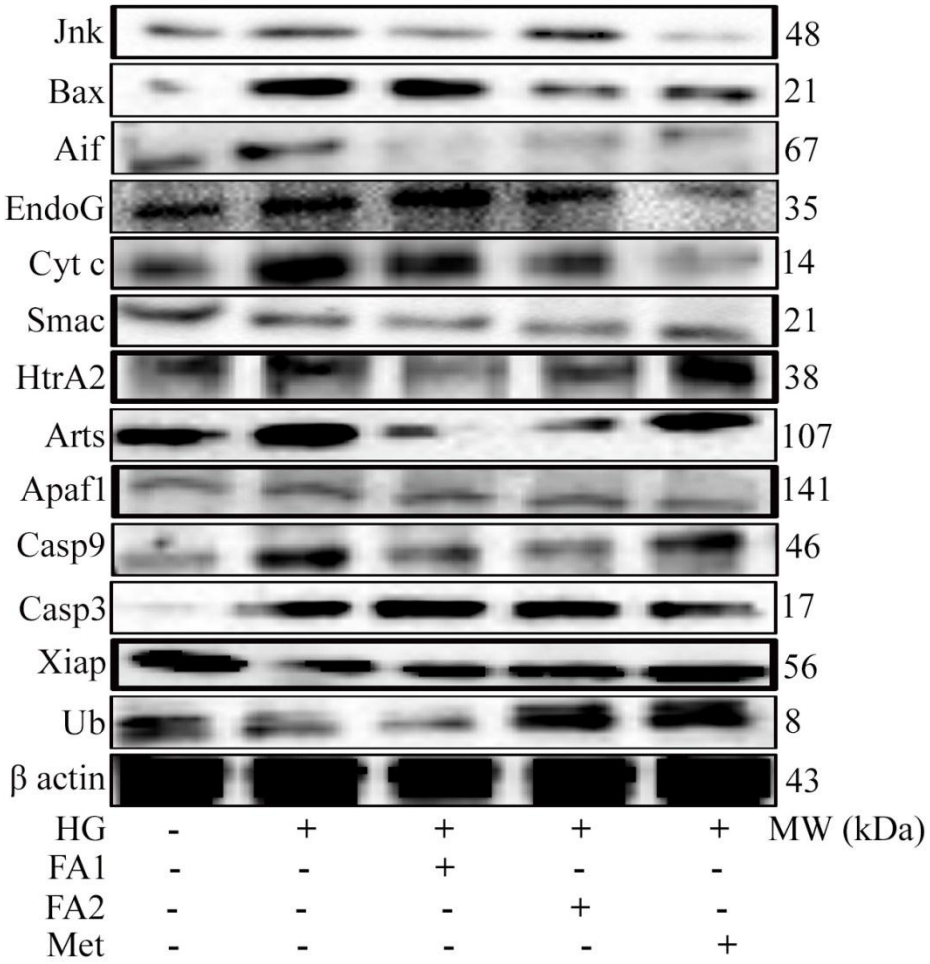

Figure. 3.10. Hyperglycaemia upregulates the mitochondrial caspase-dependent and independent apoptotic pathways in H9c2 rat cardiomyoblasts. Western blot analysis of the proteins of interest in the cell lysate prepared H9c2 cells grown under the treatment of NG (5.5 mM d-glucose), HG (33 mM d-glucose), FA (10 and 25 µM), or Met (10 µM) conditions for 48 h. Images are representative of six independent (n=6) experiments.

The HG is also found to induce Cyt c (3.9 fold) release from mitochondria. The apoptosome proteins Apaf1 (2.8 fold), Casp 9 (2.9 fold) and Casp 3 (20.2 fold) were also found upregulated in HG (n=6, $p < 0.05$). We found the treatment with FA prevented the release of Cyt c, and downregulated Apaf1 and Casp 9 in a dose dependent-manner; but no significant effect on Casp3. However, Met prevented release of Cyt c and downregulated Apaf1; but no significant effect on Casp9 and Casp3 (n=6, $p < 0.05$; **Fig. 3.10& Table 3.6**).

Groups / Proteins	Protein folds of control			
	HG	HGF1	HGF2	HGM
Jnk	2.52 ± 0.17*	1.04 ± 0.09#	2.21 ± 0.06	0.38 ± 0.03#
Bax	36.21 ± 1.81*	31.45 ± 1.66	13.29 ± 1.20#	17.42 ± 1.93#
Aif	1.90 ± 0.28*	0.76 ± 0.05#	0.95 ± 0.06	0.97 ± 0.12
EndoG	1.17 ± 0.22*	0.34 ± 0.05#	0.35 ± 0.03#	0.15 ± 0.03#
Cyt c	3.95 ± 0.28*	0.75 ± 0.04#	0.70 ± 0.10#	0.42 ± 0.05#
Smac	1.63 ± 0.29*	1.63 ± 0.19	1.43 ± 0.04#	1.73 ± 0.16
HtrA2	1.60 ± 0.21*	1.36 ± 0.14#	1.58 ± 0.16	2.31 ± 0.49
Arts	1.90 ± 0.23*	0.46 ± 0.05#	0.65 ± 0.05#	1.72 ± 0.32
Apaf1	2.89 ± 0.61*	2.68 ± 0.19	1.98 ± 0.42#	1.83 ± 0.44#
Casp9	2.98 ± 0.50*	1.28 ± 0.23#	1.04 ± 0.28#	2.51 ± 0.13
Casp3	20.24 ± 1.96*	18.09 ± 1.5	15.18 ± 1.24#	17.37 ± 0.25#
Xiap	0.54 ± 0.06*	0.77 ± 0.05	0.96 ± 0. 14#	0.97 ± 0.06#
Ub	0.47 ± 0.19*	0.69 ± 0.05#	4.59 ± 1.98#	4.59 ± 0.96#

Table. 3.6. Densitometry analysis of apoptotic and antiapoptotic proteins of H9c2 cells Folds difference values of intensity of proteins analysed by western blot. Values were folded differences of control, as control normalised to 1. HG indicates high glucose (33 mM d-glucose); HGF1, high glucose cells treated with FA - 10 µM; HGF2, high glucose cells treated with FA- 25 µM; HGM, high glucose cells treated with Met -10 µM. (mean ± SD, n=3, * $p < 0.05$ vs. control and # $p < 0.05$ vs. hyperglycaemia)

We also studied Xiap, Ub, and Xiap inhibitor proteins such as Smac/Diablo, HtrA2/Omi and Arts, because of the high significance of these

proteins in apoptosis. Smac/Diablo, HtrA2, and Arts were found upregulated (1.6, 1.6, 1.9 fold respectively) during HG. FA application downregulated significantly the Xiap inhibitors Smac/Diablo, HtrA2, and Arts in a dose-dependent manner (n=6, $p < 0.05$). But surprisingly Met has no effect on these Smac/Diablo, HtrA2 and Arts. Also, the Xiap and Ub were found downregulated significantly (0.5 and 0.4 fold respectively) in the HG group (n=6, $p < 0.05$; **Fig. 3.10 & Table 3.6**). The co-treatment with FA upregulated the Xiap and Ub significantly, which was comparable to Met treatment.

Flow cytometry analysis showed that HG caused a significant increase (19.4 %; n=6, $p < 0.05$) in the apoptotic cells compared to control. FA (10 and 25 µM) significantly reduced the apoptotic cells by 6.3 and 10.7 % compared to HG group. Met (10 µM) also reduced the apoptosis by 13.2 % compared to HG groups (n=6, **Fig. 3.11**).

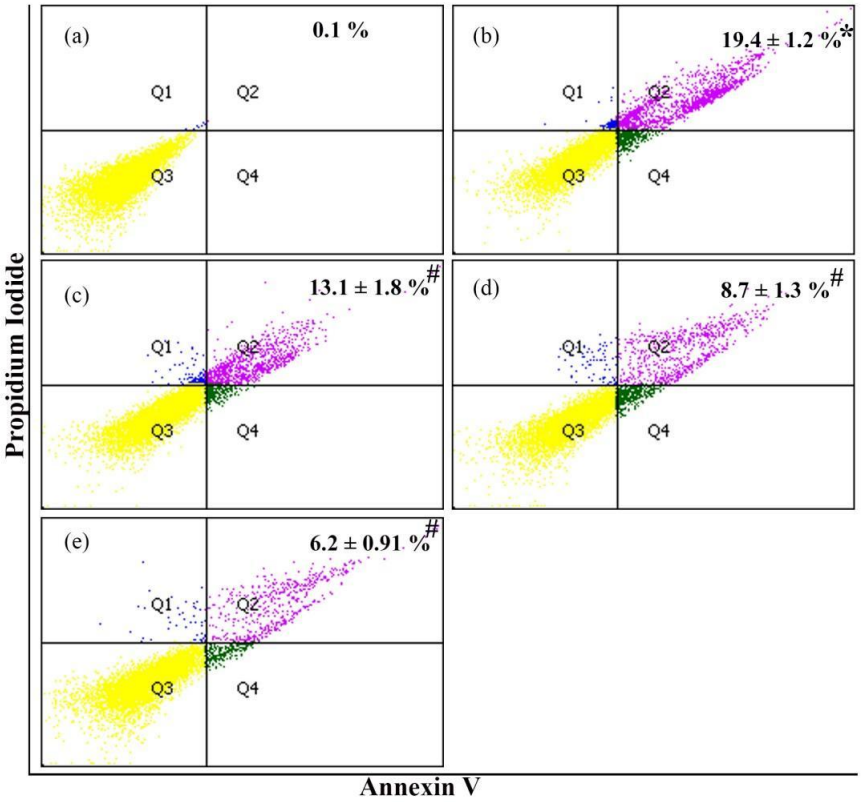

Figure.3.11. Hyperglycaemia induced apoptotic cell death in H9c2 rat cardiomyoblasts. Determination of percentage apoptotic cells by flow cytometry analysis using Annexin V/FITC – PI dual staining (mean ± SD, n=6, * $p < 0.05$ vs. control and # $p < 0.05$ vs. hyperglycaemia).

(a), indicates control (5.5 mM d-glucose); (b), HG, hyperglycaemia (33 mM d-glucose); (c & d), FA, ferulic acid (10 and 25 µM respectively); and (e), Met (metformin - 10 µM) treated conditions for 48 h

3.4. Discussion

In recent days, MAMs have been raised with great interest in heart physiology. MAMs modulate various cellular processes, namely calcium homeostasis, lipid transport, autophagy, and maintenance of redox status in the heart (Wu et al. 2017). The role of MAMs in the context of diabetes has been noticed by some researchers. However, no in-depth investigation aiming for the identification of novel pathways involved in the genesis of pathological lesions associated with DCM has been conducted. The disruption of MAMs integrity associated with the beginning of mitochondrial dysfunction and insulin resistance has been reported by some researchers (Tubbs et al. 2018). Neverthless, no study has been found about the involvement of MAMs induced apoptosis in diabetic cardiomyopathy except one which states the AMPKα2 causes DCM via promotion of MAMs (Wu et al. 2019).

The present chapter focuses on the importance of MAMs and its cross-talk with other important regulators of energy metabolism, cell respiration and redox status in the mitochondria in the genesis of DCM via apoptosis. For this, the behaviour of vital proteins of MAMs such as Pacs2, Ip3r2, Vdac1, and Fundc1 during hyperglycaemia was examined at the protein level. The mitochondrial dynamics maintained the mitochondrial population and other crucial functional properties of mitochondria including the respiratory capacity, so we also studied it in detail. Simultaneously mitochondrial components of energy metabolism - OxPhos were subjected to detailed examination. For this, various complexes of the ETC were analysed. Since the above-referred regulators are significant players of oxidative stress induced apoptosis, and the cardiomyocyte apoptosis had been observed at the final stage of DCM, we performed elaborated investigations at different pathways of apoptosis. We also checked whether FA could prevent the alterations caused by hyperglycaemia in H9c2 cells.

The roles of MAMs are being noticed in various regulatory functions of the cells and genesis of several diseases, mainly because of various special regulatory proteins such as Fundc1, Pacs2, Ip_3r2, Vdac1, Mfn2, and Drp1 in the MAM. In the present study Vdac1, Ip_3r2, Pacs2, and Fundc1 showed upregulation during hyperglycaemia in H9c2 cells. Vdac1 is an essential protein from the outer mitochondrial membrane in ER-mitochondria tethering and also functions as a regulatory component of mPTP, and on upregulation it induces cardiac injury and cell death (Camara et al. 2017). Ip_3r2 is an intracellular Ca^{2+} release channel located in ER and mediates the release of intercellular Ca^{2+} (Okubo et al. 2019). The upregulation of Ip_3r2 causes calcium overload (Galloway & Yoon, 2015), and in the present study, we observed the same trend.

We also found upregulation of Pacs2 and which is known for its role in overall control over mitochondria communication. It is also involved in Cyt c release and activation of Casp3 and the apoptosis (Simmen et al. 2005). Fundc1, a highly conserved protein localised to the mitochondria, interacts with Ip_3r2 and is essential for maintaining the structure of MAMs and ensuring appropriate Ca^{2+} transfer from the ER to mitochondria in the heart. It recruits mitochondria to autophagosomes and promotes mitochondrial fission by directly interacting with Drp1 at MAMs under pathological conditions (Wu et al. 2016). The significant upregulation observed with these proteins causes various processes of cell injury, Ca^{2+} overload, and apoptosis in H9c2 cells which are reported to be markers of DCM.

For detailed information of the underlying mechanism, we explored the SERCA/PLN pathway. SERCA/PLN/PKA C-α is a significant signalling cascade responsible for the transport of Ca^{2+} into the sarcoplasmic reticulum (SR) and regulates intracellular Ca^{2+} homeostasis, SR Ca^{2+} load, and the rate of contraction and relaxation of the heart (Gustavsson et al. 2013). The decrease in the Serca protein level leads to a decrease in SR Ca^{2+} transport, and this is characteristic of failing the human heart (Chen et al. 2005). In the cardiac myocytes, the small molecular weight protein Pln is the primary

regulator of the SERCA pump (Periasamy et al. 2008). The phosphorylation Pln leads to the opening of SRCA pump. The pPka cα, in turn, phosphorylates the Pln and itself. Western blot analysis revealed that HG downregulated the Serca2 and decreased the phosphorylation of Pln and Pka cα, which contributes significantly to the [Ca2+]i overload.

Mitochondrial function is significantly impaired by hyperglycaemic conditions, particularly the integrity markers like mPTP and membrane potential. The transition in mPTP and associated dissipation of membrane potential is reported to induce ([Ca^{2+}]i) overload through the change in membrane integrity and electrochemical concentration gradient via alteration in uniporter (Carri et al. 1997). The change in mPTP and transmembrane potential observed during HG exposure is assumed to be involved in the genesis of intracellular calcium overload (Kruman et al. 1999). We also found downregulation of Ca^{2+} transport regulator protein Mcur1, and mPTP proteins Ant1 and CypD which also have a strong link with MAM. Mcur1 plays a direct role in uniporter-mediated calcium transport via MCU.

The Ant1 catalyses the trafficking of ADP and ATP between cytosol and mitochondria and is also involved in the proton leak (Cheng et al. 2017). CypD regulates the opening of the mPTP, a large conductance pore whose opening depolarises the inner mitochondrial membrane, decreases ATP and increases ROS production (Porter Jr & Beutner, 2018). Downregulation of these proteins affects the function of mitochondria negatively via Ca^{2+} overload, depolarisation of transmembrane potential, depletion of ATP and induction of apoptosis. The study, confirms the regulatory role of MAM over mitochondrial function because of the unique chemistry of MAM comprising exceptional proteins with diverse functions. The behaviour of these critical proteins of MAMs during hyperglycaemia in H9c2 cells and the subsequent impact on the cell reveals the profound influence of MAM over various signalling pathways.

Next, we checked the impact of MAM on mitochondrial biogenesis and dynamics. The marker proteins such as Pgc1α, Opa1 and Mfn2 were found downregulated, revealing biogenesis and mitochondrial fusion were significantly depleted. Pgc1α induces mitochondrial DNA replication and catalyses mitochondrial biogenesis. The decreased expression of Pgc1α causes energy starvation and metabolic defects in the heart cells (Arany et al. 2005). The inner mitochondrial membrane protein OpA1 maintains the membrane integrity and impedes the formation of the pore; thus it mediates the mitochondrial fusion. Mfn 2, a dynamin-related GTPase in mitochondria and MAM is implicated in mitochondrial docking and fusion. Ablation of Mfn1/2 results in mitochondrial fragmentation and cardiovascular diseases (Papanicolaou et al. 2012).

Besides, Mfn2 is also essential for ER-mitochondria juxtaposition, and it is modulated by Ca^{2+} entry into cells mediated by Ip3r2 in the MAM. In the heart muscle, the vital link with mitochondrial network and myocardial contraction has been attributed by the Ip3r2 (Eisner et al. 2017). Also, the defects in Mfn2 function induce structural and functional changes such as cardiac hypertrophy and arrhythmias via impaired Ca^{2+} homeostasis (Porter Jr & Beutner, 2018). The Ca^{2+} overload and cardiac hypertrophy via fibrosis have been identified as potential markers of diabetic cardiomyopathy (Jia et al. 2018), and the alterations of these proteins are found to be the molecular basis of the same. So this is a significant finding of this study.

The upregulation of fission proteins such as Fis1 and Drp1 cause surplus fission of existing mitochondria leading to disintegration of existing mitochondria. The cytosolic protein Drp1 mediates mitochondrial fission through its interaction with the protein Fis1. The essential cell survival and cellular metabolism are affected by these processes that disturb the smooth balance of fission and fusion. In order to meet the cellular demands, ideal mitochondrial morphology and sufficient quantity of mitochondria are maintained by the well-controlled mitochondrial dynamics. Defective fission

and fusion are also linked with the occurrence of apoptotic cell death (Tan et al. 2020).

After confirming imbalance in mitochondrial dynamics with hyperglycaemia, we were eager to see whether hyperglycaemic shock had transmitted from faulty MAM to OxPhos via mitochondrial dynamics because mitochondrial bioenergetics and mitochondrial dynamics are closely related and modulate each other. Mitochondrial respiratory complexes comprise a large supramolecular assembly of individual ETC complexes such as Cx I - NADH: ubiquinone oxidoreductase (NDUF) subunits, Cx II - succinate dehydrogenase (SDH) subunits, Cx III - ubiquinol cytochrome c reductase Cx (UQCRC) subunits, Cx IV - cytochrome c oxidoreductase (MTCO) subunits and Cx V - ATP synthase subunits. They provide highly methodical ATP synthesis and minimise electron leakage and ROS generation. We observed down regulation of Cx I, II - SDH A, III, IV and V, while Cx II – SDH B is not affected during hyperglycaemia in H9c2 cells.

Because Cx I is the primary entry point for electrons to the respiratory chain and is suggested as the rate-limiting step in overall respiration, it plays a central role in energy metabolism. It has been implicated in regulating ROS, which is essential component in various signalling pathways, including apoptosis (Zhang et al. 2016). CxI is also the primary site of non-enzymatic superoxide formation within mitochondria. Cx II of OxPhos consists of four subunits - SDH A to D, and functions as a vital link between the Krebs cycle and ETC. Cx II regulates reserve respiratory capacity (RRC) and cell survival of ventricular cardiomyocyte. Since Cx II consists of multiple subunits, defects in one or more of these subunits could presumably impair RRC and ATP synthesis. We studied the Cx II subunits SDHA and SDHB. Interestingly the SDHA, linked to Krebs cycle was downregulated, and the inner membrane SDHB unaltered during HG. The dysfunction of Cx I and SDHA of Cx II followed by an increase of pro-apoptotic markers proceeds to a transition from compensated left ventricular hypertrophy to heart failure (Circu & Aw, 2010).

Cx III shunts the electrons across the intermembrane space to Cyt c, which brings electrons to Cx IV. Cx III is one of the significant sites of superoxide production inducing hypoxia in the tissue, and we found inhibition of Cx III protein expression. We assume that the defective Cx I, II &III may be the molecular mechanism behind the surplus superoxide generation reported by us in our previous study and others (Galloway & Yoon, 2015).

It is worth adding here that downregulation of CypD and Ant1, the mPTP proteins, found during initial stages of the study also contributes to the defective OxPhos through decreasing ATP synthesis and increasing proton leakage, respectively. Cx V is also found inhibited during hyperglycaemia. Cx V is a prominent player in the synthesis of ATP, and the inhibition of the same causes the depletion of ATP synthesis, which contributes to the depletion of ATP production observed in the study. Impaired OxPhos and impaired ETC function are found to be responsible for most of the cardiac diseases irrespective of causes, because the heart is the most energy-requiring organ in the body. Eventually, these events reveal the loss of integrity of mitochondrial dynamics during hyperglycaemia reduces the efficiency of OxPhos, ATP synthesis and induces surplus ROS generation, establishes the regulatory power of mitochondrial dynamics over OxPhos.

The defective ETC and OxPhos lead to the superoxide production from the mitochondria. The importance of MnSOD in the function of heart through regulation of redox status is a well-established one. Mitochondrial dysfunction causes inhibition of MnSOD and thereby oxidative stress (Preetha et al. 2018). Besides, downregulation of MnSOD paves the way for damaged mitochondrial DNA, sped up the progression of atherosclerosis and proliferation of vascular smooth muscle cells.

Based on the clue of forthcoming apoptosis from above-mentioned experiments and the available report of same in DCM, hereafter our efforts were on an investigation on various pathways leading to apoptosis. Proteins of apoptotic pathways namely Aif, EndoG, Smac/Diablo, Arts, HtrA2/Omi and

Cyt c, Jnk, Bax, Apaf1, Casp9, and Casp3 were found upregulated and antiapoptotic proteins Xiap and Ub were downregulated. From these result, we conclude genesis of apoptosis via Jnk induced Bax mediated pathway originated from mitochondria with the translocation of Cyt c from the mitochondrial intermembrane space into the cytoplasm, where it binds with Apaf1. The Cyt c/Apaf1 forms a complex “apoptosome” with Casp9 and Casp3 in the cytosol and triggers apoptosis, which was visible in this study through upregulation of cytoplasmic Cyt c during hyperglycaemia.

Another mitochondrial apoptotic pathway begins with the release of Xiap inhibitor factors such as Smac/Diablo, HtrA2/Omi, and Arts. These upregulated proteins inhibit Xiap and Ub, which in turns leads to apoptosis. In addition, mitochondria activate the caspase-independent apoptotic pathway through release of nuclear DNA damaging factors such as Aif, and EndoG (Ke et al. 2016; Liang et al. 2015), which were also found increased during hyperglycaemia in H9c2 cells. Based on the upregulation of Aif and EndoG we expect the third pathway of apoptosis in this study. Altogether confirms the role of MAM in the general energy homeostasis of cell and control over mitochondrial dynamics and OxPhos. Disturbances in MAM function lead to upregulation of pro-apoptotic signals which in turn play a prominent role in the development of DCM.

The co-treatment with FA showed significant protection against hyperglycaemia induced molecular and cellular alteration in H9c2 cells and diabetic animals. FA protected MAM integrity, maintained a balance between fission and fusion in mitochondrial dynamics and also maintained the normal status of OxPhos with ATP production almost normal in high glucose medium. It could prevent upregulation of most of the pro-apoptotic proteins. The antiapoptotic and antioxidant property of FA is well established by many researchers (Alam, 2019). Since surplus oxidative stress associated with biochemical complications are found to be the central issue of glucotoxicity, its potent antioxidant activity is found to be beneficial in this study. Contribution

of these pharmacological effects of FA may be responsible for the protective effect in this study.

Although metformin was not a drug for DCM it exhibited protection in most of the cases against hyperglycaemia induced alteration in the H9c2 cells. Similarly, it also showed the efficiency *in vivo* diabetic model. However, it was interesting to note that metformin did not protect the alteration of protein of inner mitochondrial membranes like Ant1, Smac/Diablo, HtrA2/Omi and Arts, which may be due to the non-accessibility of metformin to the inner mitochondrial matrix. Still, metformin seems to be an ideal drug for repurposing for DCM based on results from this study.

Overall, the finding in this chapter justified the importance of MAM in the genesis of hyperglycaemia associated apoptosis and its secondary complication leading to cardiac hypertrophy, fibrosis and insulin resistance. The outcome of this study suspects the common notion that mitochondrial dysfunction is the nucleus of the DCM. However, it is clear now from the study that, not only the function of mitochondria but also the integrity of MAM is also essential to keep normal cellular homeostasis intact. It requires further research on MAM to confirm the prominence of MAM in the DCM to design strategies for drug development. We found apoptosis via three distinct paths is the central root of pathophysiology. The present study opens novel avenues for research for significant drug development where not even a single drug is available exclusive for DCM. FA, a potent phytochemical from a variety of edible vegetables and fruits is found to be an attractive item for nutraceuticals development for cardiac issues arising from diabetes.

References

1. Alam MA, 2019. Anti-hypertensive effect of cereal antioxidant ferulic acid and its mechanism of action. Front. Nutr. 6:121.

2. Arany Z, He H, Lin J, et al., 2005. Transcriptional coactivator PGC-1 alpha controls the energy state and contractile function of cardiac muscle. Cell. Metab. 1:259-271.
3. Bock FJ, Tait SWG, 2020. Mitochondria as multifaceted regulators of cell death, Nat. Rev. Mol. Cell. Biol. 21:85-100.
4. Bonora M, Morganti C, Morciano G, et al., 2016. Comprehensive analysis of mitochondrial permeability transition pore activity in living cells using fluorescence-imaging-based techniques. Nat. Protocol. 11:1067-1080
5. Cai L, Li W, Wang G, et al., 2002. Hyperglycaemia-induced apoptosis in mouse myocardium: mitochondrial cytochrome C-mediated caspase-3 activation pathway. Diabetes. 51:1938-1948.
6. Camara AKS, Zhou Y, Wen PC, Tajkhorshid E, Kwok WM, 2017. Mitochondrial VDAC1: A key gatekeeper as potential therapeutic target. Front. Physiol. 8:460.
7. Carri MT, Ferri A, Battistoni A, et al., 1997. Expression of a Cu, Zn superoxide dismutase typical of familial amyotrophic lateral sclerosis induces mitochondrial alteration and increase of cytosolic Ca^{2+} concentration in transfected neuroblastoma SH-SY5Y cells. FEBS Lett. 414:365-368.
8. Chen X, Zhang X, Kubo H, et al., 2005. Ca^{2+} influx-induced sarcoplasmic reticulum Ca2+ overload causes mitochondrial-dependent apoptosis in ventricular myocytes. Circ. Res. 97:1009-1017.
9. Chen Y, Hua Y, Li X, et al., 2020. Distinct types of cell death and the implication in diabetic cardiomyopathy. Front. Pharmacol. 11:42.
10. Cheng J, Nanayakkara G, Shao Y, et al., 2017. Mitochondrial proton leak plays a critical role in pathogenesis of cardiovascular diseases, Adv. Experiment. Med. Biol. 982:359-370.
11. Circu ML, Aw TY, 2010. Reactive oxygen species, cellular redox systems, and apoptosis. Free Rad. Boil. Med. 48:749-762.
12. Eisner V, Cupo RR, Gao E, et al., 2017. Mitochondrial fusion dynamics is robust in the heart and depends on calcium oscillations and contractile activity, Proc. Natl. Acad. Sci. U.S.A. 114:E859-868.

13. Elrod JW, Molkentin JD, 2013. Physiologic functions of cyclophilin D and the mitochondrial permeability transition pore. Circ. J. 77:1111-1122.
14. Elrod JW, Wong R, Mishra S, et al., 2010. Cyclophilin D controls mitochondrial pore-dependent Ca(2+) exchange, metabolic flexibility, and propensity for heart failure in mice. J. Clin. Investig. 120:3680-3687.
15. Folmes CD, Dzeja PP, Nelson TJ, Terzic A., 2012. Mitochondria in control of cell fate. Circ. Res. 110: 526-529.
16. Galloway CA, Yoon Y, 2015. Mitochondrial dynamics in diabetic cardiomyopathy. Antioxid. Redox Signal. 22:1545-1562.
17. Galluzzi L, Blomgren K, Kroemer G, 2009. Mitochondrial membrane permeabilization in neuronal injury. Nat. Rev. Neurosci. 10:481-494.
18. Galluzzi L, Vitale I, Aaronson SA, et al., 2018. Molecular mechanisms of cell death: recommendations of the nomenclature committee on cell death 2018. Cell Death Differ. 25:486-541.
19. Gustavsson M, Verardi R, Mullen DG, et al., 2013. Allosteric regulation of SERCA by phosphorylation mediated conformational shift of phospholamban. Proc. Natl. Acad. Sci. USA. 110:17338-17343.
20. Hou Y, Ghosh P, Wan R, et al., 2014. Permeability transition pore-mediated mitochondrial superoxide flashes mediate an early inhibitory effect of amyloid beta1-42 on neural progenitor cell proliferation. Neurobiol. Aging. 35:975-989.
21. Izzo V, Bravo-San Pedro JM, Sica V, Kroemer G, Galluzzi L, 2016. Mitochondrial permeability transition: new findings and persisting uncertainties. Trends Cell Biol. 26(9):655-667.
22. Jia G, Hill MA, Sowers JR, 2018. Diabetic cardiomyopathy: an update of mechanisms contributing to this clinical entity. Circ. Res. 122:624-638.
23. Ke W, Yuan Y, Liu X, et al., 2016. Cardiac specific overexpression of mitochondrial Omi/HtrA2 induces myocardial apoptosis and cardiac dysfunction. Sci. Rep. 6:37927.
24. Kruman II, Pedersen WA, Springer JE, Mattson MP, 1999. ALS-linked Cu/Zn-SOD mutation increases vulnerability of motor neurons to

excitotoxicity by a mechanism involving increased oxidative stress and perturbed calcium homeostasis. Exp. Neurol. 160:28-39.

25. Kwong JQ, Molkentin JD, 2015. Physiological and pathological roles of the mitochondrial permeability transition pore in the heart. Cell Metab., 21:206-214
26. Liang X, Ma K, Rao Y, et al., 2015.Characterization of endonuclease G and mitochondria-sarcoplasmic reticulum-related proteins during cardiac hypertrophy. Pharmazie. 70:586-592.
27. Madamanchi NR, Runge MS, 2007. Mitochondrial dysfunction in atherosclerosis. Circ Res. 100(4):460-473.
28. Okubo Y, Kanemaru K, Suzuki J, et al., 2019. Inositol 1,4,5-trisphosphate receptor type 2-independent Ca^{2+} release from the endoplasmic reticulum in astrocytes. Glia. 67:113-124.
29. Papanicolaou KN, Ngoh GA, Dabkowski ER, et al., 2012. Cardiomyocyte deletion of mitofusin-1 leads to mitochondrial fragmentation and improves tolerance to ROS-induced mitochondrial dysfunction and cell death, Am. J. Physiol. Heart Circ. Physiol. 30:H167-179.
30. Periasamy M, Bhupathy P, Babu GJ, 2008. Regulation of sarcoplasmic reticulum Ca2+ ATPase pump expression and its relevance to cardiac muscle physiology and pathology. Cardiovasc. Res. 77:265-273.
31. Porter Jr GA, Beutner G, 2018. Cyclophilin D, somehow a master regulator of mitochondrial function. Biomolecules. 8:176.
32. Preetha Rani MR, Anupama N, Sreelekshmi M, Raghu KG, 2018. Chlorogenic acid attenuates glucotoxicity in H9c2 cells via inhibition of glycation and PKC α upregulation and safeguarding innate antioxidant status. Biomed. Pharmacother. 100:467-477.
33. Rao VK, Carlson EA, Yan SS, 2014. Mitochondrial permeability transition pore is a potential drug target for neurodegeneration. Biochim. Biophys. Acta. 1842:1267-1272.
34. Riswan NA, Bhuvaneshwari P, 2019. Apoptotic cell death in heart failure associated with diabetes. Int. J. Clinicopathol. Correl. 3:12-18.

35. Simmen T. Aslan JE, Blagoveshchenskaya AD, et al., 2005. PACS-2 controls endoplasmic reticulum-mitochondria communication and Bid-mediated apoptosis. EMBO J. 24:717-729.
36. Swapna Sasi US, Sindhu G, Salin Raj P, Raghu KG, 2020. Mitochondria associated membranes (MAMs): Emerging drug targets for diabetes, Curr. Med. Chem. 27:3362.
37. Tan Y, Zhang Z, Zheng C, et al., 2020. Mechanisms of diabetic cardiomyopathy and potential therapeutic strategies: preclinical and clinical evidence, Nat. Rev. Cardiol. 17:585-607.
38. Tubbs E, Chanon S, Robert M, et al., 2018. Disruption of mitochondria-associated endoplasmic reticulum membrane (MAM) integrity contributes to muscle insulin resistance in mice and humans. Diabetes. 67:636-650.
39. Wallace DC, 2005. A mitochondrial paradigm of metabolic and degenerative diseases, aging, and cancer: a dawn for evolutionary medicine. Annu. Rev. Genet. 39:359-407.
40. Wu S, Lu Q, Ding Y, et al., 2019. Hyperglycaemia-driven inhibition of AMP-activated protein kinase α2 induces diabetic cardiomyopathy by promoting mitochondria-associated endoplasmic reticulum membranes in vivo. Circ. 139:1913-1936.
41. Wu S, Lu Q, Wang Q, et al., 2017. Binding of FUN14 domain containing 1 with inositol 1,4,5-trisphosphate receptor in mitochondria-associated endoplasmic reticulum membranes maintains mitochondrial dynamics and function in hearts in vivo, Circ. 136:2248-2266.
42. Wu S, Zou MH, 2019. Mitochondria-associated endoplasmic reticulum membranes in the heart, Arch. Biochem. Biophys. 662: 201-212.
43. Wu W, Lin C, Wu K, et al., 2016. FUNDC1 regulates mitochondrial dynamics at the ER-mitochondrial contact site under hypoxic conditions. EMBO J. 35:1368-1384.
44. Zhang Z, Liu L, Wu S, Xing D, 2016. Drp1, Mff, Fis1, and MiD51 are coordinated to mediate mitochondrial fission during UV irradiation-induced apoptosis. FASEB J. 30:466-476.

Chapter 4

Investigation on alteration in the heart metabolism during T2DM

4.1. Introduction

The increased cardiovascular disorders are the major causes of lethal complications in diabetic patients and hypothesised due to the metabolic alterations in cardiomyocyte during DM. One of the overlooked pathophysiological conditions of DM resulting in heart failure is the DCM. The DCM is increasing day by day, but the underlying mechanisms are still incompletely understood. Human DCM has become a well-documented condition.

The understanding of the molecular mechanisms responsible for human DCM has significantly advanced with the recent research on T1DM, T2DM, and genetically engineered rodent models of obesity, insulin resistance or diabetes. The experimental techniques such as ECG, echocardiography, MRI and CT of heart, used for the investigation of cardiac physiology were adapted for the rodent models to allow comprehensive characteriaation of these models (Bugger & Abel, 2009). In experimental animal models of T1DM and T2DM, the defective cardiomyocyte contractile function and some specific proteins of cardiomyocyte were demonstrated with decreased diastolic and systolic contractile function (Trost et al. 2002). The larger size of rats compared with the mice made it a preferred model for cardiac physiologic measurements. The biochemical parameters like diminished glucose utilisation, increased fatty acid utilisation, impeded calcium handling, compromised mitochondrial energetics, and high connective tissue content in the heart were the prime characteristics of both T1 and T2DM models and were used interchangeably to understand pathophysiological mechanisms of DCM.

However, some pathophysiological mechanisms such as mitochondrial ROS production, fatty acid induced mitochondrial uncoupling of DCM may differ between the T1and T2DM (Herlein et al. 2009). The significant cardiac

abnormalities taken in account for the DCM in the selection of rodent models include decreased diastolic function, cardiac efficiency, mitochondrial energetics, and Ca^{2+} handling, and increased left ventricle mass, fatty acid oxidation, and lipid content (Bugger & Abel, 2009). In the present study, we used a high fat-high fructose diet-induced insulin resistance and diabetic model in Wistar rat model. The onset of dysfunctional cardiac markers such as myocardial steatosis, impaired contractile function and mitochondrial degeneration in Wistar rats is more rapid since these abnormalities will develop in seven weeks of Western diet feeding. The Wistar rats fed on a Western diet showed elevated sarcolemmal CD36 manifested with increased myocardial fatty acid uptake (Ouwens et al. 2007).

The biomarker (troponin, hsCRP, TNNI3K, hFabp, and copeptin) analysis and echocardiography may be employed to confirm the occurrence of hypertrophy, fibrosis, myocardial injury and other pathological lesions in the heart of DCM, which is independent of other comorbidities such as hypertension, congestive heart failure, and significant valvular diseases (Borghetti et al. 2018). The specific and early markers for the diagnosis of DCM still remain as a question due to the poor understanding of the mechanisms in the genesis of DCM.

The striated muscle-specific E3 ligase mitsugumin 53 (MG53, or tripartite motif (TRIM) 72), a newly identified TRIM-containing family protein primarily expressed in cardiac and skeletal muscles, has recently shown to be implicated in intracellular vesicle trafficking, myogenesis, and acute membrane repair in skeletal and cardiac muscles, which constitutes a primary causal factor of systemic insulin resistance and metabolic disorders. The pathophysiological role of MG53 in the induction of cardiac metabolic disorders is still unrevealed. MG53 was initially known for its role in membrane repair (Cai et al. 2009). Song et al. (2013) reported that MG53 leads to ubiquitin-dependent degradation of insulin receptor (IR) and insulin receptor substrate 1 (IRS1) as an E3 ligase, resulting in insulin resistance and metabolic disorders. In the ischemia-mediated cardiac preconditioning and

postconditioning, there reported an increased expression of MG53 in the heart and skeletal muscles (Zhang et al. 2011). The role of MG53 in the myocardial glucose and lipid metabolism remains elusive. However, insulin-dependent glucose metabolism and lipid metabolism are proposed to be regulated by the MG53 (**Fig.4.1**).

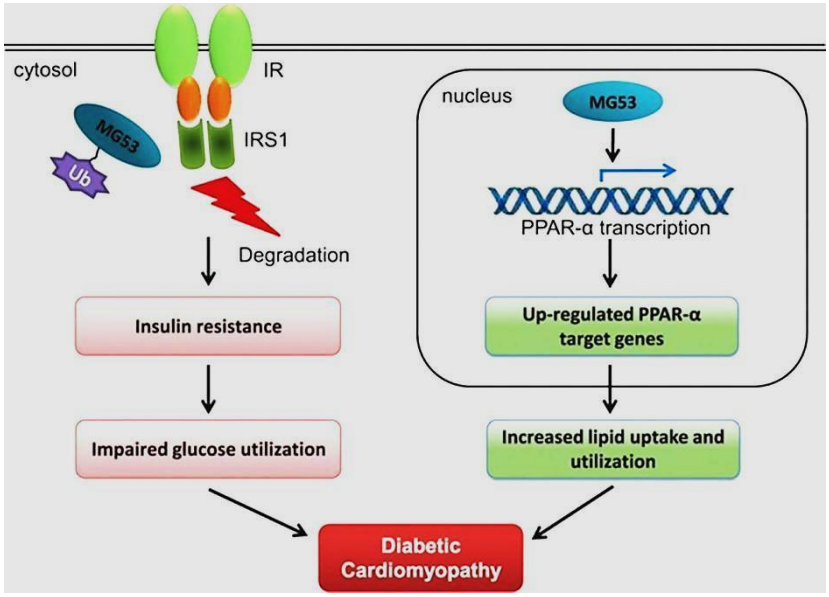

Figure. 4.1. Signalling pathways involved in MG53-induced DCM. IR indicates insulin receptor; IRS1, insulin receptor substrate 1; PPAR-α, peroxisome proliferator-activated receptor-alpha; and Ub, ubiquitin (Liu et al., Circulation. 2015; 131:795-804)

Dietary components are reported to exhibit beneficial activities against various disorders, including diabetes and cardiovascular disorders. In the present study, we have evaluated the ubiquitous phenolic phytochemical ferulic acid (FA), present as both free and covalently conjugated forms in seeds and leaves. The FA was reported to have various biological activities such as antiallergic, anticarcinogenic, antiinflammatory, antimicrobial, antioxidant, antithrombotic, antiviral, hepatoprotective, increase sperm viability, metal chelation, modulation of enzyme activity, and vasodilation. FA has also been reported to activate the transcriptional factors, gene expression, and signal transduction pathways. All these biological effects make this molecule an attractive phytochemical for DCM even though it has not been reported beneficial for DCM. So, in the present study, we are

planning to evaluate the alteration in MG53 during diabetes in order to analyse its role on myocardial lipid metabolism in the pathogenesis of DCM and the beneficial effect of FA against the MG53 mediated DCM.

4.2. Materials and methods

4.2.1. Chemicals and reagents

Ferulic acid (pharmaceutical secondary standard), gum acacia, protease inhibitor cocktail, and radioimmunoprecipitation assay (RIPA) buffer, were purchased from Sigma- Aldrich, USA. Streptozotocin, sodium citrate, citric acid, fructose, cholesterol, salt mixture, vitamin mixture, casein, and halothane were bought from Sisco Research Laboratories (SRL), Pvt Ltd., Mumbai, Maharashtra, India. Okamet 500 (metformin hydrochloride tablets) and normal saline (NS) were purchased from Cipla, Ltd., Cipla House, Ganpatrao Kadam Marg, Mumbai, India. Lard was purchased from MP Biomedicals India Pvt Ltd., Mumbai, Maharashtra, India. Standard rat feed was purchased from Feed mill unit, Kerala Veterinary and Animal Sciences University (KVASU), Mannuthy, Thrissur. Isoflurane (Forane, 250 mL solution) was bought from D. Vijay Pharma Pt. Ltd., Mumbai, India. Capillary blood collection tubes (BD SurePrep™) and serum tubes (BD Vacutainer® Plus) were purchased from Becton, Dickinson and Company, Franklin Lakes, NJ. Serum parameters were estimated using kits from Agappe diagnostics, Kerala, India.

4.2.2. Animal model and treatment protocols

The experimental procedures involving rats were approved by the Institutional Animal Ethics Committee (No. JMMC&RI/SARF/IAEC/RP-02/ 2017), Jubilee Mission Medical College and Research Institute (JMMC&RI), Thrissur, Kerala, India, and were carried out according to the guidelines of the International Guiding Principles for Biomedical Research Involving Animals, and the Committee for the Purpose of Control and Supervision of Experiments on Animals (CPCSEA) at Small Animal Research Facility,

Jubilee Mission Medical College and Research Institute (JMMC&RI), Thrissur, Kerala, India.

Forty-five male Wistar rats weighing 90-120 g were purchased from Small Animal Breeding Station, College of Veterinary and Animal Sciences, Mannuthy, Thrissur, Kerala, India, and used in this study. The rats were housed under standard environmental conditions of temperature (22 ± 2 °C) and humidity 50-60 % and with a 12/12 h light/dark cycle and acclimatised for two weeks. The experimental procedure follows the previously described procedure (Guo et al. 2016) with slight modifications. The details of animal treatments are given in the **Fig.4.2**.

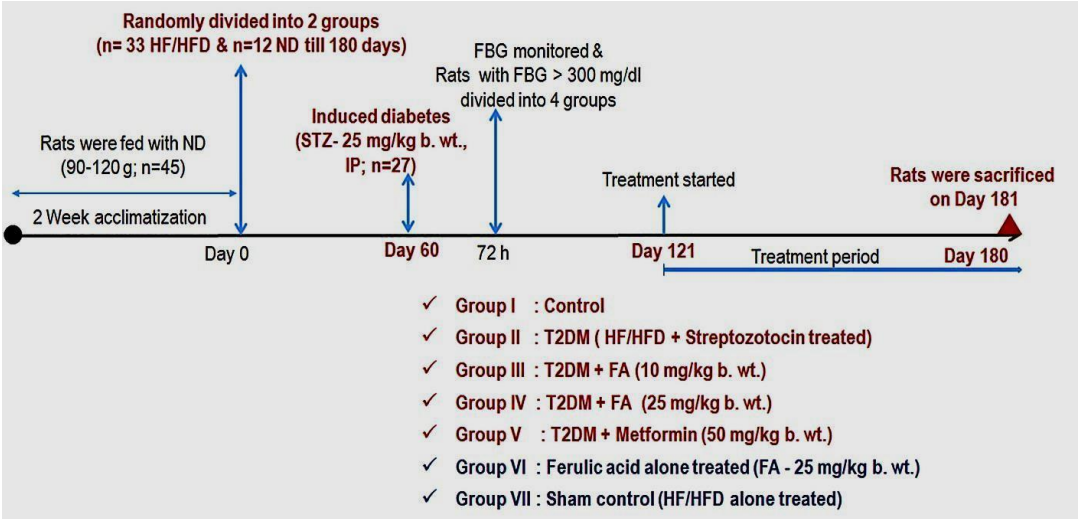

Figure. 4.2. Experimental flow chart of in vivo study. Schematic diagram of the induction and treatment schedule of diabetic rats

Briefly, after two weeks of acclimatisation, rats were divided randomly into two sets (n = 12 and n=33). The first set (n=12) were fed a standard rat chow throughout the experimental period, and the second set (n=33) were fed with a high fat/fructose (HF/F) diabetogenic diet (TD05482, Teklad, USA; 46.5 % carbohydrate, 25.7 % fat, and 18.6 % protein; 4.9 kcal/g). After 60 days 27 rats from the second set were given streptozotocin (STZ, 25 mg/kg b. wt. in 0.1 M citrate buffered saline, pH 4.5) and the other six rats were given normal saline (NS) intraperitoneally. After 72 h of STZ injection, the rats with fasting blood glucose (FBG) above 300 mg/dl were taken as diabetic.

The experimental groups were *Group I* - control; *Group II* - diabetic rats; *Group III* - diabetic rats treated with FA - 10 mg/kg b. wt./day; *Group IV* - diabetic rats treated with FA - 25 mg/kg b. wt./day; *Group V* - diabetic rats treated with Met - 50 mg/kg b. wt./day; *Group VI* - rats treated with FA - 25 mg/kg b. wt./day; and *Group VII* - sham control (rats fed with HF/F diet) (**Fig.4.2**).

FA, Met and vehicle (1 % gum acacia in NS for *groups I*, *II* and *VII*) were administered via oral gavage. The rats were continued with their respective diets throughout the experimental period (180 days). In this study, rats were treated with a FA dose of approximately 10 and 25 mg/kg/day and Met at 50 mg/kg/day; this dose corresponds to a human dose of approximately 100, 250 and 500 mg/day respectively based on body surface area comparisons between rats and humans (Reagan-Shaw et al. 2008).

For sacrifice, rats were fasted overnight, and subjected to inhale carbon dioxide gas; then under deep anaesthesia hearts were immediately dissected out and snap-frozen in liquid nitrogen for biochemical analyses, and some hearts were fixed in 10 % buffered formalin (in normal saline) for histological studies. Serum was separated from blood taken through a cardiac puncture and stored in minus 80°C for biochemical and western blot analyses.

4.2.3. Morphology analysis, estimation of body mass index (BMI) and heart mass index (HMI)

During the course of the experiment and at the end of the experiment, the photographs of animals were taken for the morphological examination. The body weights of animals were monitored fortnightly. The body weight and body length were taken and determined the BMI using the equation, BMI = body weight (g)/length^2 (cm^2). The hearts were weighed, and the HMI was calculated as the ratio of heart mass to body weight.

4.2.4. Estimation of fasting blood glucose (FBG)

At the end of the experiment, all the rats were fasted for 16 h and FBG (blood drop was collected from tail tip prick) was measured by using glucose strips in an Accu-Chek® Active blood glucose meter (Roche Diabetes Care India, Pvt. Ltd.).

4.2.5. Estimation of serum glycated haemoglobin (HbA1c)

The HbA1c level of rat serum were estimated using rat haemoglobin A1c ELISA kit from ImmunoTag (Geno Technology Inc., USA) as per the kit protocol. Briefly, 40µl of serum samples or standard, 10µl of anti-HbA1c antibody, 50µl of streptavidin-HRP were added to the wells labelled as serum samples and standards. The plate was then covered with the plate sealer, mixed well, and incubated for 60 min at 37 °C. Then, it was washed 5 times with the wash buffer, and after each wash, the plate was blotted onto absorbent filter paper. Then 50µl of substrate solution A and B were added to each well, and incubated in the dark for 10 min at 37°C. 50µl of stop solution was then added to all the wells, and the absorbance was measured immediately at 450 nm using a microplate reader (Tecan Infinite M200PRO, Tecan, Austria). A standard curve was constructed, and the HbA1c levels were estimated from the standard regression curve, and the results were expressed in ng/mL.

4.2.6. Estimation of serum insulin and HOMA-IR

The fasting serum insulin level (FBI) of the rats were estimated by ELISA method using rat insulin ELISA kit from ImmunoTag (Geno Technology Inc., USA) as per the kit protocol. Briefly, 40µl of serum samples or standards, 10µl of anti-INS antibody, and 50µl of streptavidin-HRP were added to samples and standard wells and mixed well, and incubated for 60 min at 37 °C. Then it was washed 5 times with the wash buffer, and 50µl of substrate solution A and B were added to all the wells and incubated in the dark for 10 min at 37°C. 50µl of stop solution was then added to all the wells, and the absorbance was measured immediately at 450 nm using a microplate

reader. The insulin level was calculated from the standard curve and expressed as mIU/L.

The homeostatic model assessment (HOMA) score for insulin resistance (HOMA-IR) was calculated using the formula: HOMA-IR = [Insulin (U/l) x Blood glucose (mM)]/22.5.

4.2.7. Serum atrial and b-type natriuretic peptide (ANP & BNP)

The serum ANP and BNP were estimated by ELISA method using respective ELISA kits (MyBioSource, CA, USA) according to the kit protocols. Briefly, 50 µL of standard, blank, or serum samples were taken into the corresponding labelled wells, and 50 µL of biotin-labelled antibody was added immediately to it. Then it was mixed well and incubated for 45 min at 37 °C, and washed with the wash buffer (3 times). After the washing step, 100 µL of SABC working solution (kit reagent) was added to all the wells and incubated for 30 min at 37 °C. It was then washed (5 times), and 90 µl of TMB substrate was added into each well and incubated in the dark at 37°Cfor 20 min. Then 50 µL of stop solution was added, and the absorbance was read at 450 nm. The standard curves for ANP and BNP were constructed, and ANP and BNP concentrations were determined and expressed in pg/ml.

4.2.8. Estimation of serum glutamate oxaloacetate transaminase (SGOT) activity

The serum GOT was estimated by the kinetic determination of aspartate aminotransferase (AST) using the diagnostic kit (Agappe Diagnostics Ltd., Kerala, India) according to the kit protocols. Briefly, 1 mL of working reagent (made as to the kit instructions) was mixed with 100 µL of serum samples and incubated at 37 °C for 1 min. Then the absorbance was measured at 340 nm using a multimode plate reader (Tecan Infinite M200PRO, Tecan, Austria) for 3 min with 1 min interval. The change in absorbance per min (ΔOD/min) was calculated, and the enzyme activities were estimated using the equation; enzyme activity (U/L) = (ΔOD/min) x 1745.

4.2.9. Analysis of lipid profile

The serum concentrations of total cholesterol (TC), triglyceride (TG), high-density lipoprotein (HDL), and low-density lipoprotein (LDL) were estimated using respective kits (Agappe Diagnostics Ltd., Kerala, India).

The TC was estimated enzymatically by colourimetric determination of total cholesterol following the cholesterol oxidase (CHOD) – peroxidase (POD) reactions using the kit reagents. Briefly, 1 mL of working reagent (made as to the kit instructions) was mixed with 10 µL of serum sample or standard and incubated at 37 °C for 5 min. Then the absorbance of samples and standard were measured at 630 nm using a multimode plate reader (Tecan Infinite M200PRO, Tecan, Austria), and change in absorbance was calculated against the reagent blank. The TC concentration in the serum was estimated using the equation, cholesterol (mg/dL) = (absorbance of sample/ absorbance of standard) x 200.

The TG was estimated enzymatically by colourimetric determination of triglyceride following the glycereol-3-phosphate oxidase (GPO) – peroxidase (POD) reactions using the kit reagents. Briefly, 1 mL of working reagent (made as to the kit instructions) was mixed with 10 µL of serum samples or standard and incubated at 37 °C for 5 min. Then the absorbance of samples and standard were measured at 630 nm using a multimode plate reader, and change in absorbance was calculated against the reagent blank. The TG concentration was estimated using the equation, triglyceride (mg/dL) = (absorbance of sample/ absorbance of standard) x 200.

The HDL cholesterol was determined by suppressing other lipoproteins than HDL by the electrostatic interaction between polyanions & cationic substances (kit reagents). The HDL was then estimated by cholesterol oxidase (CHOD) – peroxidase (POD) reactions using the kit reagents. Briefly, 450 µL of reagent 1 (supplied with kit) was mixed with 5 µL of serum samples or calibrator and incubated for 5 min at 37 °C. Then, 150 µL of reagent 2 was added to all the samples and calibrator, mixed well and incubated for 5 min at

37 °C. The absorbance of samples and calibrator were measured at 630 nm using a multimode plate reader against the reagent blank. The HDL concentration was estimated using the equation, HDL-C (mg/dL) = (absorbance of sample/ absorbance of calibrator) x 47 (calibrator concentration).

The LDL cholesterol was determined by selectively solubilising LDL alone by using a surfactant (kit reagent) which also inhibits other, non-LDL lipoproteins (HDL, VLDL, chilomicrons). The solubilised LDL was then estimated by cholesterol esterase - cholesterol oxidase (CHOD) – peroxidase (POD) reactions using the kit reagents. Briefly, 270 µL of reagent 1 (supplied with kit) was mixed with 3 µL of serum samples or calibrator and incubated for 5 min at 37 °C and measured the absorbance (OD1) at 600 nm using a multimode plate reader. Then, 90 µL of reagent 2 was added to all the samples and calibrator, mixed well and incubated for 5 min at 37 °C. Then, again the absorbance (OD2) of samples and calibrator were measured at 600 nm against the reagent blank. The LDL concentration was estimated using the equation, LDL-C (mg/dL) = [(OD2-OD1) sample/ (OD2-OD1) calibrator] x 97 (calibrator concentration).

4.2.10. Serum lactate dehydrogenase (S-LDH) & creatine kinase-MB (CK-MB)

The serum concentration of S-LDH was estimated by the kinetic determination of pyruvate (kit reagent) to lactate conversion by LDH using the assay kits (Agappe Diagnostics Ltd., Kerala, India) according to the kit protocols. Briefly, 1 mL of working reagent (made as to the kit instructions) was mixed with 10 µL of serum samples and incubated at 37 °C for 1 min. Then the absorbance was measured at 340 nm using a multimode plate reader (Tecan Infinite M200PRO, Tecan, Austria) for 3 min in 1 min interval. The change in absorbance per min (ΔOD/min) was calculated, and the enzyme activities were estimated using the equation; LDH activity (U/L) = (ΔOD/min) x 16030.

The CK-MB in the serum was estimated by assay kit from Agappe (Agappe Diagnostics Ltd., Kerala, India) which used CK antibody to inhibit other than CK-MB in the serum sample. Briefly, 1 mL of working reagent (made as to the kit instructions) was mixed with 40 µL of serum samples and incubated at 37 °C for 100 sec. Then the absorbance was measured at 340 nm for 5 min in 1 min interval. The change in absorbance per min (ΔOD/min) was calculated, and the enzyme activities were estimated using the equation; CK-MB activity (U/L) = (ΔOD/min) x 8254.

4.2.11. Serum myeloperoxidase (MPO) enzyme activity

The MPO activity with 3,3′,5,5′-Tetramethylbenzidine (TMB) was measured as described before (Suzuki et al. 1983). Briefly, 10 µl of different samples were mixed with 80 µl of H_2O_2 (0.75 mM) and 110 µl of TMB solution (2.9 mM TMB in DMSO (14.5%) and sodium phosphate buffer (150 mM, pH 5.4)) in a 96 well plate, and the plate was incubated for 5 min at 37 °C. The reaction was stopped by adding 50 µl of H_2SO_4 (2 M), and absorbances were measured at 450 nm and estimated the MPO activity.

4.2.12. Analysis of biochemical markers of heart

The biochemical markers of cardiac injury were assessed at protein level. The cardiovascular disease marker proteins such as hsCrp, cTnT, cTnI, Copeptin, and hFabp were examined using western blot. The band intensity was measured using ImageJ, and densitometric data was calculated to compare the protein expression to control.

4.2.13. Estimation of serum cardiac troponin I-interacting kinase (TNNI3K)

The serum concentration of TNNI3K was quantitatively determined using Rat serine/threonine-protein kinase TNNI3K ELISA kit (MyBioSource, Inc. San Diego, CA, USA) according to the kit protocol. Briefly, 100 µL of standard or samples were taken in the well plate and incubated at 37 °C for 90 min. The well contents were removed and immediately added 100 µL of

biotinylated antibody, gently mixed and incubated for 1 h at 37 °C. The wells were washed (three times) and 100 µL of HRP conjugate was added, and again incubated for 30 min at 37 °C. The wells were washed five times, and 90 µL of substrate reagent was added to each well and incubated for 15 min at 37 °C in the dark. Then 50 µL of stop solution was added to each well, and OD was measured at 450 nm with a microplate reader. A standard curve was constructed, and the TNNI3K concentrations were calculated and expressed in pg/ml.

4.2.14. Mitsugumin 53 mediated insulin resistance and fatty acid oxidation

The MG53, insulin signalling pathway and the lipid metabolism pathway were analysed in protein level. The expressions of MG53, proteins of insulin signalling such as Ir, Irs1, Akt and pAkt; and proteins of lipid metabolism such as Pparα, adiponectin (Acrp30), Cpt1, Acc1, and Fas were examined using western blot. The band intensity was measured using ImageJ, and densitometric data was calculated to compare the protein expression to control.

4.2.15. Western blot

For the western blot analysis, equal amounts of proteins (25 µg) were run in a 10 % SDS-PAGE, and transferred to PVDF membranes using Trans-Blot® Turbo™ Transfer system (Bio-Rad, USA). The membranes were then blocked with 5 % defatted (skimmed) milk in TBST (50 mM Tris, pH 7.5, 150 mM NaCl, 0.01% Tween-20) for 1 h at room temperature. The membrane was washed three times with TBST for 10 min each. The membrane was incubated in primary antibodies of various proteins of interest overnight at 4 °C. The membranes were washed with TBST and incubated with HRP-conjugated corresponding secondary antibodies for 1 h at room temperature. The membranes were again washed three times with TBST, and the proteins were visualised using Western BLoT Hyper HRP Substrate (Takara Bio Inc. USA). The protein bands were captured by stain-free imaging capabilities of

the Bio-Rad ChemiDoc MP imaging systems, using image lab software (Bio-Rad, USA). The intensity of bands was quantified using the ImageJ software and normalised to control and fold difference was calculated as the ratio of loading control proteins.

4.2.16. Histological studies

For histological studies, the pieces of the heart were fixed in 10% formol saline and processed for preparations of histological studies. After fixation, tissues were dehydrated in ethanol, cleared in xylene and embedded in paraffin wax. 5 µm thickness of the left ventricular tissue sections were prepared using a microtome and treated with haematoxylin for 10 min, washed in tap water and incubated for 2 min in van Gieson's staining solution (1% acid fuchsin in aqueous saturated picric acid). The sections were dehydrated and mounted with DPX mounting. The images were captured with 20 X objective in Nikon Eclipse TS 100 inverted microscope and morphometric analysis was carried using NIS Elements D imaging software (Nikon, Melville, NY), and images showed collagen fibres in pink/red-stained, nuclei in black, and muscle in yellow coloured.

The collagen fibres were quantitatively estimated according to the method of Segnani et al. (2015). Briefly, a square was applied upon the colour of interest (pink/red colour for collagen fibres), and the specific threshold of positive tissue areas was measured on the basis of the total pixel number and intensity using ImageJ software and expressed as a percentage of the total tissue area examined (percentage positive pixels, PPP) in 6 fields/each for each animal.

Statistical analysis

All statistical analyses were carried out using the Statistical Package for Social Science (IBM SPSS Statistics for Windows, Version 22.0. Armonk, NY). The results were expressed as the mean ± standard deviation (SD). Data were subjected to one-way ANOVA, and the differences among the

means for the groups were assessed using Duncan's multiple range tests to determine which mean values were significantly different at $p < 0.05$.

4.3. Results

4.3.1. Diabetes increased the morphometric parameters

The morphological appearances of rats were noted at the end of the experimental period. The diabetic rats showed fattier appearance (increased size) than the control animals, and the treatment with FA and Met reduced the size of rats (**Fig.4.3A**). The morphological parameters such as body length and weight were also measured, The diabetic rats showed 1.5 fold gain in the body weight, whereas the treatment with FA reduced the body weight (1.33 and 1.42 fold with 10 and 25 mg/kg b. wt./day respectively; (**Fig.4.3B & C**)

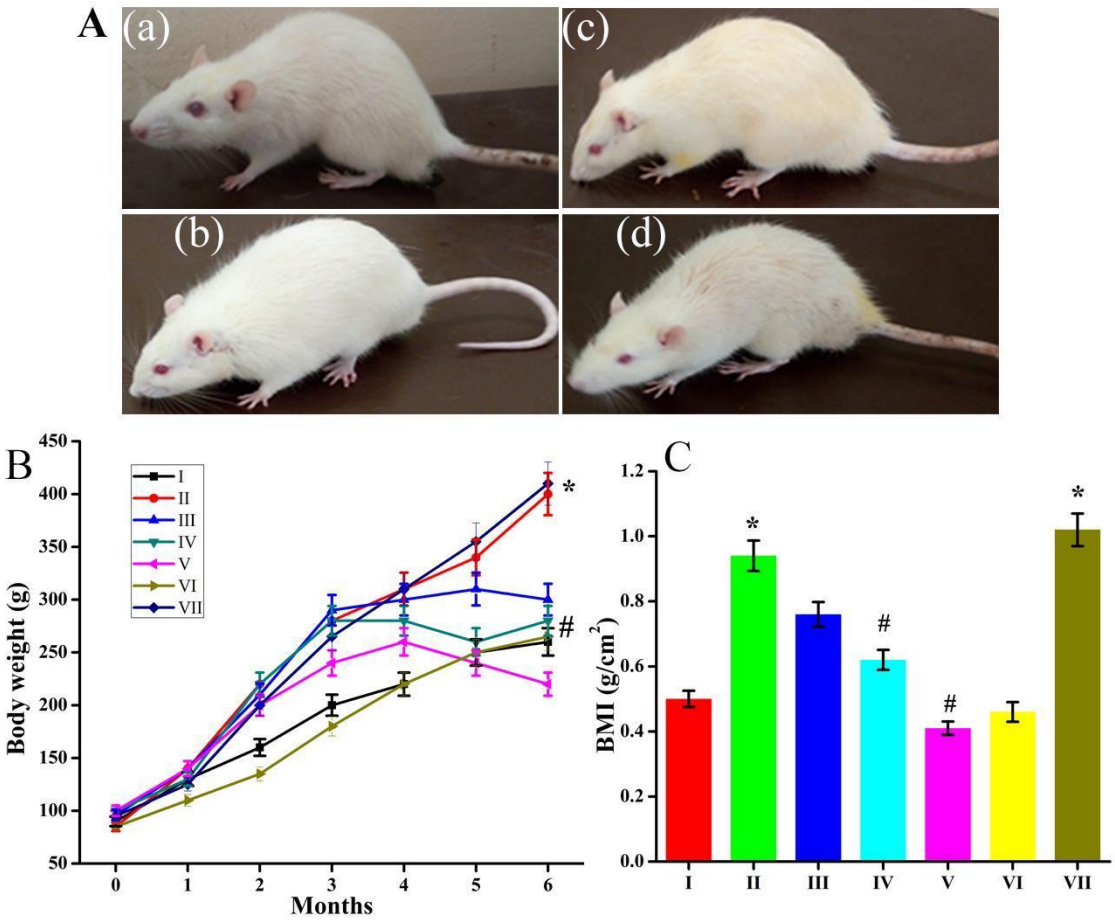

Figure. 4.3. Diabetes caused an increase in morphologic parameters in Wistar rats. A, Photograph of Wistar rats grown under the conditions of NRC (a), DM (b), DM treated with FA - 25 mg/kg b. wt./day (c), and DM treated with Met - 50 mg/kg b. wt./day (d) for 180 days. Images are representative of each group (n=6) of experiments. **B,** Body weight of rats from different groups - NRC (I), DM (II), DM treated with FA - 10 and 25 mg/kg b. wt./day (III & IV), DM treated with Met - 50 mg/kg b. wt./day (V), NRC treated with FA - 25 mg/kg b. wt./day (VI), and SC rats (VII), throughout the experimental period. **C,** BMI of different treatment group of rats (mean ± SD, n=6, * $p < 0.05$ vs. control rats and # $p < 0.05$ vs. DM rats). NRC, indicates rats fed with normal rat chow (control); DM, rats fed with high fat/fructose diet and streptozotocin (single dose - 25 mg/kg b. wt., i. p and fasting blood glucose > 300 mg/dl); BMI, body mass index; FA, ferulic acid; and Met, metformin.

which was comparable with the standard drug Met (1.81 fold with 50 mg/kg b. wt./day) (**Fig.4.3B & C**). BMI of the diabetic rats showed 1.8 fold increase and the treatment with FA reduced the BMI significantly (1.20 and 1.51 fold with 10 and 25 mg/kg b. wt./day respectively) which was comparable with the standard drug Met (2.29 fold, $p < 0.05$) (**Fig.4.3B & C**).

4.3.2. Diabetes induces insulin resistance

The serum markers like FBG, HbA1c, FBI and the insulin resistance (HOMA-IR) were measured to evaluate the diabetic complications in the heart. The rats fed with a diabetogenic diet plus mild dose of STZ (i.p) showed a 5.9 fold increase in the FBG, whereas the treatment with FA reduced the FBG in a dose-dependent manner which was comparable with the standard drug Met. The diabetes group showed 4.6 fold increase in HbA1c level (n=6, $p < 0.05$; (**Table.4.1**)) and the treatment with FA (10 and 25 mg/kg b. wt./day) reduced the HbA1c level by 1.9 and 3.0 fold respectively compared to the diabetes group. The Met (50 mg/kg b. wt./day) also reduced the HbA1c level by 3.5 fold (**Table.4.1**).

The serum insulin level was reduced to 1.8 fold in diabetic rats compared to control, whereas the treatment with different concentrations of FA increased the serum insulin by 1.4 and 1.5 fold compared to diabetic rats. The Met also increased the insulin level by 1.1 fold (**Table.4.1**). The insulin

Groups	FBG (mg/dl)	HbA1c (%)	FBI (mIU/L)	HOMA-IR (AU)
I	87.83 ± 8.81	4.53 ± 0.21	26.53 ± 1.33	5.83 ± 0.29
II	526.83 ± 60.63*	21.25 ± 1.80*	14.35 ± 0.50*	21.26 ± 0.74*
III	295.21 ± 77.13#	10.94 ± 1.35#	20.63 ± 1.31#	11.71 ± 0.74#
IV	179.50 ± 68.93#	6.87 ± 1.41#	21.58 ± 1.97#	9.59 ± 0.88#
V	133.35 ± 29.20#	5.95 ± 0.45#	17.11 ± 1.50#	5.58 ± 0.49#
VI	98.50 ± 8.87	4.94 ± 0.16	23.31 ± 1.76	5.66 ± 0.95
VII	103.66 ± 8.66	5.43 ± 0.27	39.37 ± 1.72*	9.53 ± 1.30*

Table.4.1. Diabetes induces alteration in glucose homeostasis in male Wistar rats. Biochemical parameters of glucose homeostasis estimated in rats grown under the conditions of NRC (I), DM (II), DM treated with FA - 10 and 25 mg/kg b. wt./day (III & IV), DM treated with Met - 50 mg/kg b. wt./day (V), NRC treated with FA - 25 mg/kg b. wt./day (VI), and SC rats (VII) for 180 days (mean ± SD, n=6, * $p < 0.05$ vs. control rats and # $p < 0.05$ vs. DM rats). NRC indicates rats fed with normal rat chow (control); DM, rats fed with high fat/fructose diet and streptozotocin (single dose - 25 mg/kg b. wt., i. p and fasting blood glucose > 300 mg/dl); SC, rats fed with high fat/fructose diet (sham control); FA, ferulic acid; Met, metformin; FBG, fasting blood glucose; HbA1c, haemoglobin A1c (glycated); FBI, fasting blood insulin; and HOMA-IR, homeostatic model assessment for insulin resistance.

resistance was evaluated by HOMA-IR. The diabetic rats showed 3.6 fold increase in HOMA-IR value (n=6, $p < 0.05$) and the treatment with different concentrations of FA (10 and 25 mg/kg b. wt./day) reduced the HOMA-IR by 1.8 and 2.2 fold respectively compared to the diabetes group. The Met treatment also reduced the HOMA-IR value by 3.8 fold (**Table.4.1**). The results revealed that FA could reduce insulin resistance and glycation end product formation significantly.

4.3.3. Diabetes induces lipotoxicity

The genesis of lipotoxicity by diabetes was evaluated by the lipid profile analysis. The diabetic rats showed a 3.68 fold increase in the total cholesterol (TC), whereas the treatment with FA reduced the TC in a dose-dependent manner which was comparable with the standard drug Met. The diabetes

group showed 2.67 fold increase in triglycerides (TG) level (n=6, $p < 0.05$; **Table.4.2**)

				mg/dL
Groups	**TC**	**TG**	**HDL**	**LDL**
I	33.64 ± 1.83	100.92 ± 0.67	62.61 ± 5.41	19.29 ± 3.33
II	124.03 ± 6.86 *	270.06 ± 2.61 *	18.38 ± 4.93 *	49.72 ± 2.68 *
III	92.46 ± 8.15 #	106.19 ± 4.99 #	40.45 ± 1.14 #	44.46 ± 1.92 #
IV	77.19 ± 0.27 #	86.52 ± 2.63 #	49.00 ± 4.32 #	20.64 ± 3.20 #
V	68.39 ± 2.32 #	95.27 ± 4.55 #	21.68 ± 0.54 #	12.90 ± 1.08 #
VI	40.58 ± 5.58	89.52 ± 1.71	42.89 ± 4.99	23.09 ± 2.04
VII	108.57 ± 1.46 *	112.00 ± 10.51	32.09 ± 8.24	24.95 ± 0.32

Table.4.2. Diabetes induces lipotoxicity in male Wistar rats. Lipid profile analysis in rats grown under the conditions of NRC (I), DM (II), DM treated with FA - 10 and 25 mg/kg b. wt./day (III & IV), DM treated with Met - 50 mg/kg b. wt./day (V), NRC treated with FA - 25 mg/kg b. wt./day (VI), and SC rats (VII) for 180 days (mean ± SD, n=6, * $p < 0.05$ vs. control rats and # $p < 0.05$ vs. DM rats). NRC, indicates rats fed with normal rat chow (control); DM, rats fed with high fat/fructose diet and streptozotocin (single dose - 25 mg/kg b. wt., i. p and fasting blood glucose > 300 mg/dl); SC, rats fed with high fat/fructose diet (sham control); FA, ferulic acid; Met, metformin; TC, total cholesterol; TG, triglycerides; HDL, high-density lipoprotein; and LDL, low-density lipoprotein.

and the treatment with FA (10 and 25 mg/kg b. wt./day) reduced the TG level by 2.45 and 3.12 fold respectively compared to the diabetes group. The Met (50 mg/kg b. wt./day) also reduced the TG level by 2.83 fold (**Table.4.2**).

The HDL cholesterol level was reduced to 3.40 fold in diabetic rats compared to control, whereas the treatment with different concentrations of FA increased the HDL by 2.2 and 2.66 fold compared to diabetic rats. The Met also increased the HDL level by 1.17 fold (**Table.4.2**). The diabetic rats showed 2.57 fold increase in LDL cholesterol level (n=6, $p < 0.05$) and the treatment with different concentrations of FA (10 and 25 mg/kg b. wt./day) reduced the LDL in a dose-dependent manner (1.11 and 2.40 fold

respectively) compared to the diabetes group. The Met treatment also reduced the LDL level by 3.85 fold (**Table.4.2**). The results showed the protective effect of FA against the lipotoxicity under the diabetic condition.

4.3.4. Diabetes induces cardiac hypertrophy

The HMI was found to have a 1.65 fold increase in diabetes, and the treatment with FA reduced the HMI by 1.67 fold which was comparable to Met (1.99 fold). Cardiac markers like ANP and BNP were estimated. Diabetes induced significant ($p < 0.05$) increase in the ANP and BNP level (15.6 and 7.9 fold respectively) compared to control (**Table. 4.3**). The treatment with different concentrations of FA (10 and 25 mg/kg b. wt./day) significantly decreased the ANP level (1.5 and 2.4 fold compared to the diabetes group). The treatment with Met (50 mg/kg b. wt./day) also decreased the ANP significantly (8.3 fold). The treatment with different concentrations of FA (10 and 25 mg/kg b. wt./day) significantly decreased the BNP level (1.4 and 4.5 fold compared to the diabetes group) also in a dose-dependent manner which was comparable to the Met (50 mg/kg b. wt./day) (5.2 fold) (**Table. 4.3**).

Groups	HMI	ANP (pg/mL)	BNP (pg/mL)
I	2.78 ± 0.11	4.77 ± 0.77	31.44 ± 1.42
II	4.62 ± 0.33*	71.99 ± 4.98*	248.49 ± 4.67*
III	3.36 ± 0.26	45.67 ± 2.03#	177.32 ± 0.91#
IV	2.75 ± 0.18#	21.98 ± 1.27#	54.37 ± 4.69#
V	2.31 ± 0.20#	8.68 ± 1.53#	47.38 ± 3.23#
VI	2.34 ± 0.19	7.55 ± 0.03	34.03 ± 0.30
VII	2.80 ± 0.24	7.79 ± 0.01	41.12 ± 0.27

Table. 4.3. Diabetes causes significant release of cardiac hypertrophy markers in the blood. Analysis of markers of cardiac hypertrophy in rats grown under the conditions of NRC (I), DM (II), DM treated with FA - 10 and 25 mg/kg b. wt./day (III & IV), DM treated with Met - 50 mg/kg b. wt./day (V), NRC treated with FA - 25 mg/kg b. wt./day (VI), and SC rats (VII) for 180 days (mean ± SD, n=6, * $p < 0.05$ vs. control rats and # $p < 0.05$ vs. DM rats). NRC indicates rats fed with normal rat chow (control); DM, rats fed with high fat/fructose diet and

streptozotocin (single dose - 25 mg/kg b. wt., i. p and fasting blood glucose > 300 mg/dl); SC, rats fed with high fat/fructose diet (sham control); FA, ferulic acid; Met, metformin; HMI, heart mass index; ANP, atrial natriuretic peptide; and BNP, b-type natriuretic peptide.

4.3.5. Diabetes induces cardiac dysfunction

The myocardial infarction marker SGOT was estimated. Diabetes induced significant ($p < 0.05$) increase in the SGOT level (2.98 fold respectively) compared to control (**Table. 4.4**). The treatment with different concentrations of FA (10 and 25 mg/kg b. wt./day) significantly decreased the SGOT level (1.46 and 1.73 fold compared to the diabetes group). The treatment with Met (50 mg/kg b. wt./day) also decreased the SGOT significantly (2.11 fold; **Table. 4.4**).

Group	SGOT	S-LDH	CK-MB	MPO
		(U/L)		(U/mg)
I	60.49 ± 8.10	68.21 ± 3.05	17.99 ± 12.13	1.22 ± 0.04
II	180.60 ± 14.04*	543.42 ± 27.17*	114.23 ± 21.48*	4.60 ± 0.04*
III	123.60 ± 8.10	360.32 ± 18.02 #	112.91 ± 15.64	4.49 ± 0.11
IV	104.11 ± 4.39#	363.88 ± 18.19 #	79.98 ± 11.78#	1.39 ± 0.10#
V	85.21 ± 8.78#	177.39 ± 8.87 #	62.81 ± 16.22#	3.49 ± 0.39

Table. 4.4. Diabetes increases the activities of cardiac enzymes. Analysis of enzyme activities of cardiac dysfunction in rats grown under the conditions of NRC (I), DM (II), DM treated with FA - 10 and 25 mg/kg b. wt./day (III & IV), DM treated with Met - 50 mg/kg b. wt./day (V), NRC treated with FA - 25 mg/kg b. wt./day (VI), and SC rats (VII) for 180 days (mean ± SD, n=6, * $p < 0.05$ vs. control rats and # $p < 0.05$ vs. DM rats). NRC indicates rats fed with normal rat chow (control); DM, rats fed with high fat/fructose diet and streptozotocin (single dose - 25 mg/kg b. wt., i. p and fasting blood glucose > 300 mg/dl); SC, rats fed with high fat/fructose diet (sham control); FA, ferulic acid; Met, metformin; SGOT, serum glutamate oxaloacetate transaminase; S-LDH, serum lactate dehydrogenase; CK-MB, creatine kinase-MB; and MPO, myeloperoxidase.

The cardiac dysfunction induced by diabetes was analysed by the marker enzymes like S-LDH, CK-MB, and MPO. The S-LDH activity was significantly increased (7.96 fold, $p < 0.05$) in diabetes, and the treatment with

FA and Met reduced the S-LDH activity by 1.5 and 3.06 fold respectively. Diabetes also induced a significant ($p < 0.05$) increase in the CK-MB activity (6.34 fold compared to control; **Table.4.4**). The treatment with different concentrations of FA (10 and 25 mg/kg b. wt./day) decreased the CK-MB activity (1.01 and 1.42 fold compared to the diabetes group). The treatment with Met (50 mg/kg b. wt./day) also decreased the CK-MB activity (1.81 fold). Also, the cardiac inflammatory enzyme MPO showed a significant increase (3.77 fold) in diabetic group, and the treatment with different concentrations of FA decreased the MPO activity significantly in a dose-dependant manner (1.02 and 3.23 fold compared to the diabetes group; $p < 0.05$) which was comparable to the Met (1.28 fold; **Table. 4.4**).

4.3.6. Diabetes induces systolic dysfunction and myocardial infarction

The systolic dysfunction and myocardial infarction by diabetes were analysed with markers like troponins (cTn), c-reactive protein (hs CRP), fatty acid binding protein (h Fabp), and copeptin (Cpp) in protein level. The diabetes group showed an upregulation of cTnT (2.35 fold), cTnI (2.79 fold), hs CRP (2.16 fold), and h Fabp (1.89 fold), Cpp (1.50 fold), whereas the treatment with FA and Met downregulated the expression of these proteins ($n=3$, $p < 0.05$; **Fig. 4.4A & Table 4.5**). Also, the enzyme TNNI3K was estimated; we found a 3.5 fold increase in the same compared to control (**Fig. 4.4B**). The treatment with FA reduced by 1.4 and 4.5 fold for 10 and 25 mg/kg b. wt./day respectively ($n=6$, $p < 0.05$) compared to the diabetes group. The standard drug Met also reduced the TNNI3K level significantly (4.4 fold, $n=6$, $p < 0.05$) compared to the diabetes group (**Fig. 4.4B**). The results showed the protective effect of FA against cardiac dysfunction induced by diabetes.

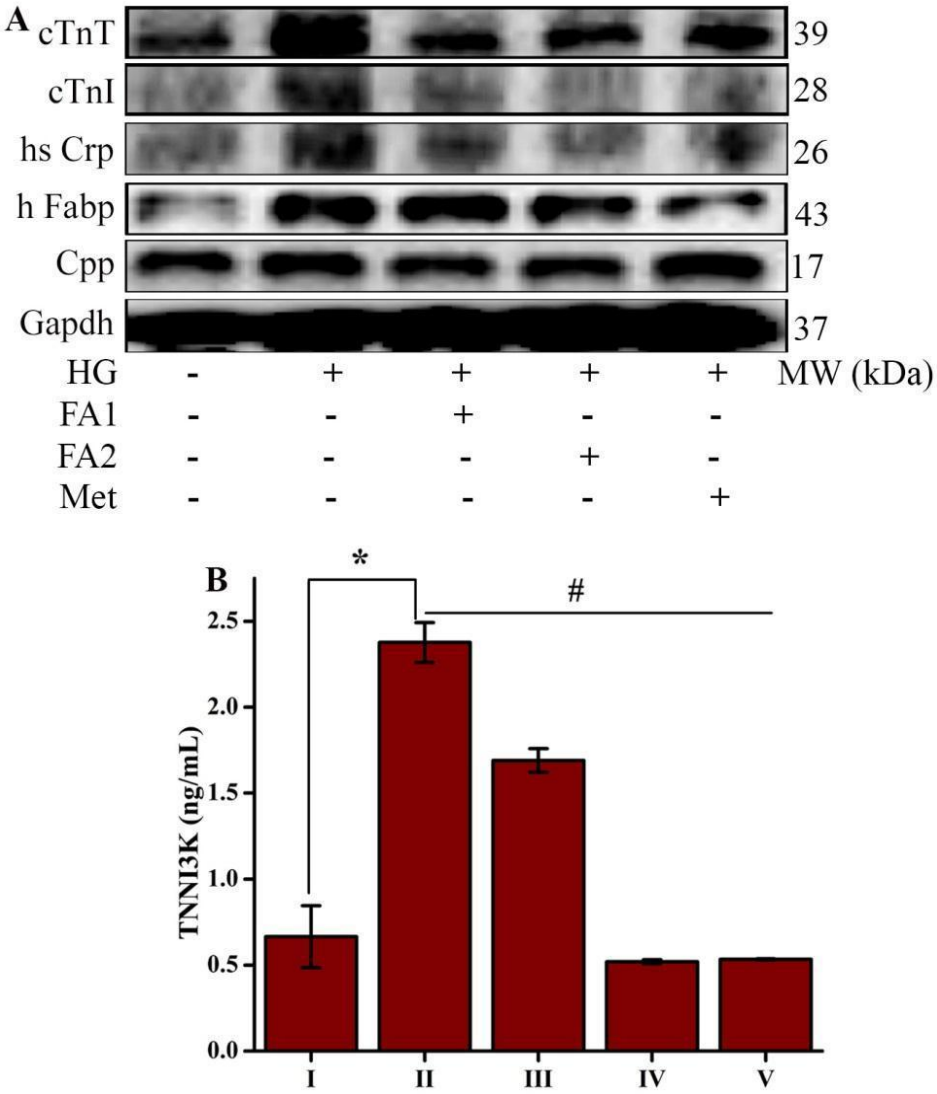

Figure. 4.4. Diabetes causes an increase in cardiac biomarkers, indicating diabetic cardiomyopathy in Wistar rats. A, Western blot analysis of the proteins of interest of cardiac dysfunction from the serum of rats grown under the conditions of NRC (I), DM (II), DM treated with FA - 10 and 25 mg/kg b. wt./day (III & IV), DM treated with Met - 50 mg/kg b. wt./day (V) for 180 days. Images are representative of six independent (n=6) experiments. **B,** Activity of TNNI3K enzyme determined by enzyme assay kit (mean ± SD, n=6, * $p < 0.05$ vs. control rats and # $p < 0.05$ vs. DM rats). NRC indicates rats fed with normal rat chow (control); DM, rats fed with high fat/fructose diet and streptozotocin (single dose - 25 mg/kg b. wt., i. p and fasting blood glucose > 300 mg/dl); cTnT & cTnI, cardiac troponins; hs CRP, high sensitive c-reactive protein; h Fabp, heart specific fatty acid binding protein; Cpp, copeptin; HG, hyperglycaemia; FA, ferulic acid; and Met, metformin.

Groups / Proteins	Protein folds of control			
	II	III	IV	V
cTnT	2.35 ± 0.41*	1.16 ± 0.09	1.25 ± 0.08 #	1.29 ± 0.07 #
cTnI	2.79 ± 0.42 *	1.91 ± 0.04	1.29 ± 0.09 #	0.82 ± 0.03 #
hsCrp	2.16 ± 0.20*	1.63 ± 0.04	0.95 ± 0.06 #	0.84 ± 0.07 #
hFabp	1.89 ± 0.07 *	1.79 ± 0.05	1.09 ± 0.01 #	0.66 ± 0.04 #
Cpp	1.50 ± 0.09 *	1.29 ± 0.05	0.89 ± 0.04 #	2.80 ± 0.02

Table. 4.5. Densitometry analysis of protein markers of cardiac dysfunction. Fold difference values of intensity of proteins analysed by western blot. Values were fold difference of control group (I), as control normalised to 1. Control (I), DM (II), DM treated with FA - 10 and 25 mg/kg b. wt./day (III & IV), and DM treated with Met - 50 mg/kg b. wt./day (V) for 180 days (mean ± SD, n=6, * $p < 0.05$ vs. control rats and # $p < 0.05$ vs. DM rats). DM, indicates rats fed with high fat/fructose diet and streptozotocin (single dose - 25 mg/kg b. wt., i. p and fasting blood glucose > 300 mg/dl); FA, ferulic acid; Met, metformin; cTnT & cTnI, cardiac troponins; hs CRP, high sensitive c-reactive protein; h Fabp, heart specific fatty acid binding protein; and Cpp, copeptin.

4.3.7. MG 53 upregulation induced diabetic cardiomyopathy

To elucidate the role of MG53 in the genesis of DCM, we examined the MG53 induced insulin signalling and lipid metabolism. The western blot analysis showed diabetes induced significant upregulation of MG53 (5.64 fold), Pparα (1.74 fold), Cpt1 (8.21 fold), Acc2 (1.24 fold) and Fas (1.05 fold) ($p < 0.05$), and downregulation of Ir (0.25 fold), Irs1 (0.50 fold), Akt (0.87 fold), pAkt (0.34 fold), and the serum marker adiponectin (Acrp30 - 0.87 fold) ($p < 0.05$) revealing the role of MG53 **(Fig.4.5 & Table 4.6)** in the genesis of DCM. The treatment with FA was effective to bring back most of the protein (MG53, Ir, Irs1, Akt, pAkt, Pparα, and Fas) level to the normal except Cpt1, Acc2, and Acrp30 where the recovery was slightly less. Met also brought back only MG53, Ir, pAkt, Pparα, Acc1 and Fas to the normal, but had little effect on Irs1, Akt, Cpt1and Acrp30 (**Fig.4.5 & Table 4.6**).

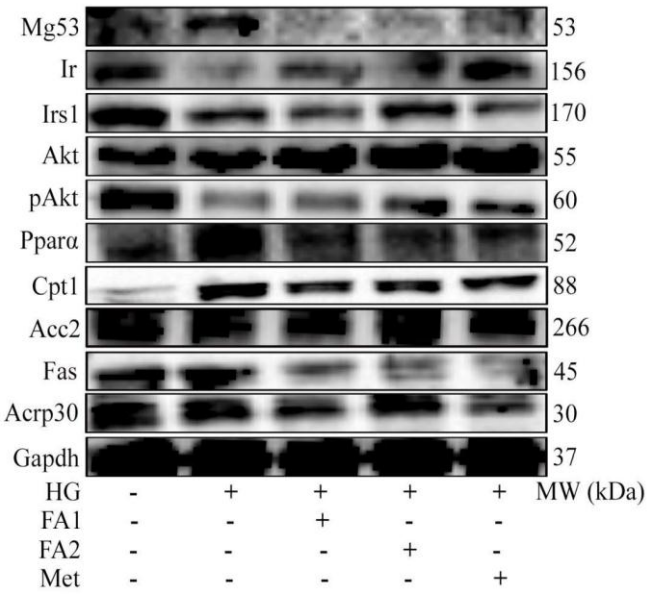

Figure. 4.5. Diabetes causes an increase in cardiomyopathy markers in Wistar rats. Western blot analysis of the cardiomyopathy marker proteins. Images are representative of six independent (n=6) experiments. HG, indicates hyperglycaemic (diabetic) rats; FA1, DM rats treated with FA - 10 mg/kg b. wt./day; FA2, DM rats treated with FA - 25 mg/kg b. wt./day; and Met, DM rats treated with Met - 50 mg/kg b. wt./day; FA, ferulic acid; Met, metformin; MG53, mitsugumin 53; Ir, insulin receptor; Irs1, insulin receptor substrate1; Akt, protein kinase B ; pAkt, phosphorylated Akt ; Pparα, peroxisome proliferator activated receptor -α; Cpt1, carnitine palmitoyl transferase 1; Acc2, acetyl CoA carboxylase; Fas, fatty acid synthase; and Acrp30, adiponectin.

Groups / Proteins	Protein folds of control			
	II	III	IV	V
MG53	5.64 ± 0.21*	1.08 ± 0.04#	0.88 ± 0.07#	0.61 ± 0.07#
Ir	0.25 ± 0.01*	0.66 ± 0.06#	0.70 ± 0.05#	0.92 ± 0.05#
Irs1	0.50 ± 0.02*	0.49 ± 0.05	0.70 ± 0.05#	0.26 ± 0.02
Akt	0.87 ± 0.02	1.14 ± 0.16#	0.92 ± 0.02#	0.84 ± 0.06
pAkt	0.34 ± 0.02*	0.43 ± 0.11	0.62 ± 0.08 #	0.51 ± 0.07#
Pparα	1.74 ± 0.07*	1.32 ± 0.07	0.84 ± 0.09 #	1.20 ± 0.03#
Cpt1α	8.21 ± 0.47*	5.15 ± 0.19#	5.66 ± 0.57#	5.85 ± 0.85#
Acc2	1.24 ± 0.05*	1.26 ± 0.02	1.38 ± 0.05	1.07 ± 0.08#
Fas	1.05 ± 0.03*	0.54 ± 0.02#	0.54 ± 0.09#	0.18 ± 0.01#
Acrp30	0.87 ± 0.04	0.60 ± 0.09	0.83 ± 0.05	0.38 ± 0.06

Table. 4.6. Densitometry analysis of MG53, insulin signaling and lipid metabolism pathway. Fold difference values of intensity of proteins analysed by western blot. Values were fold difference of control group (I), as control normalised to 1. Control (I), DM (II), DM treated with FA - 10 and 25 mg/kg b. wt./day (III & IV), and DM treated with Met - 50 mg/kg b. wt./day (V) for 180 days (mean ± SD, n=6, * $p < 0.05$ vs. control rats and # $p < 0.05$ vs. DM rats).

4.3.8. Diabetes induced cardiomyocyte fibrosis

The microscopic examination of the tissues from the left ventricle by van Gieson's staining showed a significant increase in the collagen fibres (PPP value 83.6 fold, n=6, $p < 0.05$; intensive red colour) in the diabetic rats compared to control. The treatment with FA reduced the fibrosis significantly (2.2 and 11.2 fold for 10 and 25 mg/kg b. wt./day respectively compared with diabetes rats) and which was comparable to Met (21.5 fold) (**Fig. 4.6A & B**).

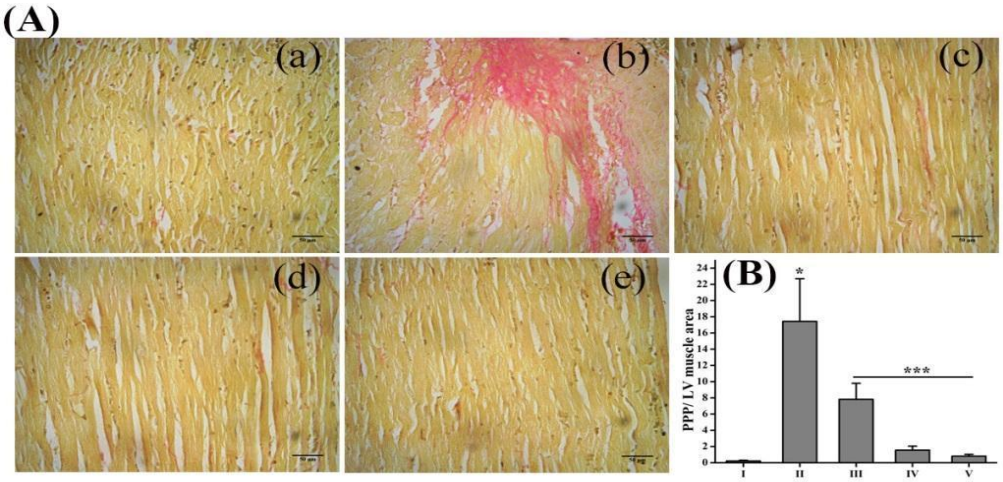

Figure.4.6. Diabetes induces cardiomyocyte fibrosis in Wistar rats. A, Representative photomicrographs of histological analysis of left ventricular tissue of rats grown under the conditions of NRC (a or I), DM (b or II), DM treated with FA - 10 and 25 mg/kg b. wt./day (c & d or III & IV), DM treated with Met - 50 mg/kg b. wt./day (e or V) for 180 days, showing the distribution pattern of collagen fibres stained with van Gieson, collagen fibres in pink, nuclei in black and muscle in yellow colour stained. Scale bars represent 50 µm. **B,** Quantitation of percentage of positive pixel (PPP) of collagen obtained from six rats in each group (mean ± SD, n=6, * $p < 0.05$ vs. control rats and *** $p < 0.05$ vs. DM rats). NRC indicates rats fed with normal rat chow (control); DM, rats fed with high fat/fructose diet and streptozotocin (single dose - 25 mg/kg b. wt., i. p and fasting blood glucose > 300 mg/dl); FA, ferulic acid; and Met, metformin.

4.4. Discussion

The significant pathophysiologies of DM include hyperglycaemia, insulin resistance, and ketoacidosis. There exist various non-invasive methods for the actual diagnosis and prognosis of DM. The DM complication of heart, especially the DCM is still run undiagnosed in many DM patients, even the advanced diagnostic methods like echocardiogram, MRI, CT scan, and ECG are available. This is because of the lack of diagnostic parameter or biochemical markers, specific to the DCM. Since DCM prolonged in different stages ends in heart failure, early detection markers should be only advisable to reduce the mortality. The general cardiac biomarkers like troponin, CK-MB, ANP, BNP, SGOT, S-LDH, left ventricular mass index (LVMI); and the DM markers like FBG, FBI, HbA1c, HOMA-IR, and lipid profile are mainly in use for the diagnosis of these disorders.

Even though the markers are helpful in the diagnosis of DM and CVDs, the early diagnosis of DCM is still a research concern due to the unavailability of specific diagnostic markers. A ubiquitin ligase from the tripartite motif (TRIM) family named mitsugumin - 53 (MG53), which is expressed exclusively in skeletal and cardiac muscle, has demonstrated to play critical roles in myogenesis, vesicle trafficking, and membrane repair (Cai et al. 2009). Mg53 was found increased in DM models, where it triggered a cascade of events that contribute to heart disease. So it is now attaining much interest in the development of novel markers for DCM, and in the present study, we evaluated the signal cascades mediated by MG53 in the genesis of DCM. Also, it is hypothesised that the inhibition of MG53 is a useful target for the development of drugs for DCM. In this regard, we evaluated FA against the MG53 and its signal cascade behind the development of DCM like insulin signalling and lipid metabolism. In the present study we evaluated various markers of DM, cardiac tissue damage, hypertrophy, fibrosis, myocardial injury, and insulin resistance in T2DM rat model.

Since DCM occurs with the absence of conventional CVDs, the rodent models with the nominal confounding implication of coronary atherosclerosis are of particular importance in the DCM research. DM induced hyperglycaemia is the primary culprit behind the complications of heart disease. The hyperglycaemia induces the glucotoxicity, which has been evidenced by oxidative stress, altered glucose metabolism, calcium homeostasis, mitochondrial dysfunction, the formation of advanced glycation end products, arterial stiffness, and atherosclerosis. The uncontrolled hyperglycaemia leads to other lethal complications such as hyperosmolar hyperglycaemic state (HHS) with an estimated mortality rate of up to 20 %. In the heart, hyperglycaemia causes cardiac lipotoxicity, mitochondrial dysfunction, ER stress, impairment in Ca^{2+} handling, and myocyte death.

HbA1c is the measure of extent of hyperglycaemic formation of glycated haemoglobin, one of the advanced glycation end products (AGE) of the haemoglobin protein. The elevated cardiac stiffness, connective tissue crosslinking, fibrosis, and impaired diastolic relaxation are contributed by the AGEs formed from the amino acids, lipids, and lipoproteins (Jia et al. 2016). In individuals with early diabetic heart failure, the increased serum levels of AGEs induced the alterations in mechanical properties of the extracellular matrix, augmented the crosslinking of collagens and laminins, elevated resistance to the connective tissue enzymatic proteolysis, and lengthened the left ventricular relaxation time. These pathophysiological alterations impart reduced cardiac compliance and left ventricular diastolic dysfunction along with the increased fibrosis (Lazo et al. 2015).

Each one percent increase in baseline and follow-up HbA1c was associated with a 2 and 11 % increased risk of CHD diabetic patients (Zhao et al. 2014). When compared to patients with HbA1c levels below 5.7%, patients with both intermediate and high HbA1c levels are associated with a more considerable extent of endothelial damage of the coronary arteries (Engel et al. 2019). HbA1c analysis of the present study also showed an increase which

is in line with these findings, and this gave us an instinct for the downstream analysis of insulin resistance in the heart.

Insulin resistance and associated hyperinsulinaemia may promote the development of DCM. In the present study, the analysis of serum fasting insulin (FBI) level and the HOMA-IR showed the DM rats developed insulin resistance. The studies revealed the translation of cellular effects of mitochondrial dysfunction and impaired Ca^{2+} homeostasis might advance to the insulin-resistant states like impaired myocardial insulin signalling, irregular coronary microcirculation, triggering off the sympathetic nervous system and renin-angiotensin-aldosterone system (RAAS), and dysfunctional immune responses. The elevated oxidative stress, fibrosis, hypertrophy, diastolic cardiac dysfunction, and finally, the systolic heart failure are the significant consequences of these changes in the heart (Jia et al., 2016).

A HOMA-IR value above the 75 % had a twice increased risk for cardiovascular events, myocardial infarction and death, and increased heart rate in healthy sedentary males (Cherkas et al. 2015). The HOMA-IR is correlated to the subclinical coronary artery disease even in the non-diabetic range HbA1c values (Chang et al. 2013). The insulin resistance in the myocardium also is reported to damage the signal transduction, substrate metabolism, and alter the delivery of substrates to the myocardium (Ormazabal et al. 2018).

After confirming the insulin resistance, we evaluated the insulin resistance mediated alteration in the levels of plasma triglycerides (TG), high-density lipoprotein (HDL), and low-density lipoprotein (LDL) which were reported to contribute to the atherosclerotic plaque formation and endothelial dysfunction. The present study showed increased blood cholesterol, triglycerides, LDL cholesterol, and reduced HDL in the DM, which agrees with the previous reports of a similar kind. In the DM heart, there is a shift from glucose to fatty acids as the energy source, and approximately 70 % of the ATP generated through oxidation of fatty acids (Fillmore et al. 2014), and may

pathologically lead to dyslipidaemia. The increased fatty acid acylcarnitine, TG, and diacylglycerol (DG) may lead to impairment of mitochondrial structure and function, as well as cardiac function.

The elevated TG levels and decreased HDL cholesterol levels is the most common pattern of dyslipidaemia in T2DM patients, which is highly correlated with atherosclerosis. The increased atherogenesis via the overproduction of small and dense forms of LDL and decreased HDL transport are the significant consequences of hypertriglyceridemia in T2DM patients. The increased LDL can become glycated and lengthens its half-life, which promotes atherogenesis. However, the glycation shortens the half-life of HDL, and its protective effect against atherosclerosis becomes diminished. HDL has antioxidant and anti-inflammatory properties and reduces LDL oxidation (Norata et al. 2006). The HDL inhibited the oxidised LDL-induced MCP-1 production and monocyte transmigration in a co-culture of human aortic endothelial and smooth muscle cells. HDL has also been demonstrated to exert anti-thrombotic, anti-apoptotic effects, and antidiabetic functions (Tabara et al. 2017).

The evidence from insulin resistance and lipotoxicity in the serum of DM rats gave way for the evaluation of markers of cardiac dysfunction for the analysis of DCM. The hypertrophy markers like HMI, ANP and BNP were evaluated. Timely identification of the increase in the left ventricular mass index (LVMI or HMI) is crucial. The LVMI is a strong predictor of mortality in both middle-aged and elderly individuals, unexpected cardiac death, and CVDs. The LVMI could be developed as a promising pre-symptomatic marker of pathophysiological structural alteration in the myocardium during T2DM since it was found elevated in T2DM patients. The hyperglycaemia induced elevation in the LVMI is associated with the higher FBG and HbA1c levels (Seferovic et al. 2018). We also found the fibrosis with surplus collagen deposition (increase in PPP value) and an increase in HMI. The failed human heart and the animal hearts with experimentally induced heart failure showed

degenerative ultrastructural changes in the cardiomyocytes, confirming the increase in collagen deposition.

In response to volume expansion and pressure overload, cardiac atria and ventricles release the circulating hormones natriuretic peptides ANP (atrial natriuretic peptide) and BNP (B-type natriuretic peptide) respectively. The regulation of intravascular blood volume and vascular tone are the primary functions of these circulatory peptide hormones. In the group of clinically established biomarkers of heart failure, both the natriuretic peptides and their N-terminal peptide fragments are also included recently. The natriuretic peptides act as physiological antagonists of the renin-angiotensin system by raising the renal sodium excretion and elicit vasodilation (Cardarelli & Lumicao, 2003). ANP has been reported to prevent the DCM by suppressing the NADPH oxidase (Ritchie et al. 2018). BNP levels are high in diabetic subjects with left ventricular dysfunction, and also exhibit antifibrotic effects on the heart muscle. BNP is now growing as a marker for early and advanced heart failure or diastolic dysfunction in association with hypertension (Epshteyn et al. 2003).

The cardiac hypertrophy will eventually lead to myocyte injury and death. Taking this into consideration, we evaluated the myocyte injury markers like SGOT, S-LDH, CK-MB, and MPO. The SGOT was proposed to be released from cardiomyocytes undergoing necrosis, and identified as the first biomarker in the diagnosis of acute MI. After an acute MI, the SGOT level was found increased in the blood in 3 to 4 h and in 15 to 28 h it peaked, and within 5 days it was shown to returns to baseline (Patibandla et al. 2020). Also, a highly significant increase in SGOT levels was observed in cardiac complications such as supraventricular and ventricular arrhythmias, complete heart block, bundle-branch block, myocardial insufficiency, and secondary cardiac arrest. In current clinical practice, SGOT has not been used to diagnose acute MI because it is not a specific marker for cardiac myocytes (Patibandla et al. 2020).

Another potential biomarker for detecting myocardial ischemia is the serum lactate dehydrogenase (S-LDH). After 6 to 12 h of acute MI, S-LDH increases in the blood and takes 24 to 72 h to peak, and within 8 to 14 days it becomes normalised. Another biomarker CK-MB has a relative specificity for cardiac tissue, so it is a useful biomarker for detecting acute MI. It is detected in the serum after 4 h and peaks within 24 h, and within 48 to 72 h it becomes normalised. Since CK-MB is normalized in 48 to 72 h after myocardial ischemia; and if levels rise again after declining, it can be considered as the re-infarction (Aydin et al. 2019).

The leukocyte derived enzyme myeloperoxidase (MPO) is involved in the formation of reactive oxygen species (Zhang et al. 2002). The evolution of CVDs, including atherosclerosis, has been attributed by the pro-atherogenic activities of MPO. The MPO activity leads to the breakdown of the fibrous cap through the promotion of endothelial cell apoptosis protease cascades in ischemic complications of atherosclerosis (Nicholls & Hazen, 2005). The CVDs such as arterial hypertension, cardiac arrhythmia, congestive heart failure, coronary artery disease, myocardial ischemia/ reperfusion injury, peripheral arterial disease, pulmonary arterial hypertension, stroke, and venous thrombosis were also associated with the MPO activity. The elevated MPO level is linked with the potential risk of CVDs related mortality and morbidity (Nicholls & Hazen, 2005).

Then we evaluated some other systolic dysfunction markers like troponin, TNNI3K, hs-CRP, H-FABP, and copeptin because of DCM after the myocyte injury evaluation. The cardiac-specific troponins (cTn) are the standard biomarkers for detection of myocardial injury (Apple et al. 2012). The troponin I (cTnI) and troponin T (cTnT) are the specific and sensitive biomarkers of cardiac myocyte injury and is currently the first-line test for acute MI. The cTnI and cTnT levels are used for the detection of initial ischemic episodes since its levels in the blood rise within 4 h and peaks in 24 to 48 h from the onset of acute MI symptoms, and remains in the elevated levels for many days.

The cardiomyocyte-specific kinase, troponin I - interacting protein kinase (TNNI3K), promotes ischemia/reperfusion injury by promoting oxidative stress induced cardiomyocyte death. In a pressure overload induced pathological hypertrophy model, the disease progression is accelerated in the overexpressed state of TNNI3K (Wang et al. 2013). The DM induced inflammation in cardiomyocytes causes a release of many systemic markers; the most promising biomarker is high-sensitivity C-reactive protein (hs-CRP), which independently predicts future coronary heart disease (CHD). The levels of hs-CRP are increased in T2DM. There exists a strong association between hsCRP and insulin resistance, and this suggests the influence of chronic inflammation and insulin resistance with the pathophysiological and metabolic mechanisms.

The fatty acid metabolism in cardiomyocytes involves a specific type of protein called heart-type fatty acid-binding protein (H-FABP), and has also been used as a marker for myocardial infarction. When compared with the sensitivity of the troponin (18.8%) and CK-MB (12.5%) as biomarkers of acute MI patients within 4 h of the onset of symptoms, the H-FABP (60 %) showed significantly higher sensitivity (Kabekkodu et al., 2016). Copeptin, the C-terminal pro-vasopressin is also proposed as a useful biomarker in cardiovascular and renal disease. It can be used for the predicted prognosis in heart failure, stroke and myocardial infarction (Katan et al., 2009).

Even though there are many markers for the diagnosis of DM and CVDs, currently there is no specific marker for DCM. The insulin resistance and metabolic alteration to lipids have been predicted to be the reason for DCM. However, the mechanism underlying DCM is poorly understood, and this generated the gap area for the diagnosis and development of drugs for DCM. Recent studies have shown that a MG53 (TRIM72) constitutes a primary causal factor of systemic insulin resistance and metabolic disorders (Song et al. 2013). It has been proposed to have different functional activities. The endogenous target of intrinsic E3 ligase activity of MG53 is insulin receptor, and insulin receptor substrate-1 (IRS-1), critical molecules in the

insulin signalling cascade (Yi et al. 2013). The reduced IRS1 protein has been the fundamental mechanism of cardiac dysfunction during insulin resistance and T2DM.

The DM models showed an increased MG53 activity, which triggers a cascade of events that contribute to heart disease. The pathophysiological factors of DCM like cardiac hypertrophy, reactivation of the foetal gene program, cardiomyocyte steatosis, and contractile dysfunction were observed in adult MG53 transgenic mice at 20 weeks of age. In the DCM model, MG53 suppressed the insulin signalling by reducing the activity of insulin receptor, IRS-1 and insulin-stimulated Akt phosphorylation. The effect was expressed by pathological factors such as insulin resistance, reduced glucose uptake, increased lipid accumulation, myocardial fibrosis, hypertrophy, and cardiac dysfunction (Liu et al., 2015). The present study in the T2DM rat model also showed a similar effect of MG53.

The insulin signalling cascade proteins IR, IRs1, Akt and pAkt were found to be downregulated with upregulation of MG53 in diabetic heart tissue, depicting the development of DCM in the present model. The Akt modulates insulin-regulated glucose metabolism, and the activation of Pi3k/Akt signalling is beneficial for the treatment of DCM. These molecular changes lead to increases in fatty acid oxidation and declines in glucose utilisation in cardiomyocytes, one of the salient features of DCM.

The increased intracellular MG53 levels upregulates the transcription of PPAR α and its target genes, which contributes to the pathogenesis of DCM through the cardiac lipid accumulation (Liu et al. 2015). In the present study, we evaluated the PPAR α and its target proteins like Cpt1, Acc2, and some other fatty acid metabolism factors such as Fas and adiponectin (Acrp30) were analysed. The transcription of the genes involved in cellular fatty acid utilisation pathways such as fatty acid transport, esterification, and oxidation is regulated by the nuclear receptor PPARα. The pathological upregulation of

PPAR-α, resulting in altered glucose transportation, increased cardiac lipid uptake in cardiomyocytes, and progressive DCM (Lee et al. 2013).

In the diabetic heart, the upregulation of PPAR-α, transcriptionally upregulate its downstream target enzyme CPT1, the rate limiting enzyme of mitochondrial β-oxidation, and thus elevates the rate of mitochondrial β-oxidation for degradation of the fatty acids (Amrutkar et al. 2015). In line with these reports, in the present study, we also found regulation of CPT-1 expression, indicating increased mitochondrial β-oxidation for degradation of the fatty acids. This may cause cellular lipotoxicity and initiation of cardiac dysfunction in the diabetic heart due to the elevation of fatty acids and following TG synthesis (Tonin et al. 2010). Another target of PPAR-α is ACC2, which is involved in the long-chain fatty acid entry into the mitochondria via the ACC2/malonyl CoA/CPT1 mechanism. ACC2 upregulation mice may have abnormal heart function because of the elevated rates of fatty acid oxidation.

The altered lipid metabolism in the diabetic heart is proposed due to the increased activity of *de novo* lipogenesis enzyme, fatty acid synthase (FAS). Insulin sensitivity and cardiovascular health is also affected by the multiple salutary effects of adipokines such as adiponectin. In both cardiac and vascular cells, adiponectin showed different activities such as anti-apoptotic, anti-inflammatory, anti-oxidative, and vasodilator activities and protected cardiovascular health. In the obesity and related pathologies like T2DM and CVDs, the plasma level of adiponectin is found decreased (Zhu et al. 2008). In the prognosis of the clinical course of CAD, and to predict the risk of myocardial infarction, the plasma levels of adiponectin can be exercised (Barseghian et al. 2011).

Alteration of MG53, PPAR-α and its target proteins in the present study, reveals the molecular mechanism in the genesis of DCM. Since MG53 is the initiator of metabolic alteration in cardiomyocytes in the initial stage of DCM, it can be developed as a tool for early diagnosis of DCM. Novel molecules which inhibit the MG53 can be developed as a better drug for the

DCM. Over the past few years, novel cardioprotective compounds, as potential drug candidates for DM and associated cardiovascular complications, from natural products have become an essential focus in drug discovery.

In this view, we evaluated the natural product FA, against the MG53 expression in the DCM rat model, and the results are promising. FA downregulated MG53 and its targeted pathways like insulin resistance and lipid metabolism. FA also found effective against the conventional cardiac dysfunction and myocardial infarction markers. FA acted as glucose-lowering agent in the DM rats, and effective against the cardiomyocyte injury, fibrosis and dysfunction. Since FA is a ubiquitous phytochemical found in a large variety of edible vegetables and fruits, it is an attractive molecule for nutraceuticals development for DCM. The metformin is also found beneficial against DCM from the present study.

References

1. Amrutkar M, Cansby E, Chursa U, et al., 2015. Genetic disruption of protein kinase STK25 ameliorates metabolic defects in a diet-induced type 2 diabetes model. Diabetes. 64(8):2791-804.
2. Apple FS, Collinson PO, 2012. IFCC task force on clinical applications of cardiac biomarkers: Analytical characteristics of high-sensitivity cardiac troponin assays. Clin. Chem. 58(1):54-61.
3. Aydin S, Ugur K, Aydin S, Sahin I, Yardim M, 2019. Biomarkers in acute myocardial infarction: current perspectives. Vasc. Health Risk Manag. 15:1-10.
4. Barseghian A, Gawande D, Bajaj M, 2011. Adiponectin and vulnerable atherosclerotic plaques. J. Am. Coll. Cardiol. 57: 761-770.
5. Borghetti G, von Lewinski D, Eaton DM, et al., 2018. Diabetic cardiomyopathy: Current and future therapies beyond glycemic control. Front. Physiol. 9:1514.

6. Bugger H, Abel ED, 2009. Rodent models of diabetic cardiomyopathy. Dis. Model. Mech. 2:454-466.
7. Cai C, Masumiya H, Weisleder N, et al., 2009. Mg53 nucleates assembly of cell membrane repair machinery. Nat. Cell. Biol. 11:56-64.
8. Cardarelli R, Lumicao TG, 2003. B-type natriuretic peptide: a review of its diagnostic, prognostic, and therapeutic monitoring value in heart failure for primary care physicians. Clin Rev. 16:327-333.
9. Chang Y, Yun KE, Jung HS, et al., 2013. A1C and coronary artery calcification in nondiabetic men and women. Arterioscler. Thromb. Vasc. Biol. 33(8):2026-2031.
10. Cherkas A, Abrahamovych O, Golota S, et al., 2015. The correlations of glycated hemoglobin and carbohydrate metabolism parameters with heart rate variability in apparently healthy sedentary young male subjects. Redox. Biol. 5:301-307.
11. Engel LC, Landmesser U, Goehler A, et al, 2019. Noninvasive imaging of endothelial damage in patients with different HbA1c levels: A proof-of-concept study Diabetes. 68 (2):387-394.
12. Epshteyn V, Morrison K, Kishnaswamy P, et al., 2003. Utility of B-type natriuretic peptide (BNP) as a screen for left ventricular dysfunction in patients with diabetes. Diabetes Care. 26:2081-2087.
13. Fillmore N, Mori J, Lopaschuk GD, 2014. Mitochondrial fatty acid oxidation alterations in heart failure, ischaemic heart disease and diabetic cardiomyopathy. Br. J. Pharmacol. 171(8):2080-2090.
14. Guo C, Li C, Yu Y, et al., 2016. Antihyperglycemic and antihyperlipidemic activities of protodioscin in a high-fat diet and streptozotocin-induced diabetic rats. RSC Adv. 6:88640-88646.
15. Herlein JA, Fink BD, O'Malley Y, Sivitz WI, 2009. Superoxide and respiratory coupling in mitochondria of insulin-deficient diabetic rats. Endocrinology. 150:46-55.
16. Jia G, DeMarco VG, Sowers JR, 2016. Insulin resistance and hyperinsulinaemia in diabetic cardiomyopathy. Nat Rev Endocrinol. 12(3):144-53.

17. Kabekkodu SP, Mananje SR, Saya RP, 2016. A Study on the role of heart type fatty acid binding protein in the diagnosis of acute myocardial infarction. J Clin Diagn Res. 10(1):OC07-10.
18. Katan M, Fluri F, Morgenthaler NG, 2009. Copeptin: a novel, independent prognostic marker in patients with ischemic stroke. Ann. Neurol. 66:799-808.
19. Lazo M, Halushka MK, Shen L, et al., 2015. Soluble receptor for advanced glycation end products and the risk for incident heart failure: The atherosclerosis risk in communities study. Am. Heart J. 170(5):961-7.
20. Lee TI, Kao YH, Chen YC, et al., 2013. Peroxisome proliferator-activated receptors modulate cardiac dysfunction in diabetic cardiomyopathy. Diabetes Res. Clin. Pract. 100:330-339.
21. Liu F, Song R, Feng Y, et al., 2015. Upregulation of MG53 induces diabetic cardiomyopathy through transcriptional activation of peroxisome proliferation-activated receptor α. Circulation. 131(9):795-804.
22. Nicholls SJ, Hazen SL, 2005. Myeloperoxidase and cardiovascular disease. Arterioscler. Thromb. Vasc. Biol. 25:1102-1111.
23. Norata GD, Pirillo a, Catapano AL, 2006. Modified HDL: Biological and physiopathological consequences. Nutr. Metab. Cardiovasc. Dis. 16(5):371-386.
24. Ormazabal V, Nair S, Elfeky O, et al., 2018. Association between insulin resistance and the development of cardiovascular disease. Cardiovasc. Diabetol. 17:122.
25. Ouwens DM, Diamant M, Fodor M, et al., 2007. Cardiac contractile dysfunction in insulin-resistant rats fed a high-fat diet is associated with elevated CD36-mediated fatty acid uptake and esterification. Diabetologia. 50:1938-1948.
26. Patibandla S, Gupta K, Alsayouri K, 2020. Cardiac Enzymes. In: StatPearls [Internet]. Treasure Island (FL): StatPearls Publishing. https://www.ncbi.nlm. nih.gov/ books/NBK545216/

27. Qi Y, Xu Z, Zhu Q, et al., 2013. Myocardial loss of IRS1 and IRS2 causes heart failure and is controlled by p38α MAPK during insulin resistance. Diabetes. 62(11):3887-3900.
28. Reagan-Shaw S, Nihal M, Ahmad N, 2008. Dose translation from animal to human studies revisited. FASEB J. 22:659-661.
29. Ritchie RH, Cao AH, Kiriazis H, et al., 2006. Atrial natriuretic peptide (ANP) prevents diabetic cardiomyopathy via suppression of NADPH oxidase. Circulation. 114(S18):II_132.
30. Seferovic JP, Tesic M, Seferovic PM, et al., 2018. Increased left ventricular mass index is present in patients with type 2 diabetes without ischemic heart disease. Sci Rep. 8:926.
31. Segnani C, Ippolito C, Antonioli L, et al., 2015. Histochemical detection of collagen fibers by sirius red/fast green is more sensitive than van Gieson or sirius red alone in normal and inflamed rat colon. PLoS One 10(12), e0144630
32. Song R, Peng W, Zhang Y, et al., 2013. Central role of E3 ubiquitin ligase MG53 in insulin resistance and metabolic disorders. Nature. 494:375-379.
33. Suzuki K, Ota H, Sasagawa S, Sakatani T, Fujikura T, 1983. Assay method for myeloperoxidase in human polymorphonuclear leukocytes. Anal Biochem. 132(2):345-52.
34. Tabara Y, Arai H, Hirao Y, et al., 2017. Nagahama study group: different inverse association of large high-density lipoprotein subclasses with exacerbation of insulin resistance and incidence of type 2 diabetes: the Nagahama study. Diabetes Res. Clin. Pract. 127:123-131.
35. Tonin AM, Grings M, Busanello EN, et al., 2010. Long-chain 3-hydroxy fatty acids accumulating in LCHAD and MTP deficiencies induce oxidative stress in rat brain. Neurochem Int. 56:930-936.
36. Trost SU, Belke DD, Bluhm WF, Meyer M, Swanson E, Dillmann WH, 2002. Overexpression of the sarcoplasmic reticulum Ca(2+)-ATPase improves myocardial contractility in diabetic cardiomyopathy. Diabetes. 51:1166-1171.

37. Wang X, Wang J, Su M, et al., 2013. Tnni3k, a cardiac-specific kinase, promotes physiological cardiac hypertrophy in transgenic mice. PLoS One. 8:e58570.
38. Yamagishi SI, Matsui T, 2018. Role of hyperglycaemia-induced advanced glycation end product (AGE) accumulation in atherosclerosis. Ann. Vasc. Dis. 11(3):253–258.
39. Yi JS, Park JS, Ham YM, et al., 2013. MG53-induced IRS-1 ubiquitination negatively regulates skeletal myogenesis and insulin signalling. Nat. Commun. 4:2354.
40. Zhang R, Shen Z, Nauseef WM, Hazen SL, 2002. Defects in leukocyte-mediated initiation of lipid peroxidation in plasma as studied in myeloperoxidase-deficient subjects: systematic identification of multiple endogenous diffusible substrates for myeloperoxidase in plasma. Blood. 99:1802–1810.
41. Zhang Y, Lv F, Jin L, et al., 2011. MG53 participates in ischaemic post conditioning through the RISK signalling pathway. Cardiovasc. Res. 91:108-115.
42. Zhao W, Katzmarzyk PT, Horswell R, et. al., 2014. HbA1c and coronary heart disease risk among diabetic patients. Diabetes care. 37(2):428-435.
43. Zhu W, Cheng KK, Vanhoutte PM, Lam KS, Xu A, 2008. Vascular effects of adiponectin: molecular mechanisms and potential therapeutic intervention. Clin. Sci (Lond). 114(5):361-74.

Chapter 5

Summary and conclusion

5.1. Summary

In the H9c2 cells, the hyperglycaemia caused alterations on the Ca^{2+} homeostasis, mitochondrial function, MAMs, induced oxidative stress, and increased apoptotic cell death (**Fig.5.1**). The mechanism underlying hyperglycaemia induced oxidative stress was analysed and found that different mechanisms such as increased intracellular Ca^{2+} ions, defective mitochondrial ETC complexes, dysregulation of HSPs were involved. The detailed investigation on the intracellular Ca^{2+} ion revealed the role of novel SERCA pathway and the MAMs. The proteins of the SERCA pathway like Serca2/1, pPln, and pPka cα were found downregulated, which lead to the dysregulation of Ca^{2+} ion transport. Also, the Ca^{2+} ion transporters of MAM like Ip_3r2 and Pacs2 were found upregulated, and the regulator protein Mcur1 was downregulated in hyperglycaemia, which resulted in defective Ca^{2+} ion handling in mitochondria and resulted in intracellular Ca^{2+} overload.

The overall effects of hyperglycaemic stress were found to have resulted in the oxidative damages to lipids, proteins, DNA, mitochondria, and MAMs, which caused the release of cardiomyocyte injury markers like ANP, BNP, and LDH. The mitochondria were found dysfunctional with dissipated membrane potential, aberrant mPTP opening, dysregulated dynamics (increased fission and decreased fusion), defective OxPhos complex activities with reduced ATP production, and the increased mitochondrial superoxide. The present study assessed the crosstalk between mitochondria and MAMs in various functions. The protein expression of MAMs during hyperglycaemia revealed that the mitochondrial fusion protein Mfn2 was downregulated, whereas fission protein Fis1 was upregulated, revealing the regulatory function of MAMs over mitochondrial dynamics. MAMs also showed to have a regulatory effect on mPTP opening via the Vdac1 protein, which is the central channel protein of mPTP. Thus MAMs were involved in mitochondrial membrane potential indirectly via mPTP. The present study also showed that dysfunctional mitochondria release various pro-apoptotic proteins of multiple

apoptotic pathways and finally cardiomyocyte death, which is the endpoint of DCM.

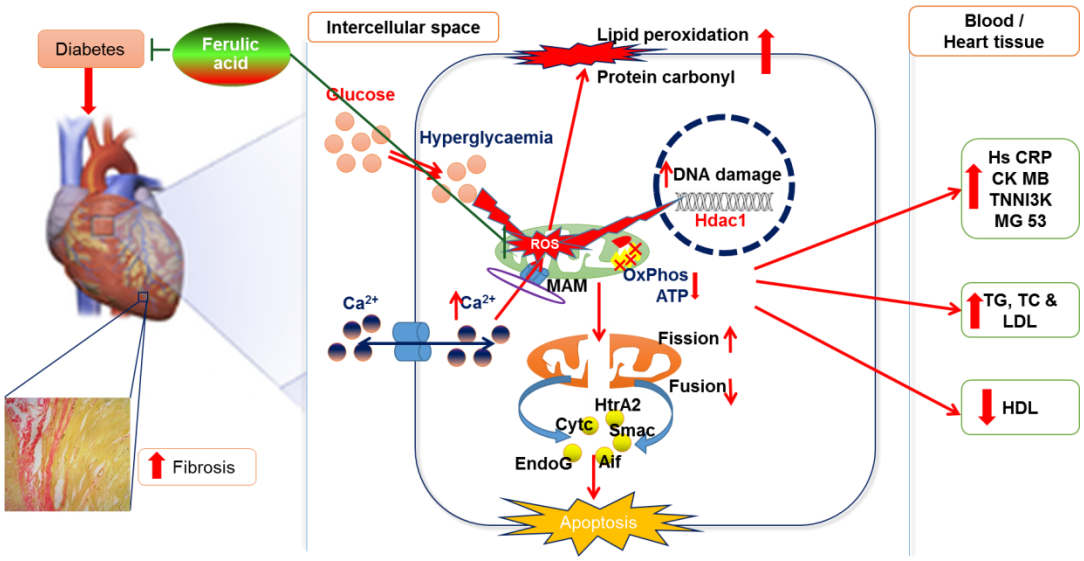

Fig.5.1. Schematic representation of the effect of ferulic acid against DCM

The study on diabetic rats showed that the hyperglycaemia induced damages in vitro system had been translated into the animal system. The diabetic rats showed increased HbA1c and HOMA-IR values and insulin resistance. This model of diabetes also increased the TC, TG and LDL-C, and reduced the HDL-C, which gave the future cardiac complications of diabetes. The cardiomyocyte injury and dysfunction were increased in the diabetic rats evidenced with increased SGOT, S-LDH, CK-MB, MPO, troponins (cTnT & cTnI), TNNI3K, hs-Crp, hFabp, copeptin, ANP, and BNP levels (**Fig.5.1**). The HMI was also found to increase with increased collagen fibre content.

One of the novel mechanisms underlying DCM was studied with the mitsugumin 53 (MG53) mediated insulin resistance and lipid metabolism pathways in heart tissue. MG53 was found upregulated, which in turn downregulated the Ir/Irs1/pAkt insulin signalling pathway to induce insulin resistance one of the central pathophysiologies of DCM. The upregulated MG53 causes the upregulation of Pparα and its targeted proteins Cpt1 and Acc2, and other fatty acid metabolising factors such as Fas and adiponectin.

These effects are predicted to induce lipotoxicity in cardiomyocyte and the DCM.

The phytochemical FA and the standard drug metformin were also evaluated against these pathophysiological and molecular mechanisms in both *in vitro* and *in vivo* model systems. The results revealed that FA could attenuate hyperglycaemic stress and protect the mitochondria. Also, FA showed beneficial effects on Ca^{2+} homeostasis via SERCA pathway and MAMs. In the diabetic rats, FA reduced the HbA1c, HOMA-IR, lipid profile, and most of the biochemical markers of cardiac dysfunction. FA also acted as an inhibitor of MG53 and attenuated the insulin resistance and lipotoxicity in heart tissue (**Fig.5.1**). Overall results revealed the cardioprotective effect of FA during hyperglycaemia/ diabetes.

5.2. Conclusion

Overall, the present study generated highly novel data on the mechanisms of DCM employing various established experimental techniques. The results are highly promising and report novel molecular targets and biomarkers for the development of diagnostic parameters and medicine for the management of DCM. The results of the studies in this dissertation establish specific molecular pathways such as SERCA pathway of Ca2+ homeostasis and MAMs as novel targets for the analysis of DCM. The MG53 protein is suggested as a novel biomarker for the early diagnosis of DCM, which demands more elaborative research. We are postulating that the inhibitors of MG53 as the drugs for DCM. The activities of FA are found promising, and since it is from edible plants, it can be developed as nutraceuticals for the DCM with extensive research.

5.3. Future prospects

Even though the communicable diseases like the on-going pandemic of novel Covid-19 affecting large numbers of the population over the World, the non-communicable disorders like diabetes and heart disorders are still run as

the largest killers in the World. The findings from the present study pave a new way of research in the development of novel biomarkers and the identification of molecular mechanisms in the genesis of DCM. The results of the present study propound some exciting indications which demand elaborative research in future, and we summarise some of the perspective as follows:

- Investigation on SERCA pathway and MAMs using specific inhibitors or by genetic knockout/knockdown analysis for much deeper foundation of these pathways as biomarkers for DCM.
- The analysis of MG53 in the gene level and also the development of specific inhibitors for it, in order to develop novel drug molecules for the treatment of DCM.

ABSTRACT

Name of the Student : Salin Raj P **Registration No. :** 10BB15A39025
Faculty of Study : Biological Sciences **Year of Submission :** September 2020
AcSIR academic centre/CSIR Lab: NIIST **Name of the Supervisor:** Dr K G Raghu

Title of the thesis: Elucidation of hyperglycaemia mediated mitochondrial dysfunction and associated complications in heart and evaluation of ferulic acid against the same

Diabetic cardiomyopathy (DCM) is the existence of abnormal myocardial structure and function in the absence of other cardiac risk factors during diabetes. This investigation deals with alteration in mitochondrial functions during DCM and possible protection with ferulic acid (FA) exploring in vitro and in vivo models. In this study, an in vitro model of hyperglycaemia had been developed by incubating H9c2 cells with glucose for 48 h. For the *in vivo* model, male Wistar rats were fed with a high fat-fructose diet for two months after that a single dose of streptozotocin (25 mg/kg b. wt.) was given to induce diabetes, and the rats having fasting blood glucose above 300 mg/dl were used. The hyperglycaemic pathology was investigated by cardiomyocyte injury markers, mitochondrial function, dynamics, Ca^{2+} homeostasis, apoptosis, and oxidative stress. The molecular pathways like SERCA pathway of Ca^{2+} homeostasis and MAMs (mitochondria-associated ER membranes) in the mitochondrial dynamics and energy metabolism (OxPhos) were studied. MAMs were subjected to detailed investigation selecting critical proteins such as Pacs2, Ip3r2, Fundc1, Vdac1, Ant1, CypD, Mcur1, Mfn2, and Drp1. MAMs were also explored for its functional link with mitochondrial dynamics by studying alteration in its core proteins namely Mfn2, Opa1, Drp1 and Fis1; electron transport chain by alteration in various OxPhos complexes, and Ca^{2+} homeostasis by Mcur1. The *in vivo* study was conducted to check whether the cellular events and apoptosis occurred in the H9c2 cells during hyperglycaemia transform to insulin resistance, fibrosis, hypertrophy and injury in the diabetic heart. From various biomarker analyses, we confirmed the development of DCM with above mentioned pathological lesions. A novel molecular mechanism of mitsugumin 53 (MG53) mediated insulin resistance, and lipid metabolism was explored, and this study is the first report of this kind. Overall this study confirms the significant role of MAM, SERCA pathway, and MG53 in the aetiology of DCM. The evaluation of FA against DCM showed it is beneficial and an attractive phytochemical for nutraceuticals development for DCM.

PUBLICATIONS

Publications from the thesis

1. **Salin Raj P**, Swapna Sasi US, Raghu KG (2019). High glucose induced calcium overload via impairment of SERCA/PLN pathway and mitochondrial dysfunction leads to oxidative stress in H9c2 cells and amelioration with ferulic acid. Fund. Clin. Pharmacol. 33(4):412-425.

2. **Salin Raj P**, Anupama Nair, Preetha Rani MR, Ranjith S, Rajankutty K, Raghu KG (2020). MAM regulated mitochondrial dynamics and ETC causing multiple pathways of apoptosis is the basis of diabetic cardiomyopathy, and evaluation of efficacy of ferulic acid. (*submitted to journal*)

Manuscript to be communicated

3. **Salin Raj P**, Anupama Nair, Preetha Rani MR, Ranjith S, Rajankutty K, Raghu KG (2020). MG53 mediated insulin resistance and lipid metabolism mechanism in the genesis of diabetic cardiomyopathy and effect of ferulic acid (*under preparation*)

Publications from other than thesis

1. **Salin Raj P**, Prathapan A, Sebastian J, Antu KA, Riya MP, Preetha Rani MR, Biju H, Priya S, Raghu KG (2014). *Parmotrema tinctorum* exhibits antioxidant, antiglycation and inhibitory activities against aldose reductase and carbohydrate digestive enzymes: an *in vitro* study. Nat. Prod. Res. 28(18):1480-1484.
2. **Salin Raj P** ‡, Sankar V ‡, Athira R, Soumya RS, Raghu KG (2015). Cerium nanoparticles synthesized using aqueous extract of *Centella asiatica*: characterization, determination of free radical scavenging activity and evaluation of efficacy against cardiomyoblast hypertrophy. RSC Adv. 5:21074-21083. (‡*These authors contributed equally to the work and deserve to have the status of first author*)

3. Prathapan A, **Salin Raj P**, Raghu KG (2016). Attenuation of oxidative damage by *Boerhaavia diffusa L*. against different neurotoxic agents in rat brain homogenate. J. Diet. Suppl. 13(3):300-12.
4. Prathapan A, **Salin Raj P**, Priya Rani M, Raghu KG (2018). Apoptosis in angiotensin II-stimulated hypertrophic cardiac cells -modulation by phenolics rich extract of *Boerhavia diffusa* L. Biomed. Pharmacother. 108:1097-1104.
5. Swapna Sasi US, Sindhu G, **Salin Raj P**, Raghu KG (2020). Mitochondria Associated Membranes (MAMs): Emerging drug targets for diabetes. Curr. Med. Chem. 27(20):3362-3385.
6. Soumya RS, Prathapan A, **Salin Raj P**, Vineetha VP, Raghu KG (2018). Selenium incorporated guar gum nanoparticles safeguard mitochondrial bioenergetics during ischemia reperfusion injury inH9c2 cardiac cells. Int. J. Biol. Macromol. 107:254-260
7. Soumya RS, Vineetha VP, **Salin Raj P**, KG Raghu (2014). Beneficial properties of selenium incorporated guar gum nanoparticles against ischemia/reperfusion in cardiomyoblasts (H9c2). Metallomics. 6(11):2134-2147.
8. Priyanka A, Shyni GL, Anupama Nair, **Salin Raj P**, Anusree SS, Raghu KG (2017). Development of insulin resistance through sprouting of inflammatory markers during hypoxia in 3T3-L1 adipocytes and amelioration with Curcumin. Eur. J. Pharmacol. 812:73-81
9. Prathapan A, Varghese MV, Abhilash S, **Salin Raj P**, Mathew AK, Anupama Nair, Harikumaran Nair R, Raghu KG (2017). Polyphenol rich ethanolic extract from Boerhavia diffusa L. mitigates angiotensin II induced cardiac hypertrophy and fibrosis in rats. Biomed. Pharmacother. 87:427-436.
10. Jaiswal N, Maurya CK, Arha D, Avisetti DR, Prathapan A, **Salin Raj P**, Raghu KG, Kalivendi SV, Tamrakar AK (2015). Fructose induces mitochondrial dysfunction and triggers apoptosis in skeletal muscle cells by provoking oxidative stress. Apoptosis. 20(7):930- 947.

CONFERENCE PRESENTATIONS

Oral paper presentations

1. IBS award for best paper presentation: **Salin Raj P**, Sruthi Krishna K, Raghu KG (2019). Cardioprotective, alpha-glucosidase inhibition activity and antioxidant potential of Boeravinone B, a rotenoid isolated from *Boerhaavia diffusa* Lin. In National Conference on Biotechnology Innovations & Annual Meet of Society for Biotechologists (India) held at SRMU, Lucknow, Uttar Pradesh.

2. **Salin Raj P,** Raghu KG (2018). Ferulic acid ameliorates the hyperglycaemia induced mitochondrial dysfunction and deregulation of calcium homeostasis through SERCA/PLB regulatome in H9c2 cardiomyoblasts. In International conference on Biochemical innovations: translating cellular cues to novel therapeutics & 7th Annual meet of Indian Academy of Biomedical Sciences held at SKIMS, Srinagar, Jammu & Kashmir.

3. Young Scientist Award for best paper presentation: **Salin Raj P,** Sindhu G, Raghu KG (2016). Fukugiside from *Garcinia travancorica* Bedd. acts as anti-obesity agent via regulating lipid metabolism through PPAR α and AMPK signalling pathways in HepG2 cells. In International Conference on Nutraceuticals and Chronic Diseases held at Cochin, Kerala

Poster presentations

4. **Salin Raj P**, Sreelekshmi Mohan, Shyni GL, Mangalam SN, Raghu KG (2017). Licarin B, a novel insulin sensitizer from *Myristica fragrans* acts *via* PPARγ and GLUT4 in the IRS-1/PI3K/AKT pathway in 3T3-L1 adipocytes. In International conference on Current Trends in Healthcare - Advances in New Drug Discovery And Development & 8th RBF symposium, Ahmedabad, Gujarat.

5. **Salin Raj P**, Prathapan A, Raghu KG (2015). α-Amyrin ameliorates the hyperglycemia induced oxidative stress and Ca^{2+} overload in H9c2 cardiomyocytes. In International Conference on Recent Advances in Research and Treatment of Human Diseases and 4th Annual Meeting of Indian Academy of Biomedical Sciences, Hyderabad.

doi: 10.1111/fcp.12452

ORIGINAL ARTICLE

High glucose induced calcium overload via impairment of SERCA/PLN pathway and mitochondrial dysfunction leads to oxidative stress in H9c2 cells and amelioration with ferulic acid

Palayyan Salin Raj[a,b], Sasi U. S. Swapna[a,b], Kozhiparambil G. Raghu[a,b]*

[a]Biochemistry and Molecular Mechanism Laboratory, Agro-Processing and Technology Division, CSIR - National Institute for Interdisciplinary Science and Technology (NIIST), Thiruvananthapuram 695019, Kerala, India
[b]Academy of Scientific and Innovative Research (AcSIR), CSIR-HRDC Campus Ghaziabad, Uttar Pradesh 201 002, India

Keywords
brain natriuretic peptide,
calcium overload,
diabetic cardiomyopathy,
H9c2,
mitochondria,
SERCA

Received 4 September 2018;
revised 15 January 2019;
accepted 31 January 2019

*Correspondence and reprints:
raghukgopal@niist.res.in;
raghukgopal2009@gmail.com

ABSTRACT

Oxidative stress and associated complications are the major pathological concerns of diabetic cardiomyopathy (DC). We aim to elucidate the mechanisms by which high glucose (HG) induced alteration in calcium homeostasis and evaluation of the beneficial effect of two concentrations (10 and 25 μM) of ferulic acid (FA). HG was induced in H9c2 cardiomyoblast by treating with glucose (33 mM) for 48 h, and FA was co-treated. Intracellular calcium ([Ca^{2+}]i) overload was found increased significantly with HG. For elucidation of mechanism, the SERCA pathway and mitochondrial integrity (transmembrane potential and permeability transition pore) were explored. Then, we assessed oxidative stress, and cell injury with brain natriuretic peptide (BNP), atrial natriuretic peptide (ANP), and lactate dehydrogenase (LDH) release. HG caused significant [Ca^{2+}]i overload through downregulation of SERCA2/1, pPLN, and pPKA C-α; and upregulation of PLN and PKA C-α and alteration in the integrity of mitochondria with HG. The [Ca^{2+}]i overload in turn caused oxidative stress via generation of reactive oxygen species, lipid peroxidation, and protein carbonylation. This resulted in cell injury which was evident with significant release of BNP, ANP, and LDH. FA co-treatment was effective to mitigate all pathological changes caused by HG. From the overall results, we conclude that [Ca^{2+}]i overload via SERCA pathway and altered mitochondrial integrity is the main cause for oxidative stress during HG. Based on our result, we report that FA could be an attractive nutraceutical for DC.

INTRODUCTION

Diabetic cardiomyopathy (DC), a diabetic-associated complication of heart, is emerging as a leading cause of diabetic mortality. DC, a clinical condition independent of conventional coronary artery disease, valvular disease, hypertension, and/or dyslipidemia, has been increasingly recognized by clinicians and epidemiologists as a serious health issue of unmet category [1]. Oxidative stress and multiple associated complications are primarily responsible for the development of DC [2].

The existence of crosstalk between calcium (Ca^{2+}) homeostasis and redox status in the cells has been well established. Literature reveals that the hyperglycemia alters Ca^{2+} homeostasis [3]. The facilitated Ca^{2+} homeostasis has been suggested as a potential choice for treatment of DC [4]. There are some reports available on the mechanism underlying high glucose (HG) induced

© 2019 Société Française de Pharmacologie et de Thérapeutique

intracellular calcium ([Ca^{2+}]i) overload in H9c2 cells. Kumar et al. [3] reported that HG treated H9c2 cells showed increased [Ca^{2+}]i with a concomitant increase in intra-mitochondrial calcium ([Ca^{2+}]m) which resulted in enhanced reactive oxygen species (ROS) generation, mitochondrial dysfunction, and apoptosis.

But no detailed investigation is done to check the involvement of sarcoplasmic reticulum Ca^{2+}-ATPase (SERCA)/phospholamban (PLN) in HG-induced Ca^{2+} overload in H9c2 cells. Here, in first time, we report the contribution of SERCA/PLN signalling pathway downregulation and mitochondrial dysfunction together in the genesis of [Ca^{2+}]i overload during HG shock. Mitochondrial dysfunction initiates with transition (opening) of membrane permeability transition pore (mPTP) which in turn causes a change in permeability of the mitochondrial membrane. This causes dissipation of mitochondrial transmembrane potential, followed by irregular calcium influx to cytoplasm leading to [Ca^{2+}]i overload.

Ferulic acid (FA), a ubiquitous phenol compound, occurs as the main constituent of the cell wall of annual plants. It occurs as a bioactive ingredient of many foods such as grain bran, whole-grain foods, citrus fruits, banana, coffee, orange juice, eggplant, bamboo shoots, beetroot, cabbage, spinach, broccoli, etc [5]. Some of the studies reported that FA had been a potential agent for the treatment of diabetes, cancer, Alzheimer's disease, skin disease, cardiovascular diseases, etc. [6]. But the precise role of FA and the details of the underlying mechanism of HG-induced DC remain largely unclear.

Considering the importance of Ca^{2+} homeostasis in heart function and its crosstalk with redox status, the present study is focused on elucidation of the effect of HG on cardiomyocyte Ca^{2+} homeostasis and role of FA on possible recovery and mechanism. H9c2 rat ventricular myoblast cells are the one more similar to primary cardiac myocytes in phenotype, energy metabolism, and gene expression patterns; and also the cell responses to metabolic and gene expression remodelling with different stimuli [7,8]. So in this study, H9c2 cell line was used as an in vitro model system.

MATERIALS AND METHODS

Chemicals and reagents

Ferulic acid, metformin hydrochloride, D-glucose, mannitol, 2′,7′- dichlorofluorescin diacetate (DCFDA), cobalt chloride ($CoCl_2$), 1-(4,5-Dimethylthiazol-2-yl)-3, 5-diphenyl formazan (MTT), dimethyl sulfoxide (DMSO), Krebs-Ringer bicarbonate buffer (KRB), MitoSOX, and JC-1 mitochondrial staining kit were purchased from Sigma-Aldrich, St. Louis, MO, USA. Dulbecco's Modified Eagle's Medium (DMEM), fetal bovine serum (FBS), Hank's Balanced Salt Solution (HBSS), penicillin-streptomycin solution, and trypsin-EDTA solution were from GIBCO®, Life Technologies, Waltham, MA, USA. Fura-2 AM and Calcein-AM were purchased from Invitrogen™, Fisher Scientific, Houston, TX, USA. Primary and secondary western blot antibodies for SERCA 2/1, PLN, pPLN, PKA C-α, pPKA C-α, β-actin proteins were from Cell Signalling Technology, Danvers, MA, USA. The solvents and reagents used were analytical grade unless/otherwise mentioned.

Cell culture and induction of HG

H9c2 cardiomyoblast cells (American Type Culture Collection (ATCC), CLR-1446; Rockville, MD USA) were maintained in DMEM supplemented with 10% FBS, 1% penicillin-streptomycin solution and incubated at 5% CO_2 and 37 °C in a humidified incubator (Eppendorf, Hauppauge, NY, USA). HG condition was induced according to the previous protocol [9]. Briefly, when the cell populations reached 40–50% confluence, the cells were exposed to 33 mM of glucose for 48 h, to investigate the pathological changes associated with HG. The cells with 5.5 mM D-glucose were control. To exclude a hyperosmolar effect, we added identical concentrations of mannitol (5.5 and 33 mM) and evaluated cytotoxicity and ROS generation. No significant effect was seen compared to respective groups (data not shown).

Experimental groups

C – control (5.5 mM glucose); CF – control + ferulic acid (FA -25 μM); HG – high glucose (33 mM glucose); HGF1 – high glucose + FA (10 μM); HGF2 – high glucose + FA (25 μM); HGM – high glucose + metformin (Met -10 μM). The FA and Met were co-treated with the HG group for 48 h.

Cytotoxicity assay

The cytotoxicity evaluation was done by MTT assay according to the protocol of Mosmann [10]. Briefly, once the experimental duration is over, the cells were incubated with MTT solution (5 mg/mL MTT in DMEM) for 4 h at 37 °C with 5% CO_2 atmosphere. The metabolically active cells reduce the yellow tetrazolium MTT, by the action of dehydrogenase enzymes, NAD(P)

© 2019 Société Française de Pharmacologie et de Thérapeutique

H-dependent oxidoreductase, to formazan, an insoluble crystalline product with a deep purple color. The purple-colored MTT formazan was dissolved in DMSO, and the absorbance was read at 570 nm by a microplate reader (Infinite® M200 PRO; Tecan Group Ltd, Männedorf, Switzerland); and the results were expressed as % cytotoxicity.

Estimation of intracellular Ca^{2+} ($[Ca^{2+}]i$) overload

The $[Ca^{2+}]i$ overload was determined using the calcium indicator dye, fura-2 AM. Briefly, the cells from all groups were incubated with fura-2 AM (5 μM in PBS) for 20 min at 37 °C and then washed twice with PBS. The cells were then visualized using BD Pathway™ 855 High-Content BioImager (AttoVision software; BD Biosciences, San Jose, CA, USA) at an excitation/emission of 375/510 nm wavelengths. The images were analyzed using ImageJ software (U. S. National Institutes of Health, Bethesda, MD, USA).

Western blot examination of SERCA/PLN pathway

After the particular treatment, the total protein was extracted in RIPA buffer [11], and quantified using the bicinchoninic acid protein assay kit (BCA kit; Pierce, Rockford, IL, USA). An equal amount of proteins (20 μg) were separated by 10% SDS-PAGE and transferred to PVDF membranes using the Trans-Blot® Turbo™ Transfer system (Bio-Rad, Hercules, CA, USA). The membranes were blocked with 5% skimmed milk in TBST (50 mM Tris, pH 7.5, 150 mM NaCl, 0.01% Tween-20) for 1 h at room temperature. The membrane was washed three times with TBST for 10 min each. After that, membrane was incubated at 4 °C overnight with primary antibodies of SERCA 2/1, PLN, pPLN, PKA C-α, pPKA C-α, and β- actin proteins. After washing with TBST, the membrane was incubated with HRP-conjugated corresponding secondary antibodies for 1 h at room temperature. Again washed three times with TBST, then the membranes were developed using Western BLoT Hyper HRP Substrate (Takara Bio Inc., Mountain View, CA, USA), and the protein bands were analyzed (Bio-Rad ChemiDoc MP imaging systems, USA).

Analysis of mitochondrial transmembrane potential (ΔΨm) and opening of mitochondrial permeability transition pore (mPTP)

The change in ΔΨm was detected using the JC-1 mitochondria staining kit (Sigma-Aldrich). Briefly, after experiments, 5 μM of JC-1 was added to wells and incubated for 30 min at 37 °C. In the live cells, JC-1 exists either as a green-fluorescent monomer at depolarized membrane potentials or as an orange fluorescent J-aggregate at hyperpolarized membrane potentials. The cell images were taken by BD Pathway™ 855 High-Content BioImager (BD, Franklin Lakes, NJ, USA) on excitation at 490 nm, and the emission was collected at 530 nm (monomer) and 590 nm (aggregate) and analyzed with ImageJ software, U. S. National Institutes of Health, Bethesda, MD, USA. Valinomycin was used as negative control.

The mPTP opening was observed with calcein-AM dye in the presence of $CoCl_2$ as previously described protocol [12]. Briefly, after the respective experiments, the culture medium was removed and washed with KRB, and added 1 mL of calcein loading solution (containing 1 μM calcein- AM and 2 mM $CoCl_2$ in KRB); and incubated for 15 min at 37 °C in a 5% CO_2 atmosphere. Then, washed twice with KRB and images of cells were taken (BD Pathway™ 855 High-Content BioImager System, BD, USA); and fluorescent intensity was measured by microplate reader (Infinite® M200 PRO; Tecan Group Ltd) at excitation/emission of 488/525 nm.

Estimation of cytosolic ROS and mitochondrial superoxide production

The cytosolic ROS formation was evaluated using DCFH-DA fluorescent dye (excitation/emission: 488/525 nm). Briefly, DCFH-DA was added (3 μg/mL in PBS) to the cells, and incubated for 20 min at 37 °C, washed three times with PBS and images were taken (BD, USA). The fluorescence intensity was measured using microplate reader (Tecan Group Ltd) and flow cytometry analysis by BD FACS Aria II flow cytometer (BD Biosciences, San Jose, CA, USA.).

The mitochondrial superoxide productions were evaluated with MitoSOX dye. Briefly, the cells were incubated with MitoSOX (5 μM in HBSS) dye for 10 min at 37 °C, then washed three times with HBSS and images were taken as described above sections. The fluorescent intensity was analyzed as before.

Analysis of lipid peroxidation and protein carbonyl content

The lipid peroxidation was estimated spectrophotometrically using the lipid peroxidation assay kit (Sigma-Aldrich). The lipid peroxidation is the degradation of lipids that occurs as a result of oxidative damage resulting in the production of end products such as

© 2019 Société Française de Pharmacologie et de Thérapeutique

malondialdehyde (MDA). The cell lysate was prepared in MDA lysis buffer (supplied with the kit) and used for analysis. The lipid peroxidation was determined by the reaction of MDA with thiobarbituric acid to form a colorimetric (532 nm) product proportional to the MDA, and calculated using MDA standard curve and expressed as nM/μL.

The protein carbonyl content was analyzed with colorimetric assay kit of Cayman Chemical (Ann Arbor, USA). Briefly, the protein was extracted in ice cold PBS (50 mM) (pH 6.7 containing 1 mM EDTA) and estimated using Pierce™ BCA protein assay kit (Thermo Scientific, Rockford, IL, USA). Then, the protein samples were derivatized by the reaction between 2,4- dinitrophenyl hydrazine and protein carbonyls; and the formed Schiff base produce the corresponding protein-hydrazone which was estimated spectrophotometrically at 370 nm.

Estimation of atrial natriuretic peptide and brain natriuretic peptide

The level of atrial natriuretic peptide (ANP) in the medium was estimated by competitive ELISA method using the Rat ANP ELISA kit (Elabscience®, Houston, TX, USA) in the ANP pre-coated ELISA plate. The ANP in the sample (cell culture medium) competes with a fixed amount of ANP on the solid phase supporter for sites on the biotinylated detection antibody specific to ANP. Then, it was incubated with avidin conjugated to horseradish peroxidase (HRP) and a TMB substrate solution. The enzyme-substrate reaction was terminated by the addition of stop solution, and the color change was measured spectrophotometrically at 450 nm. The concentration of ANP was determined from the standard curve, and the results were expressed as pg/mL.

The brain natriuretic peptide (BNP) level was determined by RayBio® Human/Mouse/Rat Brain Natriuretic Peptide EIA Kit (RayBiotech, Inc., Norcross, GA, USA). The samples were added to the plate pre-coated with the anti-BNP antibody. The biotinylated BNP peptide competes with the BNP in the sample for binding to the anti-BNP antibody. After a wash step, any bound biotinylated BNP then interacted with horseradish peroxidase (HRP)-streptavidin, catalyze a color development reaction. The intensity of the colorimetric signal is directly proportional to the amount of captured biotinylated BNP peptide and inversely to the amount of BNP in the samples. The concentration of BNP was determined from the standard curve; and expressed as pg/mL.

Lactate dehydrogenase leakage assay

Lactate dehydrogenase (LDH) is a stable cytoplasmic enzyme released only when the cytoplasmic membrane is damaged, and quantification of it in the cell culture supernatant depicts the depth of cell injury. LDH release was quantified using the LDH cytotoxicity detection kit (Takara Bio Inc., Kusatsu, Japan). Briefly, after the respective treatment, the medium was taken and incubated for 30 min at room temperature with the reaction mixture. The yellow tetrazolium salt (INT) was converted into a red formazan product through a coupled reaction by the released LDH enzyme, which was read at 490 nm (Infinite® M200 PRO; Tecan Group Ltd). The amount of LDH enzyme activity directly correlates with the number of injured cells in culture.

Statistical analysis

The results were presented as the mean ± standard deviation (SD) ($n = 6$) for the control and experimental groups. Statistical analyses were done using SPSS statistical programme (SPSS/PC+, Version 11.0, Chicago, IL, USA). Data were subjected to one-way ANOVA, and the differences among the means for the groups were assessed using Duncan's multiple range tests to determine which mean values were significantly different at $P \leq 0.05$.

RESULTS

FA protects H9c2 cardiomyoblasts against HG-induced cell death

Significant cell death with HG was observed (27.80% compared to control; $P \leq 0.05$, *Table I*) and

Table I Evaluation of cytotoxicity (MTT assay) induced by hyperglycemia and protection by ferulic acid (FA) in H9c2 cardiomyoblast cells.

Groups	% Cell death
C	0.00
CF	1.73 ± 0.13
HG	27.80 ± 1.54[a]
HGF1	15.89 ± 0.47[b]
HGF2	10.24 ± 0.45[b]
HGM	7.38 ± 0.26[b]

C – control (5.5 mM glucose), CF – control + FA (25 μM), HG – high glucose (33 mM glucose), HGF1 – high glucose + 10 μM FA, HGF2 – high glucose + 25 μM FA and HGM – high glucose + metformin (10 μM) treated groups. Values are Mean ± SD ($n = 6$).

[a]Mean values are significantly different from the control group ($P \leq 0.05$).

[b]Mean values are significantly different from high glucose group ($P \leq 0.05$).

© 2019 Société Française de Pharmacologie et de Thérapeutique

co-treatment with FA (10 and 25 μM) showed protection against HG. (15.89 and 10.24%, respectively, compared to control, $P \leq 0.05$; *Table I*). The treatment with positive control metformin (7.38%; *Table I*) also showed significant protection.

FA prevented the HG-induced intracellular Ca^{2+} ($[Ca^{2+}]i$) overload in H9c2 cardiomyoblasts

Intracellular calcium was found increased significantly with the HG group. The treatment with FA and Met decreased the $[Ca^{2+}]i$ overload indicated by diminished blue fluorescence (Bioimaging; *Figure 1A*). This was again confirmed by fluorescent intensity analysis with plate reader and found that 31% increase of $[Ca^{2+}]i$ concentration in HG compared with control ($n = 6$, $P \leq 0.05$). The FA treatment decreased $[Ca^{2+}]i$ overload (16% and 20% with 10 and 25 μM, respectively; *Figure 1B*) which was comparable to Met (23%). These results reveal the efficacy of FA in maintaining the $[Ca^{2+}]i$ homeostasis during HG.

FA reverses the HG-induced decrease of SERCA and PLN activation in H9c2 cardiomyoblasts

To elucidate the mechanism by which HG-induced defect in Ca^{2+} homeostasis, we examined the SERCA pathway. The western blot analysis showed that HG downregulated the SERCA2/1, and decreased the expression of phosphorylated PLN and cAMP-dependent protein kinase A catalytic subunit α (PKA C-α)- an activator of PLN, revealing the HG-induced impairment in Ca^{2+} homeostasis. The treatment with FA significantly reversed the effect of HG; it upregulated the SERCA2/1 and increased the phosphorylation of PLN and PKA C-α ($n = 6$) and this was comparable with the positive control Met (*Figure 2*).

FA prevented HG-induced dissipation of mitochondrial membrane potential (ΔΨm) and permeability transition pore (mPTP) opening in H9c2 cardiomyoblasts

The ΔΨm was assessed by bio-imaging with mitochondrial stain JC-1. In the functional mitochondria, the JC-1 dye was found in aggregate (red) form, and in the dysfunctional mitochondria the JC-1 was found in monomeric (green) form due to the dissipation of ΔΨm. HG caused increased green fluorescence indicating the dissipation of ΔΨm. The co-treatment with FA (10 and 25 μM) and Met reduced the green fluorescence and increased red fluorescence preventing ΔΨm dissipation (*Figure 3A,B*).

The mPTP opening is also an indicator of functional mitochondria. So we evaluated the mPTP opening by calcein-AM/$CoCl_2$ bio-imaging. The calcein fluorescence (green) was compartmentalized within mitochondria until PTP opening permits the distribution of cobalt inside mitochondria, which results in the quenching of calcein fluorescence in the mitochondrial matrix. The PTP opening thus leads to the de-compartmentalization (decrease) of calcein fluorescence. The HG showed a decrease in calcein fluorescence

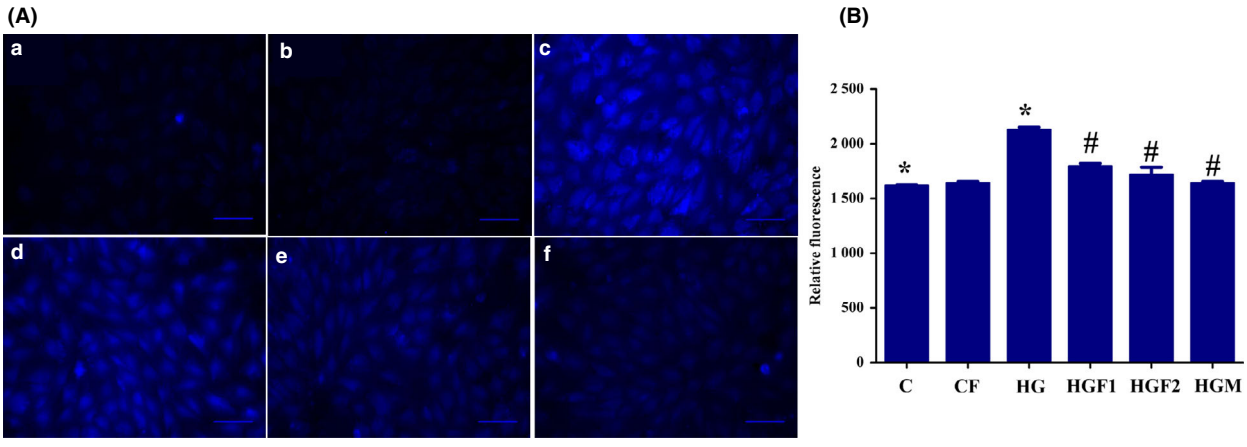

Figure 1 Analysis of intracellular Ca^{2+} overload: (A) Confocal bio-imaging of Fura-2AM fluorescence and (B) Relative fluorescent intensity. (a) C – control (5.5 mM glucose), (b) CF – control + 25 μM ferulic acid (FA), (c) HG – high glucose (33 mM glucose), (d) HGF1 – high glucose + 10 μM FA, (e) HGF2 – high glucose + 25 μM FA and (f) HGM – high glucose + metformin (10 μM) treated groups. Values are Mean ± SD ($n = 6$). * Mean values are significantly different from the control group ($P \leq 0.05$). # Mean values are significantly different from the high glucose treated group ($P \leq 0.05$). Scale bar 50 μM.

© 2019 Société Française de Pharmacologie et de Thérapeutique

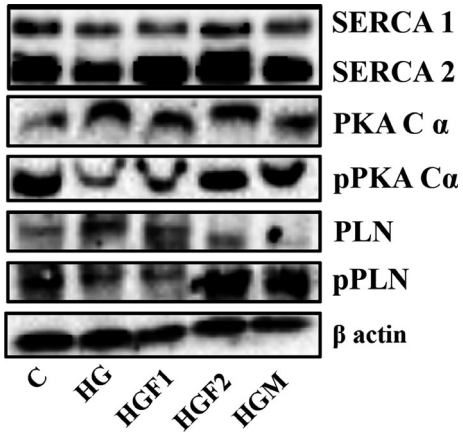

Figure 2 Effect of ferulic acid (FA) and high glucose (HG) on SERCA/PLN pathway: C – control (5.5 mM glucose) (*lane 1*), HG – high glucose (33 mM glucose) (*lane 2*), HGF1 – high glucose + 10 μM FA (*lane 3*), HGF2 – high glucose + 25 μM FA (*lane 4*) and HGM – high glucose + 10 μM metformin (*lane 5*) treated groups. SERCA 2/1 – sarcoplasmic reticulum Ca^{2+}-ATPase 2/1; PLN – phospholamban, pPLN – phosphorylated PLN; PKA C-α – cAMP-dependent protein kinase A catalytic subunit α, and pPKA C-α – phosphorylated PKA C- α. β- actin served as loading control.

indicating the aberrant opening of mPTP and the co-treatment with FA showed increased calcein fluorescence showing the protection of mPTP (*Figure 4A*). It was further confirmed by fluorescent intensity analysis (*Figure 4B*). The results indicated the beneficial effect of FA in maintaining the mitochondrial function during HG in H9c2 cardiomyoblasts.

FA ameliorated the HG-induced mitochondrial superoxide and ROS production; and oxidative damage on lipid and protein in H9c2 cardiomyoblasts

We analyzed the cytosolic ROS production by DCFH-DA dye and mitochondrial superoxide by MitoSOX dye. HG induced 6.5-fold increase in the mitochondrial superoxide generation (compared to the control, $P \leq 0.05$) and is reduced significantly by FA (4.75- and 3.5-fold with 10 and 25 μM, respectively, compared to the control, $P \leq 0.05$; *Figure 5A,B*). The cytosolic ROS analysis also showed increased production with HG evidenced by the increase in green fluorescence, while FA prevented ROS which was comparable to Met (*Figure 6A*). This was again confirmed by fluorescent intensity analysis and showed a significant (60% compared with control) production of ROS whereas the treatment with FA (10 and 25 μM) showed 10% and 22% reduction of the ROS production, respectively ($P \leq 0.05$). The Met application also caused ROS reduction (30%) compared to the HG group (*Figure 6B*). Further confirmatory analysis by flow cytometry also showed the same trend (*Figure 6C*).

In addition, HG-induced lipid peroxidation and protein carbonylation were also investigated. HG caused a significant increase in lipid peroxidation and protein carbonylation (1.70- and 3.33-fold, respectively; compared to control). The treatment with FA (10 and 25 μM) reduced lipid peroxidation (1.45- and 1.52-fold) and protein carbonylation (1.45- and 1.84-fold) significantly (compared to HG; $P \leq 0.05$) in a dose-dependent manner which was comparable to Met (1.96-fold; *Table II*).

FA protects H9c2 cardiomyoblasts against HG-induced myocyte injury

Cell injury with HG was evaluated by measuring cardiac health markers such as BNP and ANP release into the medium. H9c2 cardiomyoblasts treated with HG showed significant release of BNP and ANP (9.73- and 2.47-fold, respectively, $P \leq 0.05$) and co-treatment with FA significantly reduced the release of both NPs (BNP – 3.94- and 6.10-fold; ANP – 1.33- and 1.81-fold; $P \leq 0.05$; *Table III*) in a dose-dependent manner (for 10 and 25 μM, respectively) which is comparable with positive control Met (BNP – 5.25 and ANP – 1.91; *Table III*). Further, the cell injury was confirmed by LDH leakage assay (expressed as % cytotoxicity) which showed a significant release of the enzyme with HG (12.16%; $P \leq 0.05$) whereas co-treatment with FA significantly reduced the cytotoxicity (9.98 and 6.93%, respectively, $P \leq 0.05$; *Table III*) comparable with Met (5.91%; $P \leq 0.05$; *Table III*) These results indicate that FA can protect the cardiac myocyte from the HG-induced injury.

DISCUSSION

The pathogenesis of DC has been found to be multifactorial in origin, and evidence indicates that the defects in Ca^{2+} homeostasis are a major pathological reason for cardiac dysfunction [13]. Herein, we describe the sequences of various biochemical process induced by HG in H9c2 cells which ultimately terminates in oxidative stress via calcium overload and mitochondrial dysfunction. Normal Ca^{2+} homeostasis is very much essential for cardiac function. One of the most

© 2019 Société Française de Pharmacologie et de Thérapeutique

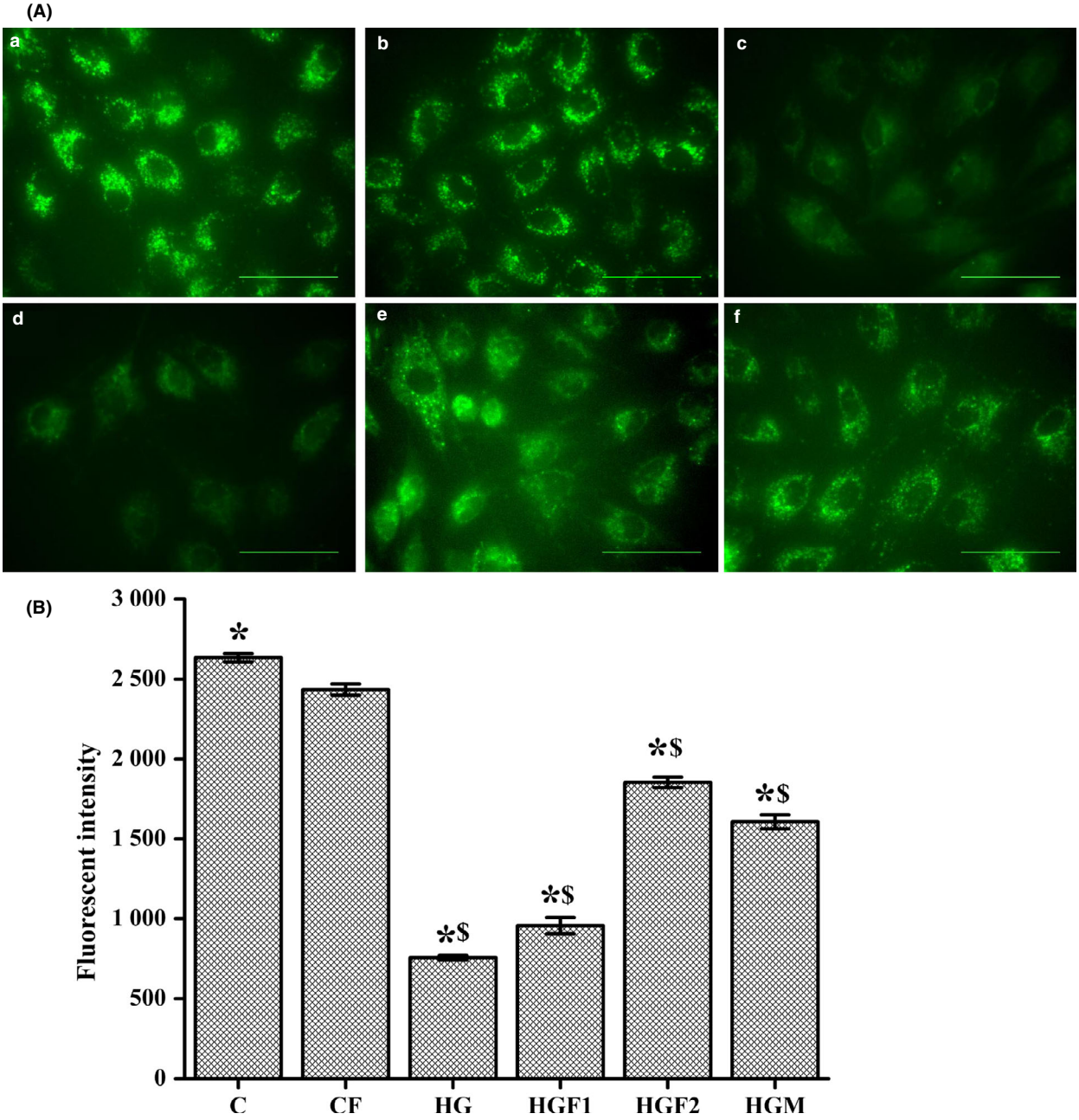

Figure 3 Effect of ferulic acid (FA) on high glucose (HG) induced dissipation of mitochondrial membrane potential (ΔΨm): (A) Confocal bio-imaging of calcein/$CoCl_2$ fluorescence and (B) Relative fluorescent intensity. (a) C – control (5.5 mM glucose), (b) CF – control + 25 μM FA, (c) HG – high glucose (33 mM glucose, (d) HGF1 – high glucose + 10 μM FA, (e) HGF2 – high glucose + 25 μM FA and (f) HGM – high glucose + metformin (10 μM) treated groups. Values are Mean ± SD (n = 6). *Mean values are significantly different from the control group ($P \leq 0.05$). $Mean values are significantly different from the high glucose treated group ($P \leq 0.05$). Scale bar 50 μM.

detrimental factors in the genesis of various heart diseases is the unbalanced change in Ca^{2+} homeostasis [14]. Ca^{2+} overload in post-ischemic cardiomyocytes is the leading cause of cell death either through apoptosis or necrosis [15,16]. Intracellular calcium concentration ($[Ca^{2+}]i$) is finely regulated through the control of flux

© 2019 Société Française de Pharmacologie et de Thérapeutique

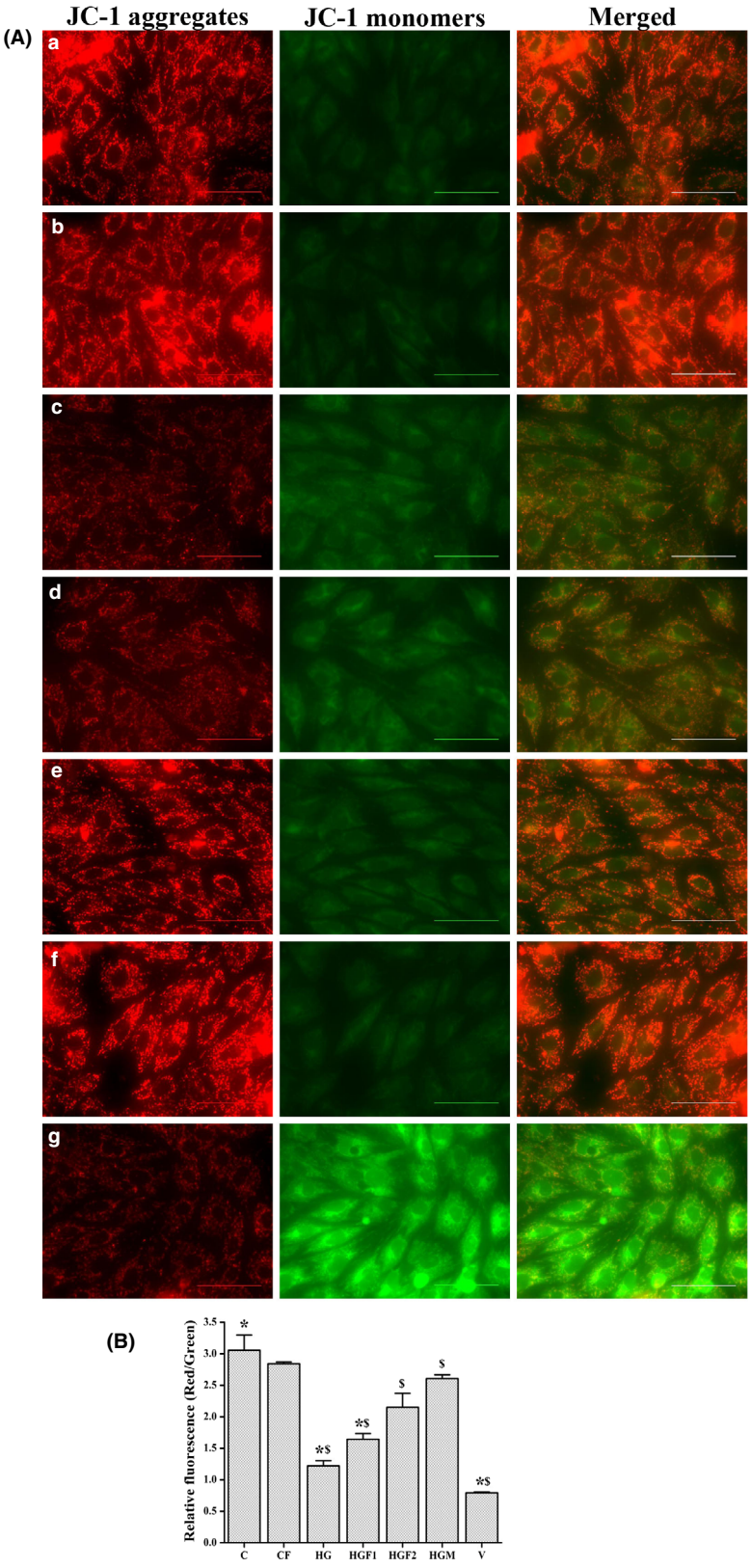

Figure 4 Effect of ferulic acid (FA) on high glucose (HG) induced mitochondrial permeability transition pore (mPTP) opening: (A) Bio-imaging of JC-1 fluorescence and (B) Relative fluorescent intensity. (a) C – control (5.5 mM glucose), (b) CF – control + 25 μM FA, (c) HG – high glucose (33 mM glucose), (d) HGF1 – high glucose + 10 μM FA, (e) HGF2 – high glucose + 25 μM FA, (f) HGM – high glucose + metformin (10 μM), and (g) Valinomycin (negative control) treated groups. Values are Mean ± SD (n = 6). *Mean values are significantly different from the control group ($P \leq 0.05$). $Mean values are significantly different from the high glucose treated group ($P \leq 0.05$). Scale bar 50 μM.

© 2019 Société Française de Pharmacologie et de Thérapeutique

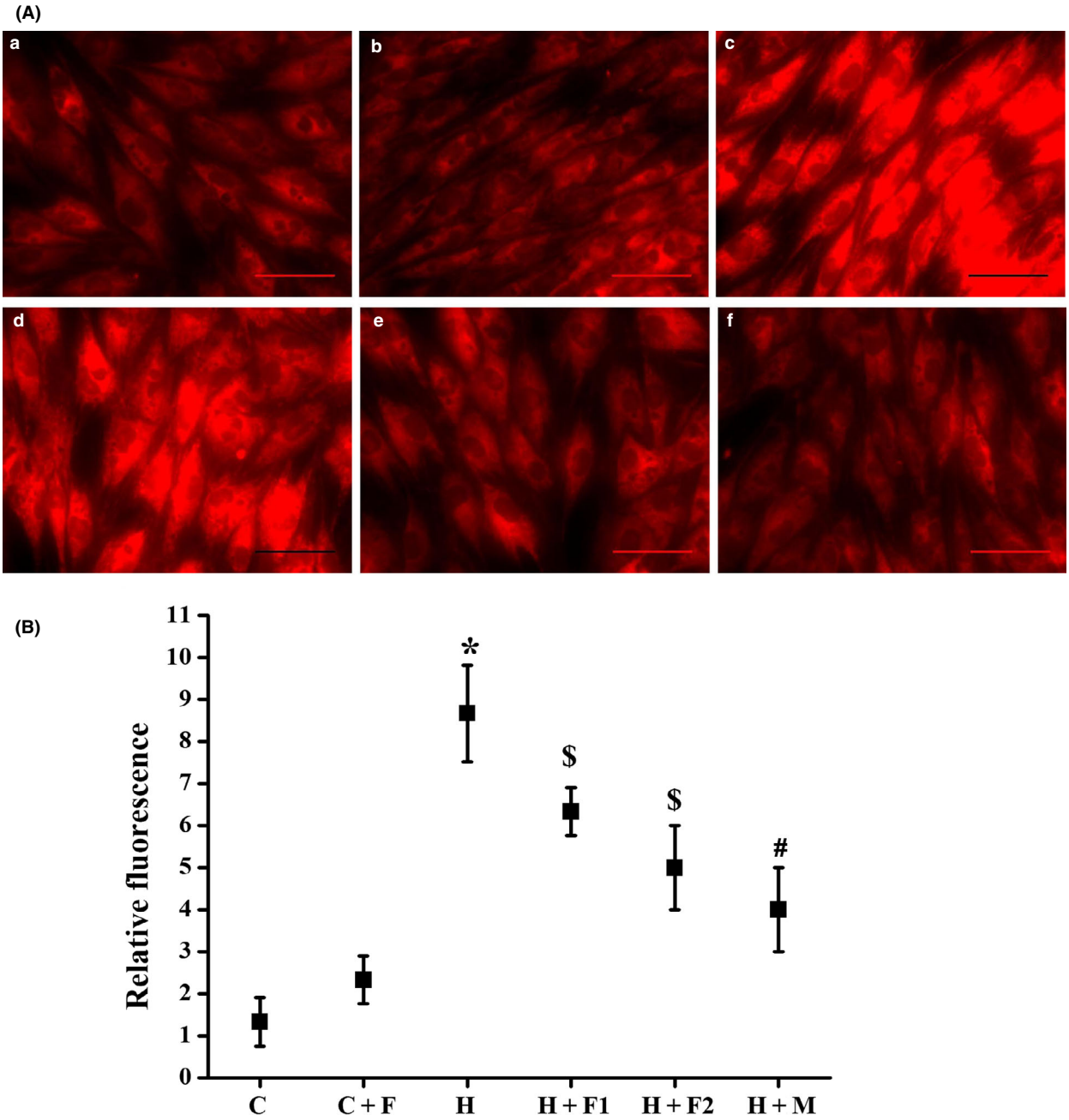

Figure 5 Analysis of mitochondrial superoxide generation: (A) Confocal bio-imaging of MitoSOX fluorescence and (B) Relative fluorescent intensity. (a) C – control (5.5 mM glucose), (b) CF – control + 25 μM FA, (c) HG – high glucose (33 mM glucose), (d) HGF1 – high glucose + 10 μM FA, (e) HGF2 – high glucose + 25 μM FA and (f) HGM – high glucose + metformin (10 μM) treated groups. Values are Mean ± SD (n = 6). * Mean values are significantly different from the control group ($P \leq 0.05$). #, $ Mean values are significantly different from the high glucose treated group ($P \leq 0.05$). Scale bar 50 μM.

from the extracellular compartment and internal reservoirs [16]. Alteration of this triggers a plethora of effects. There are reports available stating that HG is responsible for alteration of Ca^{2+} homeostasis in diabetes patients [3]. For detailed information of underlying mechanism, we explored the SERCA/PLN pathway. SERCA/PLN/PKA C-α is a very important signalling cascade responsible for the transport of Ca^{2+}

© 2019 Société Française de Pharmacologie et de Thérapeutique

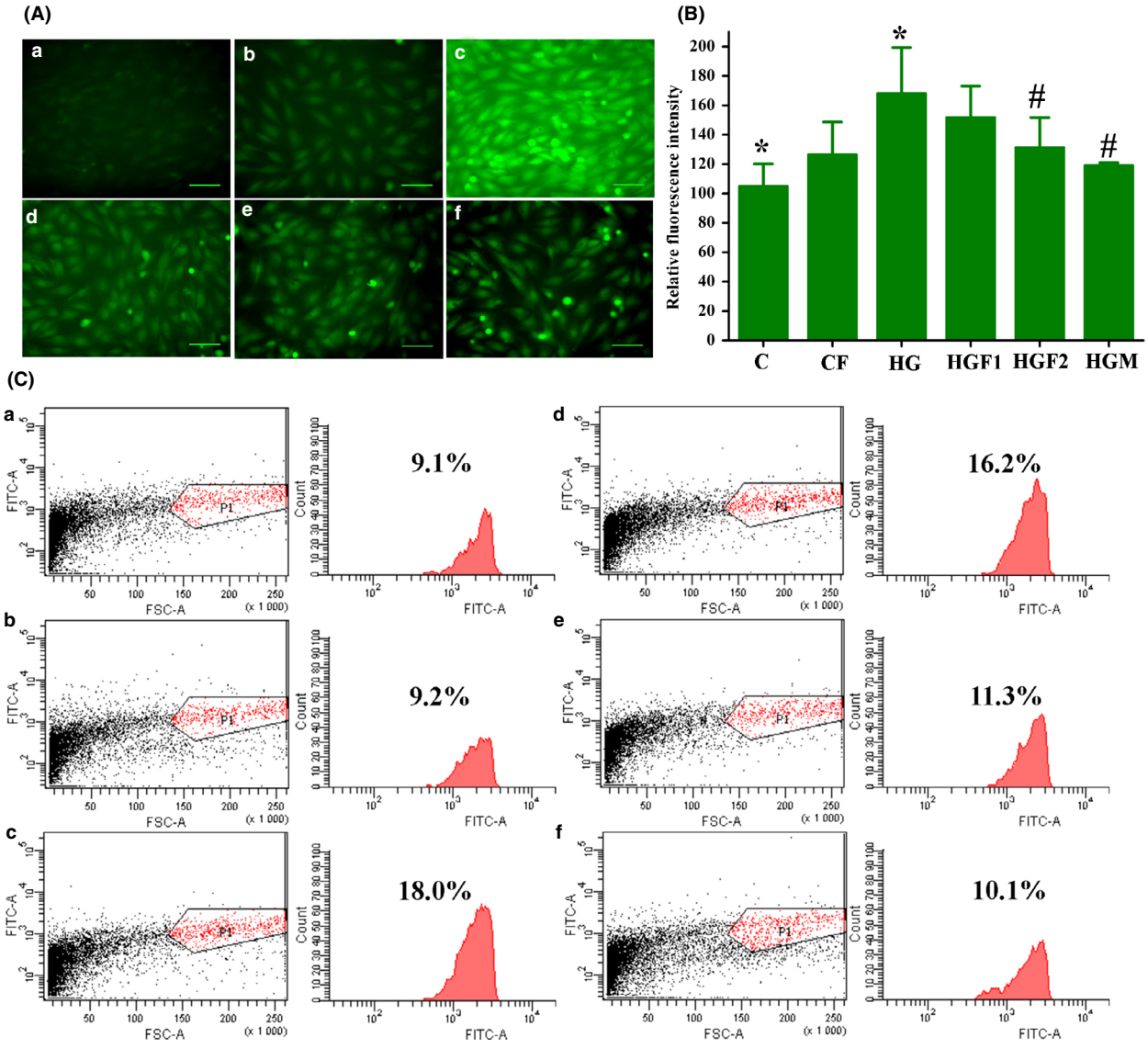

Figure 6 Analysis of cytosolic ROS generation: (A) Confocal bio-imaging DCF fluorescence, (B) Relative fluorescent intensity, and (C) Flow cytometry analysis. (a) C – control (5.5 mM glucose), (b) CF – control + 25 μM ferulic acid (FA), (c) HG – high glucose – 33 mM glucose, (d) HGF1 – high glucose + 10 μM FA, (e) HGF2 – high glucose + 25 μM FA and (f) HGM – high glucose + metformin (10 μM) treated groups. Values are mean ± SD (n = 6). * Mean values are significantly different from the control group ($P \leq 0.05$). # Mean values are significantly different from the high glucose treated group ($P \leq 0.05$). Scale bar 50 μM.

into the sarcoplasmic reticulum (SR) and regulates intracellular Ca^{2+} homeostasis, SR Ca^{2+} load, and the rate of contraction and relaxation of the heart [17]. The decrease in the SERCA protein level leads to a decrease in SR Ca^{2+} transport, and this is characteristic of failing human heart [18–20]. In the cardiac myocytes, the small molecular weight protein PLN is the primary regulator of the SERCA pump [19]. The phosphorylation of PLN leads to the opening of SRCA pump. The pPKA C-α, in turn, phosphorylates the PLN. Western blot analysis revealed that HG downregulated the SERCA2 and decreased the phosphorylation of PLN and PKA C-α. This contributes significantly to the $[Ca^{2+}]i$ overload.

In addition to SERCA/PLN/PKA C-α, defective mitochondria also contribute to intracellular calcium overload [21]. Mitochondria are known for its involvement in the regulation of calcium mobilization through the

© 2019 Société Française de Pharmacologie et de Thérapeutique

Table II Estimation of lipid peroxidation and protein carbonylation in control and experimental groups.

Groups	Lipid peroxidation (nM/μL) (fold change)	Protein carbonyl content (nM/mg protein) (fold change)
C	0.205 ± 0.02[a]	0.27 ± 0.03[a]
CF	0.204 ± 0.02	0.25 ± 0.02
HG	0.348 ± 0.02 (1.70)[a]	0.90 ± 0.14 (3.33)[a]
HGF1	0.240 ± 0.07 (1.45)[b]	0.62 ± 0.09 (1.45)[b]
HGF2	0.229 ± 0.05 (1.52)[b]	0.49 ± 0.11 (1.84)[b]
HGM	0.175 ± 0.02 (1.99)[b]	0.46 ± 0.09(1.96)[b]

C – control (5.5 mM glucose), CF – control + ferulic acid (FA -25 μM), HG – high glucose (33 mM glucose), HGF1 – high glucose + 10 μM FA, HGF2 – high glucose + 25 μM FA and HGM – high glucose + metformin (10 μM) treated groups. Values are Mean ± SD (n = 6).

[a]Mean values are significantly different from the control group ($P \leq 0.01$).

[b]Mean values are significantly different from high glucose treated group ($P \leq 0.01$).

uniporter in the cell. Mitochondrial function is significantly impaired by hyperglycemic conditions, particularly the integrity markers like mPTP and membrane potential. The transition in mPTP and associated dissipation of membrane potential is reported to induce ([Ca^{2+}]i) overload through the change in membrane integrity and electrochemical concentration gradient via alteration in uniporter [22]. The changes in mPTP and transmembrane potential observed during HG exposure are assumed to be involved in the genesis of intracellular calcium overload [23]. So these findings establish the combined role of SERCA/PLN/PKA C-α and integrity of mitochondria in the genesis of calcium overload during HG.

Role of intracellular calcium in the generation of the oxidative stress is well established in various studies [16,24,25]. One explanation has been that Ca^{2+} induces a three-dimensional conformation change of the respiratory chain complexes which leads to surplus mitochondrial ROS generation [26,27]. There is further evidence that the metabolic state of the mitochondria determines the effects of calcium on mitochondrial ROS levels [28]. We also checked lipid peroxidation and genesis of carbonyl content to confirm alteration in redox status. A significant rise in lipid peroxidation and carbonyl content was found during HG condition.

Oxidative stress causes multiple injuries in the cardiac cell [29] which is reflected in the surplus secretion of various marker proteins like ANP and BNP [30,31]. HG-induced cardiac dysfunction has been confirmed with the quantification of cardiac markers like BNP and ANP. These proteins have been found increased with incubation of cells with the HG medium. It is established that these natriuretic peptides from the heart are released in response to changes in the physiology of the heart [32–34]. The level of BNP goes up when heart failure develops or gets worse, and it goes down when the condition is stable. ANP, another marker peptide from the heart is released during stressed conditions like cardiac ischemia and heart failure [33]. In early heart failure, these peptides have a significant role in keeping the compensated state of asymptomatic left ventricular dysfunction [34,35]. We also found a surplus release of LDH during HG shock. This confirms the cardiac injury during HG concentrations.

Co-treatment of FA was found effective against HG-induced alterations in H9c2 cells. In details, FA upregulated phosphorylation of PLN and PKA C-α and decreased the level of non-phosphorylated forms, and thus activated the SERCA pathway. This activation of

Table III Estimation of cardiac myocyte injury markers (atrial natriuretic peptide (ANP), brain natriuretic peptide (BNP), and lactate dehydrogenase (LDH)) in control and experimental groups.

Groups	ANP (pg/mL) (fold change)	BNP (pg/mL) (fold change)	LDH release (% cytotoxicity)
C	149.80 ± 24.88[a]	48.83 ± 4.89[a]	0.00[a]
CF	176.59 ± 16.59 (0.18)	57.93 ± 3.55 (0.18)	1.43 ± 0.33
HG	369.48 ± 4.85 (2.47)[a]	475.01 ± 30.90 (9.73)[a]	12.16 ± 1.63[a]
HGF1	277.18 ± 9.92 (1.33)[b]	120.32 ± 18.81 (3.95)[b]	9.98 ± 0.41[a,b]
HGF2	218.67 ± 0.05 (1.81)[b]	77.93 ± 0.72 (6.10)[b]	6.93 ± 0.51[a,b]
HGM	193.03 ± 23.25 (1.91)[b]	90.46 ± 8.52 (5.25)[b]	5.91 ± 0.90[a,b]

C – control (5.5 mM glucose), CF – control + ferulic acid (FA -25 μM), HG – high glucose (33 mM glucose), HGF1 – high glucose + 10 μM FA, HGF2 – high glucose + 25 μM FA and HGM – high glucose + metformin (10 μM) treated groups.

Values are Mean ± SD (n = 6).

[a]Mean values are significantly different from the control group ($P \leq 0.01$).

[b]Mean values are significantly different from high glucose treated group ($P \leq 0.01$).

© 2019 Société Française de Pharmacologie et de Thérapeutique

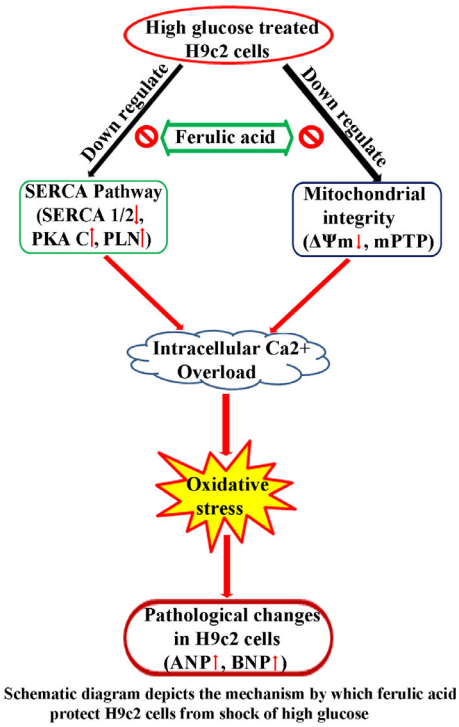

Figure 7 Schematic diagram of mechanism of action of ferulic acid during high glucose in H9c2 cardiomyoblasts.

SERCA pathway led to the reduction in the $[Ca^{2+}]i$ level accumulated during HG exposure. Further, it safeguarded the integrity of mitochondria which is also expected to contribute to the decrease of $[Ca^{2+}]i$ overload. Mitigation of lipid peroxidation and carbonyl content is also observed with FA co-treatment. Finally, FA was able to keep all cardiac pathological indicators like LDH, ANP, and BNP in the normal range. Our result is in line with a previous study by Song et al. [36], reported that FA is effective against HG-induced oxidative stress. FA through its antioxidant properties is reported to be beneficial in prevention and/or treatment of disorders linked to oxidative stress, including Alzheimer's disease [37], diabetes [38–41], cancers [42], hypertension, dyslipidemia, and atherosclerosis [43,44]. In addition, its derivatives have been found effective against several inflammatory diseases due to its anti-inflammatory properties [45–47]. There are reports on FA for its potential against diabetes and associated complications. It improves insulin sensitivity [48,49], hepatic glycogenesis and inhibits gluconeogenesis [50]. It is also found to reduce diabetic induced complications like nephropathy [51], inflammation, splenotoxicity (stress mediated) [52]. These pleiotropic effects of FA were attraction for us to work on FA to see its efficacy against HG-induced pathological manifestation in H9c2 cells. Most of the various pharmacological effects of FA are associated with its ability to break free radical chain reactions [53], but not all. The positive impact of FA observed in the present study on calcium homeostasis glorifies its status in the drug discovery field. FDA has approved FA as food additive and sports food. The remarkable array of pharmacological properties of FA and lack of side effects make it an exciting compound for use as a functional food as well as a substitute for synthetic drugs. However, detailed preclinical and clinical studies are required before recommending FA for human use both as a nutrient supplement as well as a therapeutic agent against human diseases.

The current study concludes that FA protects H9c2 cardiomyoblasts from HG-induced oxidative stress damages. This protection is mediated by the maintenance of Ca^{2+} homeostasis via safeguarding SERCA/PLN pathway and mitochondrial function (*Figure 7*). From the overall results, we suggest that FA should be further explored in vitro and in vivo studies for the development of novel nutraceuticals in the prevention and treatment of DC.

ACKNOWLEDGEMENTS

Salin Raj P thanks, Council of Scientific and Industrial Research (CSIR) and Department of Health Research (DHR) New Delhi for Research Fellowship. Swapna Sasi U S acknowledges University Grants Commission (UGC), New Delhi, India for Junior Research Fellowship We thank the Director, CSIR-NIIST, for providing necessary facilities.

DECLARATION OF INTEREST

The authors declare that they have no conflict of interests regarding the data of this paper.

REFERENCES

1 Zhang X., Chen C. A new insight of mechanisms, diagnosis and treatment of diabetic cardiomyopathy. Endocrine (2012) **41** 398–409.
2 Kayama Y., Raaz U., Jagger A. et al. Diabetic cardiovascular disease induced by oxidative stress. Int. J. Mol. Sci. (2015) **16** 25234–25263.

© 2019 Société Française de Pharmacologie et de Thérapeutique

3 Kumar S., Kain V., Sitasawad S.L. High glucose-induced Ca^{2+} overload and oxidative stress contribute to apoptosis of cardiac cells through mitochondrial dependent and independent pathways. Biochim. Biophys. Acta (2012) **1820** 907–920.

4 Huang X., Liu S., Wu D. et al. Facilitated Ca^{2+} homeostasis and attenuated myocardial autophagy contribute to alleviation of diabetic cardiomyopathy after bariatric surgery. Am. J. Physiol. Heart Circ. Physiol. (2018) **15**(5) H1258–H1268.

5 Zhao Z., Moghadasian M.H. Chemistry, natural sources, dietary intake and pharmacokinetic properties of ferulic acid: a review. Food Chem. (2008) **109** 691–702.

6 Shahidi F., Chandrasekara A. Millet grain phenolics and their role in disease risk reduction and health promotion: a review. J. Funct. Foods (2013) **5** 57081.

7 Kuznetsov A.V., Javadov S., Sickinger S., Frotschnig S., Grimm M. H9c2 and HL-1 cells demonstrate distinct features of energy metabolism, mitochondrial function and sensitivity to hypoxia-reoxygenation. Biochim. Biophys. Acta (2015) **1853** 276–284.

8 Branco A.F., Pereira S.P., Gonzalez S., Gusev O., Rizvanov A.A., Oliveira P.J. Gene expression profiling of H9c2 myoblast differentiation towards a cardiac-like phenotype. PLoS ONE (2015) **10** e0129303.

9 Cai L., Li W., Wang G., Guo L., Jiang Y., Kang Y.J. Hyperglycemia-induced apoptosis in mouse myocardium: mitochondrial cytochrome C-mediated caspase-3 activation pathway. Diabetes (2002) **51** 1938–1948.

10 Mosmann T. Rapid colorimetric assay for cellular growth and survival: application to proliferation and cytotoxicity assays. J. Immunol. Methods (1983) **65** 55–63.

11 Priyanka A., Shyni G.L., Anupama N., Raj P.S., Anusree S.S., Raghu K.G. Development of insulin resistance through sprouting of inflammatory markers during hypoxia in 3T3-L1 adipocytes and amelioration with curcumin. Eur. J. Pharmacol. (2017) **812** 73–81.

12 Bonora M., Morganti C., Morciano G., Giorgi C., Wieckowsk M.R., Pinton P. Comprehensive analysis of mitochondrial permeability transition pore activity in living cells using fluorescence-imaging-based techniques. Nat. Protocol. (2016) **11** 1067–1080.

13 Singh R.M., Waqar T., Howarth F.C., Adeghate E., Bidasee K., Singh J. Hyperglycemia-induced cardiac contractile dysfunction in the diabetic heart. Heart Fail. Rev. (2018) **23** 37–54.

14 Dhalla N.S., Temsah R.M., Netticadan T., Sandhu M.S. Calcium overload in ischemia/reperfusion injury, in: Sperelakis N. (Ed), Heart physiology and pathophysiology, Academic Press, San Diego, CA, 2001, pp. 949–965.

15 Altamirano F., Wang Z.V., Hill J.A. Cardioprotection in ischaemia-reperfusion injury: novel mechanisms and clinical translation. J. Physiol. (2015) **593** 3773–3788.

16 Soumya R.S., Vineetha V.P., Salin Raj P., Raghu K.G. Beneficial properties of selenium incorporated guar gum nanoparticles against ischemia/reperfusion in cardiomyoblasts (H9c2). Metallomics (2014) **6** 2134–2147.

17 Gustavsson M., Verardi R., Mullen D.G. et al. Allosteric regulation of SERCA by phosphorylation mediated conformational shift of phospholamban. Proc. Natl Acad. Sci. USA (2013) **110** 17338–17343.

18 Hasenfuss G. Alterations of calcium-regulatory proteins in heart failure. Cardiovasc. Res. (1998) **37** 279–289.

19 Periasamy M., Bhupathy P., Babu G.J. Regulation of sarcoplasmic reticulum Ca^{2+} ATPase pump expression and its relevance to cardiac muscle physiology and pathology. Cardiovasc. Res. (2008) **77** 265–273.

20 Chen X., Zhang X., Kubo H. et al. Ca^{2+} influx-induced sarcoplasmic reticulum Ca^{2+} overload causes mitochondrial-dependent apoptosis in ventricular myocytes. Circ. Res. (2005) **97** 1009–1017.

21 Soumya R.S., Prathapan A., Salin Raj P., Vineetha V.P., Raghu K.G. Selenium incorporated guar gum nanoparticles safeguard mitochondrial bioenergetics during ischemia reperfusion injury in H9c2 cardiac cells. Int. J. Biol. Macromol. (2018) **107** 254–260.

22 Carri M.T., Ferri A., Battistoni A. et al. Expression of a Cu, Zn superoxide dismutase typical of familial amyotrophic lateral sclerosis induces mitochondrial alteration and increase of cytosolic Ca^{2+} concentration in transfected neuroblastoma SH-SY5Y cells. FEBS Lett. (1997) **414** 365–368.

23 Kruman I.I., Pedersen W.A., Springer J.E., Mattson M.P. ALS-linked Cu/Zn-SOD mutation increases vulnerability of motor neurons to excitotoxicity by a mechanism involving increased oxidative stress and perturbed calcium homeostasis. Exp. Neurol. (1999) **160** 28–39.

24 Prathapan A., Salin Raj P., Raghu K.G. Attenuation of oxidative damage by *Boerhaavia diffusa* L. against different neurotoxic agents in rat brain homogenate. J. Diet Suppl. (2016) **13** 300–312.

25 Prathapan A., Varghese M.V., Abhilash S. et al. Polyphenol rich ethanolic extract from *Boerhavia diffusa* L. mitigates angiotensin II induced cardiac hypertrophy and fibrosis in rats. Biomed. Pharmacother. (2017) **87** 427–436.

26 Brookes P.S., Yoon Y., Robotham J.L., Anders M.W., Sheu S.S. Calcium, ATP, and ROS: a mitochondrial love-hate triangle. Am. J. Physiol. Cell Physiol. (2004) **287** C817–C833.

27 Adam-Vizia V., Starkov A.A. Calcium and mitochondrial reactive oxygen species generation: how to read the facts. J. Alzheimers Dis. (2010) **20** S413–S426.

28 Jaiswal N., Maurya C.K., Arha D. et al. Fructose induces mitochondrial dysfunction and triggers apoptosis in skeletal muscle cells by provoking oxidative stress. Apoptosis (2015) **20** 930–947.

29 Giugliano D., Ceriello A., Paolisso G. Oxidative stress and diabetic vascular complications. Diab. Care. (1996) **19** 257–267.

30 Waldman M., Cohen K., Yadin D. et al. Regulation of diabetic cardiomyopathy by caloric restriction is mediated by intracellular signaling pathways involving 'SIRT1 and PGC-1α'. Cardiovasc. Diabetol. (2018) **17** 111.

© 2019 Société Française de Pharmacologie et de Thérapeutique

31 Dietz J.R. Mechanisms of atrial natriuretic peptide secretion from the atrium. Cardiovasc. Res. (2005) **68** 8–17.
32 Sergeeva I.A., Christoffels V.M. Regulation of expression of atrial and brain natriuretic peptide, biomarkers for heart development and disease. Biochim. Biophys. Acta (2013) **1832** 2403–2413.
33 Wong P.C., Guo J., Zhang A. The renal and cardiovascular effects of natriuretic peptides. Adv. Physiol. Educ. (2017) **41** 179–185.
34 Yoshimura M., Yasue H., Ogawa H. Pathophysiological significance and clinical application of ANP and BNP in patients with heart failure. Can. J. Physiol. Pharmacol. (2001) **79** 730–735.
35 Maisel A.S., Koon J., Krishnaswamy P. et al. Utility of B-natriuretic peptide (BNP) as a rapid, point-of-care test for screening patients undergoing echocardiography for left ventricular dysfunction. Am. Heart J. (2001) **141** 367–374.
36 Song Y., Wen L., Sun J. et al. Cytoprotective mechanism of ferulic acid against high glucose induced oxidative stress in cardiomyocytes and hepatocytes. Food Nutr. Res. (2016) **60** 30323.
37 Jin Y., Yan E.Z., Fan Y., Zong Z.H., Qi Z.M., Li Z. Sodium ferulate prevents amyloid-beta-induced neurotoxicity through suppression of p38 MAPK and upregulation of ERK-1/2 and Akt/protein kinase B in rat hippocampus. Acta Pharmacol. Sin. (2005) **26** 943–951.
38 Shahidi F., Chandrasekara A. Hydroxycinnamates and their in vitro and in vivo antioxidant activities. Phytochem. Rev. (2010) **9** 147–170.
39 Pluemsamran T., Onkoksoong T., Panich U. Caffeic acid and ferulic acid inhibit UV A-induced matrix metalloproteinase-1 through regulation of antioxidant defense system in keratinocyte HaCaT cells. Photochem. Photobiol. (2012) **88** 961–968.
40 Kim E.O., Min K.J., Kwon T.K., Um B.H., Moreau R.A., Choi S.W. Anti-inflammatory activity of hydroxyl cinnamic acid derivatives isolated from corn bran in lipopolysaccharide-stimulated Raw 264.7 macrophages. Food Chem. Toxicol. (2012) **50** 1309–1316.
41 Jung E.H., Kim S.R., Hwang I.K., Ha T.Y. Hypoglycemic effects of a phenolic acid fraction of rice bran and ferulic acid in C57BL/KsJ-db/db mice. J. Agri. Food Chem. (2007) **55** 9800–9804.
42 Janicke B., Hegardt C., Krogh M. et al. The antiproliferative effect of dietary fiber phenolic compounds ferulic acid and p-coumaric acid on the cell cycle of Caco-2 cells. Nutr. Cancer (2011) **63** 611–622.
43 Suzuki A., Yamamoto M., Jokura H. et al. Ferulic acid restores endothelium-dependent vasodilation in aortas of spontaneously hypertensive rats. J. Am. Soc. Hypertens. (2007) **20** 508–513.
44 Wang B.H., Ou Yang J.P. Pharmacological actions of sodium ferulate in cardiovascular system. Cardiovasc. Drug Rev. (2005) **23** 161–172.
45 Bumrungpert A., Lilitchan S., Tuntipopipat S., Tirawanchai N., Komindr S. Ferulic acid supplementation improves lipid profiles, oxidative stress, and inflammatory status in hyperlipidemic subjects: a randomized, double-blind, placebo-controlled clinical trial. Nutrients (2018) **10** 713.
46 Srinivasan M., Sudheer A.R., Menon V.P. Ferulic acid: therapeutic potential through its antioxidant property. J. Clin. Biochem. Nutr. (2007) **40** 92–100.
47 Ghosh S., Basak P., Dutta S., Chowdhury S., Sil P.C. New insights into the ameliorative effects of ferulic acid in pathophysiological conditions. Food Chem. Toxicol. (2017) **103** 41–55.
48 Chang C.I., Hsu C.M., Li T.S. et al. Constituents of the stem of *Cucurbita moschata* exhibit antidiabetic activities through multiple mechanisms. J. Funct. Food. (2014) **10** 260–273.
49 Roy S., Metya S.K., Sannigrahi S., Rahaman N., Ahmed F. Treatment with ferulic acid to rats with streptozotocin-induced diabetes: effects on oxidative stress, pro-inflammatory cytokines, and apoptosis in the pancreatic β cell. Endocrine (2013) **44** 369–379.
50 Rukkumani R., Aruna K., Suresh V.P., Padmanabhan M.V. Hepatoprotective role of ferulic acid: a dose-dependent study. J. Med. Food (2004) **7** 456–461.
51 Alam M.A., Sernia C., Brown L. Ferulic acid improves cardiovascular and kidney structure and function in hypertensive rats. J. Cardiovasc. Pharmacol. (2013) **61** 240–248.
52 Ghosh S., Chowdhury S., Sarkar P., Sil P.C. Ameliorative role of ferulic acid against diabetes associated oxidative stress induced spleen damage. Food Chem. Toxicol. (2018) **118** 272–286.
53 Nenadis N., Zhang H.Y., Tsimidou M.Z. Structure-antioxidant activity relationship of ferulic acid derivatives: effect of carbon side chain characteristic groups. J. Agri. Food Chem. (2003) **51** 1874–1879.

© 2019 Société Française de Pharmacologie et de Thérapeutique

Annexure I: List of proteins

Acc1	Acetyl CoA carboxylase	Ho-1	Haem Oxygenase 1
Acrp30	Adiponectin	hs CRP	High sensitivity C-reactive protein
Aif	Apoptosis Inducing Factor	Hsp	Heat Shock Proteins
Akt	Protein kinase B	HtrA2/Omi	High temperature requirement protein A2
Anp	Atrial natriuretic peptide	Ip3r2	Inositol 1,4,5-trisphosphate receptor, type 2
Ant1	Adenine nucleotide translocator 1	Ir	Insulin receptor
Apaf 1	Apoptotic protease activating factor-1	Irs1	Insulin receptor substrate 1
Arts	Apoptosis-related protein in the TGF-β signalling	Jnk	c-Jun N-terminal kinase
ATP 5A	ATP synthase F1 subunit alpha (Complex V)	Mcur1	Mitochondrial Calcium Uniporter Regulator 1
Bax	Bcl-2-associated X protein	Mfn 2	Mitofusin 2
Bnp	b-Type natriuretic peptide	MG53	Mitsugumin 53
Casp 3	Cysteine-aspartic acid protease 3	MTCO1	Mitochondrially encoded cytochrome C Oxidase 1 (Complex IV)
Casp 9	Cysteine-aspartic acid protease 9	NDUFB8	NADH: ubiquinone oxidoreductase 1 beta subcomplex subunit 8 (Complex I)
COX IV	Cytochrome C oxidase IV	Opa1	Optic Atrophy 1
Cpp	Copeptin	Pacs2	Phosphofurin Acidic Cluster Sorting Protein 2
Cpt1	Carnitine palmitoyl transferase 1	Pgc 1α	Peroxisome proliferator-activated receptor gamma coactivator-1α
cTnI	Cardiac Troponin I	Pka cα	Protein kinase A catalytic subunit α
cTnT	Cardiac Troponin T	Pln	Phospholamban
Cyp D	Cyclophilin D	Pparα	Peroxisome proliferator activated receptor -α
Cyt c	Cytochrome c	Rac1	Ras-related C3 botulinum toxin substrate 1
Drp 1	Dynamin-related protein 1	SDHA	Succinate dehydrogenase complex, subunit A (Complex II)
EndoG	Endonuclease G	SDHB	Succinate dehydrogenase complex, subunit B (Complex II)
Fas	Fatty acid synthase	Serca	Sarco/endoplasmic reticulum Ca^{2+}-ATPase
Fis1	Mitochondrial fission 1 protein	Smac/ Diablo	Second Mitochondria-derived Activator of Caspases
Fundc1	FUN14 domain-containing protein 1	Ub	Ubiquitin
Gapdh	Glyceraldehyde 3-phosphate dehydrogenase	UQCRC2	Ubiquinol-Cytochrome C Reductase Core Protein 2 (Complex III)
Hdac1	Histone Deacetylase 1 (HDAC1)	Vdac1	Voltage-dependent anion-selective channel 1
hFabp	heart-specific Fatty acid binding protein	Xiap	X-linked inhibitor of apoptosis

Annexure II

AcSIR course work

Course code	Course Name	Credits	Status
BIO-NIIST-1-0001	Biostatistics	1	Completed
BIO-NIIST-1-0002	Computation/bioinformatics	1	Completed
BIO-NIIST-1-0003	Basic Chemistry	1	Completed
BIO-NIIST-1-0004	Research Methodology, Communication/ethics/safety	1	Completed
BIO-NIIST-2-4101	Bio-techniques and Instrumentation	1	Completed
BIO-NIIST-2-4102	Protein Science and Proteomics	2	Completed
BIO-NIIST-2-4104	Basic Molecular Biology	2	Completed
BIO-NIIST-3-4101	Seminar course	1	Completed
BIO-NIIST-3-4109	Cardiovascular Disease Biology	2	Completed
BIO-NIIST-3-4110	Molecular Biology of Diabetes	2	Completed
BIO-NIIST-4-0001	Project Proposal Writing	2	Completed
BIO-NIIST-4-0002	Review Article Writing	2	Completed
BIO-NIIST-4-0003	CSIR-800 Project Work	4	Completed